Geophysical Investigations of Tasmania at Multiple Scales

Esmaeil Eshaghi

School of Physical Sciences (Earth Sciences)

Submitted in fulfilment of the requirements for the degree of

Doctor of Philosophy

University of Tasmania- Australia

March, 2017

Declaration of originality

This thesis contains no material which has been accepted for a degree or diploma by the University or any other institution, except by way of background information and duly acknowledged in the thesis, and to the best of my knowledge and belief no material previously published or written by another person except where due acknowledgement is made in the text of the thesis, nor does the thesis contain any material that infringes copyright.

Authority of access

This thesis may be made available for loan and limited copying and communication in accordance with the Copyright Act 1968.

Statement regarding published work contained in thesis

Chapters 4, 5 and 6 may contain copyright material and access to the material may need to be sought from the respective journal.

Esmaeil Eshaghi

February, 2016

Statement of Co-Authorship

The following people and institutions contributed to the work undertaken as part of this thesis:

Esmaeil Eshaghi, School of Physical Sciences – Earth Sciences	= **Candidate**
Anya Reading, University of Tasmania	= **Author 1**
Michael Roach, University of Tasmania	= **Author 2**
Mark Duffett, Mineral Resources Tasmania	= **Author 3**
Daniel Bombardieri, Mineral Resources Tasmania	= **Author 4**
Matthew Cracknell, University of Tasmania	= **Author 5**
Stephen Kuhn, University of Tasmania	= **Author 6**
John Everard, Mineral Resources Tasmania	= **Author 7**
Grace Cumming, Mineral Resources Tasmania	= **Author 8**

Paper 1, The onshore and offshore tectonic structure of Tasmania from 3D gravity modelling:

Chapter 4 comprises material to be reformatted for submission to Australian Journal of Earth Sciences (AJES).

The Candidate was the primary author and with Author 1, Author 2 and Author 3 contributing to the development of research ideas.

The Candidate performed data processing, modelling and interpretation.

Author 4, Author 5 and Author 6 contributed to the assessment and interpretation of results and presentation.

Paper 2, Major granite bodies beneath prospective regions of West Tasmania: geometry redefined by potential field modelling:

Chapter 5 comprises a manuscript to be submitted to Ore Geology Reviews.

The Candidate was the primary author with Author 1, Author 2, Author 3 and Author 4 contributing to the development of research ideas and modelling.

The Candidate performed model construction, modelling and interpretation.

Author 5 contributed to the discussion of research findings and presentation.

Paper 3, 3D inverse modelling of the prospective Heazlewood-Luina-Waratah region combining improved geological mapping and constraints from petrophysics:

Chapter 6 comprises a manuscript to be submitted to the journal, Interpretation.

The Candidate was the primary author and with Author 1, Author 2 and Author 3 contributing to the development of research ideas.

The Candidate performed model construction, modelling and interpretation.

Author 4 and Author 5 contributed to modelling and presentation.

Author 7 and Author 8 contributed to model construction and geological interpretation.

Signed

Anya M. Reading

Supervisor

School of Physical Sciences (Earth Sciences)
University of Tasmania

Date: 21 Nov 2017

John M. Dickey

Head of School

School of Physical Sciences
University of Tasmania

24/11/17

Abstract

Tasmania, part of east Australia, is notable for its diverse geology. It contains rocks ranging in age from Mesoproterozoic to Cainozoic. Multiple orogenic events associated with granite intrusions have affected Tasmania during the Neoproterozoic, Cambrian and Devonian. Therefore, the tectonic structure of Tasmania is complex and many aspects of its evolution are the subject of current geological debate. The multiple orogenic and intrusive events have produced environments for mineralisation and Tasmania is prospective for a wide range of economic deposits.

In this study, geophysical data, geological information and an improved petrophysical database have been used to investigate Tasmania at multiple scales including a sub continental scale study, a regional scale study, a local scale investigation and a prospect scale study. Deep tectonic boundaries and major geological features have been investigated using modelling techniques (e.g. 2D and 3D inversions of potential field data) to facilitate a better understanding of the tectonic evolution and present day geological structures of Tasmania. Modelling of local and prospect scale studies was performed using 3D inversion of gravity and magnetic data upon a geologically constrained initial model. Petrophysical properties (i.e. density and magnetic susceptibility) of major subsurface units are characterised in this research and used to better constrain properties during modelling.

At the sub continental scale across east Australia, the Curie Point Depth (CPD) is estimated using spectral analysis of magnetic data with a low resolution of 100 × 100 km across east Australia and 50 × 50 km across Tasmania. The interpreted CPD is relatively deep across north of the Delamerian, Thomson and Lachlan Orogens and shallower throughout regions associated with Cainozoic volcanism and in the northern part of Queensland. While the CPD and Moho depth determined from seismic data generally correlate, the CPD is dominantly deeper than Moho across the Thomson Orogen and north of the Lachlan Orogen. Tasmania is characterised by CPDs ranging from ~25 km to ~40 km that correlate with seismic Moho depth reasonably well.

At the regional scale study, gravity derived Moho depth has been investigated throughout onshore and offshore Tasmania. At this scale, Moho depth determined from seismic data has been reinvestigated based on 3D modelling of well distributed onshore and offshore gravity Bouguer anomaly with a resolution of 1 km × 1 km. The modelled gravity Moho depth is

inferred to be generally deeper than seismic Moho depth across onshore Tasmania. In addition, the gravity derived Moho depth map delineates ocean-ward crustal thinning and relatively shallow Moho depth across Bass Strait compatible with failed rifting in the Cretaceous.

At the local scale of investigation, the geometry of granites and major geological features is refined within West Tasmania, at a 500 m × 500 m resolution, with a focus on major subsurface units to improve previous models and identify new prospective regions. A new sub-surface granite body is inferred that underlies much of the eastern region of Rocky Cape Group outcrop. This interpreted intrusion may be either Neoproterozoic or Devonian. The subsurface geometry of the known Devonian Granites in western Tasmania was also refined using both geometry and property inversions.

At the prospect scale study, the Heazlewood-Luina-Waratah region, which hosts a series of significant deposits, is investigated, at 250 m × 250 m resolution, to provide a platform to facilitate further refinement and opportunities for discovery in future research. Using this model, the geometry of the Meredith Batholith and ultramafic complexes were refined, resulting in the identification of three regions prospective for mineralisation including: 1) northeast of the Waratah region associated with a newly identified granite cupolas, 2) above the Bells Syncline associated with high magnetic intensity, and lithologically prospective for skarn mineralisation, and 3) across the recently re-mapped ultramafic complexes linking the Heazlewood and Mt Stewart ultramafic complexes.

Acknowledgement

I would like to express my utmost gratitude toward all who have assisted me during my PhD, aiding me with their worthwhile and friendly advice and comment. Firstly, I'd like to deeply thank my primary supervisor, Anya Reading. Thank you so so much, Anya, for trusting me and giving the chance to an unknown candidate to commence his PhD under your supervision and continuous support during the last 3.5 years. You have kept supporting me especially during the first year of this PhD when I was frustrated with lots of unfamiliar ideas and not certain whether I can get through this challenge or not. Furthermore, you never gave up on encouraging me, tolerating my English language and providing me scientific feedback. I'd also like to acknowledge my other supervisors, Michael Roach and Mark Duffett. Thank you Michael for your significant ideas which firstly looked scary and unresolvable, but helped me to improve the quality of my outcomes. Mark, you allowed me to feel free to contact you whenever I had any questions and then provided me your advice and excellent support. Thank you and thank you and again thank you Anya, Michael and Mark.

Special thanks must go to Daniel Bombardieri for instructing me on using GOCAD and inversion workflow. Thanks also to Matthew Cracknell for his support on bringing up new ideas and revising my written pieces.

I would like to acknowledge the help of Stephen Kuhn as my officemate with regular conversations and sharing ideas about the PhD, global warming and other topics. In addition, I would also like to thank people from Earth Science and CODES, especially the geophysics group, Deborah Macklin, Ian Little, Sasha Stepanov, Ron Berry, Alexander Cuison, Jodi Fox, Jacob Mulder, Jeff Steadman and Selina Wu and also Joanne Whittaker from Institute for Marine and Antarctic Studies (IMAS). Hey Auntie Jane, I have not forgotten to appreciate your kind manner, answering my paper work questions and yummy rhubarb that helped me to restart the creativity in my brain.

I also like to acknowledge the help from MRT staff, especially Andrew McNeill, John Everard, Grace Cumming, Kyen Knight, Lia Unwin and Andrew Eastaugh. Andrew, I will never forget our chats about timber cutting and other conversations. RIP Andrew Eastaugh, and you will be respectfully remembered by your friend.

I also like to thanks Hossein Ferdowsi from Geological Survey of Iran (GSI) for assisting me in spectral analysis of magnetic data and Michael Morse from the Geoscience Australia for providing offshore gravity data in east Tasmania.

Finally, I would like to express my endless thanks to my lovely family, dad, mum, brothers and lovely 2 years old niece. I do know that my success makes you happy and I am doing my best to make you proud as you did the same to me. Thank you for all the ongoing support and emotional backup on your behalf which persuades the universe to stay behind me. (MERSIIIIIIIIIIIII my family).

Contents

List of Figures

List of Tables

Abbreviations

1D	One dimensional
2D	Two dimensional
3D	Three dimensional
CCW	Cambrian Cleveland-Waratah association
CMUC	Cambrian Mafic-Ultramafic Complexes
CMUC- unit 1	Cambrian Mafic-Ultramafic Complexes unit 1
CMUC- unit 2	Cambrian Mafic-Ultramafic Complexes units 2
COB	Continental-oceanic boundary
DRTP	Differential reduction to the pole
ETT	Eastern Tasmanian Terrane
FMC	Franklin Metamorphic Complex
GA	Geoscience Australia
GDA	Geocentric Datum of Australia
GSV	Geological Survey of Victoria
Gx	Geometry inversion
HDR	Hot Dry Rocks samples
IGRF	International Geomagnetic Reference Field
IQR	Interquartile range
MC	Metamorphic Complex
MGA	Map Grid of Australia
Moho	Mohorovičić discontinuity
MRT	Mineral Resources Tasmania
MRV	Mount Read Volcanics
NOAA	National Oceanic and Atmospheric Administration
PGE	Platinum-group element
Px	Property inversion
RMS	Root mean squared

RCG	Rocky Cape Group
RTP	Reduction to the pole
SMRS	Southern Margin Rift System
TFS	Tamar Fracture System
TMF	Tyennan Margin Fault
TMI	Total magnetic intensity
UBC-GIF	University of British Columbia-Geophysical Inversion Facility
UC	Ultramafic complexes
UCCL	Unstretched continental crust limit
V_p	P-wave velocity
V_s	S-wave velocity
WTT	Western Tasmanian Terrane

Mathematical nomenclature

A	Constant
C	Constant
C_m	Proportionality constant
E	Maximum error
H	Strength of the Magnetic field
k	Magnetic susceptibility
k_x	Wavenumber in x direction
k_y	Wavenumber in y direction
M	Applied magnetic field
m_w	Mass of saturated sample suspended in water
m_a	Mass of saturated sample in air
P	Radially averaged spectrum of the anomaly
Z_t	Top bound of the magnetic source
Z_c	Centroid depth of the magnetic source
Z_b	Basal depth of the magnetic source
ρ	Density
Θ_m	Factor for magnetisation direction
Θ_f	Factor for geomagnetic field direction

Chapter 1 – Introduction

Potential field datasets (i.e. gravity and magnetic) have been acquired across the planet at different scales throughout recent decades (e.g. Chulliat, et al. 2015, Sandwell, et al. 2014, Sandwell and Smith 2009, Sandwell and Smith 1997, Sandwell and Smith 2005). These data enable the lithological character and geometry of subsurface units to be estimated, through a modelling approach, constrained by density and magnetic properties (Reynold, 1997). Petrophysical measurements (e.g. density, magnetic susceptibility) help to constrain the geological model parameters to realistic values and reduce model ambiguity resulting in an improved understanding of the geological structure. Petrophysics, therefore, provides an important link between geophysics and geology that is essential for credible modelling and interpretation of geophysical data (e.g. Clark, 1997; Heincke et al., 2010; Kamm et al., 2015; Williams, 2008).

Two dimensional (2D) modelling of geophysical data has been standard since the 1950s. During the last two decades, there has been a shift toward fully three dimensional (3D) modelling of geophysical data consistent with all available information (e.g. McGaughey, 2006; Fullagar and Pears, 2007; Calcagno, et al. 2008, Guillen, et al. 2008). An inherently complex lithological structure can be represented as a 3D model. Integration of geophysics and geology into a consistent 3D model has become more feasible due to advances in 3D modelling and inversion software packages, and computational power (e.g. Fullagar and Pears, 2007; McGaughey, 2006; Calcagno, et al. 2008; Guillen, et al. 2008; Monoury et al., 2015). 3D inversion of geophysical data based on an initial 3D geological model often provides the most efficient mechanism to maximise the extracted information. The initial model needs to provide a general fit to the observations, and is refined during the inversion process (e.g. Farquharson et al., 2008; Pilkington, 1997). Commercially available 3D inversion packages of potential field data such as the University of British Columbia-Geophysical Inversion Facility (UBC-GIF) packages: GRAV3D and MAG3D (Li and Oldenburg, 1998; Li and Oldenburg, 1996), Geomodeller (Calcagno, et al. 2008, Guillen, et al. 2008) and VPmg^{TM} software (Fullagar, 2013; Fullagar et al., 2004; Fullagar et al., 2008) have made it possible to perform 3D inversion upon complex geological structures.

Tasmania is well endowed with diversity of mineral deposits, but notable for its diverse geology and exploration difficulties. Therefore, some of available models and interpretations need a better refinement which might lead to a significant improvement in geometry of geological features, reconciling tectonic boundaries and identifying new mineral deposits. In this research, I have investigated tectonic boundaries and subsurface geological structures at multiple scales, with a focus on Tasmania, using spectral analysis, 2D and 3D modelling and inversion of gravity and magnetic data. Major tectonic boundaries and geological features can be traced using these data with interpretation undertaken in conjunction with other available knowledge (e.g. geological observations, petrophysical measurements and seismic data). The two-fold aims of these investigations are to 1) generate knowledge on the structure and evolution of Tasmania, with a focus on West Tasmania and its context in southeast Australia; and 2) improve the pre-competitive information available to mineral explorers in West Tasmania by generation of new geologically constrained 3D models. The scales used in the investigations include: sub continental, regional, local and prospect scale studies that encompass eastern Australia and Tasmania (Figure 1.1).

In this research, Tasmania has been investigated at multiple scales. Information and knowledge gained at a larger scale has been integrated with previously available geological, geophysical and tectonic information to identify areas associated with some misfit contradicting with available models. The new information contributed with the larger scale models in this study have been used to determine regions for further investigation, understand the problem and discuss different solutions.

Eastern Australia has gradually evolved through a series of orogenies with progressive accretion of new crust during the Phanerozoic (e.g. Betts et al., 2002; Glen, 2005; Cayley 2011, Cayley and Musgrave 2013, Cayley, et al. 2002, Musgrave 2015). Tasmania contains rocks ranging in age from Mesoproterozoic to Cainozoic with very complex structure in some regions (Berry and Crawford, 1988; Crawford and Berry, 1992; Halpin et al., 2014). The investigations presented in this thesis are carried out at multiple scales in order to try to understand the diverse influences on the resulting 3D structures.

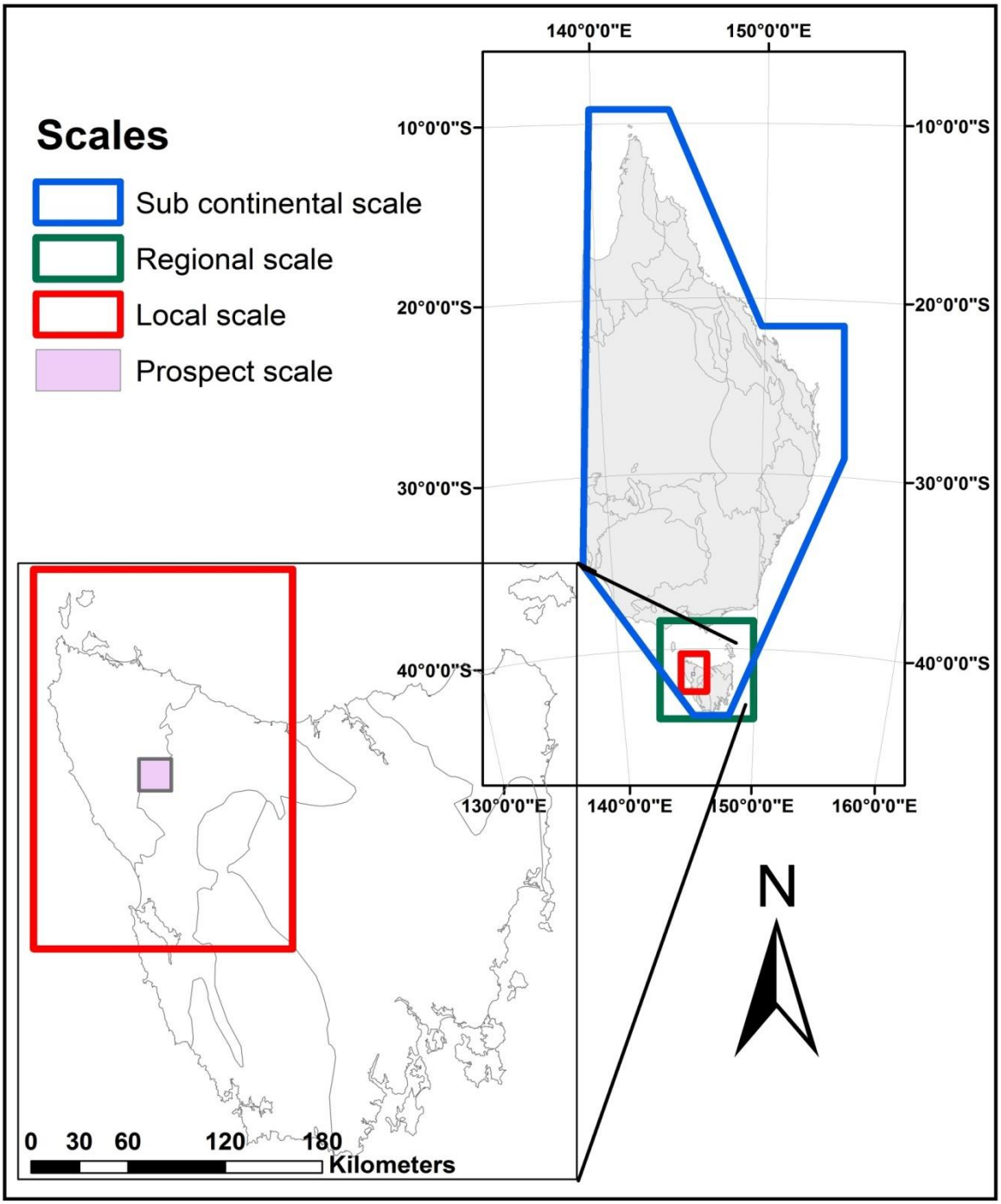

Figure 1. 1 - The multiple scale study areas described in this thesis. The sub continental scale study (blue polygon) investigates the Curie Point Depth across eastern Australia; the regional scale study (green polygon) investigates the Moho depth throughout onshore and offshore Tasmania; the local scale study (red polygon) models the 3D distribution of major geological units throughout West Tasmania; the prospect scale study (plum region) focuses on the Heazlewood-Luina-Waratah region.

1.1. Tectonic and geological background

1.1.1. Tectonic background of east Australia

The exposed geology of the Australian continent is composed of an assemblage of crustal blocks that can broadly be grouped into the Precambrian western and central tectonic zones and the Phanerozoic eastern province. Disparate Archean crustal elements were assembled into three major cratonic zones in the Proterozoic. The West Australian Craton, North Australian Craton, and South Australian Craton were joined to the Rodinian supercontinent by 1300—1100 Ma (Cawood and Korsch, 2008). This supercontinent broke up at ~800 Ma. Subsequently, the fold belt structures of the Phanerozoic Tasman Orogen that comprises much of the eastern third of Australia were accreted, in stages, onto the eastern margin of the Precambrian cratons. Accretion occurred primarily through supersubduction involving a sequence of subduction complexes during the late Palaeozoic (e.g. Direen and Crawford, 2003; Doutch and Nicholas, 1978; Cayley 2011, Cayley and Musgrave 2013, Cayley, et al. 2002, Everard and Cumming 2016, Foster and Gray 2000, Glen 2006, Glen and Roberts 2012, Glen 2013, Glen 2005, Glen, et al. 2009, Musgrave 2013, Musgrave 2015). This extended region is known as the Tasmanides. In addition to the Palaeozoic accreted terranes, eastern Australia geology includes both Precambrian and Cambrian basements elements, extensive late Palaeozoic and Mesozoic continental basins, and extensive areas of Mesozoic-Cainozoic volcanic rocks (e.g. Betts et al., 2002; Glen, 2005; Fergusson, et al. 2017; Foster and Gray 2000; Gibson, et al. 2011; Williams 2008). The term Tasman Line refers to the boundary between cratonised Precambrian material to the west and the Tasmanide to the east. The Tasman Line is thought of as the edge of the Australia continent at the time of the break-up of Rodinia and its position has been interpreted by numerous authors based on lineations derived from potential field measurements (e.g. Direen and Crawford, 2003). Although the Tasman Line marks the major upper crustal boundary, the main seismic boundary lies somewhat to the east in the mantle (Cayley, 2011; Fishwick et al., 2008; Kennett et al., 2004).

The tectonic evolution of eastern Australia commenced with the breakup of Rodinia in the Neoproterozoic. Convergent margin tectonism characterised the evolution of the Tasmanides from the Middle Cambrian to the Late Triassic. Eastern Australia developed through a succession of subduction and orogenic events incorporating both oceanic crustal blocks and micro-continents. Significant sedimentation in, arc, and back-arc and foreland settings accompanied these orogenic events (Glen, 2005). Toward south of the Tasmanides, orogens progressively young toward the eastern edge of the Australian continent and include: the

~520—490 Ma Delamerian Orogen, the ~450—340 Ma Lachlan-Thomson Orogen, and the ~320—300 Ma New England Orogen (Gray and Foster, 2004). In Central and northern Queensland, the major orogenies were the Thomson Orogeny and the North Queensland Orogeny (Glen, 2005). These orogenic events successively brought arc material and possible continental ribbons onto the growing eastern margin of Australia. Figure 1.2 shows the major orogens and basements elements across eastern Australia. The Phanerozoic succession abuts Precambrian basements blocks such as the Mount Isa Region and Curnamona Craton in the west and a Precambrian basement inlier, the Georgetown Inlier is also present east of the Tasman Line (Betts et al., 2002).

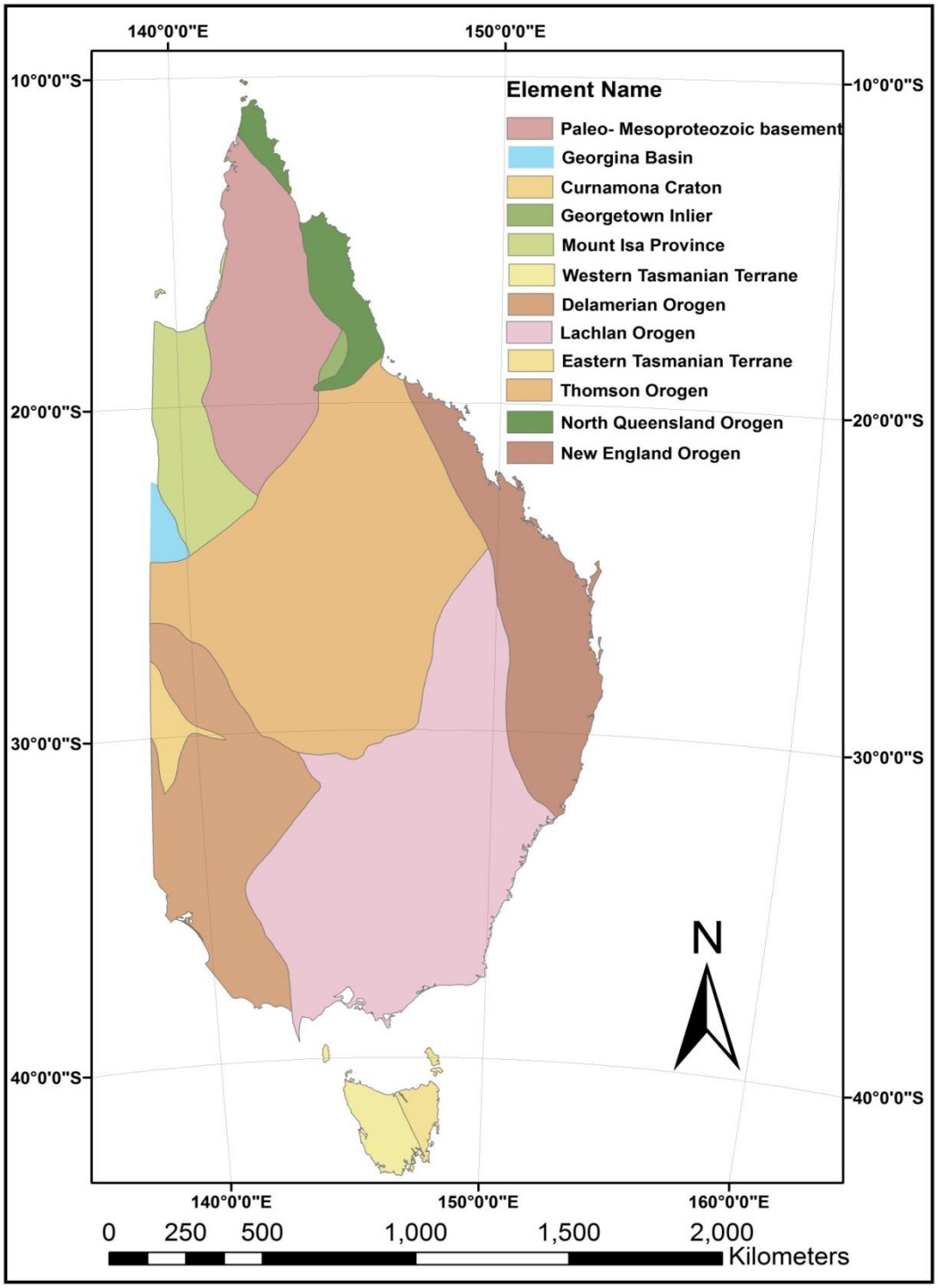

Figure 1. 2 - Terrane map of east Australia (Reference: Major Crustal Boundaries of Australia; Korsch and Doublier 2015). For the detail of tectonic units in Tasmania and Bass Strait, refer to Figures 1.3 and 4.1.

The Delamerian Orogeny is a compressional orogenic zone with westward-verging folds. This orogeny was associated with convergence along the proto-Pacific margin of the continent and also caused overprinting of the Precambrian cratons in the western part of the Tasmanides

(Glen, 2005). The Lachlan Orogen preserves Cambrian-Ordovician remnants of crustal material. The Lachlan Supercycle consists of three main cycles of Benambran, Tabberabberan and Kanimblan Orogenies during the Ordovician to Carboniferous. This supercycle evolved with the development of the Cambrian oceanic island arc and back-arc basement followed by a widespread Ordovician turbidite deposition (Glen, 2005). The basement beneath the majority of the Lachlan Orogen is predominantly oceanic lithosphere (Glen, 2005; Gray and Foster, 2004). The boundary between the Delamerian and Lachlan Orogens is controversial (Hallett et al., 2005). Glen (2006) suggested this boundary lies along the Avoca Fault, west of the Bendigo Zone.

The New England Orogen on the eastern margin of the continent comprises a series of north-northwest trending belts representing volcanic-arc, fore-arc/back-arc basins and subduction assemblages (Betts et al., 2002). Unlike the Lachlan Orogen, substrate beneath the New England Orogen is a mixture of oceanic and continental crust (Glen, 2005). The orogen is separated from the Lachlan and Thomson Orogens by a rift-foreland basin system of the Permian-Triassic age Bowen-Gunnedah-Sydney Basin System (Glen, 2005).

The Thomson Orogeny comprised several episodes of deposition, deformation and plutonism during the Cambrian to Carboniferous (Murray and Kirkegaard, 1978). The boundaries of the Thomson Orogen with the Delamerian and Lachlan Orogens are concealed, but discordant potential field lineaments suggest that these boundaries are abrupt and correspond to a curvilinear, east-west trending thrust in the Tibooburra-Brewarrina area (Glen, 2005; Murray and Kirkegaard, 1978). The North Queensland Orogen contains rocks from the Neoproterozoic to Permian and inliers of the Proterozoic metamorphic complexes. The North Queensland Orogen links to the western Proterozoic craton along the Palmerville Fault System and to the Thomson Orogen through the Anakie Inlier (Glen, 2005).

Many different scenarios have been proposed for the tectonic evolution of the Lachlan Orogen and the southern parts of the Tasmanides during the Phanerozoic: the formation of multiple subduction zones (Gray and Foster, 2004), the strike-slip emplacement of the continental margin terranes (Glen et al., 2009), VanDieland microcontinent scenario (Cayley, 2011), and subduction with subsequent orocline evolution (e.g. Musgrave, 2013; Cayley and Musgrave, 2013; Moresi et al., 2014).

Cayley (2011) suggested an exotic Proterozoic microcontinental block called ‘VanDieland’ encompassing Western Tasmania and the Selwyn Block of central Victoria (Cayley et al.,

2002), together with the adjacent oceanic plateaus (the South Tasman Rise continental fragment). This microcontinent originated from either the edge of the Laurentia or perhaps south China (Cayley, 2011) or south of Victoria Land, Antarctica (Gibson et al., 2011). VanDieland was placed on the Paleo-Pacific plate and subduction-accretion along the eastern margin of Gondwana moved the block toward the supercontinent. The block arrived at the margin and then accreted to east of Gondwana south of western Victoria, Australia, and north of North Victoria Land, Antarctica in the Late Cambrian at ~515—510 Ma (Cayley, 2011). After at least a 50 Ma hiatus, while the southwestern part of the block remained attached to east Gondwana, other parts of the microcontinent transported out into the paleo-Pacific by the mid-Ordovician (~470 Ma). The block accreted onto the eastern Gondwanaland margin during the Late Ordovician to Silurian (Cayley, 2011).

It has been proposed that the tectonic development of eastern Australia was partially controlled by orocline evolution (Moresi et al., 2014). Several oroclines are identified across the Tasmanides such as the Texas, Coffs Harbour, Manning and Nambucca oroclines across the New England Orogen (e.g. Li and Rosenbaum, 2014; Li et al., 2012b; Rosenbaum, 2012) and the Lachlan Orocline and Macquarie Arc located in the Lachlan Orogen (e.g. Cayley and Musgrave, 2013; Musgrave, 2013; Tetley et al., 2013). Moresi et al. (2014) suggested a 3D dynamic orocline evolution model in the southern Tasmanides, consisting of three stages: 1) a collisional stage, 2) a transitional stage, and 3) the re-initiation of a stable subduction system. The collision stage resulted in accretion of VanDieland to the overriding plate in the Ordovician. Subduction in the congested region of the trench rapidly stalled and the slab began to stretch, creating a window or tear in the slab resulting in trench-perpendicular extension and rifting of the overriding plate. The transitional stage happened where the convergent subducting plate and trench reorganised through coeval trench advance and retreat in different parts of the boundary during the Silurian. In this stage, first, the trench advanced in the south and subduction rollback occurred in the central Tasmanides in a transitional configuration of back-arc extension and, then, the margin parallel trench retreated behind the accreted terrane. The laterally retreating part of the slab underwent pure trench rollback subduction. The progression of the boundary from the top of the ribbon to its interior created the orocline. During the last stage, stable subduction system began outboard of the orocline in the Early Devonian and represents the present distribution of the major tectonic elements across southeast Australia (Moresi et al., 2014).

The Tabberabberan Orogeny (390 Ma; Black et al., 2004) affected most of the Tasmanides through emplacement of volcanic-volcanoclastic rocks, metamorphism and granite intrusion/emplacement. It is characterised by an intra-oceanic arc and convergent margin phase during the Late Silurian to Middle Devonian. This orogeny led to the deformation of the intrabasin unconformities, presence of the volcanic and volcanoclastic rocks, intrusion of granite and granodiorites, and deposition of sediments (Glen, 2005).

During the Mesozoic, Australia was a continental margin of the subducting Pacific Plate and subsequently a chain of hotspot-related volcanism developed through eastern Australia (Johnson et al., 1989). In addition, eastern Australia was affected by extensive Mesozoic continental- foreland basin sedimentation such as Bowen- Gunnedah- Sydney basin system overlying and obscuring lower Palaeozoic successions (Fielding et al., 2001). Australia separated from East Antarctica at ~80 Ma by the opening of the Southern Ocean followed by the opening of the Tasman Sea at 80—50 Ma (Gaina et al., 1998). The fault-system opening from the west to east, across southern Australia, failed to propagate into the Tasmania-Selwyn Block crust. The spreading between Australia and Antarctica was, therefore, forced to step south by passing Tasmania and reactivating the north-south trending suture zone between the former Cambrian East Gondwanaland margin and VanDieland (Cayley, 2011; Royer and Rollet, 1997).

1.1.2. Tectonic and geological background of Tasmania

Tasmania forms an enigmatic province that encompasses rocks ranging in age from the Mesoproterozoic to Cainozoic. At a regional scale, Tasmania is characterised by two main geological domains (Chappell et al., 1988; Williams, 1989): 1) the Western Tasmanian Terrane (WTT), with exposed Mesoproterozoic basement rocks (Berry et al., 2008), and 2) the Eastern Tasmanian Terrane (ETT), dominated by Palaeozoic rocks and no evidence for Proterozoic basement (Reed, 2001). The WTT is dominated by Neoproterozoic continental shelf depositions (Calver et al., 2004; Calver and Walter, 2000) and has common structural sequences to East Antarctica in the Cambrian and parts of North America (Berry et al., 2008). The WTT consists of volcanic rocks that formed largely along the proto-Pacific margin of East Gondwana due to the subduction-accretion during the Palaeozoic (Berry et al., 2008; Williams, 1989). In contrast, the ETT shares an affinity with the Lachlan Fold Belt and was thrust over the WTT during the Early to Middle Devonian (Reed, 2001). The ETT was emplaced from episodic accretion of oceanic crust and sediment deposition along Tasmania's eastern margin

from the Early Ordovician to the Early Devonian (Reed, 2001) and finally docked with western Tasmania during the Middle Devonian (Seymour et al., 2007). While the ETT is thought to be underlain by a mafic oceanic crust, the WTT is underlain by more silicic continental crust (Rawlinson et al., 2010).

Berry et al. (2008) proposed that the WTT rifted from the Neoproterozoic Australian-Antarctic margin in the late Proterozoic and was reattached to the ETT by the early Ordovician. The nature of the boundary between the WTT and ETT is controversial. A broad and complex area of deformation has been discussed by Reed (2001) between the distinctive outcrops of the WTT and ETT in northern Tasmania but there is very limited surface exposure of lower Palaeozoic rocks in this area. The Tamar Fracture System (TFS) has been suggested by Williams (1989) as the approximate location of a crustal-scale suture zone. This broad zone, extending SSE across Tasmania from between Port Sorell and the Tamar River has been indicated as the approximate location of a crustal-scale suture by other studies (e.g. Leaman et al., 1994; Rawlinson et al., 2010; Reed, 2001; Young et al., 2011).

Tasmanian basement rocks have been divided into seven stratotectonic elements with different tectonic histories and chronostratigraphies. These are the King Island, Rocky Cape, Dundas, Sheffield, Tyennan, Adamsfield-Jubilee, and Northeast Tasmania Elements (Seymour and Calver, 1995).

The King Island Element comprises Mesoproterozoic metamorphic rocks. The Surprise Bay Formation toward the western half of the King Island includes more than 1000 m of multiply-deformed amphibolite facies metasedimentary rocks with minor mafic intrusives with the deposition age after 1350 Ma (Black et al., 2004; Cox, 1973) that was intruded by 760 Ma granitic rocks (Berry et al., 2008; Seymour et al., 2007).

The Rocky Cape Element dominantly encompasses the Rocky Cape Group and its correlates, the Arthur Lineament (or the Arthur Metamorphic Complexes), parts of the Burnie and Oonah Formations, the Smithton Synclinorium and the Togari Group (Seymour and Calver, 1995). The Rocky Cape Group contains the oldest exposed rocks in Tasmania with a depositional age of 1450—1330 Ma (Halpin et al., 2014) and represents a block of an autochthonous basement of the mainly open shallow-marine shelf sedimentation. It contains ~10 km thicknesses of quartzarenite-siltstone-pelite-dominated successions, with evidence of active extensional tectonics of the east Antarctic Shield during the sedimentation (Calver et al., 2012; Seymour et al., 2007). Toward the northwest, the Rocky Cape Group is unconformably overlain by

Precambrian sequences of clastic sedimentary rocks, mafic volcanic rocks, dolomite and chert of the Togari Group in the Smithton Synclinorium (Seymour et al., 2007). The Rocky Cape Group is separated from the Neoproterozoic-Late Cambrian sandy turbidite-facies and metasedimentary rocks of the Oonah and Burnie Formations by the Arthur Lineament; a narrow, Cambrian northeasterly-trending metamorphic belt (110 km long by up to 10 km wide; Seymour and Calver, 1995; Seymour et al., 2007). Across this metamorphic belt, a transitional decrease in the grade of the metamorphism exists from the highly metamorphosed rocks within the complex toward the relatively unmetamorphosed sediments of the Rocky Cape Group and the Oonah Formation (Seymour and Calver, 1995; Seymour et al., 2007). The Tenth Legion Thrust defines the eastern boundary of the Rocky Cape Element near Zeehan (Brown and Findlay, 1992).

The Tyennan Element represents a central, autochthonous basement zone that comprises the largest area of exposed Proterozoic rocks in Tasmania. This element shows evidence of a shared protolith with the Rocky Cape Group (Seymour et al., 2007). Unlike the Rocky Cape Group, Tyennan rocks experienced greater metamorphism and deformation. High grade rocks (garnet amphibolite schists) are exposed in the Franklin Metamorphic Complex (FMC) in the central part of the Tyennan element. The FMC reached peak metamorphic conditions of 730—715^{o} C at 1700—1560 MPa (Kamperman, 1984) or 698 $\pm$ 28^{o} C at 1520 $\pm$ 105 MPa (Goscombe, 1990) with a burial depth of 30—50 km and probable partial melting at ~780 Ma (Seymour and Calver, 1995; Seymour et al., 2007).

The palaeogeographic feature lying between the Tyennan Element to the east and the Rocky Cape Element to the west is defined as the Dundas Element. This feature, often described as the Dundas Trough, developed after a major arc-continent collision event in the Middle Cambrian (Berry and Crawford, 1988; Seymour and Calver, 1995). The Dundas Element consists of sedimentary and volcanic rock formations and sequences from the Neoproterozoic to Early-Middle Palaeozoic. Neoproterozoic sequences of the Oonah Formation within this element are overlain by the Neoproterozoic Success Creek and Crimson Creek Formations. The Success Creek Formation comprises 750—1000 m of shallow-water, tidal flat-flood sediments. In contrast, the Crimson Creek Formation consists of 4000—5000 m of commonly interbedded volcaniclastic turbiditic wacke and siltstone-mudstone, with numerous tholeiitic basalt lava horizons and associated intrusive sills (Brown, 1986; Seymour and Calver, 1995; Seymour et al., 2007). Cambrian Mafic-Ultramafic Complexes and associated allochthonous sequences overlie the older successions and were emplaced during the Tyennan Orogeny. The

Tenth Legion Thrust is the most westerly occurrence of the Cambrian Mafic-Ultramafic Complexes in West Tasmania (Brown and Findlay, 1992).

The Mount (Mt) Read Volcanics and associated volcano-sedimentary sequences are Middle Cambrian units within the Dundas Element. They form a narrow volcanic belt (~250 km long by 0—15 km wide) lying along the eastern side of the Dundas Element and the southern margin of the Sheffield Element (Seymour and Calver, 1995; Seymour et al., 2007). The Mt Read Volcanics comprise felsic, intermediate and minor mafic volcanic rocks, dominantly of calc-alkaline type (Corbett and Solomon, 1989). The Mt Read Volcanics were predominantly deposited in a submarine environment during the Middle Cambrian. The major units in this belt are: 1) the Western Volcano-Sedimentary Sequences, 2) the Central Volcanic Complex, 3) the Eastern Quartz-phyric Sequence and 4) the Tyndall Group and correlates. The Tyndall Group and correlates are young sequences (~494.4 $\pm$ 3.8 Ma) in comparison with other units (~502.6 $\pm$ 3.5 Ma) (Seymour et al., 2007). The Middle Cambrian volcano-sedimentary successions unconformably lie on the following two major associations: 1) the rifted successions of the Burnie and Oonah Formations, Success Creek and Crimson Creek Formations, or Togari Group correlates, and 2) the Early Cambrian oceanic allochthons (Seymour and Calver, 1995; Seymour et al., 2007).

The Sheffield Element refers to a large rectangular area of Neoproterozoic-Early Palaeozoic basin sequences bounded to the west by the northern part of the Arthur Lineament, to the south by the Tyennan Element, to the east by the Tamar River (Seymour and Calver, 1995) and links to the Dundas Element through the Machinery Creek Fault (Murphy et al., 2003). This element dominantly consists of parts of the Burnie Formation, the Dial Range and Fossey Mountain Troughs. The Forth Metamorphic Complex around the western and southern margins of the Forth Inlier is interpreted as a “pop-up” allochthonous piece of the high-grade metamorphosed Tyennan basement and is overlain by the Burnie Formation. The largely fault-bounded Badger Head Inlier, near the northeastern margin of the element, consists of polydeformed correlates of the Burnie Formation. The Middle Cambrian Cateena Group and the late Middle to early Late Cambrian Radfords Creek Group form parts of the continuous sedimentary and volcaniclastic successions of the Dial Range Trough (Jago and Brown, 1989). The volcanic sequences in Fossey Mountain Trough are quartz-feldspar phyric with sequences equivalent to the Dundas and Tyndall Groups with a possible origin age of the Middle to Late Cambrian (Seymour and Calver, 1995; Seymour et al., 2007).

The Adamsfield-Jubilee Element consists of the deformed but relatively unmetamorphosed Proterozoic and lower Palaeozoic rocks located east of the Tyennan Element. This element is located between the Cambrian Lake Gordon Fault in the west and the Lake Crescent Fault in the east (Murphy et al., 2003). The main exposed parts of the element consist of the mainly Proterozoic rocks in the Jubilee region and Cambrian rocks in the Adamsfield district. The Florentine Synclinorium preserves a sequence of unmetamorphosed Ordovician to Devonian predominantly shallow marine sediments. (Seymour and Calver, 1995).

While elements in the western part of Tasmania have common structures and Precambrian and Cambrian basement rocks, the Northeast Tasmania Element is characterised by the lower Palaeozoic, Ordovician to Devonian, turbiditic rocks with no evidence of the Proterozoic exhumation (Seymour and Calver, 1995). Deep marine sedimentation in the Northeast Tasmania element contrasts with synchronous shallow marine sedimentation in basement elements further to the west. The western boundary between the Northeast Tasmania Element and others is debated. The Port Sorell Fault marks the western edge of the Northeast Tasmania Element, whilst the Verwood Fault marks the eastern edge of western Tasmania and a ~30 km wide zone is the boundary between these two faults (Murphy et al., 2003). The TFS is considered as the boundary between the Northeast Tasmania Element and the Sheffield Element (Seymour and Calver, 1995). Figure 1.3 shows major surface geological features across Tasmania.

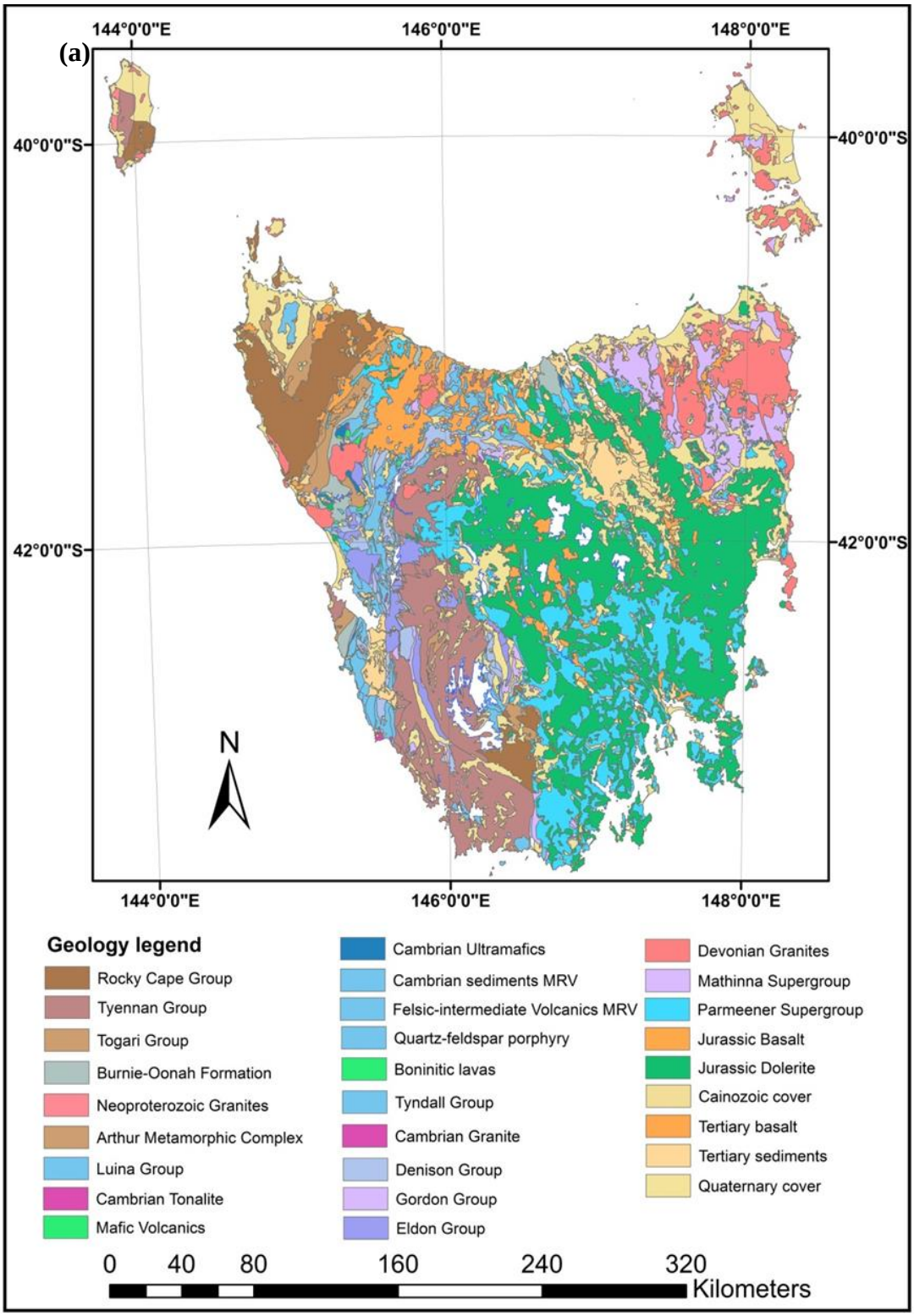

Figure 1. 3 – (a) geological map of major rock units across Tasmania (Reference: 1:500,000 geology map; Brown et al., 2012).

The tectonic evolution of Tasmania is predominantly affected by three major orogenic events the Wickham Orogeny (~760 Ma; Black et al., 1997), the Tyennan Orogeny (520—490 Ma;

Berry and Crawford, 1988; Crawford and Berry, 1992), and the Tabberabberan Orogeny (390 Ma; Black et al., 2004). In the Proterozoic, the evolution of Tasmania involved three episodes of passive margin sedimentations and continental shelf depositions (e.g. the Rocky Cape Group, Oonah Formation and correlates) on the margin of Gondwana over a duration of 900 million years (Berry and Bull, 2012; Calver et al., 2004; Calver and Walter, 2000). A second cycle of deposition (the Togari Group and correlates) from 740—540 Ma comprises a major basaltic event at 540 Ma (Meffre et al., 2004). The main Proterozoic basement units across Tasmania are the Rocky Cape Group (Mesoproterozoic, 1450), the Surprise Bay Formation of King Island (Mesoproterozoic, 1350 Ma), the Tyennan region (lower Neoproterozoic, 1000—750 Ma), the Oonah and Burnie Formations (lower Neoproterozoic, 1000—750 Ma), and the Togari Group and correlates (Neoproterozoic-Lower Cambrian; 750—520 Ma; Seymour and Calver, 1995; Seymour et al., 2007). The Wickham Orogeny, resulted from the rifting and breakup of Rodinia at ~760 Ma, affected King Island and mainland Tasmania through intrusion of granite rocks (Black et al., 1997). The granite intrusions caused metamorphism at temperatures of 580—470^{o} C and low pressure of 300—100 MPa (Blackney, 1982; Seymour and Calver, 1995; Turner, 1989).

A new cycle of passive margin sedimentation affected parts of Tasmania from 600 Ma to the early Cambrian. A major episode of rifting affected much of the eastern Gondwanaland including Tasmania, western Victoria, eastern South Australia, and western New South Wales resulting in deposition of a shallow water sequence at ~600 Ma. Tholeiitic basalts dykes intruded the Rocky Cape and Tyennan Blocks at this time, and erupted onto the passive margin often associated with abundant volcaniclastic greywackes and a major component of glassy mafic volcanic detritus (Berry and Crawford, 1988; Crawford and Berry, 1992; Direen and Crawford, 2003; Seymour and Calver, 1995; Seymour et al., 2007). At the end of the early Cambrian, the WTT collided with an oceanic island arc and Tasmania was accreted back onto the craton margin in the middle to late Cambrian (Berry and Crawford, 1988; Crawford and Berry, 1992).

The Cambrian Tyennan Orogeny represents the most prominent event in the tectonic evolution of western Tasmania and, comprises three major phases. The first phase is ophiolite allochthon emplacement resulting from the development of an intra-oceanic island arc at ~520—515 Ma. Boninitic lavas and their cumulate complements were erupted in the fore-arc sections of the arc above an east-dipping subduction zone and an arc-continent collision occurred within < 10 m.y. (Berry and Crawford, 1988; Crawford and Berry, 1992). This resulted in the allochthonous

emplacement of the Mafic-Ultramafic Complexes (Berry and Crawford, 1988) and structural emplacement of other blocks including the Forth Metamorphic Complex, the Badger Head Metamorphic Complexes, the Port Davey Metamorphic Complexes, the Franklin Metamorphic Complexes, the Mersey River Complexes, the Arthur Metamorphic Complexes (Meffre et al., 2000), and the Wings Sandstone (Black et al., 2004). The Arthur Lineament defines the western limit of allochthonous blocks and marks the maximum preserved extent of the thrust complex. The Rocky Cape Group is outside of the zone of influence of the Tyennan Orogeny and hence experienced negligible metamorphism (Berry and Bull, 2012; Holm and Berry, 2002).

The second stage of the Tyennan Orogeny is post collisional volcanism and extension which occurred after cessation of subduction and either jumping, or rolling back ocean-ward of the trench at ~505 Ma. This short lived extensional regime (~5 m.y.) resulted in emplacement of volcanic complexes and sedimentary sequences including the Mt Read Volcanics, Dial Range Trough, Fossey Mountain, Que Hellyer Volcanic Complexes, Northern Felsic Volcanic Complexes, and Southern Felsic Volcanic Complexes (Berry and Bull, 2012; Berry and Crawford, 1988; Corbett and Vicary, 2012; Crawford and Berry, 1992; Seymour and Calver, 1995; Seymour et al., 2007). The last phase of the Tyennan Orogeny involved basin inversion associated with compressional deformation and reverse reactivation of earlier extensional faults (e.g. the Henty Faults) in the Late Cambrian. It resulted in the Late Cambrian-Early Ordovician exhumation and uplift of the Tyennan Block (Berry and Crawford, 1988; Crawford and Berry, 1992; Seymour and Calver, 1995; Seymour et al., 2007).

The Arthur Lineament marks a zone of significant metamorphism and deformation associated with the Tyennan Orogeny. Parts of the Burnie and Oonah Formations and lower units of the Smithton Synclinorium (Seymour and Calver, 1995; Seymour et al., 2007) underwent deformation with the peak of metamorphism at ~515—496 Ma for the Tyennan Element, ~510—494 Ma for the Arthur Metamorphic Complex, and ~510—493 Ma for sedimentary rocks of the Forth Inlier in the Sheffield Element (Turner et al. 1994; 1992). Sub-volcanic Cambrian Granites such as the Murchison and Darwin Granites, were erupted at ~500 Ma (perhaps 503—498 Ma) between the Henty Fault in the west and the Tyennan Margin Fault in the east (Seymour and Calver, 1995; Seymour et al., 2007).

The Tyennan Orogeny was followed by a period of sedimentation, with depositional of the Wurawina Supergroup. The Wurawina Supergroup in western Tasmania comprises three sedimentary sequences; the Late Cambrian- Ordovician Owen Group of coarse siliciclastic

conglomerate and sandstone; the Ordovician Gordon Group comprised predominantly of shallow-marine limestone sequence with subordinate siltstone and minor sandstone; and the predominantly clastic Silurian-Devonian Eldon Group of quartz sandstone and siltstone with minor conglomerate horizons and limestone lenses (Seymour and Calver, 1995; Seymour et al., 2007).

During the Mid- to Late Devonian, Tasmania was affected by the Tabberabberan Orogeny which is manifest as polyphase deformation and reactivation of older structures, followed by intrusion of late- to post kinematic high-level granite batholiths (Black et al., 2004). The granites intrusion across Tasmania began at ~400 Ma before the onset of the Tabberabberan Orogeny in the northeast Tasmania and continued until the early Carboniferous (Black et al., 2005). Toward the west and northwest of Tasmania, granite intrusions range from 375 to 330 Ma, with younging toward the west (Black et al., 2005; Seymour et al., 2007). The Housetop Granite (~380—343 Ma), the Heemskirk Granite (~362—330.5 Ma), the Pieman Granite (~356.5—338.5 Ma), the Meredith Batholith (~338.5—336 Ma), the Granite Tor Granite (~375—344 Ma) are surface exposures of a major distributed granite intrusion across the west and northwest of Tasmania (Black et al., 1997; Seymour and Calver, 1995; Seymour et al., 2007).

After the Devonian, large scale erosion and subsidence resulted in the deposition of the mostly flat-lying rocks of the Tasmania Basin throughout the central and eastern Tasmania. Late Carboniferous to Late Triassic Parmeener Supergroup shallow marine and terrestrial sedimentary rocks in the Tasmania Basin are intruded by Jurassic Dolerite across Tasmania. Individual dolerite sheets range up to a six hundred metres in thickness and extend for 10s of km (Seymour et al., 2007).

Offshore basins including the Bass (north and northeast), Durroon (northeast) and Sorell (west, northwest and southwest) Basins contain predominantly sedimentary successions and were initiated due to the extension related to rifting between Australia and Antarctica in the latest Jurassic to Early Cretaceous (Seymour and Calver, 1995; Seymour et al., 2007).

1.2. Geophysical data

1.2.1. Gravity data

Gravity data have been assembled from across onshore and offshore Tasmania in this study. Two databases have been used for both the regional and local scale models. For the regional scale study, over 700,000 gravity observations were compiled from multiple sources including: Geoscience Australia (GA), Mineral Resources Tasmania (MRT), Geological Survey of Victoria (GSV) and National Oceanic and Atmospheric Administration (NOAA) (For details refer to Chapter 4, Table 4.1). These data were processed for latitude, free-air and Bouguer corrections. For the Bouguer correction, I calculated the terrain correction for a radius of 167 km to minimise the effects of the difference between the spherical cap and infinite horizontal slab (Nowell, 1999). The terrain correction varies between 0.05 and 142.86 mGal in this study. The Bullard B correction has been calculated for onshore gravity data to calculate the curvature of the Earth (Nowell, 1999).

To study Tasmania at a local scale, the residual Bouguer gravity anomaly grid sourced from MRT online database (2016) was used to assess the contribution of the geological features within the upper 10 kilometres of the crust (Figure 1.4). The Bouguer grid was compiled from ~ 81500 onshore gravity observations and the residual anomaly was calculated using the MANTLE09 model (Leaman, 2009).

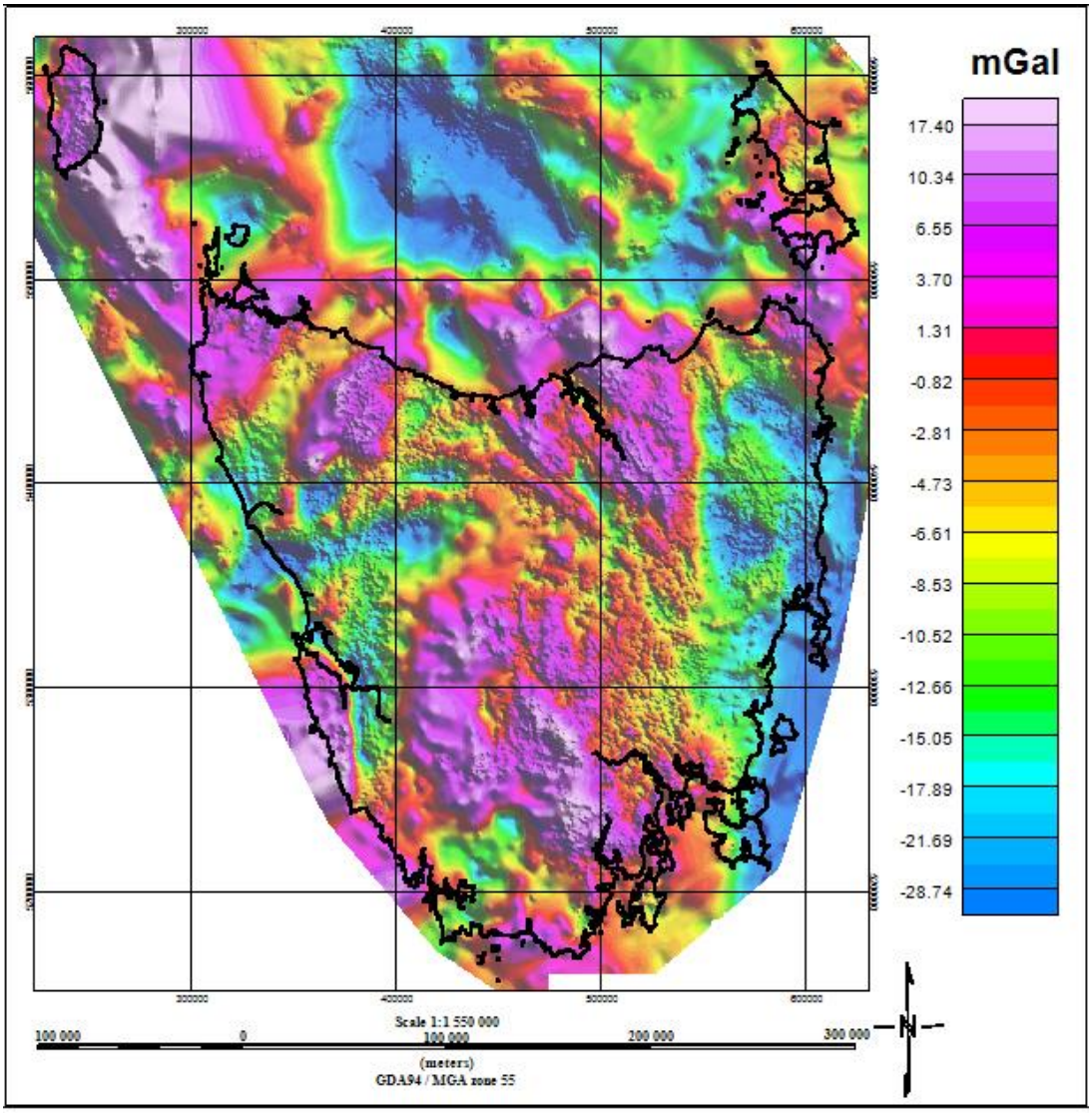

Figure 1. 4 - Residual gravity map of Tasmania calculated using MANTLE09 model (Leaman, 2009) upon Bouguer anomaly data (Reference: MRT online database, 2016).

1.2.2. Magnetic data

For regional studies in eastern Australia, the fifth edition of the total magnetic intensity (TMI) map of Australia was sourced from Geoscience Australia (GADDS, 2016; Figure 1.5). This grid includes airborne-derived TMI data for onshore and near-offshore continental areas with a resolution of ~80 m (Milligan et al., 2010). The International Geomagnetic Reference Field (IGRF) has been removed from TMI. Due to the large area covered by these data, the differential reduction to the pole (DRTP) technique proposed by Arkanihamed (2007), has been applied to avoid artefacts.

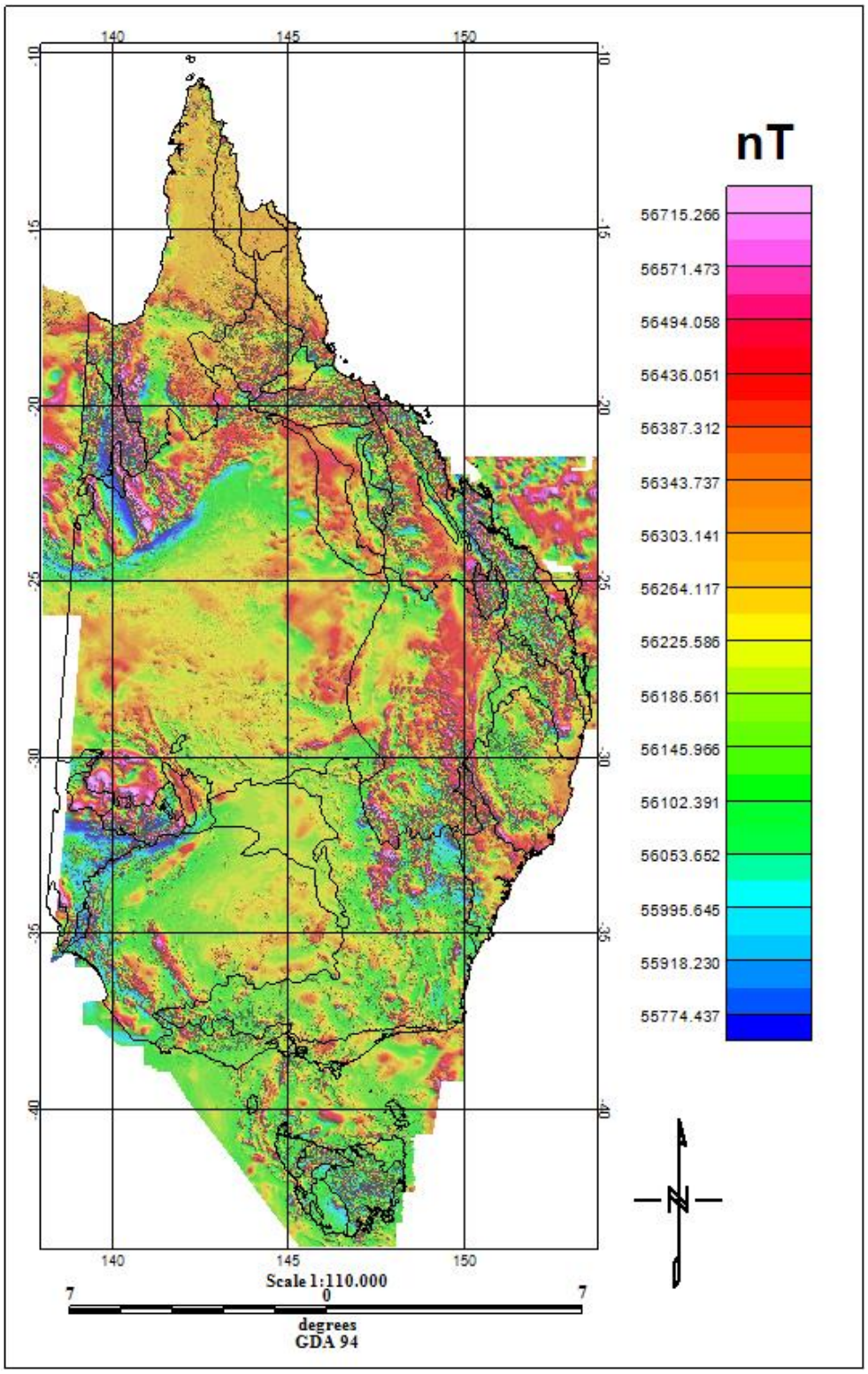

Figure 1. 5 - Total magnetic intensity map of east Australia (GDA94 datum; Reference: GADDS, 2016).

For Tasmania, gridded TMI data with a cell size of 100 m available from MRT online Database (2016) compiled by Reynold (1997) has been used. This grid was compiled from various TMI airborne surveys with different specifications and line spacing (Figure 1.6).

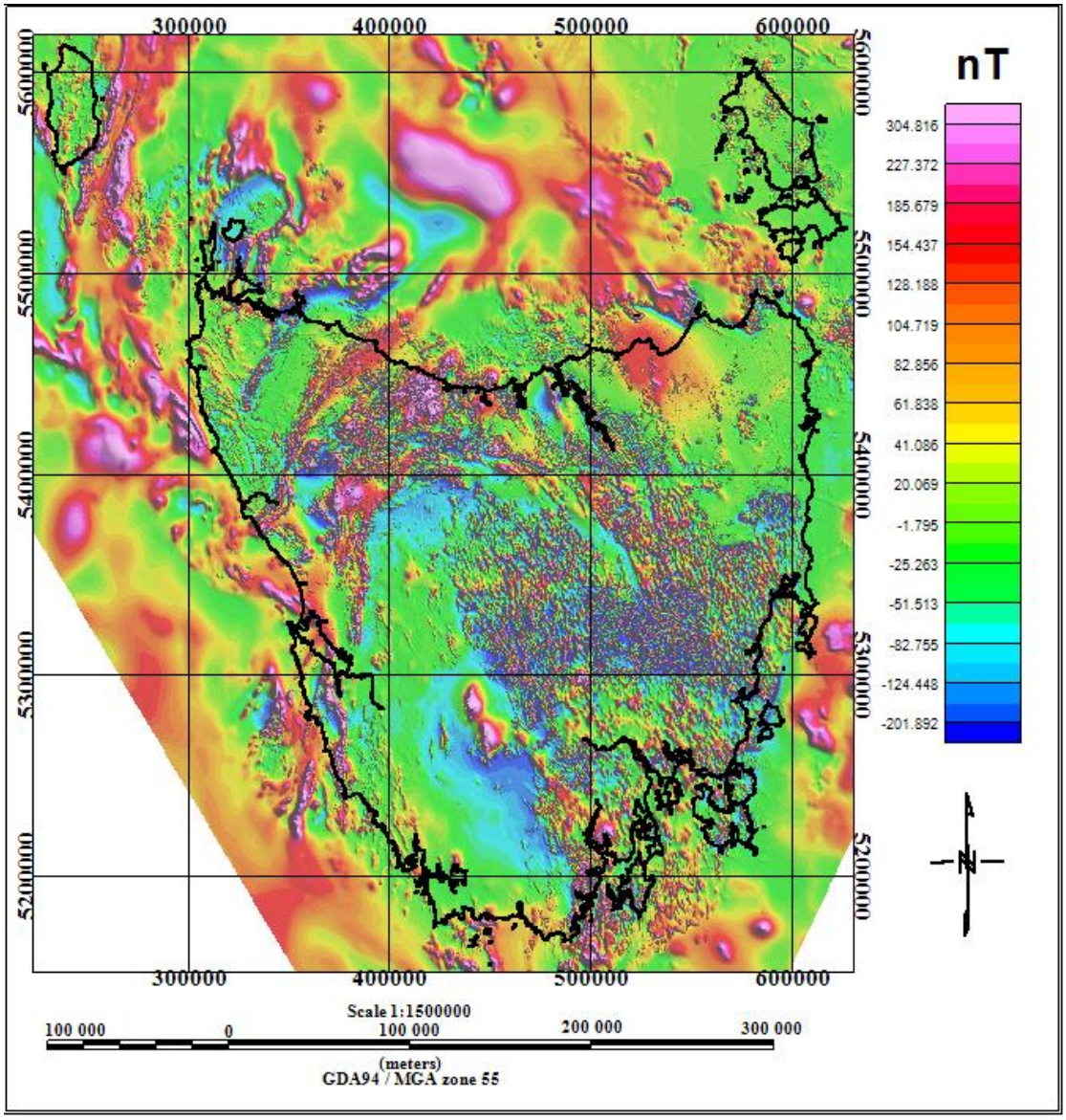

Figure 1. 6 - Reduction to pole map of magnetic data across Tasmania (GDA94 datum/ MGA 55; reference: (Duffett and Richardson, 2014)).

1.3. A tectonic context for improved information for mineral explorers

Mineral deposits are directly linked to long-term geodynamic cycles and metallogenic processes (Kerrich and Wyman, 1997). An understanding of the tectonic context and investigation of timing and kinematics of major tectonic events can lead to better understanding of ore-forming process and classification of mineral deposits. For example, hydrothermal veins containing Au form in tectonic settings including destructive plate margin and/ or intracratonic settings during circulation of hot (> 200^{o} C) hydrothermal fluids (epigenetic processes). In addition, Au-rich epigenetic skarn and porphyry deposits form in the shallow ($\leq$ 5 km) parts of both island and continental arcs in compressional through extensional regimes (e.g. Edwards and Atkinson, 1986; Groves et al., 1998).

The mineral system concept by Wyborn et al. (1994) has been focus of many investigations (e.g. Champion and Huston, 2016; González-Álvarez et al., 2013; Huston et al., 2016; Jaireth et al., 2016; Jaques et al., 2002; Joly et al., 2012; Joly et al., 2015; Kreuzer et al., 2015; Lisitsin et al., 2013; Lisitsin and Pitcairn, 2016; McCuaig et al., 2010; McCuaig and Hronsky, 2014; Pirajno, 2016; Porwal et al., 2015). The mineral system approach focuses on mineral exploration strategies on incorporating primary datasets helpful to map the critical elements at multiple scales (McCuaig and Hronsky, 2014). Increasing the scale can be utilised to understand wider features of the crustal and lithospheric geometry, and source of fluids. According to the space and time illustration of a mineral system by Huston et al. (2012a), initial metal enrichment begins from crustal differentiation at global-craton scales. Geodynamic and tectonic process drive the mineral system throughout craton-province scales. At the deposit scale, gradients are initiated by changes in the physical and/or chemical conditions. Consequently, metals are deposited and the remaining fluid expelled and dispersed. Hronsky (2015) discussed four key areas of development for exploration performance based on mineral system approach: 1) better characterisation of mineral systems at multiple, continental to deposit, scales, 2) improved integration between geological and geophysical observations at multiple scales, 3) improved capabilities to image critical deep-seated ore-controlling structures and perhaps metal-enriched deep source regions, and 4) more specific rather than just more sensitive detection technologies.

Mineral systems are complex dynamic systems comprising four critical elements that must be combined in nested scales investigations: whole lithosphere architecture, transient favourable geodynamics, fertility and preservation of the primary deposition zone. The primary deposition zone, metal deposition window, is usually within the upper 10—15 km of crustal section during the ore-forming orogenic cycle (McCuaig et al., 2010; McCuaig and Hronsky, 2014). It is challenging to image source-regions and link them to deposits. Mapping in 3D at multiple scales is a significant step in linking deposits to their wider context and is made more feasible by the integration of geological and geophysical data (Hronsky, 2015).

1.4. Major research questions to be addressed

I address the following major research questions in this thesis:

1. On a sub continental scale, does the Curie Point Depth (CPD) determined from spectral analysis of magnetic data correlate with Moho depth determined from seismic data

throughout east Australia? What do any disparities between these depth surfaces tell us about the overall context of tectonic structure and evolution?

2. Does the Moho depth defined by gravity data correlate with the Moho depth defined by seismic data for the Tasmania region? What do any disparities between these depth surfaces tell us about the evolution of Tasmania?
3. Is it possible to better constrain subsurface geology in the region of West Tasmania using a multi-disciplinary approach and 3D potential field modelling? How might any improvements aid the understanding of tectonic processes and help to direct the activities of mineral explorers?
4. Is it possible to make similar improvements on a local and prospect scale and how might these improvements help to direct the activities of mineral explorers?

In order to produce multiple models and facilitate discussions that answer the research questions posed, it is necessary to compile all available data for analysis in a single platform. For this I have compiled multi-disciplinary data (i.e. gravity, magnetic, seismic, geology, 2D and 3D models, geothermal maps and topography) and used Oasis Montaj, Paradigm GOCAD Version 2009.4 and VPmg^{TM} Version 7.1 for processing and modelling of potential field data. A key research activity to support this modelling has been the improvement of the petrophysics database for West Tasmania.

1.5. Thesis structure

This thesis contains eight chapters, describing the magnetic features of eastern Australia at a sub continental scale, onshore and offshore Tasmania at regional scale, a local scale study encompassing West Tasmania and finally a prospect scale model investigating the Heazlewood-Luina-Waratah region. Tectonic boundaries and geological units have been investigated at multiple scales, and are synthesised and discussed in terms of the research questions outlined previously and also within a mineral systems framework. As chapters intended for publication are self-contained, there is some necessary repetition of introductory material.

A summary of the contents of chapters and the structure of this thesis are as follows:

- Chapter 2: estimation of the CPD using spectral analysis of magnetic data across east Australia. Estimated CPD is compared with the Moho depth determined by seismic data and geothermal models.

- Chapter 3: characterisation of the petrophysical properties in significant rock units, providing better constraints for 3D modelling of potential field data across West Tasmania.
- Chapter 4: investigation of Moho depth across onshore and offshore Tasmania using gravity data. From an initial model constrained by the seismic Moho model, a combination of 3D geometry and property inversions of gravity data are utilised to refine this boundary. The newly refined gravity Moho depth successfully delineates crustal thinning ocean-ward, and the crustal thinning beneath the Bass Basin.
- Chapter 5: investigation of regional geological components, particularly granite bodies, across a prospective region of West Tasmania based on geological and geophysical studies. Petrophysical properties estimated in Chapter 3 have been used to constrain properties of major rock units during modelling. An initial geological model is assessed against gravity and magnetic data and new property and geometry inversions are performed. A new subsurface geometry for Devonian Granites and insights into ultramafic complexes are described in this chapter. This chapter proposes two new granitic intrusions at depth based on Bouguer gravity anomalies.
- Chapter 6: a detailed 3D inverse model of the prospective Heazlewood-Luina-Waratah region. An initial 3D model is constructed using recently published geological maps and sections. Inversion has been used to refine the geometry of granites and suggests a new ultramafic complex unit within the study area. Regions prospective for future mineral exploration are discussed in this chapter.
- Chapter 7: a synthesis and discussion of the key findings in this thesis. This is carried out firstly with regard to the tectonic evolution of Tasmania and secondly with a view to aiding mineral explorers.
- Chapter 8: summary.

Chapter 2 - Curie Point Depth investigation across eastern Australia: A broad scale tectonic context constrained by geophysical data

The lithosphere of east Australia is made up of mainly Phanerozoic basement impacted by the Mesozoic volcanism along the eastern margin of the continent and possibly by including some older, Proterozoic, basement fragments (e.g. Betts et al., 2002; Fergusson et al., 2017; Glen, 2005). Therefore, investigation of east Australia at a sub continental scale potentially provides new insights into basement provinces with different tectonic histories (refer to Chapter 1). Investigating east Australia sets the structure and evolution of Tasmania in the context of its position in southeast Australia. In this chapter, magnetic data are used to calculate the CPD across east Australia. At Curie temperature, materials pass from a ferromagnetic state to the paramagnetic state and their ability to generate detectable magnetic anomalies disappears (Bhattacharyya and Leu, 1975). Ferromagnetism occurs in materials characterised by parallel alignment of magnetic moments/domains to produce strong permanent magnets, while in paramagnetic materials individual moments do not interact resulting in small magnetic susceptibilities (White 2007). The CPD, correlating with Curie temperature, can be interpreted as the boundary of magnetic and non-magnetic subsurface materials. As temperature increases with depth it reaches the Curie-point temperature and the basal depth of a magnetic body is essentially corresponding to this depth. The CPD can be determined using: 1) magnetic methods, 2) seismic tomography models, and 3) geothermal data such as heat flow (Abd El Nabi, 2012; Artemieva, 2006). The current limited availability of seismic and heat flow data means that magnetic methods are an efficient alternative technique for calculating the CPD at regional scales. The estimated CPD values in this study are compared with Moho depth determined from seismic data and the CPD predicted from geothermal data.

2.1. CPD investigations as a tool for investigating crustal structure and evolution on a broad scale

The CPD is the depth that crustal ferromagnetic rocks undergo a sharp change in their magnetic properties and rocks become paramagnetic as a result of the increase of the temperature in the crust above the Curie temperature. At this temperature, the ability of rocks to generate detectable magnetisation disappears (Bhattacharyya and Leu, 1975). It is suggested that the world average Curie temperature for upper lithosphere ranges between 550^0 C and 580^0 C associated with ferromagnetic (Fe_3O_4) minerals (Okubo et al., 1989). Maus et al. (1997)

discussed that the CPD normally varies between 10 and 50 km. These ranges are functions of different upper crustal conditions such as the heat flow rate, the amount and type of magnetic minerals within upper crustal rocks (Bansal et al., 2013) and geological context (e.g. presence of titanomagnetite reduces the CPD; Tanaka et al., 1999).

The Earth's geomagnetic field is produced by complex hydrodynamic processes (convection) of the liquid outer core. In contrast, the Earth's mantle does not have an important effect in this field because it generally behaves as a non-magnetic body (Blakely, 1995). Therefore, the magnetic observations are sum of magnetic values resulted from the outer core and the crust. The IGRF model can be used to remove the effect of the core and, therefore, the remnant magnetic field mainly represents the magnetic field of the structures in the Earth's upper crust, i.e. 10s of kilometres. Therefore, the CPD can be estimated by calculation of the bottom of deepest magnetic source from magnetic data (Blakely, 1995; Spector and Grant, 1970; Tanaka et al., 1999).

Application of the CPD cannot completely determine the regional heat flow rate contributing to the Curie temperature. This is due to the difficulty of removing the contribution of composition, the Curie temperature of the magnetic minerals (e.g. titanomagnetite and magnetite) and the accuracy and resolution of the determined depths from magnetic interpretation methods (Tanaka et al., 1999). Nevertheless, estimation of depths to the Curie temperature can provide valuable insights into assessment of the geothermal energy and tectonic/geodynamic evolution (Bektaş, 2013; Tanaka et al., 1999). In addition, the CPD can be interpreted in comparison with observable information such as seismic Moho (e.g. Tanaka et al., 1999).

2.1.1. Estimations of CPD in different tectonic settings

It is suggested that estimated CPDs display two types of relationships with crustal boundaries: 1) CPDs that coincide with Moho depth represented by vertical changes in crustal composition, typical for regions associated with normal and/or low heat flow values (Bansal et al., 2013; Wasilewski and Mayhew, 1992) such as north China (Li et al., 2012a) and Venezuela and eastern Caribbean (Arnaiz-Rodríguez and Orihuela, 2013); and 2) CPDs that are shallower than Moho depth that are typical for regions characterised by volcanic and geothermal activities associated with high heat flow (Bansal et al., 2013) such as the Moldanubian region, Germany (Bansal et al., 2011), the Ikogosi warm spring, Nigeria (Olorunfemi et al., 2011), the Death

Valley region, USA (Hussein et al., 2012), the Aeolian Island, Italy (Ritis et al., 2013) and the Central Eastern Desert Province, Red Sea, Egypt (Abd El Nabi, 2012).

CPDs is directly related to geothermal gradient correlating with some factors such as geological history and tectonic evolution, type of the crust (continental or oceanic), and magnetic minerals present within subsurface features. Shallow CPDs are expected in regions linked to geothermal potential, young volcanism and also thinned crust (Abd El Nabi, 2012). Deep CPDs correlate with areas of low heat flow associated with plate cooling (e.g. northwestern Pacific off northeast Japan), while regions characterised by high heat flow coincide with shallow CPDs (e.g. Japan Trenches; Tanaka et al., 1999; Yoshii, 1979). Tanaka et al. (1999) summarised CPD values for different regions correlating with dominating tectonic characters. According to Tanaka et al. (1999), the CPD across geothermal and volcanic areas is ~10 km or less and increases in island arcs and back-arc rift ridges to 15—25 km, it exceeds 20 km depth at continental plateaus and Trenches have the highest CPDs (> 30 km depth). The CPD is generally deeper in continental areas compared to regions of oceanic crust (Tanaka et al., 1999). The CPD in subduction zones correlates with the boundary between the brittle and ductile crustal regime (Doser and Kanamori, 1986). Based on Harrison (1976) and Arkanihamed (1991), the lower crust in the oceanic domain is magnetic as well as the uppermost mantle. There is a correlation between the age of tectonic settings and surface processes reflecting the tectonic stabilisation of the crust: high heat flow rates are observed in younger orogens (e.g. Cermak and Hurtig, 1979) and typically older regions show a lower heat flow (e.g Abd El Nabi, 2012). In addition, Stacey and Banerjee (1974) showed that the Curie temperature estimation depends on the magnetic minerals present within subsurface rocks. Magnetic sources concentrate in one tectonic setting and change the CPD in that area. For example, Jenning (1997) showed that deeper magnetic sources are located under Precambrian lithologies in California.

2.1.2. Previous CPD and geothermal studies of Australia

Across Australia, estimation of the CPD at continental scales has been the focus of several studies (e.g. Chopping, 2013; Chopping and Kennett, 2015; Fox Maule et al., 2009). A temperature model of the Australian continental uppermost mantle was derived by Goes et al. (2005) who interpreted the Earth's temperature between 80 and 350 km depth using seismic models. In addition, the geothermal temperature at 5 km depth across Australia is interpolated by Gerner and Holgate (2010). Fox Maule et al. (2009) used radial components of the magnetic

fields of sattelite data to discuss that the CPD in eastern Australia is shallower than Moho depth, whereas elsewhere in Australia these apparently closely correspond. In contrast, Chopping and Kennett (2015) inferred generally deeper CPDs than Moho depth across eastern Australia. These two studies used different methods to estimate the CPD. Fox Maule et al. (2009) used the equivalent source magnetic dipole method and Chopping and Kennett (2015) applied radially averaged 1D power spectra of magnetic data using an entirely automatic nonlinear direct sampling inverse technique. In this study, the CPD is investiagted across eastern Australia and new results have been compared with previous CPD estimations.

2.2. Data and methods

Magnetic data across east Australia (sources as given in Chapter 1) were first transformed to the Geocentric Datum of Australia 1994 (GDA 1994, MGA 55S). In order to enhance broad crustal features associated with deep structures, the Butterworth low pass filter (cut-off frequency = 0.015 km^{-1}) was applied on DRTP data. The cut-off frequency, k = 0.015 km^{-1}, for low pass filtering was estimated through spectral analysis of the DRTP data. Therefore, magnetic anomalies with likely shallow sources and topographic effects were removed from the data.

The magnetic method used in this investigation to estimate the CPD is based on the theory proposed by Bhattacharyya (1966). The CPD can be derived from spectral analysis of magnetic anomaly data based on two different methods: 1) using the shape of isolated magnetic anomalies and 1D spectral methods (Bhattacharyya and Leu, 1975); and 2) using 2D statistical properties of magnetic anomaly patterns (Spector and Grant, 1970). Both of these methods transform the spatial data into frequency domain and provide the relationship between spectrum of magnetic anomalies and depth of the magnetic sources (Tanaka et al., 1999). These methods are appropriate to determine the regional CPD by examining the spectral properties of the magnetic anomalies over relatively large regions (Blakely, 1988). Shuey et al. (1977) indicated that the method presented by Spector and Grant (1970) is more appropriate for regional magnetic anomalies. The main problem with these methods is that small scale variations in the CPD result in difficulty in determination of the depth-to-base of a magnetic source (Hussein et al., 2012). Tanaka et al. (1999) suggested a spectral analysis method investigating the depth-to-base of a magnetic source through calculating the radially averaged 2D power density spectra of the magnetic anomalies. According to Tanaka et al. (1999) and Spector and Grant (1970) the study area are divided into overlapping 2D windows and both

radially-averaged amplitude spectrum and wavenumber-scaled counterparts for each single window are simultaneously estimated. By assuming random 2D magnetisation within each window, this method estimates the depth-to-top of magnetic sources directly from a least-square linear regression on the logarithmic radially- averaged 1D amplitude spectrum at middle to high wavenumber band and consequently the centroid depth of the magnetic source. Finally, the obtained basal depth of the magnetic source is assumed as the CPD.

In this chapter, the CPD is estimated based on statistical methods from the radial power spectrum of the magnetic field. This method is discussed by Tanaka et al. (1999) and is similar to the method of Spector and Grant, (1970) which is appropriate for regional compilation of magnetic anomalies (Shuey et al., 1977). The top bound, Z_t, and the centroid, Z_c, of a magnetic source are estimated from the power spectrum of magnetic anomalies, and used to estimate the basal depth, Z_b, of the magnetic source, i.e. the interpreted CPD. The power spectrum or the radially averaged spectrum of the anomaly, P, for the 2D assemblage of bodies can be estimated by (Blakely, 1995; Spector and Grant, 1970; Tanaka et al., 1999):

$$P(k_x, k_y) = 4\pi^2 C_m^2 \phi_m(k_x, k_y)|\Theta_m|^2|\Theta_f|^2 \exp(-2|k|Z_t) \times \{1 - \exp[-|k|(Z_b - Z_t)]\}^2 \quad (2.1)$$

Where k_x and k_y are the wavenumbers in the x and y directions, C_m is proportionality constant, Θ_m is factor for magnetisation direction and Θ_f is factor for the geomagnetic field direction. After annular averaging, Equation 2.1 can be simplified to:

$$P(k) = A[exp(-2|k|Z_t)]\{1 - \exp[-(Z_b - Z_t)]\}^2 \quad (2.2)$$

Where A is a constant related to the dimensions of the magnetic source, magnetisation and geomagnetic field directions. By assuming that signals from the top of source dominate the power spectrum and for the wavelengths less than about twice the thickness of the magnetic source, Equation 2.2 can be further simplified into:

$$\ln[P(k)]^{\frac{1}{2}} = \ln B - |k|Z_t \quad (2.3)$$

and

$$\ln\left\{\frac{\left[P(k)^{\frac{1}{2}}\right]}{k}\right\} = \ln C - |k|\, Z_c \quad (2.4)$$

Where B and C in Equations 2.3 and 2.4 are constants. So Z_b is:

$$Z_b = 2Z_c - Z_t \quad (2.5)$$

This method of obtaining the basal depth of the magnetic source, Z_b, is known as the centroid method that reflects the average CPD across the window (Tanaka et al., 1999).

Okubo et al. (1985; 1989) suggested that the centroid method is advantageous because large window dimensions are not necessary to estimate the CPD. In general, the area to determine the Z_b must be at least three to four times of the depth of the source (Bouligand et al., 2009). However, blocks of large extent could obscure local geological structures and make accurate estimation difficult (Bansal et al., 2011).

In this study, grids with extensions of 200 km × 200 km and overlapping 100 km have been created to cover an extensive area of east Australia. Across Tasmania, based on the geological extent and other geophysical information, it is summarised that the CPD does not generally exceed 40 km. Hence, Tasmania was studied with a higher resolution of 150 km × 150 km windows and overlapping 100 km. Therefore, the magnetic data were digitised and reduced to a regular grid using an interpolation program resulting in points for each square sub-region. In order to divide the entire data into the grids, a Python script was used and processing was carried out using the Oasis Montaj software package. Overall, 261 windows throughout east Australia and 42 windows covering Tasmania have been created and the CPD was estimated for these windows.

2.3. Results

Spectral analyses for three example windows spanning south of the Mt Isa Block, northern Queensland and northern Tasmania are shown in Figure 2.1. Gradient values for Z_b and Z_c were taken from the spectral plots and the CPD was estimated using Equation 2.5. Locations of centre of windows are displayed in Figure 2.1a. This process was carried out for all windows and shows that the estimated CPD through east Australia varies from ~24 to ~62 km as in the summary contour maps in Figures 2.2b. The Proterozoic basement within the study area is identified with average deeper CPDs. Tasmania is characterised by relatively shallow CPDs, varying from ~30 to ~40 km.

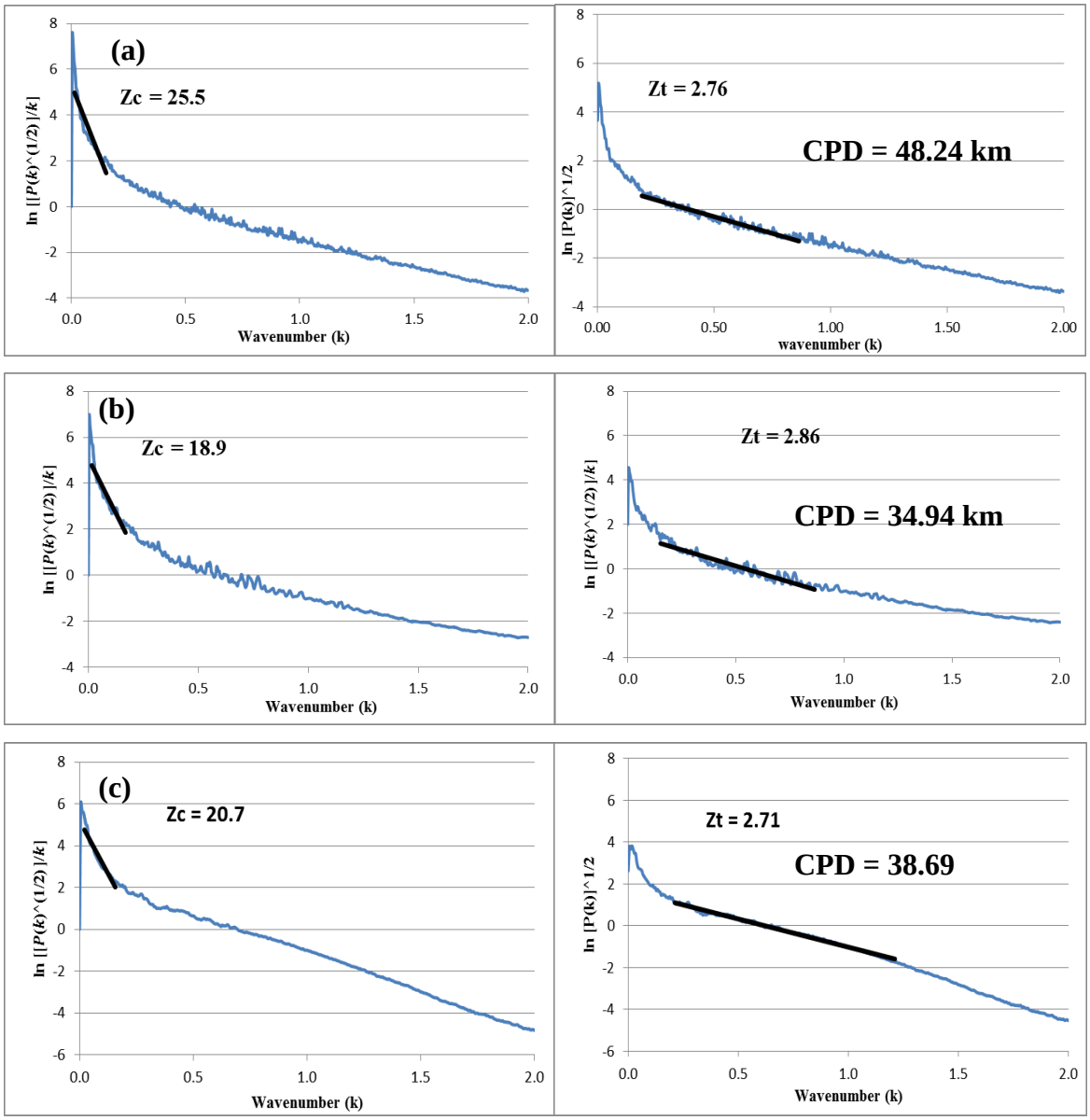

Figure 2. 1 - Estimation of depth to top of the deepest magnetic unit (gradient, Z_t), depth to the centre of the deepest magnetic unit (gradient, Z_c) and the Curie Point Depth (CPD) in (a) south of Mt Isa; (b) northern Queensland; (c) northern Tasmania.

2.4. Discussion

Spectral analysis of magnetic data and estimation of the CPD is dependent on size of the study area and windows. The obtained CPD reflects the average value of the created grid and, therefore, is limited in terms of resolving very detailed anomalies (Tanaka et al., 1999). In this study, I have determined the appropriate window size that can detect average deep CPDs and capture major basements. The CPD for each point is the average CPD across the window covering the basements and can be considered as representative for the window. Another principal difficulty is uncertainty of the quantitative interpretation of geophysical models.

Spectral analysis, particularly in deep investigations, provides an estimation of average depth to the source with the uncertainty in order of 10% (Mishra and Pedersen, 1982). Hence, I used the term of the 'estimation' for the CPD in this study to acknowledge this uncertainty.

The CPD values of major units (Figure 2.2b) vary between ~25 km and ~62 km across east Australia. Similarly, Chopping and Kennett (2015) discussed a CPD range of ~25—70 km throughout east Australia. Newly estimated CPDs well correlate with results discussed by Chopping and Kennett (2015) with similar trends and an average difference of ~10 km. This difference is acceptable based on the range of uncertainties of models. Unlike Chopping and Kennett (2015), there is a significant difference between newly estimated CPDs and results presented by Fox Maule et al. (2009). The newly estimated CPDs show that the northern part of Queensland associated with shallow CPDs (25—30 km) with a distinctive boundary with deeper CPDs (> 40 km) toward the south of the Georgetown Inlier and the north of the Thomson Orogen. The central western part of the Thomson Orogen is associated with relatively shallow CPDs (~25 km) which is compatible with high geothermal gradient in this area. However, this region is limited by relatively deep CPDs toward the south which contradicts with the extent of the high geothermal region. Proterozoic terranes of the Mt Isa Region and Curnamona Craton generally highlight deep CPDs compared to Phanerozoic basements. Some studies have discussed that the Mt Isa Region is characterised by a high geothermal gradient (e.g. Howard and Sass 1964, McLaren, et al. 1999, Sandiford, et al. 1998), while this study and model provided by Chopping and Kennett (2015) estimate relatively deep CPDs associated with dominant low geothermal gradient across this region. One possibility for this contradiction is likely underlying of a very cold basement across this region that changes the geothermal gradient at depth. The other scenario could be the uncertainty of CPD estimations across this region due to the large size of windows and likely impact of magnetic data from adjacent regions. Lack of information across the deep structures prevents a reliable interpretation throughout this region. The CPD is relatively deep throughout middle of the New England Orogen (up to 40 km depth) and smoothly shallows toward the south and north of this orogen (down to 30 km depth). Regions associated with the Mesozoic volcanism in the eastern margin generally return shallow CPD values. Northern parts of the Thomson and Lachlan Orogens display deep CPDs (> 50 km).

Across Tasmania, relatively shallow CPDs are observed with smoothly shallower CPDs across northeast Tasmania (< 30 km) compared to its western threshold. This estimated CPD is consistent with Patison et al. (2001) who suggested that an abundance of granite intrusions

resulted in higher geothermal gradient across northeast Tasmania compared to the western components. In addition, shallow CPDs across Bass Strait are consistent with the crustal thinning during the Gondwana breakup.

Comparing lateral variations of estimated depths in this study with those estimated by Chopping and Kennett (2015) shows that CPDs in both studies increase towards the northern parts of the Thompson and Lachlan Orogens. Nevertheless, Chopping and Kennett (2015) estimated deeper CPDs across Tasmania and north of Queensland compared to adjacent regions which contradicts with my estimations. This contradiction requires further detailed investigations as tectonic evolution and geothermal data suggest these regions as geothermally active areas associated with potentially shallow CPDs.

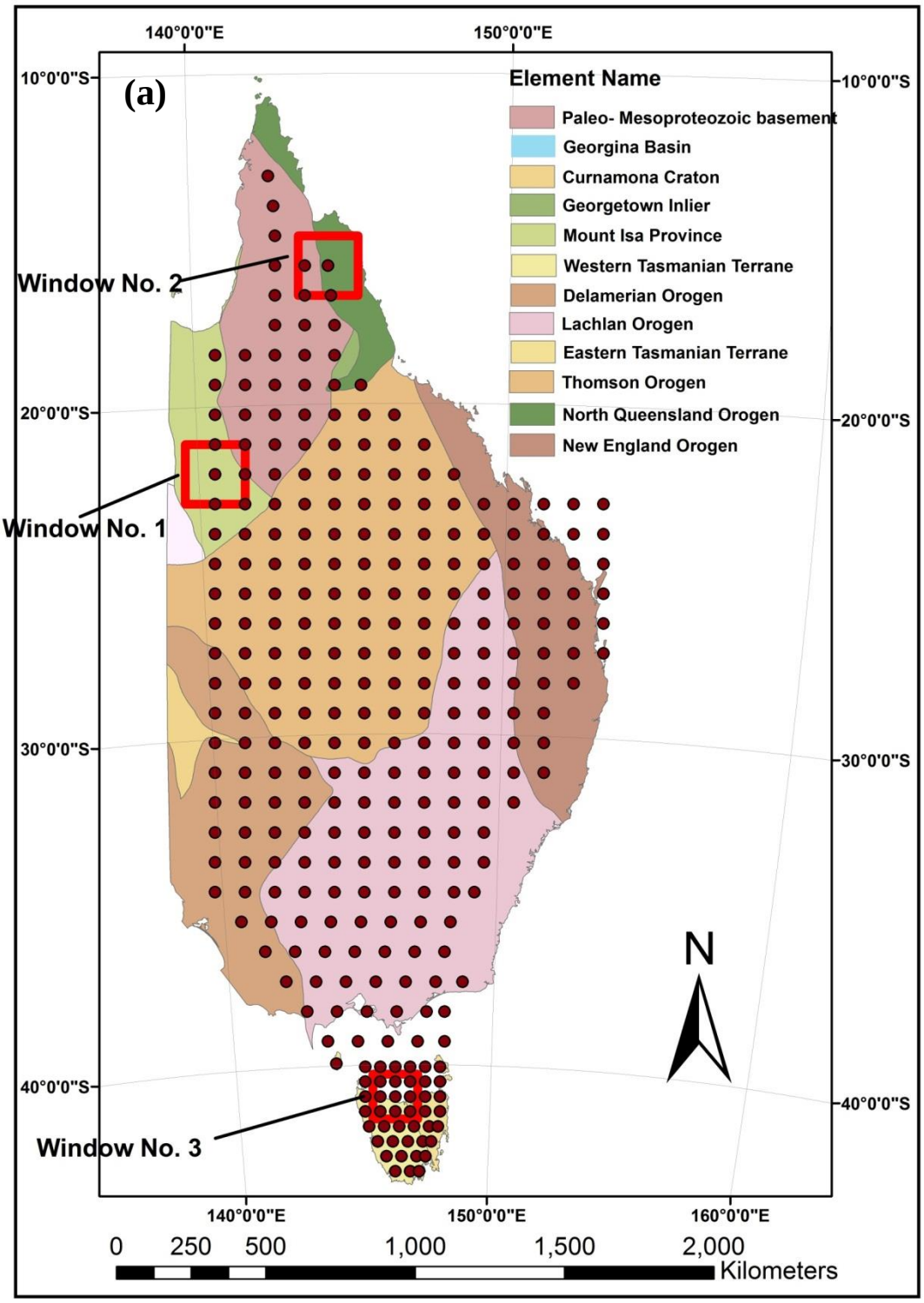
(a)
Element Name
Paleo- Mesoproteozoic basement
Georgina Basin
Curnamona Craton
Georgetown Inlier
Mount Isa Province
Western Tasmanian Terrane
Delamerian Orogen
Lachlan Orogen
Eastern Tasmanian Terrane
Thomson Orogen
North Queensland Orogen
New England Orogen
Window No. 1
Window No. 2
Window No. 3
N
140°0'0"E
150°0'0"E
160°0'0"E
10°0'0"S
20°0'0"S
30°0'0"S
40°0'0"S
0 250 500 1,000 1,500 2,000
Kilometers

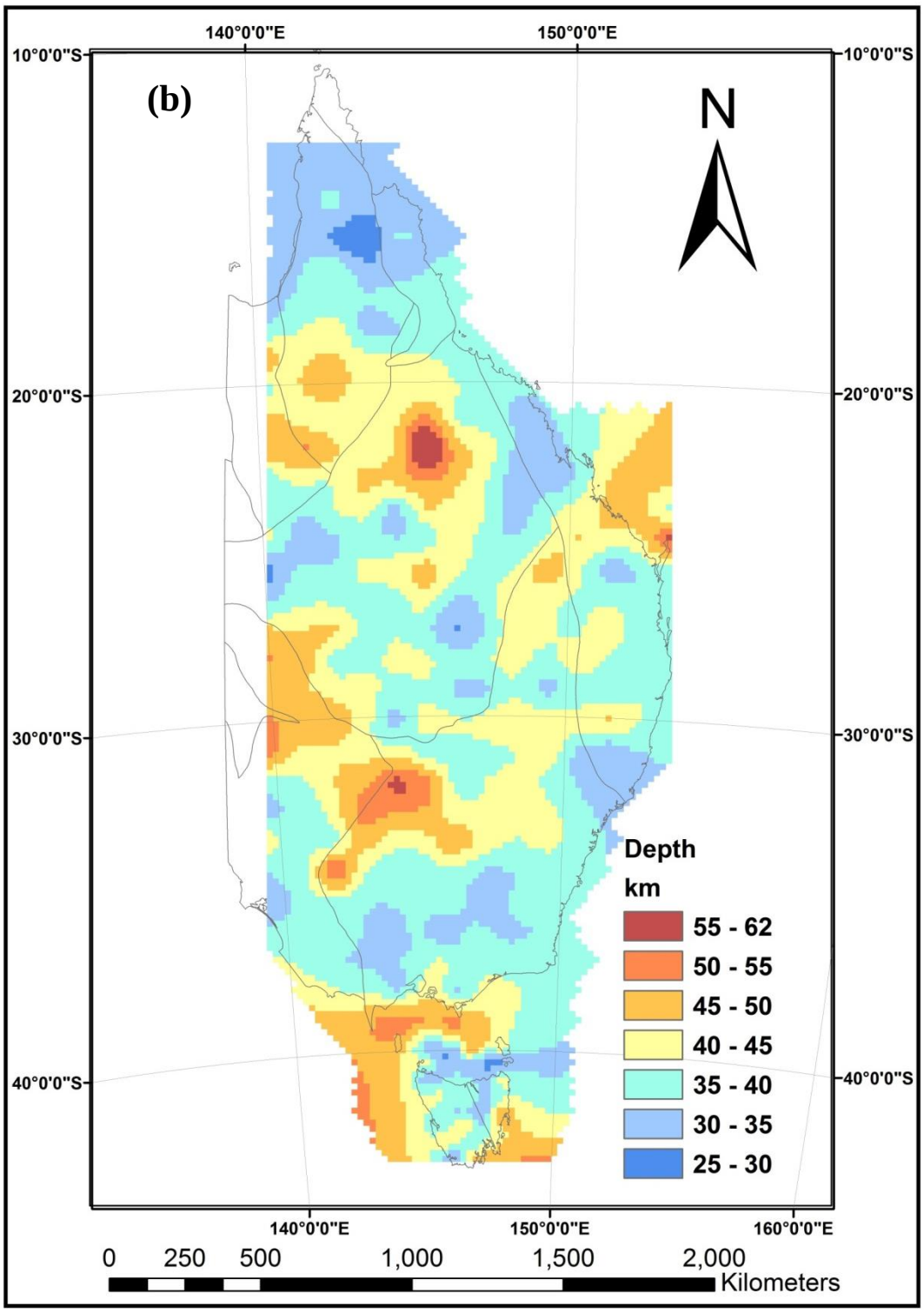

Figure 2. 2 - Calculation of the Curie Point Depth (CPD) across east Australia, (a) centre of windows used to estimate the CPD and major tectonic terranes across east Australia. Three displayed windows correspond to Figure 2.1 (Window No. 1, south of Mt Isa- Figure 2.1a; Window No. 2, north of Queensland- Figure 2.1b; Window No. 3, north of Tasmania- Figure 2.1c). Terrane boundary locations in the background basement map are given as a reference, as first shown in Figure 1.2. (b) the CPD across east Australia with tectonic basement map.

The relationship between the CPD and Moho depth determined from seismic data (Kennett et al., 2011; Salmon et al., 2013) has been displayed in Figure 2.3. Chopping and Kennett (2015) estimated a general 7—10 km uncertainty for their estimated magnetic CPDs across Australia. The Moho depth models have uncertainties of ±2—5 km using seismic data and ±3 km using gravity observations (Aitken, 2010). Hence, the quantitative interpretation of the relationship between the estimated CPD and Moho depth can be debated. Nevertheless, similar to Chopping and Kennett (2015), the relationship between these two boundaries can be considered which predominantly indicates a slight correlation across east Australia with misfits within the expected uncertainties. Tasmania consistently displays slightly deeper CPDs (up to 15 km), while regions associated with Mesozoic volcanism along the eastern margin, offshore east and west Tasmania and northern Queensland are characterised by deeper Moho depths. Regions with pronounced deeper CPDs correspond to the Proterozoic basement, and the northern parts of the Thomson and Lachlan Orogens. Deeper CPDs compared to Moho depth may be characterised by magnetised upper parts of the lithosphere (Li et al., 2010). While the mantle is a non-magnetic feature, the Moho boundary is not necessarily a magnetic boundary (McEnroe et al., 2009; Wasilewski and Mayhew, 1992). Furthermore, across very low heat flow regions (e.g. cratonic areas), low thermal gradients may result in CPDs that lie deeper than Moho depth. Since mantle rocks are non-magnetic, the CPDs deeper than Moho depth correspond to the Moho boundary (Saad, 1969).

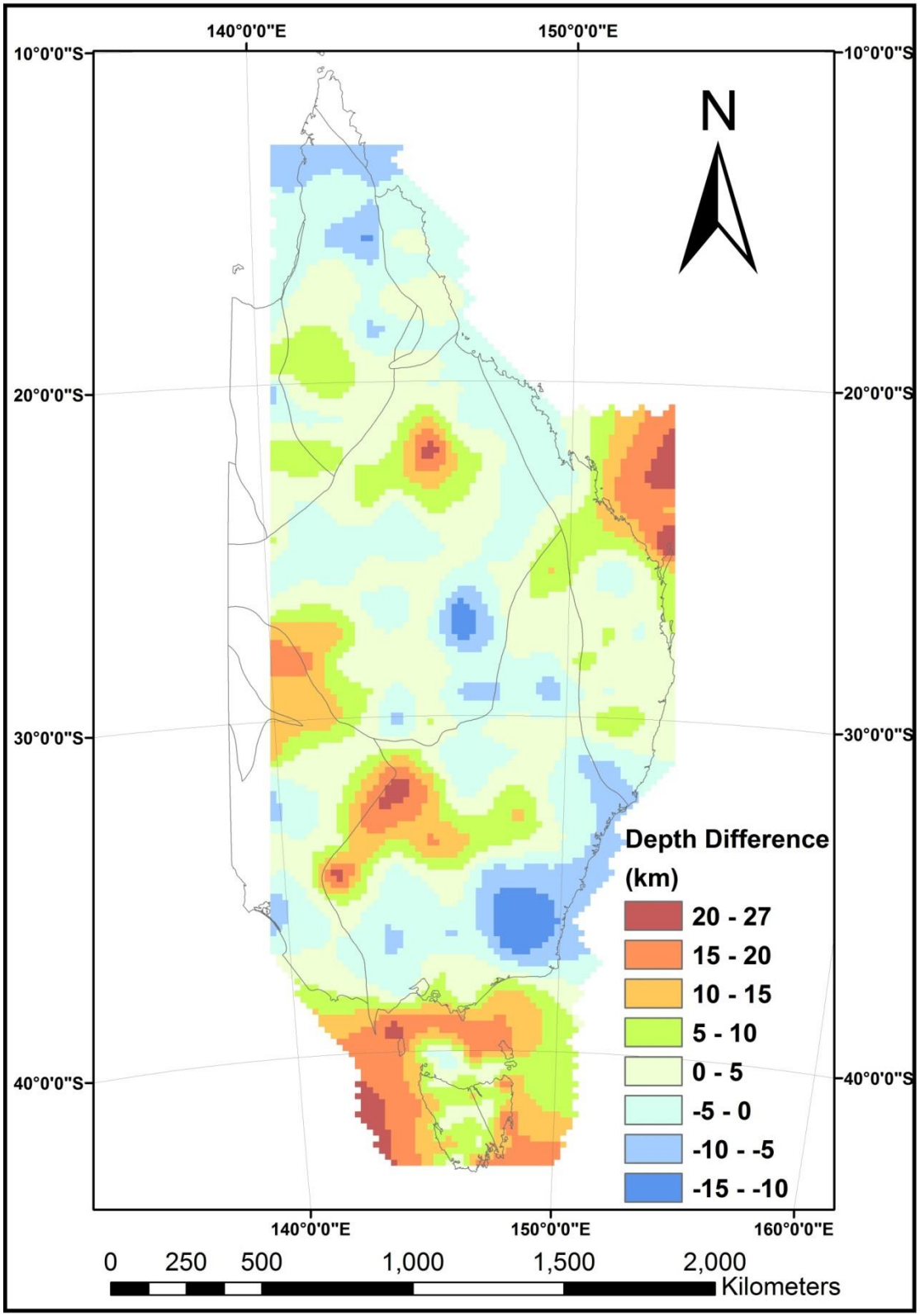

Figure 2. 3 - Relationship between the estimated Curie Point Depth (CPD) from magnetic data and Moho depth determined from seismic data across east Australia (estimated CPD - seismic Moho depth). Background basement map refers to Figures 1.2 and 2.2a.

The relationship between the estimated CPDs in this study and the expected CPDs from the OZTemp model is displayed in Figure 2.4. Estimated CPDs consistently indicate deeper depths. This difference may be from the incomplete understanding of the thermal regime (Chopping and Kennett, 2015) or inherent uncertainty in estimations of our results or/and interpolations of the OZTemp model. Local geothermal anomalies have likely been obscured due to the average spectral analysis of windows (Bansal et al., 2011; Chopping and Kennett, 2015) and large window sizes (200 km × 200 km and 150 km × 150 km) and window steps (100 and 50 km) while estimating the CPD in this study. An alternative scenario for the deeper estimated CPDs is possible underlying cold Precambrian basement with lower geothermal gradient beneath active geothermal features. For example, while west of the Thomson Orogen is characterised by an anomalously high temperature gradient in the OZTemp model, this region is associated with relatively deep CPDs. This could imply the presence of underlying cold Precambrian features of the Arunta and Warumpi provinces beneath this orogen.

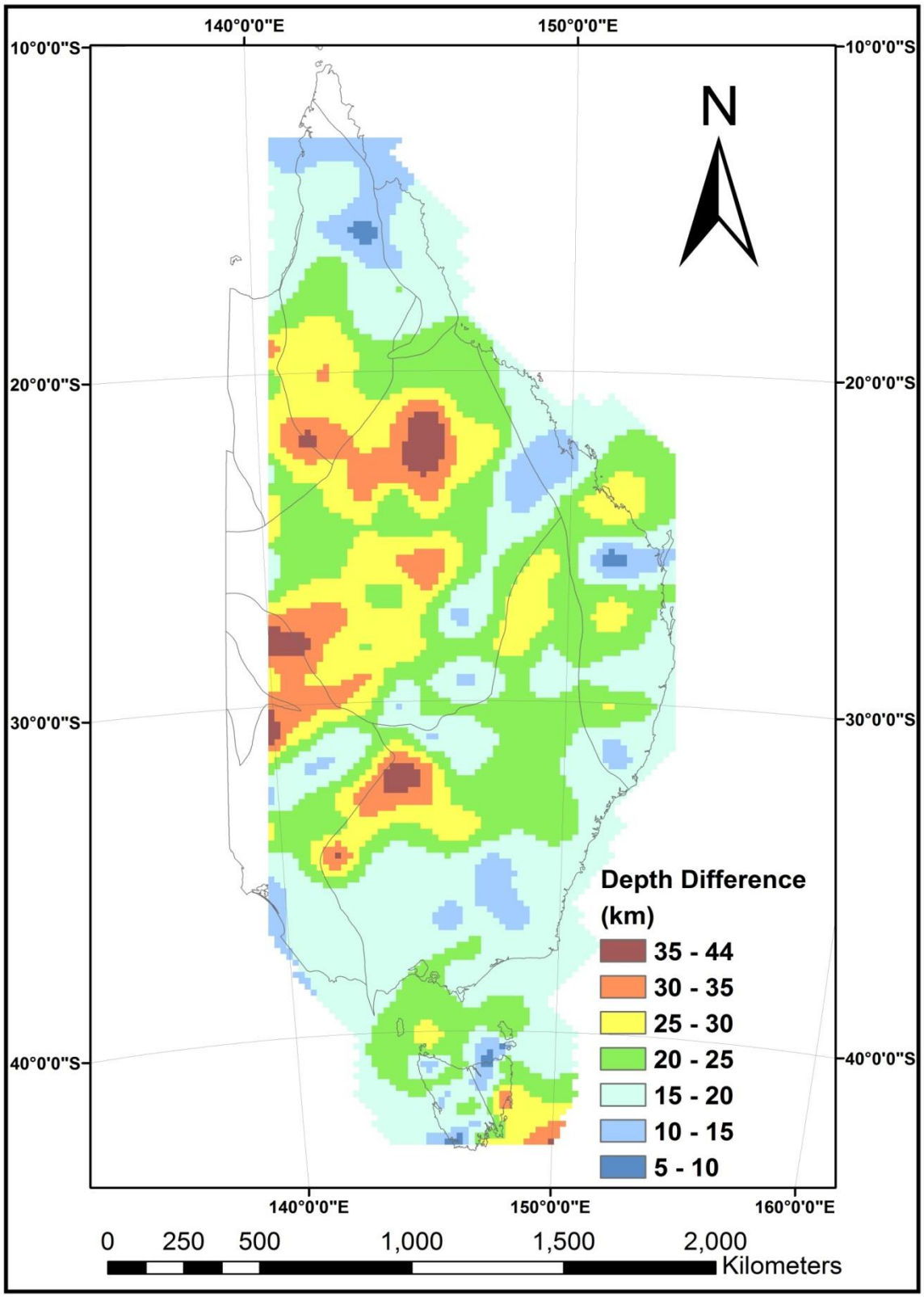

Figure 2. 4 - Relationship between the estimated Curie Point Depth (CPD) from magnetic data and expected CPD form OZTemp model (estimated CPD - expected CPD). Background basement map refers to Figures 1.2 and 2.2a.

2.5. Results

The CPD across eastern Australia has been estimated using spectral analysis of magnetic data. Estimated CPDs are compared with Moho depth determined from seismic data and the expected CPD based on the OZTemp model. The CPD is generally deeper across regions characterised by Precambrian basements. In contrast, the north of Queensland and regions associated with the Mesozoic volcanism across eastern margin relatively display shallow CPDs. The north of the Thomson Orogen and Lachlan Orogen are characterised by deep CPDs. The CPD and Moho depth correlate to some extent across east Australia. Nevertheless, CPDs are dominantly deeper than Moho depth across north of the Lachlan Orogen and Curnamona Craton. East of the Thomson and Lachlan Orogen display shallower CPDs than Moho depth. In contrast, estimated CPDs in this study are predominantly deeper than expected CPDs based on the OZTemp model which could be due to underlying cold basement and/or uncertainties in estimation and interpolation of results.

Across Tasmania, relatively shallow CPDs are observed ranging between 25 and 40 km. Northeast Tasmania and Bass Strait display relatively shallow CPDs compared to the western part of the island. Comparing CPD between northeast and western part of Tasmania emphasizes the higher geothermal gradient in northeast part and is compatible with abundance of granites intrusions. Recent tectonic activities and failed rifting across Bass Strait could result in high geothermal gradient across this region and consequently relatively shallow CPDs are interpreted across this region. Comparison of the CPD and Moho depth indicates that the CPD is consistently a few kilometres deeper than Moho depth across onshore Tasmania, while toward offshore east and west Tasmania, the CPD is dominantly deeper than Moho depth.

Chapter 3 - Petrophysical measurements of rock units from West Tasmania

Modelling of the gravitational, magnetic and seismic response of rocks may be improved through careful characterisation of their petrophysical properties including density, magnetic susceptibility and seismic velocity. This chapter describes core sampling, petrophysical property measurements of key rock units from West Tasmania and analysis of property values. The aim of this chapter is to document the building of a comprehensive petrophysical database for the Proterozoic and Palaeozoic rocks of West Tasmania to provide constraints for modelling of geophysical data. Density, magnetic susceptibility, and both P-wave and S-wave velocities were measured to improve the database.

3.1. Density

Density (ρ) is defined as the mass per unit volume of a substance. There is often significant variability associated with the measured density of a given rock unit which is related to lithological variations, contrasting alteration and weathering (Telford et al., 1990a). Sedimentary rocks are typically less dense than igneous or metamorphic rocks due to their higher porosity. Porosity of sedimentary rocks varies as a function of pressure with an increase in depth of burial. In the case of igneous rocks, density differences are due primarily to the mineral assemblage present and the rock texture. An increase in the metamorphic grade generally increases density (Telford et al., 1990a).

3.1.1. Data acquisition

To measure density, samples were immersed in water for a minimum period of 48 hours and weighed to attain the mass of the wet, saturated sample suspended in water (m_w). The saturated samples were then removed from the water, surface dried and weighed again, in air, to determine the dry mass (m_a). According to Archimedes' Principle, the density of each sample is calculated from wet and dry measured masses. The bulk density (g cm^{-3} or tonnes m^{-3}) is equal to:

$$\rho = \frac{Mass}{Volume} = \frac{m_a}{m_a - m_w} \quad (3.1)$$

3.2. Magnetic susceptibility

A magnetic material contains a distribution of magnetic moments caused by the spin of unpaired electrons. Magnetisation in each material is defined as the magnetic dipole moment per unit volume (Clark, 1997). The total magnetisation of a rock is the vector sum of the induced and remanent magnetisation. Induced magnetisation is the magnetisation due to an applied field and is proportional to the magnetic susceptibility of the object and the strength of the applied field. Remanent magnetisation can be observed, if present, when this induced field is removed but some "permanent" magnetisation remains (Telford et al., 1990b).

Magnetic susceptibility, k, is defined as the degree to which a substance can be magnetised by the process of induction. The magnetic susceptibility is, therefore, proportional to the strength of magnetisation that a material assumes in response to an applied magnetic field (M), divided by the strength of the applied magnetic field (H; Clark, 1997).

$$k = \frac{M}{H} \tag{3.2}$$

M and H have the same dimensions and hence magnetic susceptibility is a dimensionless property but the value of k depends on the system of units and may be specified CGS and SI. The relationship between k measured in these two systems is given by:

$$K_{SI} = K_{CGS} \times 4\pi \tag{3.3}$$

3.2.1. Data acquisition

The magnetic susceptibility of samples was measured using an Exploranium KT-9 Kappameter magnetic susceptibility meter, with a measurement sensitivity of 1×10^{-5} SI units (GEO F/X, 1997). Approximately 90% of measured magnetic susceptibility can be attributed to material within a distance of 20 mm from the sensor. Multiple readings per sample were collected to provide a representative measure of magnetic susceptibility. Within this thesis, all values of magnetic susceptibility are provided in $\times 10^{-3}$ SI units.

3.3. Seismic velocity

Seismic velocity measurements are conducted by timing ultrasonic pulses through a sample known length. P-wave velocity (V_p) is the speed at which longitudinal, pressure waves, or 'primary', waves propagate through a material. S-wave velocity (V_s) is the speed at which shear, or 'secondary', waves propagate through a solid material. S-waves displacements are in

a plane normal to the direction of propagation; they are slower than the P-wave and do not propagate in liquids. Both P-wave and S-wave velocity measurements can be utilised to study the 'quality' of natural materials and to investigate homogeneity, degree of alteration, geotechnical and mining parameters (e.g. Mamillan, 1972; Vasconcelos et al., 2007). The velocity of ultrasonic pulses travelling through a solid material is a function of both the elasticity and the density of the material (Telford et al., 1990c).

3.3.1. Data acquisition

A Pundit Lab instrument, manufactured by Proceq, was used for ultrasonic pulse velocity measurements. The Pundit Lab consists of a sound pulse emitting transducer, a sound transducer, and a control unit that measures the delay time between pulse transmission and reception (Proceq, 2016). Samples were prepared with parallel cut faces and appropriate couplant to each end (as recommended by the manufacturer) was applied to these surfaces prior to measurement. Before collecting velocity measurements, the Pundit Lab requires calibration. This is achieved using the calibration rod. Operating frequencies of 54 kHz and 250 kHz were used for P-wave and S-wave velocity measurements respectively. The sonic velocity for each sample can easily be calculated by dividing the length of the sample by the measured travel time.

3.3.2. Seismic velocity error

For seismic velocity measurements, the distance (path length) between transducers was obtained using digital callipers or manual ruler with an accuracy of 0.01—0.5 mm. The resolution of Pundit Lab is 0.5 µs. Hence, the maximum error (E) for a 15 cm sample with assumption of normal 0.5 mm error and arrival time of 25 µs is 25.75 m/s. This error may be regarded as negligible because it is only 0.43 percent of the average velocity of 6000 m/s for this sample.

$$E = \frac{150\ mm \pm 0.5\ mm}{25\ \mu s \pm 0.5\ \mu s} = \frac{150\ mm \pm 0.333\%}{25\ \mu s \pm 2\%} = 6000\ \text{m/s} \pm 2.33\% = 6000\ \text{m/s} \pm 25.75\ \text{m/s} \quad (3.4)$$

However, the more critical issue is achieving good contact between the transducers and the sample as this can significantly affect the measured transit time. The positions of transducers on the sample ends were adjusted to achieve the highest amplitude signal and the shortest transit time which are interpreted to indicate the best transducer coupling.

3.4. Sampling

Multiple pre-existing petrophysical data sources are available across Tasmania (e.g. Webster, 2008; Roach, 1994; Leaman, 2003; Keele, 1992; Payne, 1991, MRT online database, 2016; Poker, 2013; McAdam, 2015). Available databases have generally focused on small and anomalous regions or samples were measured from shallow depth affected by weathering. These factors can result in inaccurate characterisation. A first step in improving the petrophysical database is to select drill holes that intersect rock units of greatest interest. The likely contribution of the rock unit to the gravity, magnetic or seismic response should also be taken into consideration in prioritising samples for collection. The MRT database formed the basis for sample selection and contains over 9300 drill holes distributed across the study area with depths ranging from a few metres to a maximum of 1540 m. Drill holes and intervals for analysis were selected based on the units that likely contribute significantly to gravity and magnetic responses and were undersampled in previous studies. In general, the number of samples should be guided by the number of rock units, the diversity of mineralogy and textures (Fullagar et al., 1996).

The initial criteria to select appropriate drill holes were:

1. location within the study area

2. depth likely to be >100 m to minimise the effect of weathering on measured values

3. known intercept of major geological units

4. the absence of unrepresentative (e.g. very locally metamorphosed) samples

5. availability of core at the MRT Mornington Library.

6. a reasonable spread of drill holes across the study area.

7. available geological reports or logs for drill holes

Initially, 400 drill holes were selected, based on the above criteria and their drill logs and reports were accessed via the MRT public domain drill holes database (MRT online database, 2016). The drill logs were studied and appropriate intervals were determined. Due to the time taken to access samples in the MRT core library, the number of drill holes was reduced to 101 for the sampling to obtain sufficient numbers of samples for most of the stratigraphic units within the limited permitted time for sampling and petrophysical measuring summarised in

Figure 3.1. Core samples collected from the MRT core library, ranged in length between 11 and 24 cm. Intervals that were found to be crushed or unavailable were substituted with alternative drill holes. A total of 443 samples were obtained from a variety of rock units. Density and magnetic susceptibility measurements by McAdam (2015), Poker (2013) and relevant MRT petrophysics values were collated and combined with the new measurements to construct a more comprehensive and representative combine petrophysical database. Table 3.1 outlines the number of samples associated with major rock units.

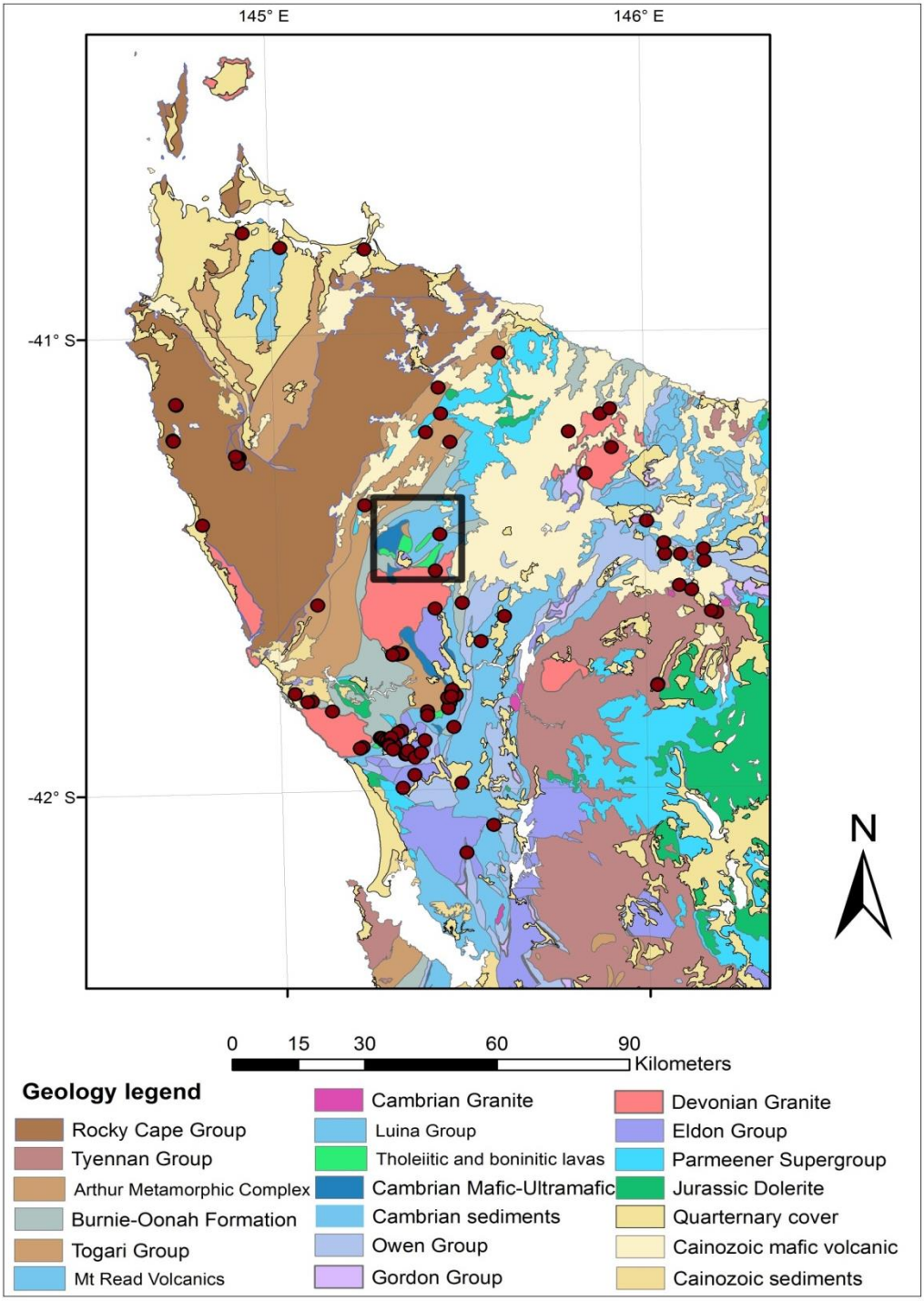

Figure 3. 1 - Final 101 selected drill holes for sampling to provide representative petrophysical properties across northwest Tasmania. The geology map of the study area is shown. The black rectangle bounding the map is the extent of the West Tasmania study (Chapter 5) and the small black rectangle shows the extent of the more detailed Heazlewood- Luina-Waratah study (Chapter 6).

Unit	No. drill holes	No. collected samples	Total No. samples adding other measurements			
			Density	Magnetic Susceptibility	P-wave velocity	S-wave velocity
Rocky Cape Group	11	48	48	48	35	20
Tyennan region	4	16	16	16	11	10
Togari Group	5	28	28	28	20	19
Arthur Metamorphic Complex	6	24	24	24	10	10
Burnie-Oonah Formations	20	80	110	396	53	39
Success Creek Formation	4	16	108	108	15	15
Crimson Creek Formation	8	44	153	155	31	28
Cambrian Mafic-Ultramafic Complexes	9	40	93	498	27	25
Cambrian Granite	3	16	41	41	19	18
Owen Group	5	24	66	65	18	17
Gordon Group	5	20	39	39	16	15
Eldon Group	3	8	17	17	3	2
Devonian Granite	9	36	68	123	24	19

Table 3. 1 - Major units across the study area, number of drill holes, obtained samples for each unit and total number of samples used for petrophysical characterisation including measurements by other studies.

3.5. Assessment of measurements

In extending a petrophysical database, it is important to test whether a new set of contributed measurements is likely to be consistent with other samples. A set of 43 samples, previously analysed by Hot Dry Rocks Pty Ltd (HDR; Hot Dry Rocks Pty Ltd, 2013) and accepted as 'correct' values was remeasured using the laboratory equipment described earlier in this chapter. New density, magnetic susceptibility, P-wave velocity, and (where possible) S-wave velocity measurements were compared with the available HDR values.

Figure 3.2 shows the density and magnetic susceptibility measurements for this study (labelled CODES) compared with the HDR values. There is a negligible difference and high correlation

between density measurements (Figure 3.2a). Comparison of magnetic susceptibility values (Figure 3.2b) is not easy because small changes in the proportion of magnetite within samples can result in large variations in magnetic susceptibility. Magnetic susceptibility values measured at CODES are consistently higher than HDR measurements for magnetic susceptibility values $< 1 \times 10^{-3}$ SI but higher values are similar. The discrepancy at low magnetic susceptibility values likely represents differences in the instrumentation used in the two studies and these variations are not important for modelling purposes because of the influence of units with high magnetic susceptibility in the measured magnetic intensity.

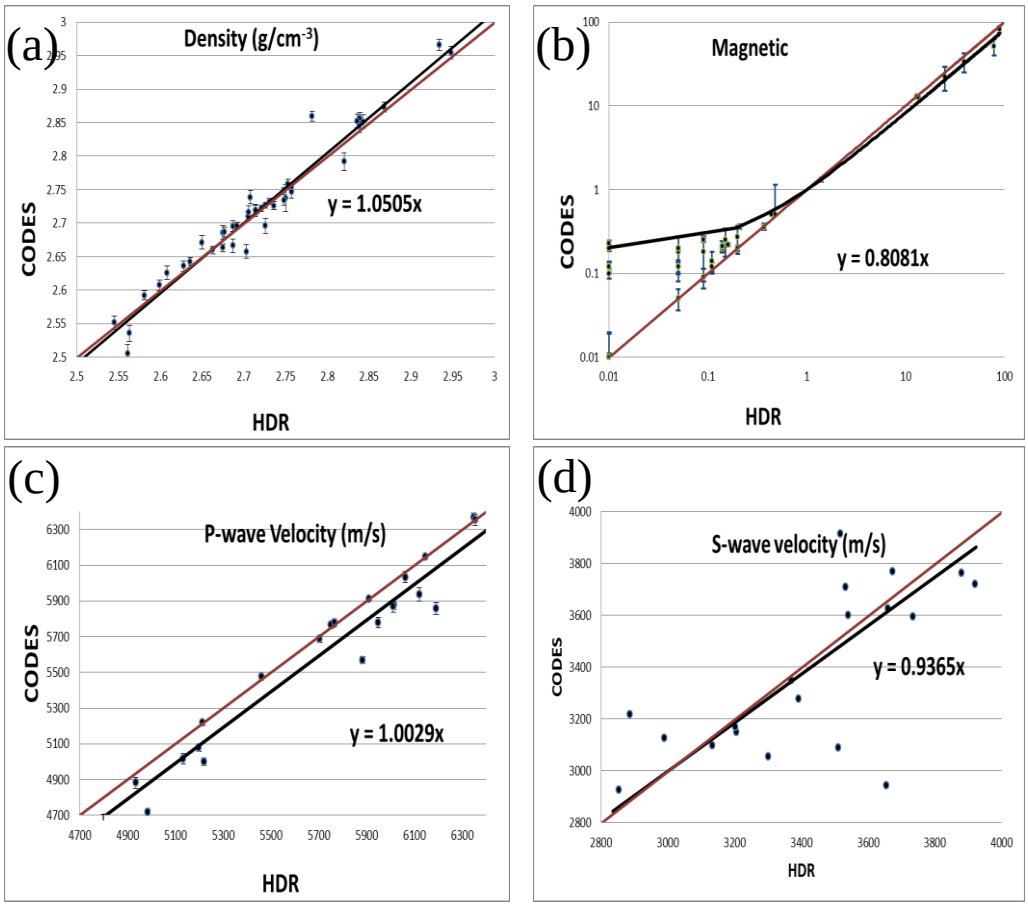

Figure 3. 2 - Comparison of petrophysical measurements between this study (CODES) and Hot Dry Rocks (HDR); (a) density, (b) magnetic susceptibility in logarithmic scale axes, (c) P-wave velocity and (d) S-wave velocity. The trend line (black line) and its equation are determined, and the line showing a 1:1 ratio (red line) is plotted. Measurement error bars are shown on measurements. Broad error bars within magnetic susceptibility measurements indicate the large impact that small amounts of irregularly distributed magnetite may have on susceptibility. No error bar is given for S-wave velocity because this error could be due to misidentification of arrival times.

P-wave velocity values (Figure 3.2c) indicates a reasonable correlation between CODES and HDR measurements with a negligible average difference of ~104 m/s (~1.66% misfit for a P-wave velocity of 6000 m/s). Comparison of S-wave measurements (Figure 3.2d) shows that nine out of the total 22 samples exhibit a relatively high difference between measurements. The difference of values between CODES and HDR could be due to the human error in selecting the S-wave arrival time. To record the arrival time of the S-waves using the Pundit Lab instrument, the operator must manually determine the arrival of S-waves. S-waves have low amplitudes which are amplified to be detectable. This could result in misidentification of noise source as the S-wave. This misidentification of arrival wave is plausible in CODES or HDR or both measurements. While this misfit cannot completely be removed, it can be reduced through user experience.

3.6. Discussion of newly measured rock properties

In this section, all measurements available for each rock unit (newly measured, recently measured by other researchers and those contained in the pre-existing MRT database) are analysed and discussed. A summary of petrophysical values for all rock units is given in section 3.8, and section 3.9 explains the values to be used as model inputs.

Tables 3.2, 3.3, 3.4 and 3.5 summarise density, magnetic susceptibility, P-wave velocity and S-wave velocity for rock units within the study area. The number of samples used for each rock unit is shown in Table 3.2.

Unit	No. samples	Minimum	Maximum	Mean	Median	Geometric Mean	Standard Deviation
Rocky Cape Group	48	2.61	2.87	2.74	2.74	2.74	0.05
Tyennan region	16	2.69	2.84	2.77	2.78	2.77	0.04
Togari Group	28	2.75	2.86	2.8	2.81	2.80	0.03
Arthur Metamorphic Complex	24	2.66	2.93	2.79	2.81	2.79	0.08
Burnie-Oonah Formations	110	2.45	3.11	2.74	2.73	2.74	0.09
Success Creek	108	2.48	3.15	2.8	2.77	2.8	0.10
Crimson Creek	153	2.74	3.18	2.88	2.86	2.88	0.10
Cambrian Mafic-Ultramafic Complex	93	2.2	3.39	2.73	2.75	2.72	0.23
Cambrian Granite	41	2.57	2.84	2.69	2.68	2.69	0.06
Owen Group	66	2.35	2.81	2.63	2.64	2.63	0.07
Gordon Group	39	2.6	2.81	2.71	2.7	2.71	0.04
Eldon Group	17	2.51	2.75	2.64	2.67	2.64	0.07
Devonian Granite	68	2.47	2.8	2.62	2.62	2.62	0.05

Table 3. 2 - Summary statistics of density (g cm^{-3}) from major geological units across West Tasmania examined in this study.

Unit	No. samples	Minimum	Maximum	Mean	Median	Geometric Mean	Standard Deviation
Rocky Cape Group	48	0.09	1.59	0.42	0.32	0.35	0.29
Tyennan region	16	0.09	0.45	0.27	0.28	0.23	0.13
Togari Group	28	0.01	8.50	0.77	0.10	0.15	1.92
Arthur Metamorphic Complex	24	0.01	0.63	0.16	0.10	0.07	0.19
Burnie-Oonah Formations	396	0.01	27.00	0.59	0.29	0.32	1.59
Success Creek Formation	108	0.05	21.00	2.29	0.65	0.53	3.79
Crimson Creek Formation	155	0.05	129.00	7.26	0.77	1.29	19.92
Cambrian Mafic-Ultramafic Complex	498	0.02	138.00	10.29	5.62	2.64	14.82
Cambrian Granite	41	0.01	58.00	25.70	28.00	11.40	17.20
Owen Group	65	0.01	16.40	1.25	0.08	0.12	3.52
Gordon Group	39	0.01	2.20	0.28	0.12	0.12	0.44
Eldon Group	17	0.01	0.25	0.08	0.05	0.04	0.08
Devonian Granite	123	0.01	11.40	0.39	0.15	0.14	1.19

Table 3. 3 - Summary statistics of magnetic susceptibility ($\times 10^{-3}$ SI) from major geological units across West Tasmania examined in this study.

Unit	No. samples	Minimum	Maximum	Mean	Median	Geometric Mean	Standard Deviation
Rocky Cape Group	35	4559	6047	5356	5467	5336	462
Tyennan region	11	4017	6171	5498	5526	5467	576
Togari Group	20	4258	6568	5900	5958	5873	555
Arthur Metamorphic Complex	10	5606	7021	6378	6475	6360	513
Burnie-Oonah Formations	53	4343	6609	5585	5632	5558	553
Success Creek Formation	15	4799	6363	5895	5921	5883	383
Crimson Creek Formation	31	5573	7259	6057	5924	6044	420
Cambrian Mafic-Ultramafic Complex	27	5000	6899	6087	6246	6062	551
Cambrian Granite	19	5472	6108	5873	5899	5871	167
Owen Group	18	5309	5901	5578	5576	5575	165
Gordon Group	16	4788	6443	5929	6085	5913	438
Eldon Group	3	4198	5886	5223	5317	5199	497
Devonian Granite	24	4559	6047	5356	5467	5336	462

Table 3. 4 - Summary statistics of P-wave velocity (m/s) from major geological units across West Tasmania examined in this study.

Unit	No. samples	Minimum	Maximum	Mean	Median	Geometric Mean	Standard Deviation
Rocky Cape Group	20	3038	3945	3539	3567	3528	279
Tyennan region	10	3648	4756	4068	3976	4056	339
Togari Group	19	2386	4302	3546	3728	3512	485
Arthur Metamorphic Complex	10	3804	4146	3948	3950	3947	100
Burnie-Oonah Formations	39	3050	4343	3678	3706	3670	253
Success Creek Formation	15	3109	4554	3943	4081	3914	480
Crimson Creek Formation	28	2861	4330	3617	3624	3598	371
Cambrian Mafic-Ultramafic Complex	25	3196	4613	3916	3898	3905	306
Cambrian Granite	18	3195	4166	3780	3838	3771	269
Owen Group	17	2865	4164	3648	3755	3630	366
Gordon Group	15	3276	3952	3733	3791	3727	218
Eldon Group	2	2601	4398	3543	3474	3517	552
Devonian Granite	19	3038	3945	3539	3567	3528	279

Table 3. 5 - Summary statistics of S-wave velocity (m/s) from major geological units across West Tasmania examined in this study.

Tables 3.6 and 3.7 compare the density and magnetic susceptibility values for different rock units adopted by past studies and compare them to the assigned values in this study. New petrophysical measurements acquired in this study characterise more geological units and provide a more comprehensive petrophysical constraints. These tables indicate that density values obtained in this study and those recorded previously are generally consistent, except for the Precambrian Basement of the Rocky Cape Group and Tyennan region and other Neoproterozoic units of the Togari Group and Arthur Metamorphic Complexes. Magnetic susceptibility values show a greater variability between studies.

Unit	Webster 2008	Roach 1994	Leaman 2003	Keele 1992	Payne 1991	MRT		Eshaghi
						Density	Range	
Precambrian Basement	2.69	2.69	-	2.64-2.66	2.67	-	-	
Rocky Cape Group	-	-	-	-	-	-	-	2.74
Tyennan region	-	-	-	-	-	-	-	2.77
Togari Group	-	-	-	-	-	-	-	2.80
Arthur Metamorphic Complex	-	-	-	-	-	-	-	2.79
Burnie-Oonah Formations	-	-	2.75	-	-	-	-	2.74
Success Creek Formation	-	-	> 2.74	-	2.75	2.82	2.79-2.85	2.80
Crimson Creek Formation	2.71	2.72	> 2.68	-	2.80	2.92	2.88-2.96	2.88
CMUC- unit 1	-	-	-	-	-	-	-	2.65
CMUC- unit 2	-	-	-	-	-	-	-	2.86*
Cambrian Granites	2.68	2.68	2.62-2.69	2.64	2.64-2.66	2.66	2.62- 2.70	2.68
Owen Group	2.73	2.65	-	-	2.63	2.65	2.60-2.69	2.63
Gordon Group	-	2.73	2.74	2.73	-	2.73	2.70-2.76	2.71
Eldon Group	-	2.69	-	2.69	-	2.62	2.66-2.68	2.64
Devonian Granite	2.60	2.60	2.60-2.62	-	2.60	-	-	2.62

Table 3. 6 - Density (g cm^{-3}) of major geological units across West Tasmania as interpreted in previous publications and in this study (labelled Eshaghi in this table). Densities marked with * in this study are median values and other values are means. In this table, the Cambrian Mafic-Ultramafic Complexes unit is divided into two subunits of CMUC- unit 1 characterised by low density and high magnetic susceptibility values and CMUC- unit 2 characterised by high density and low magnetic susceptibility values.

Magnetic Susceptibility	Webster 2003	Roach 1994	Leaman 2003	Keele 1992	Payne 1991	MRT	Eshaghi
Precambrian Basement	-	1.30	0.13	0.01	0	0	
Rocky Cape Group	0	-	-	-	-	-	0.415
Tyennan region	0	-	-	-	-	-	0.265
Togari Group	-	-	-	-	-	-	0.100*
Arthur Metamorphic Complex	> 2.5	-	-	-	-	-	0.161
Burnie-Oonah Formations	< 6	0	-	-	6.28	0	0.588
Success Creek Formation	0	0	-	-	0	3	0.650*
Crimson Creek Formation	> 10	6.28	6.5	-	12.57	10	7.250
CMUC- unit 1	> 120	-	-	-	-	-	14.451
CMUC- unit 2	> 120	-	-	10	-	-	0.745
Cambrian Granites	> 6	37.7	40	3	0	18.2	25.720
Owen Group	0	1.26	-	0.01	0	0	0.080*
Gordon Group	0	0.13	-	0.01	0	0.1	0.280
Eldon Group	0	1.26	1.3	0.01	0	0.1	0.070
Devonian Group	0	0	0	-	6.28	0	0.390

Table 3. 7 - Magnetic Susceptibility (10^{-3} SI) of major geological units as interpreted in previous publications and in this study (labelled Eshaghi in this table) across West Tasmania. Magnetic susceptibility values marked with * in this study are median values and other values are mean. In this table, the Cambrian Mafic-Ultramafic Complexes unit is divided into two subunits of CMUC- unit 1characterised by low density and high magnetic susceptibility and CMUC- unit 2 characterised by high density and low magnetic susceptibility.

Histograms of physical properties for different lithological units are presented in Figures 3.3 and 3.4. These histograms illustrate the availability of physical properties within major lithological units. This section presents rock units individually, and section 3.9 summarises the values for each rock unit that are used to constrain the modelling in later chapters.

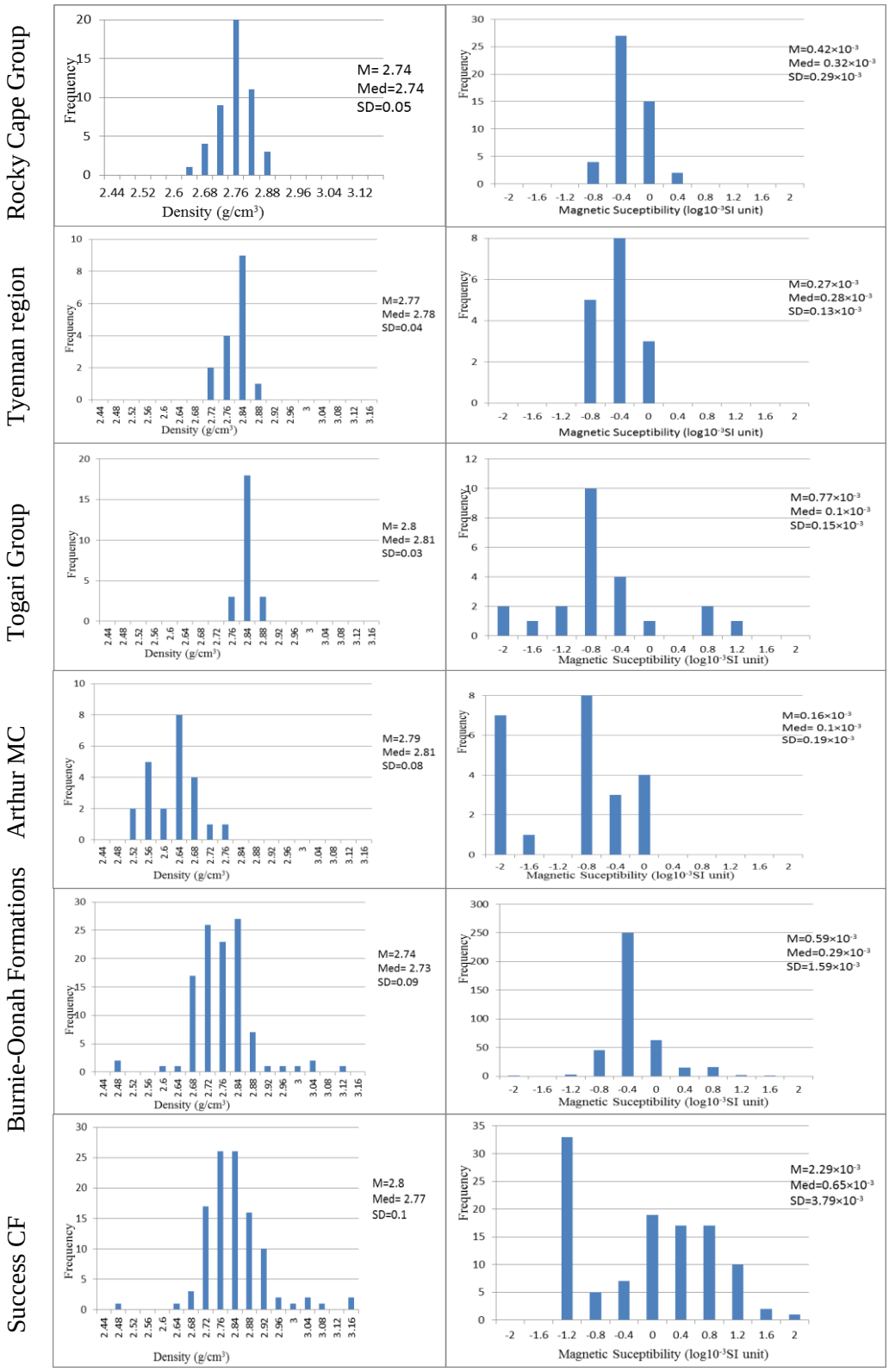
Rocky Cape Group
Tyennan region
Togari Group
Arthur MC
Burnie-Oonah Formations
Success CF
Frequency
Density (g/cm³)
M= 2.74
Med=2.74
SD=0.05
M=0.42×10⁻³
Med= 0.32×10⁻³
SD=0.29×10⁻³
Magnetic Suceptibility (log10⁻³SI unit)
M=2.77
Med= 2.78
SD=0.04
M=0.27×10⁻³
Med=0.28×10⁻³
SD=0.13×10⁻³
M= 2.8
Med= 2.81
SD=0.03
M=0.77×10⁻³
Med= 0.1×10⁻³
SD=0.15×10⁻³
M=2.79
Med= 2.81
SD=0.08
M=0.16×10⁻³
Med= 0.1×10⁻³
SD=0.19×10⁻³
M=2.74
Med= 2.73
SD=0.09
M=0.59×10⁻³
Med=0.29×10⁻³
SD=1.59×10⁻³
M=2.8
Med= 2.77
SD=0.1
M=2.29×10⁻³
Med=0.65×10⁻³
SD=3.79×10⁻³

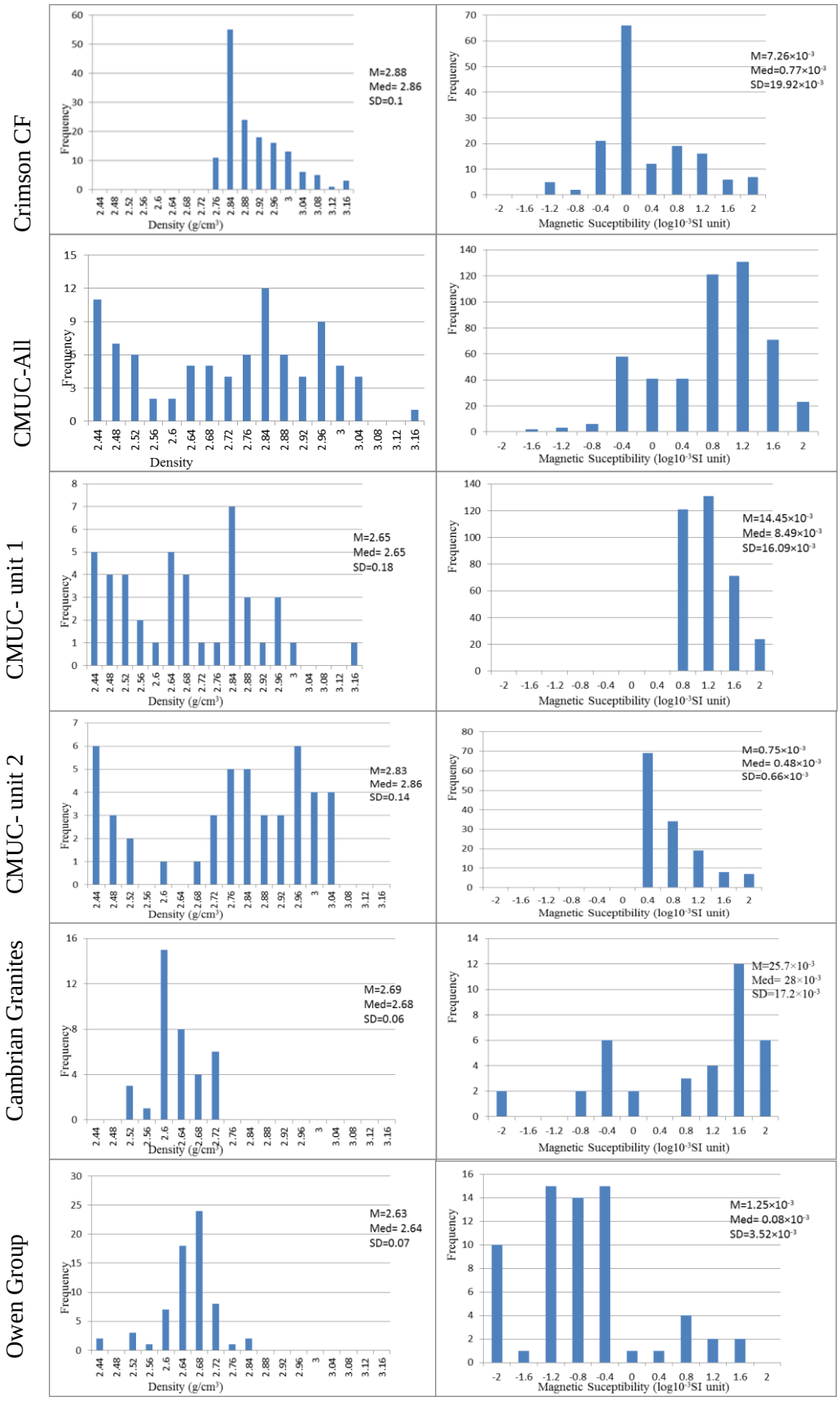
Crimson CF
M=2.88
Med= 2.86
SD=0.1
Frequency
Density (g/cm³)
M=7.26×10⁻³
Med=0.77×10⁻³
SD=19.92×10⁻³
Magnetic Suceptibility (log10⁻³SI unit)
CMUC-All
Density
CMUC- unit 1
M=2.65
Med= 2.65
SD=0.18
M=14.45×10⁻³
Med= 8.49×10⁻³
SD=16.09×10⁻³
CMUC- unit 2
M=2.83
Med= 2.86
SD=0.14
M=0.75×10⁻³
Med= 0.48×10⁻³
SD=0.66×10⁻³
Cambrian Granites
M=2.69
Med=2.68
SD=0.06
M=25.7×10⁻³
Med= 28×10⁻³
SD=17.2×10⁻³
Owen Group
M=2.63
Med= 2.64
SD=0.07
M=1.25×10⁻³
Med= 0.08×10⁻³
SD=3.52×10⁻³

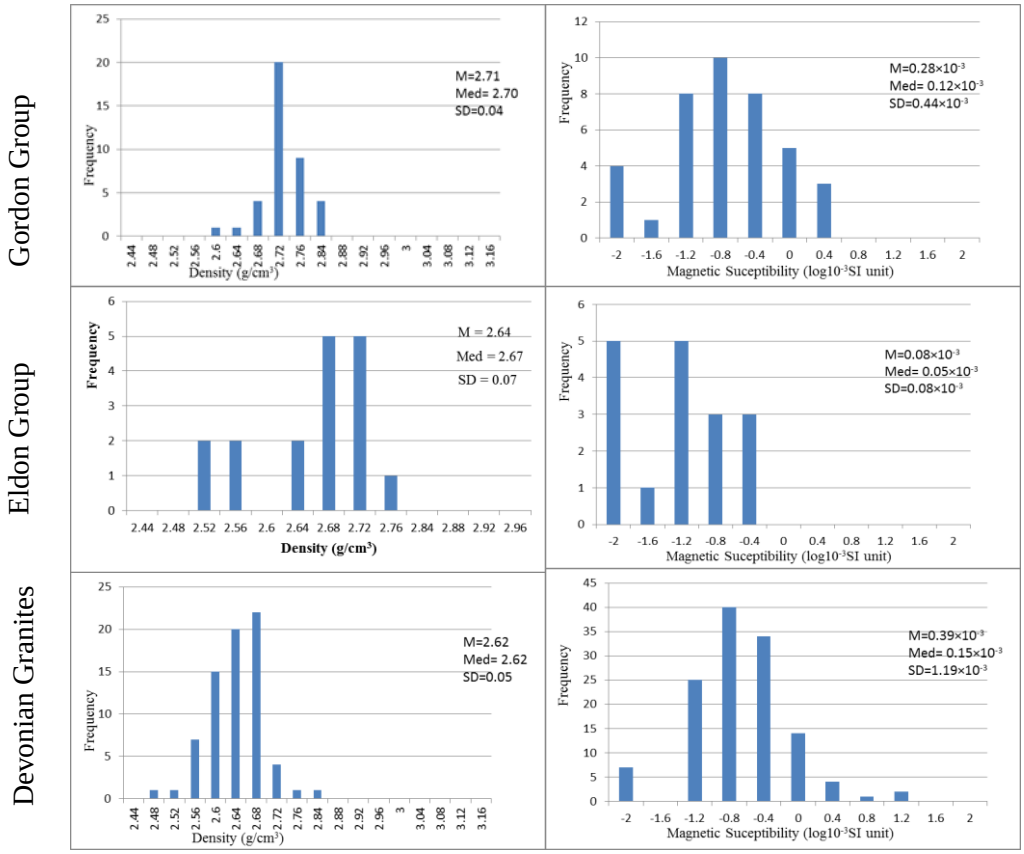

Figure 3. 3 - Petrophysical measurements of major lithological units in West Tasmania. Histograms display the density (g cm^{-3}) in the left column and log_{10} magnetic susceptibility ($\times 10^{-3}$SI) in the right column. Mean, median and standard deviation statistics of density and magnetic susceptibility are included in each histogram. In this figure, the Cambrian Mafic-Ultramafic Complexes (CMUC-all) unit is divided into two subunits: CMUC- unit 1 characterised by low density and high magnetic susceptibility values and CMUC- unit 2 characterised by high density and low magnetic susceptibility values.

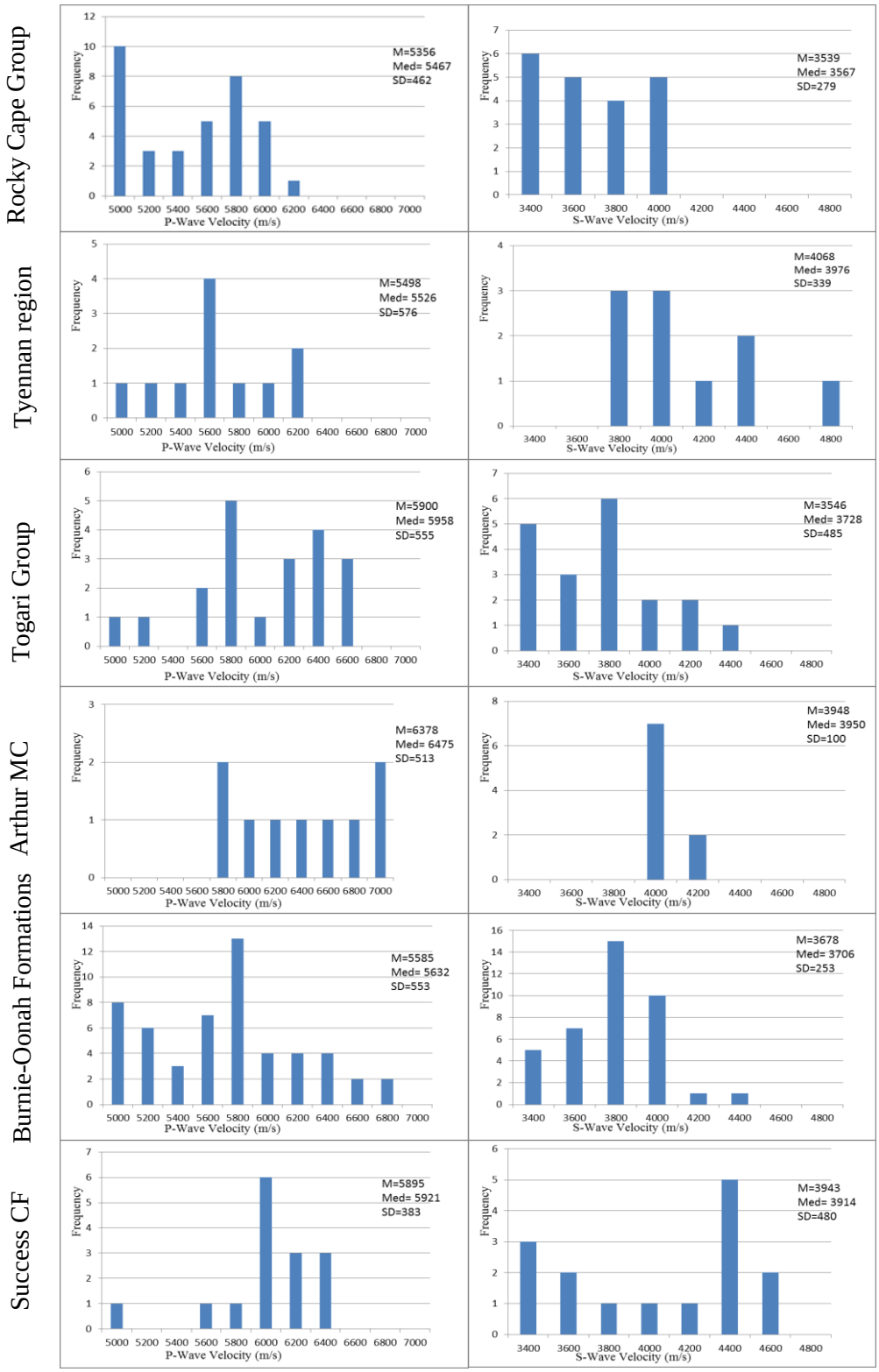
Rocky Cape Group
Tyennan region
Togari Group
Arthur MC
Burnie-Oonah Formations
Success CF
Frequency
P-Wave Velocity (m/s)
S-Wave Velocity (m/s)
M=5356
Med= 5467
SD=462
M=3539
Med= 3567
SD=279
M=5498
Med= 5526
SD=576
M=4068
Med= 3976
SD=339
M=5900
Med= 5958
SD=555
M=3546
Med= 3728
SD=485
M=6378
Med= 6475
SD=513
M=3948
Med= 3950
SD=100
M=5585
Med= 5632
SD=553
M=3678
Med= 3706
SD=253
M=5895
Med= 5921
SD=383
M=3943
Med= 3914
SD=480

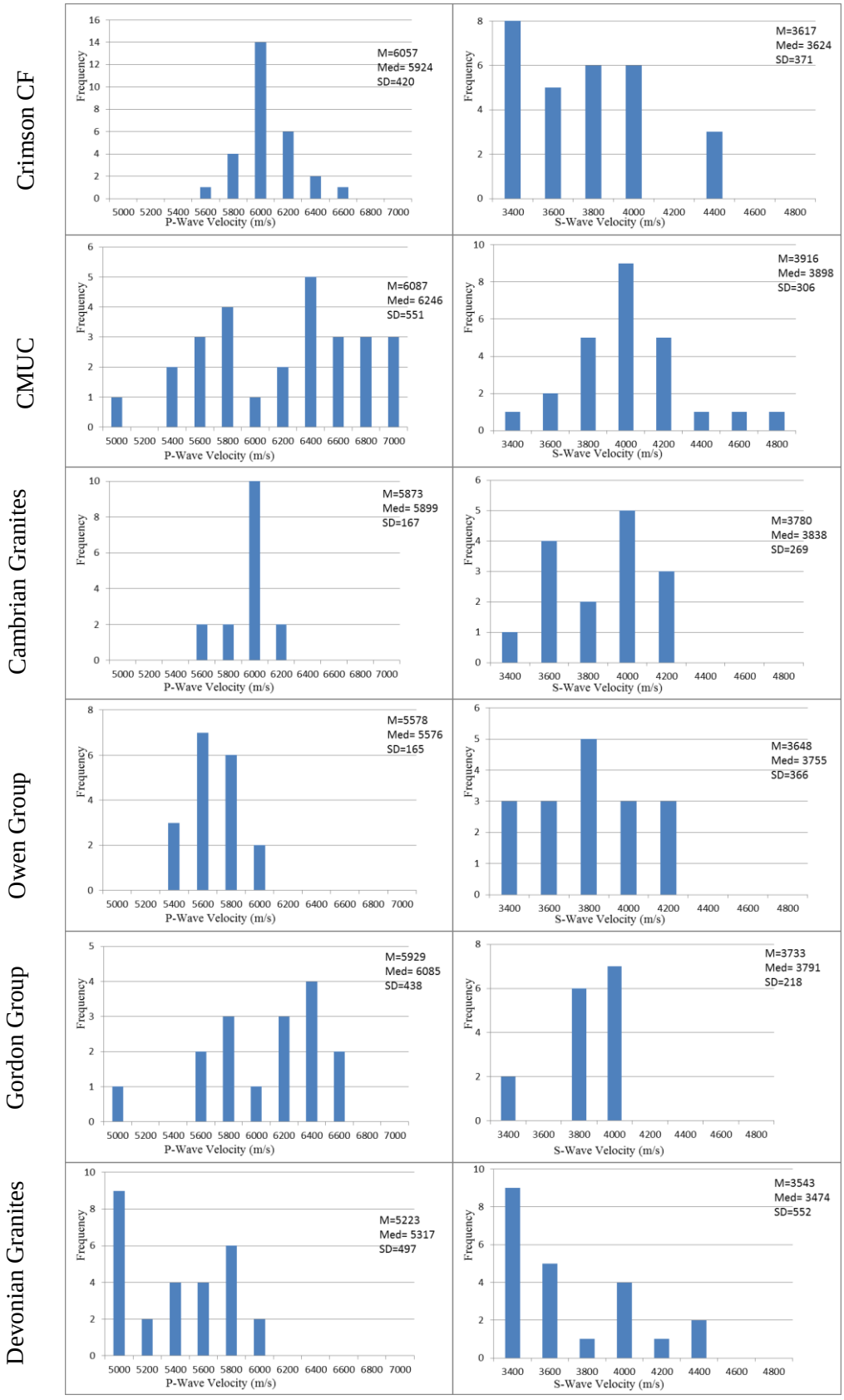

Figure 3. 4 - Seismic velocity measurements of major lithological units across West Tasmania. Histograms display the P-wave velocity (m/s) in the left column and S-wave velocity (m/s) in the right column. Mean, median and standard deviation statistics of seismic velocities are included. CMUC represents the Cambrian Mafic-Ultramafic Complexes unit.

3.6.1. Rocky Cape Group

Siliciclastic shelf sequences of the Rocky Cape Group were characterised using 48 samples taken from 11 drill holes. Petrophysical data provided by MRT are mostly from weathered surface samples. Density and magnetic susceptibility measurements (all 48 samples), P-wave velocity measurements (35 samples) and S-wave velocity measurements (20 samples) were collected for this sample suite.

The density and magnetic susceptibility histograms for samples from the Rocky Cape Group are uni-modal with mean density of 2.74 g cm^{-3} and mean magnetic susceptibility of 0.415×10^{-3} SI. Hence, the Rocky Cape Group is a non-magnetic unit with medium density.

P-wave velocities for the Rocky Cape Group range from 4556 to > 6000 m/s. Velocities less than 5000 m/s were measured in 10 samples leading to the overall bimodal distribution and the mean density of this unit has more than one population (Figure 3.4). However, without the low velocity outliers, the other samples indicate a uni-modal distribution and the bulk mean could be used to represent this unit in large scale for practical modelling. P-wave velocity measurements indicate median and mean values of 5468 and 5355 m/s respectively. The S-wave velocity measurements are relatively consistent and display median and mean velocities of 3568 and 3539 m/s respectively.

3.6.2. Tyennan region

The Proterozoic metamorphosed rocks of the Tyennan region are mostly weathered at surface. Only a few drill holes that intersect this unit are deep enough to collect samples from intact rocks with negligible weathering. Petrophysical measurements for this unit were conducted using 16 samples from four drill holes. Previous studies have not taken measurements from this unit, so the new measurements represent an important addition to the petrophysical database. Measurements of density and magnetic susceptibility (all 16 samples), P-wave velocity measurements (11 samples) and S-wave velocity measurements (10 samples) were used to characterise the properties of this unit.

The Tyennan region displays uni-modal distributions of density, magnetic susceptibility and seismic velocities. The unit has a mean density of 2.77 g cm^{-3} and low magnetic susceptibility of 0.265×10^{-3} SI.

The wave velocity measurements for this unit are limited, and thus the velocities should be regarded as reconnaissance values. These measurements indicate means of 5498 m/s and 4067 m/s for P-wave and S-wave velocities, respectively.

3.6.3. Togari Group

For the rift related sedimentary units of the Togari Group, 28 samples from five drill holes were collected. Four samples from drill hole 'CSM-2 Corinna Silica Mine' are considered to be weathered and present outlier densities and magnetic susceptibilities which have been excluded. Petrophysical properties of this unit were characterised using 28 density measurements, 28 magnetic susceptibility measurements, 20 P-wave velocity measurements and 19 S-wave velocity measurements.

Density for this unit is uni-modal distribution with a mean of 2.80 g cm^{-3}. This unit has three magnetic susceptibility sub populations (Figure 3.3) but the unit is predominantly non-mgnetic. Due to the presence of outlying susceptibility values, the median of 0.1×10^{-3} SI may better represent the central tendency of this population.

P-wave velocity has three main velocity domains (Figure 3.4) and significant variability, between 4258 and 6568 m/s. The median P-wave velocity of 5957 m/s was assigned to this unit. In contrast, S-wave velocity is bimodal with a mean velocity of 3546 m/s.

3.6.4. Arthur Metamorphic Complex

The Arthur Metamorphic Complex (MC) was characterised based on 24 samples collected from six drill holes. Density and magnetic susceptibilities were measured for all collected samples. Seismic velocities were measured upon 10 samples. One sample displayed outlier low density and magnetic susceptibility values and was discarded from calculations.

This unit has a bimodal density distribution with density values between 2.66 and 2.93 g cm^{-3}, indicative of the wide range of properties due to the variety of protolith and metamorphic lithologies. However, the majority of samples display a density range of 2.70 to 2.82 g cm^{-3}. This complex has been assigned a density value of 2.79 g cm^{-3} representing most of the measurements exhibiting high densities. The magnetic susceptibility distribution of this unit is bimodal. Nevertheless, both populations are non-magnetic and the maximum magnetic susceptibility measurement for this unit is 0.63×10^{-3} SI. Therefore, the mean magnetic susceptibility of 0.161×10^{-3} SI was assigned to this complex.

Seismic velocity measurements were under sampled and do not adequately represent P-wave and S-wave velocities. P-wave velocities for this unit display median of 5990 m/s and mean of 6378 m/s. A standard deviation of 513 m/s and difference of 1400 m/s between maximum and minimum P-wave velocities indicate a high degree of variability for this unit. S-wave velocities have a median of 3950 m/s and mean of 3948 m/s with a standard deviation of 100 m/s. These values can be regarded as reconnaissance values for this complex.

3.6.5. Burnie-Oonah Formations

Precambrian rift related turbiditic successions of Burnie-Oonah Formations were characterised using 80 samples collected from 20 drill holes. Density and magnetic susceptibility measurements for Oonah Formation by Poker (2013) were added to this database. Overall, 110 density values, 396 magnetic susceptibility values, 53 P-wave velocity measurements and 39 S-wave velocity measurements were collected to estimate the properties.

These units display a uni-modal density distribution, excluding some outliers, with a mean value of 2.74 g cm^{-3} (Figure 3.3). The Burnie-Oonah Formations display relatively low susceptibility, with a uni-modal distribution and with an average magnetic susceptibility of 0.588×10^{-3} SI.

Eight samples have P-wave velocity measurements less than 5000 m/s, and 13 samples display velocity between 5600 and 5800 m/s. The median and mean P-wave velocities in these formations are 5632 m/s and 5585 m/s respectively. S-wave velocities display a uni-modal distribution with a mean velocity of 3679 m/s.

The Rocky Cape Group, Tyennan region, Arthur MC and Burnie-Oonah Formations are all examples of the Precambrian basement within Tasmania. Previously reported density values for basement are between 2.64 and 2.70 g cm^{-3} as shown in Table 4.6 (i.e. Payne, 1991, Keele, 1992; Leaman, 2003; Roach et al., 1993). However, new measurements indicate that these units were characterised by higher densities in this study (i.e. the Rocky Cape Group, 2.74 g cm^{-3}; Tyennan region, 2.78 g cm^{-3}; Togari Group, 2.80 g cm^{-3}; Arthur MC with 2.81 g cm^{-3}; Burnie-Oonah Formations, 2.73 g cm^{-3}). This suggests that the basement is likely to be denser than previously understood. Precambrian basement units are essentially non-magnetic based on this study and previous measurements (i.e. Payne, 1991, Keele, 1992; Leaman, 2003; Roach et al., 1993).

3.6.6. Success Creek Formation

The Success Creek Formation was characterised by 16 samples collected from four drill holes. All collected samples are from East Renison drill holes, which can result in a bias in estimations because of local distribution of samples. Density and magnetic susceptibility value measurements by MRT from this unit were added to the East Renison data. Overall, 108 density measurements and magnetic susceptibility readings, and 15 P-wave and S-wave velocity measurements were used to estimate properties of this unit.

Excluding outliers from the data, the density of the Success Creek Formation is uni-modal displaying relative high density values centred on a mean density of 2.80 g cm^{-3}. A wide range of magnetic susceptibilities from non-magnetic to moderate magnetism was recorded for the formation. This unit has a generally bimodal susceptibility distribution with one population essentially non-magnetic and the other sub population with elevated but still generally low magnetic susceptibility. Due to the presence of outlying susceptibility values, the median of 0.650×10^{-3} SI may better represent the data. Large differences between median and average values and a standard deviation of 3.79×10^{-3} SI confirms that this unit has a high variation of magnetic properties.

P-wave velocity measurements are uni-modal and indicate a mean value of 5895 m/s. S-wave velocity is has a bimodal distribution with a few samples indicating relative low velocities ($\leq$ 3400 m/s) and mean S-wave velocity of 3943 m/s.

3.6.7. Crimson Creek Formation

The Neoproterozoic greywacke, mudstone and pillow lavas of the Crimson Creek Formation were characterised using 44 samples collected from eight drill holes. Previous density and magnetic susceptibility measurements were added to these new measurements. Overall, 153 density values, 155 magnetic susceptibility measurements, 31 P-wave velocity measurements, and 28 S-wave velocity measurements were used to estimate the properties.

The distribution of density for the Crimson Creek Formation is uni-modal with a positive skew (Figure 3.3). The formation has a relatively high density characterised by a mean of 2.88 g cm^{-3}, which is generally slightly higher than recorded from other sources. The magnetic susceptibility is uni-modal, excluding some outliers, with a mean susceptibility of 7.25×10^{-3} SI.

P-wave velocity measurements are uni-modal (Figure 3.4) with a mean of 6057 m/s. In contrast, S-wave velocities is characterised by a bimodal distribution and a mean of 3617 m/s.

3.6.8. Cambrian Mafic-Ultramafic Complexes

The Cambrian Mafic-Ultramafic Complexes (CMUC) were characterised using 40 samples collected from nine drill holes. Density and magnetic susceptibility measurements by Poker (2013) were added to these new measurements. In total, 93 density values, 498 magnetic susceptibility values, 27 P-wave velocity measurements and 25 S-wave velocity measurements were analysed.

The CMUC is characterised by high variations of both density and magnetic susceptibility. This unit displays three main density sub-populations and a bimodal magnetic susceptibility distribution (Figure 3.3). This marked variability in density and magnetic susceptibility means that adoption of single values for all models is not appropriate. Magnetic susceptibility versus density is plotted in Figure 3.5 and clearly shows two main units. The first sub-population is characterised by relative low density and high magnetic susceptibility, and has been named CMUC- unit 1 in this study. In contrast, the second population represents lithologies with higher density and lower magnetic susceptibility, called CMUC- unit 2. The line plotted in Figure 3.5 defines a boundary between these two populations. A difference in the degree of serpentinisation might have contributed to the large density and magnetic variations observed within this unit (Griggs, 2002). Dunites and harzburgites are typically characterised by higher density and less magnetic susceptibility values than equally serpentinised peridotites (Saad, 1969).

The first sub population with lower density, CMUC- unit 1, displays the median and mean density of 2.66 and 2.68 g cm^{-3} respectively. This sub population indicates relatively high magnetic values with median of 8.56×10^{-3} SI and mean of 14.45×10^{-3} SI. The second sub population, CMUC- unit 2, indicates the median and mean densities of 2.86 and 2.83 g cm^{-3} respectively. This unit is essentially non-magnetic, presenting a median of 0.48×10^{-3} SI and mean of 0.75×10^{-3} SI.

Unlike density and magnetic susceptibility, seismic velocity values are relatively consistent and values can be summarised as one unit. P-wave velocity values are bimodal with a mean of 6087 m/s. The S-wave velocity values are uni-modal and display mean of 3017 m/s.

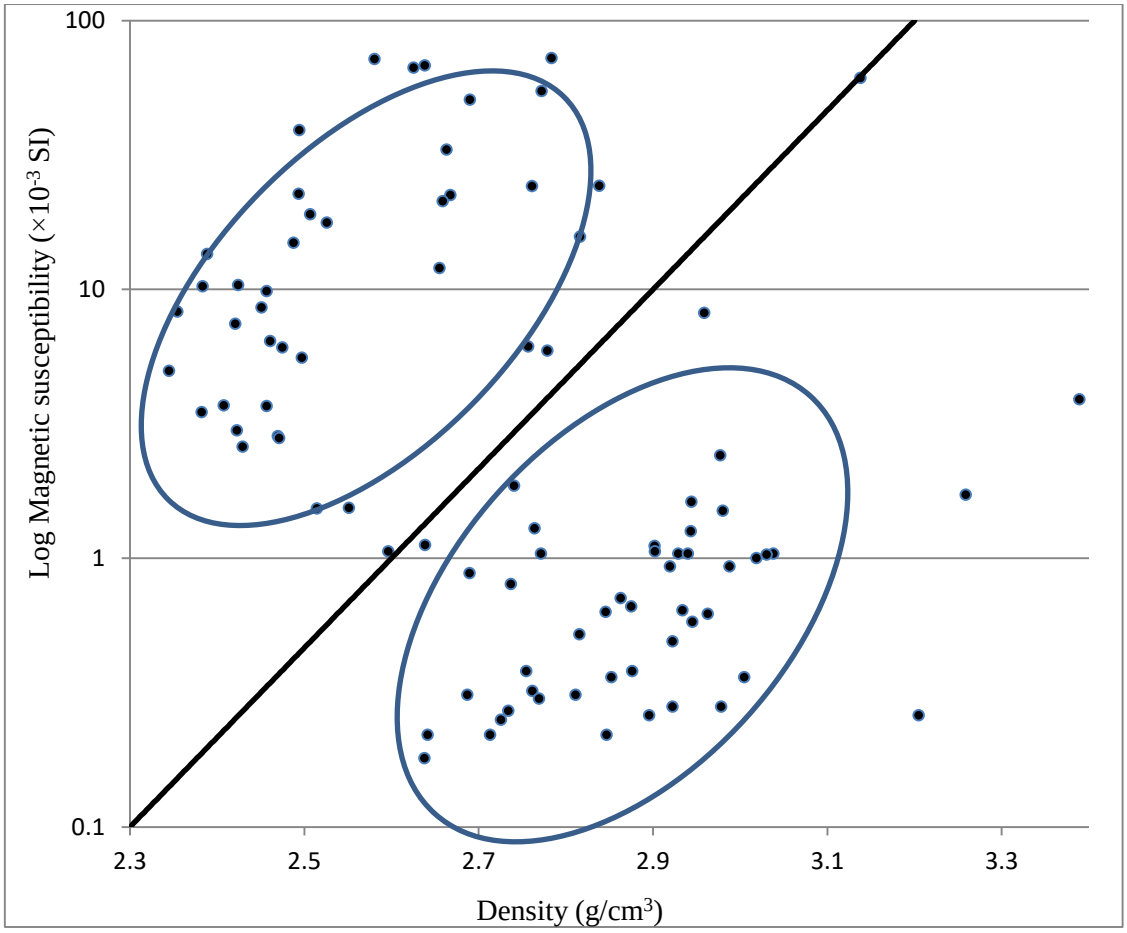

Figure 3. 5 - Magnetic susceptibility (logarithmic scale) vs density (linear scale). This plot shows two sub populations within the Cambrian Mafic-Ultramafic Complexes. CMUC- unit 1 displays relatively low density and high magnetic susceptibility values and CMUC- unit 2 is characterised by higher density and low magnetic susceptibility values. An estimated line displays the boundary between these two units.

3.6.9. Cambrian Granite

To characterise the Cambrian Granite, 20 samples were taken from four drill holes. Previous density and magnetic susceptibility measurements were added to the measurements. Overall, 41 density and magnetic susceptibility values, 19 P-wave velocity measurements, and 18 S-wave velocity measurements were analysed.

The density distribution of the Cambrian Granites is uni-modal, excluding outliers with high density, and characterising a mean density of 2.68 g cm^{-3}. In contrast, the Cambrian Granite displays a large variation of magnetic susceptibility preventing any meaningful statistical analysis (Figure 3.3). This unit has three main magnetic susceptibility sub-populations, two non-magnetic and one highly magnetic. All magnetic susceptibility measurements in this study and most of those acquired by MRT come from the high magnetic susceptibility sub-

population. Data presented by McAdam (2015) show a non-magnetic population associated with the Cambrian Dove Granites. The highly magnetic population has a uni-modal magnetic susceptibility distribution with a mean value of 25.72×10^{-3} SI.

P-wave velocities have a uni-modal distribution with the average velocity of 5825 m/s. S-wave velocity distributions are bimodal, with a major peak around 3800 m/s with a mean velocity of 3768 m/s.

3.6.10. Owen Group

The Late Cambrian-Ordovician syn-orogenic sediments of the Owen Group were characterised by 24 samples from five drill holes. Density and magnetic susceptibility measurements from McAdam (2015) were added to these measurements. In total, 66 density, 65 magnetic susceptibility, 16 P-wave velocity and 15 S-wave velocity measurements have been used to characterise this unit.

This unit displays a uni-modal density distribution, excluding a few outliers, with a mean of 2.63 g cm^{-3}. Magnetic susceptibility measurements display low to moderate values with three modal peaks, two non-magnetic and the third indicating a moderately magnetic domain. High magnetic susceptibility measurements ($> 1 \times 10^{-3}$ SI) were recorded for nine samples which are likely associated with mineralisation effects. Discarding outliers, a bimodal distribution of magnetic susceptibility is achieved with two sub-populations of non-magnetic properties. A median magnetic susceptibility value of 0.08×10^{-3} SI is representative of both non-magnetic sub-populations.

Seismic velocity measurements display uni-modal distributions. The mean of 5578 m/s for P-wave velocity and 3648 m/s for S-wave velocity are assigned to this unit.

3.6.11. Gordon Group

The Ordovician shallow-marine carbonate successions of the Gordon Group were characterised using 20 samples taken from five drill holes. Overall, 39 density and magnetic susceptibility samples including previous and new measurements from McAdam (2015) and MRT database (2016), 15 P-wave velocity and 15 S-wave velocity measurements were analysed.

The Gordon Group density distribution is uni-modal with a mean of 2.71 g cm^{-3}. This unit is essentially non-magnetic unit with a mean magnetic susceptibility of 0.28×10^{-3} SI.

P-wave velocity distribution is bimodal, excluding the low velocity outlier, with mean values of 5649 m/s. In contrast, the S-wave velocity measurements form a tight range with a mean value of 3803 m/s.

3.6.12. Eldon Group

Only eight samples from two drill holes were collected for the Siluro-Devonian marine sandstones and shales of the Eldon Group unit due to relatively few drill holes intersecting this lithology. A further difficulty in finding suitable samples is the shallow depth of the drill holes and consequent weathering. This number of samples was not considered sufficient for a robust estimation of petrophysical properties. Overall, 17 density and magnetic susceptibility values were available for this unit including new and previously measured samples.

The Eldon Group is characterised by a uni-modal density distribution, excluding outliers, with a mean value of 2.64 g cm^{-3}. This unit is non-magnetic with a mean magnetic susceptibility property of 0.07×10^{-3} SI.

The P-wave and S-wave velocity measurements across the Eldon Group are substantially under sampled (3 P-wave and 2 S-wave measurements). Hence, these measurements are disregarded for petrophysical characterisation of this unit.

3.6.13. Devonian Granites

To characterise Devonian Granites, 36 new samples were collected from nine drill holes. In total, including previous and new measurements (MRT database, 2016; McAdam, 2015, Poker, 2013), 68 densities and 123 magnetic susceptibilities 24 P-wave velocity and 19 S-wave velocity measurements were analysed across the Devonian Granites.

Density displays a uni-modal distribution with negative skew. The mean value of 2.62 g cm^{-3} is assigned to this unit. The magnetic susceptibility distribution is uni-modal, ignoring outliers, displaying a mean value of 0.39×10^{-3} SI indicating an essential non-magnetic unit.

The P-wave velocity is bimodal with one population of velocities < 5000 m/s and another population of higher velocity. The mean P-wave velocity of 5223 m/s has been assigned to this unit. Likewise, S-wave velocity measurements display significant scatter with generally low velocities and a mean of 3544 m/s. These values are generally lower than velocities for other units measured in this study.

3.7. Petrophysical Summary

This section uses box-and-whisker diagram (Box: median; whiskers: quartiles 1 and 3) to display the range of the petrophysical properties for each rock unit and compare these properties. Estimated mean or median properties can be used as initial values during forward modelling and the range of measurements guides the maximum and minimum values that rock units can vary during property inversions.

A boxplot of density data for all stratigraphic units measured is shown in Figure 3.6, and emphasises the high degree of variability in density measurements for the CMUC. The CMUC-unit 1 displays relative high variability of density values with an interquartile range (IQR) between 2.50 and 2.78 g cm^{-3} and median value of 2.65g cm^{-3}. In contrast, the CMUC- unit 2 has an IQR between 2.74 and 2.94 g cm^{-3} and median value of 2.86 g cm^{-3}. The Oonah Formation, Success Creek and Crimson Creek Formations and Owen Group also display outlying values and relatively large density variations. Anomalous outliers likely do not reflect the true bulk density of these units as these samples likely affected by weathering, alteration or mineralisation affecting the samples. For example, the usual purpose of drilling was to explore mineralised zones which results in obtaining samples near prospective mineral deposits associated with likely alteration and/or thermal interactions with granites and consequently affects the estimation. Precambrian sedimentary basement units (i.e. the Rocky Cape Group, Tyennan region, Togari Group, Arthur MC and Burnie-Oonah Formations) show an IQR between 2.69 and 2.84 g cm^{-3}, higher than that proposed by previous studies as detailed in Table 4.6. CMUC- unit 1 and the Crimson Creek Formation record the minimum and maximum measured densities respectively. Precambrian units, Cambrian and Devonian Granites and the Gordon Group have consistent density values that provide on reliable inputs for modelling these units. The Cambrian Granite displays relative higher density than Devonian Granites.

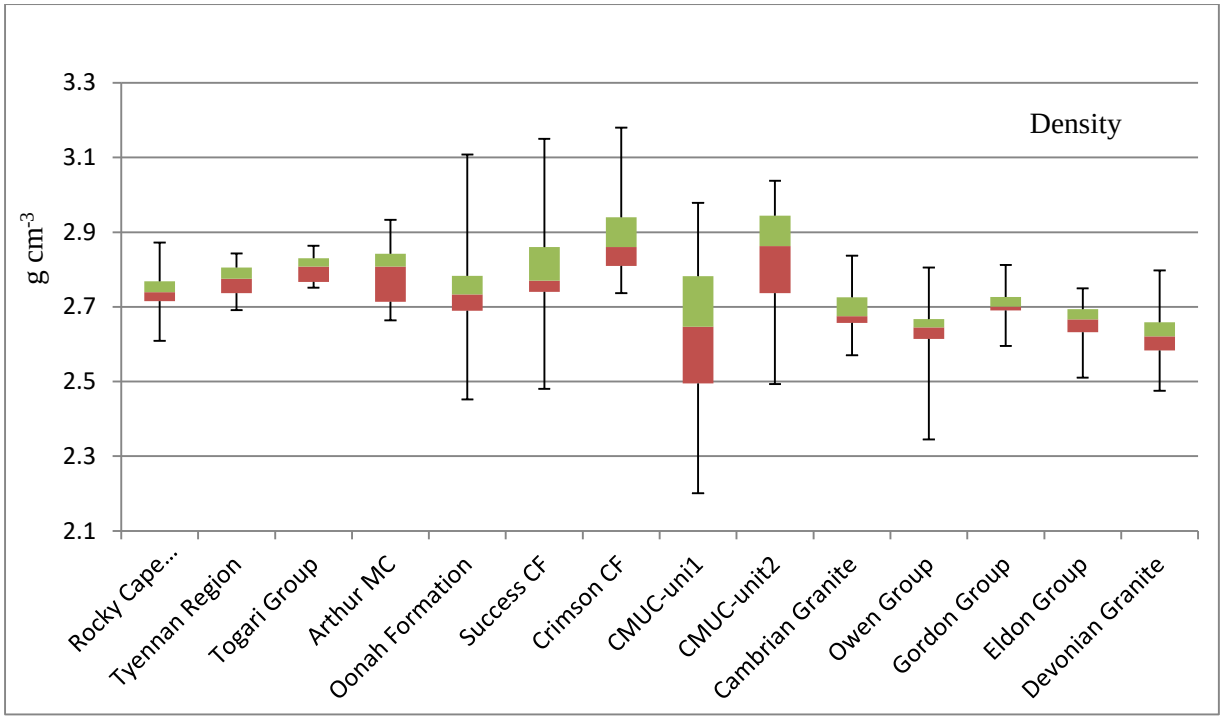

Figure 3. 6 - Boxplot analysis of density measurements represented by stratigraphic units.

Figure 3.7 displays a boxplot summary of the logarithm of magnetic susceptibility for all stratigraphic units. Most units are essentially non-magnetic with median magnetic susceptibilities $< 1 \times 10^{-3}$ SI. Two major units clearly have elevated susceptibility are the CMUC- unit 1 and Cambrian Granites. Some anomalous magnetic susceptibility values are present within the Success Creek and Crimson Creek Formations, but the medians for these rock packages are effectively non-magnetic. The Cambrian Granites unit is magnetic with high range of magnetic susceptibility values and an IQR between 0.25 and 32.7×10^{-3} SI and median of 25.72×10^{-3} SI. CMUC- unit 1 displays high magnetic susceptibility with an IQR between 5.3 and 16.5×10^{-3} SI and the median of 8.5×10^{-3} SI. The Arthur MC, Success Creek and Crimson Creek Formations display a wide range of values and have medians of 0.1×10^{-3}, 0.65×10^{-3} SI and 0.77×10^{-3} SI respectively. All remaining rock units have overlapping susceptibility ranges with IQR's between 0.05 and 3.9×10^{-3} SI and medians between 0.1 and 0.48×10^{-3} SI.

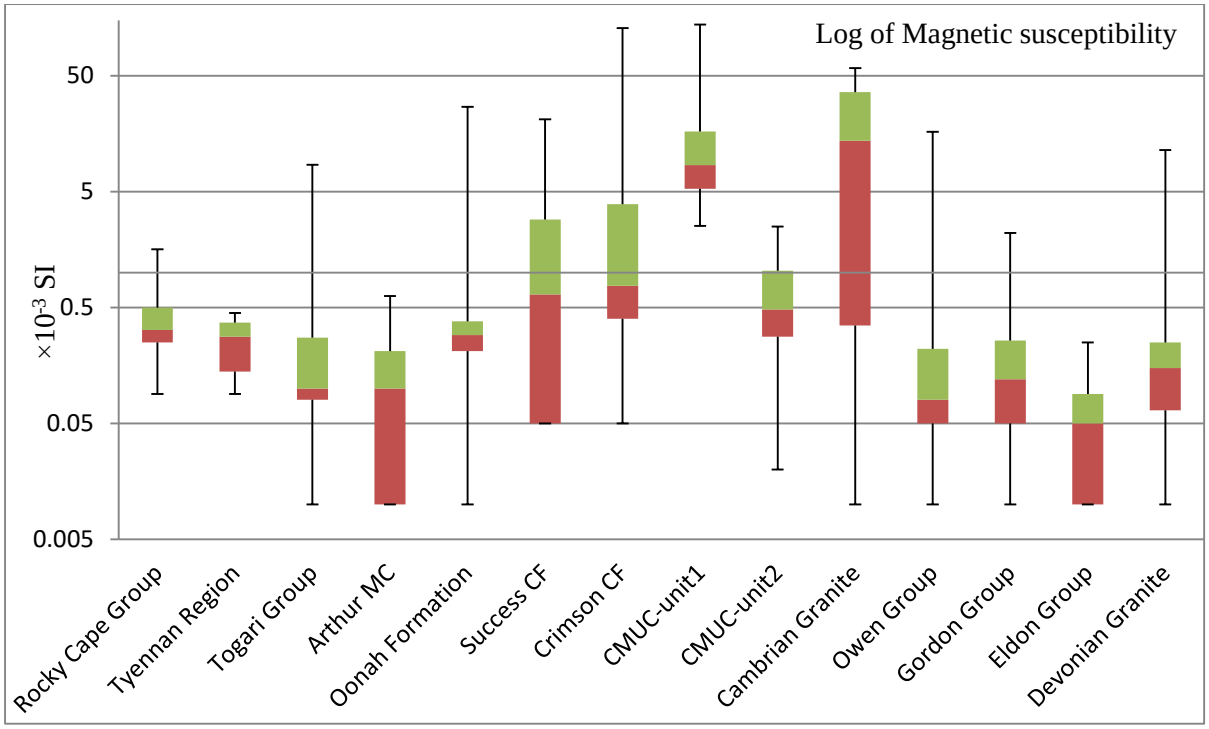

Figure 3. 7 - Boxplot analysis of magnetic susceptibility measurements represented by stratigraphic units.

Figures 3.8, 3.9 and 3.10 illustrate boxplot summaries of seismic velocity measurements and V_p/V_s ratios. The median P-wave velocities are between ~5300 m/s (Devonian Granites) and ~ 6450 m/s (Arthur MC). The S-wave velocities are between ~2950 m/s (Devonian Granites) and ~4100 m/s (Success Creek Formation). The Arthur MC, CMUC and Gordon Group display relatively high P-wave velocities but not significantly elevated S-wave velocities. Devonian Granites display the lowest seismic velocities recorded in this study, and also high variability of V_p/V_s ratios.

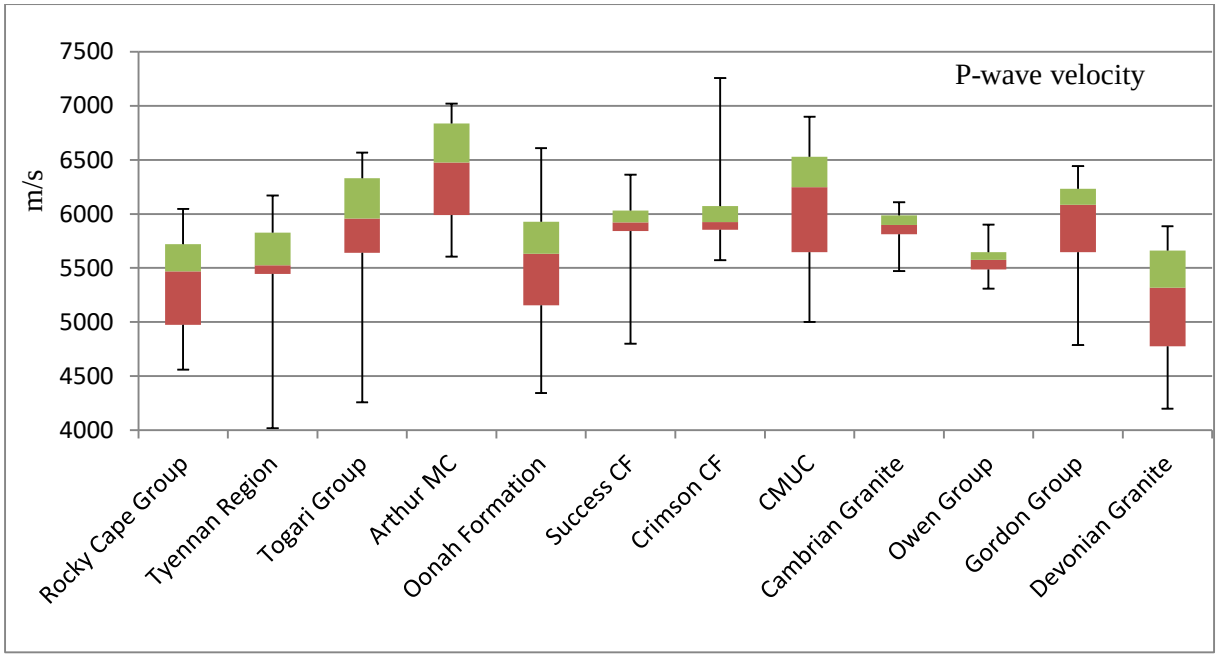

Figure 3. 8 - Boxplot analysis of P-wave velocity measurements (m/s) represented by stratigraphic units.

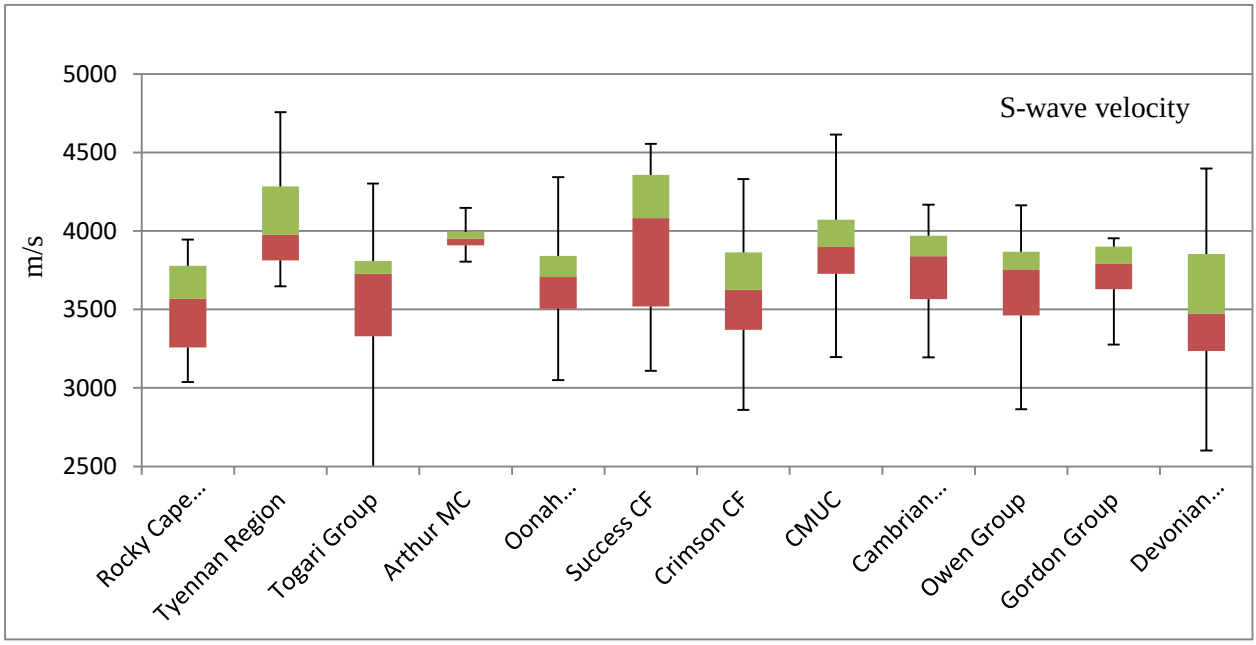

Figure 3. 9 - Boxplot analysis of S-wave velocity measurements (m/s) represented by stratigraphic units.

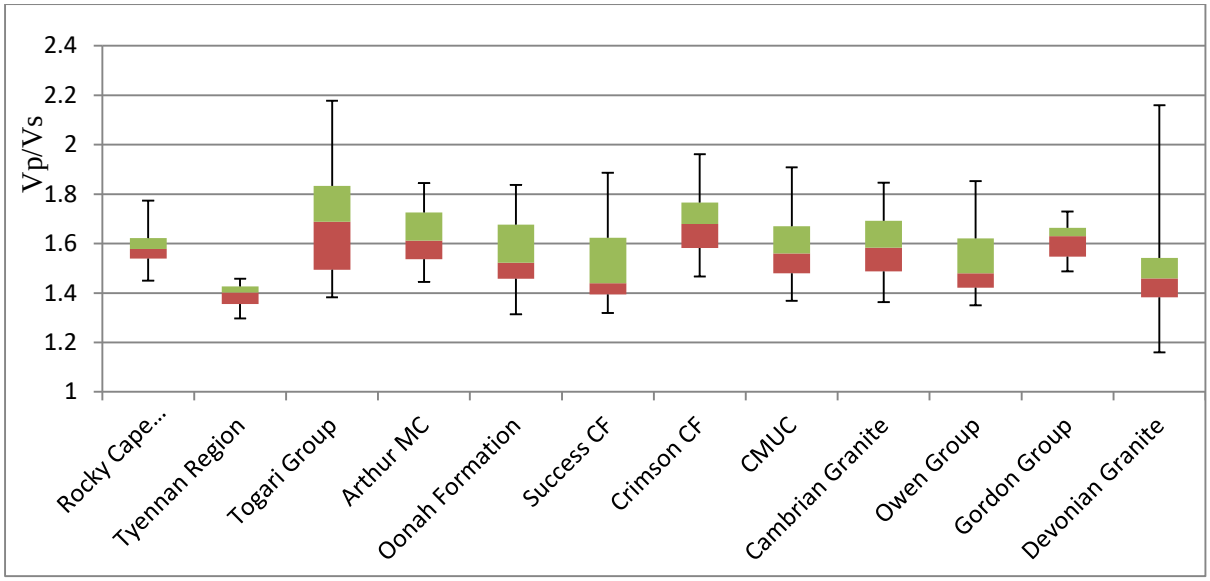

Figure 3. 10 - Boxplot analysis of ratio of P-wave and S-wave velocities represented by stratigraphic units.

A scatter plot of magnetic susceptibility values (logarithmic scale) versus density values (linear scale) for all samples is displayed in Figure 3.11. In order to successfully discriminate individual units in potential field modelling, units must be differentiated based on measured variations in these two physical properties. Three main petrophysical subgroups can be identified on the scatterplot. The Cambrian Granites (dark-blue circle) are distinguished by consistent intermediate density and high magnetic susceptibility. In contrast, the Devonian Granites (red circle) are distinguished by their low density and magnetic susceptibility readings. The CMUC- unit 2 (purple circle), the third obvious subgroup, displays high density and low magnetic susceptibility.

The Success Creek Formation has slightly higher density and magnetic susceptibility values compared to the Crimson Creek Formation. The Rocky Cape Group, Tyennan region, Togari Group, Gordon Group, Arthur MC rocks display significant overlap with medium density and low magnetic susceptibility values. The Owen Group plots as a relatively tight cluster with low densities and magnetic susceptibilities. There is a wide variation in magnetic susceptibility for the CMUC- unit 1, and also a wide variation in density for the non-magnetic Oonah Formation.

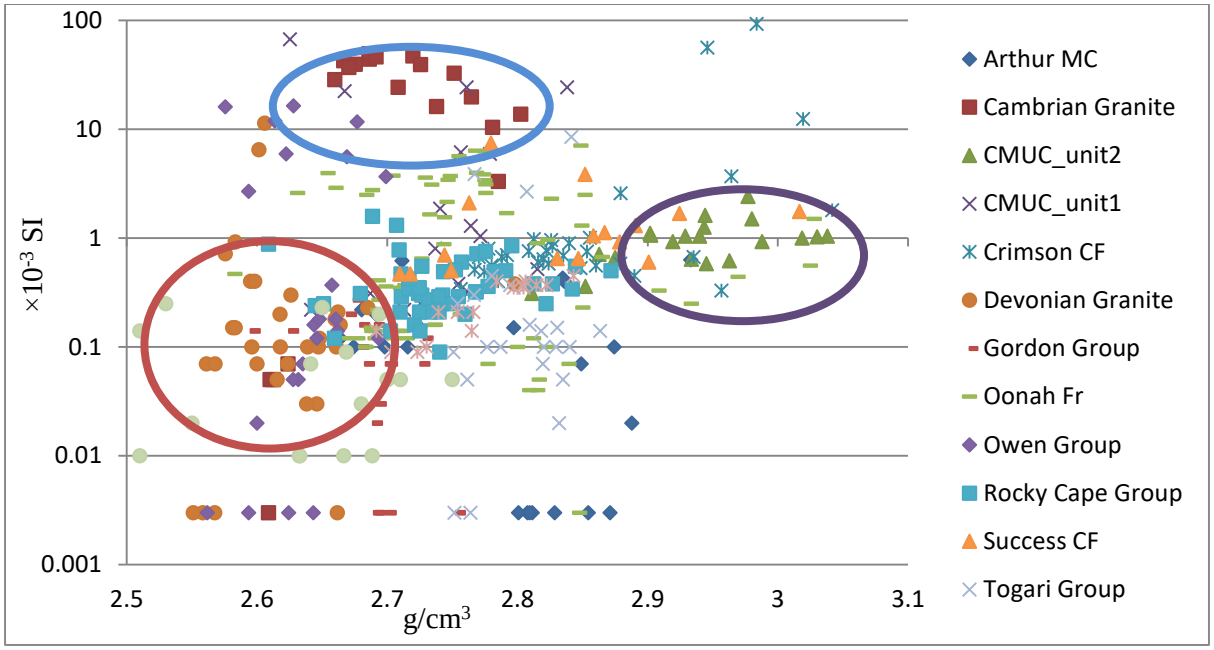

Figure 3. 11 - Scatter plot of magnetic susceptibility measurements ($\times 10^{-3}$ SI) on a logarithmic scale versus density measurement (g cm^{-3}) on a linear scale. Individual stratigraphic units are differentiated by colour as shown in the legend. Blue and red circles represent distribution of the Cambrian Granite and Devonian Granites respectively. Purple circle represents the CMUC- unit 2.

Velocity ratios (V_p/V_s) versus V_p has been reported for a variety of volcanic, igneous, and metamorphic rocks (Christensen, 1996) and sedimentary rocks (Mavko et al., 1998). Figure 3.12 illustrates the V_p/V_s ratio versus V_p values. Tyennan region (green circle) is determined with median P-wave velocities and low V_p/V_s ratios. The Crimson and Success Creek Formations, Owen Group and Rocky Cape Groups show a narrow range of variations. In contrast, the values for the Arthur MC, Oonah Formation, Togari Group, CMUC and Devonian Granites are more scattered with a wide range of values.

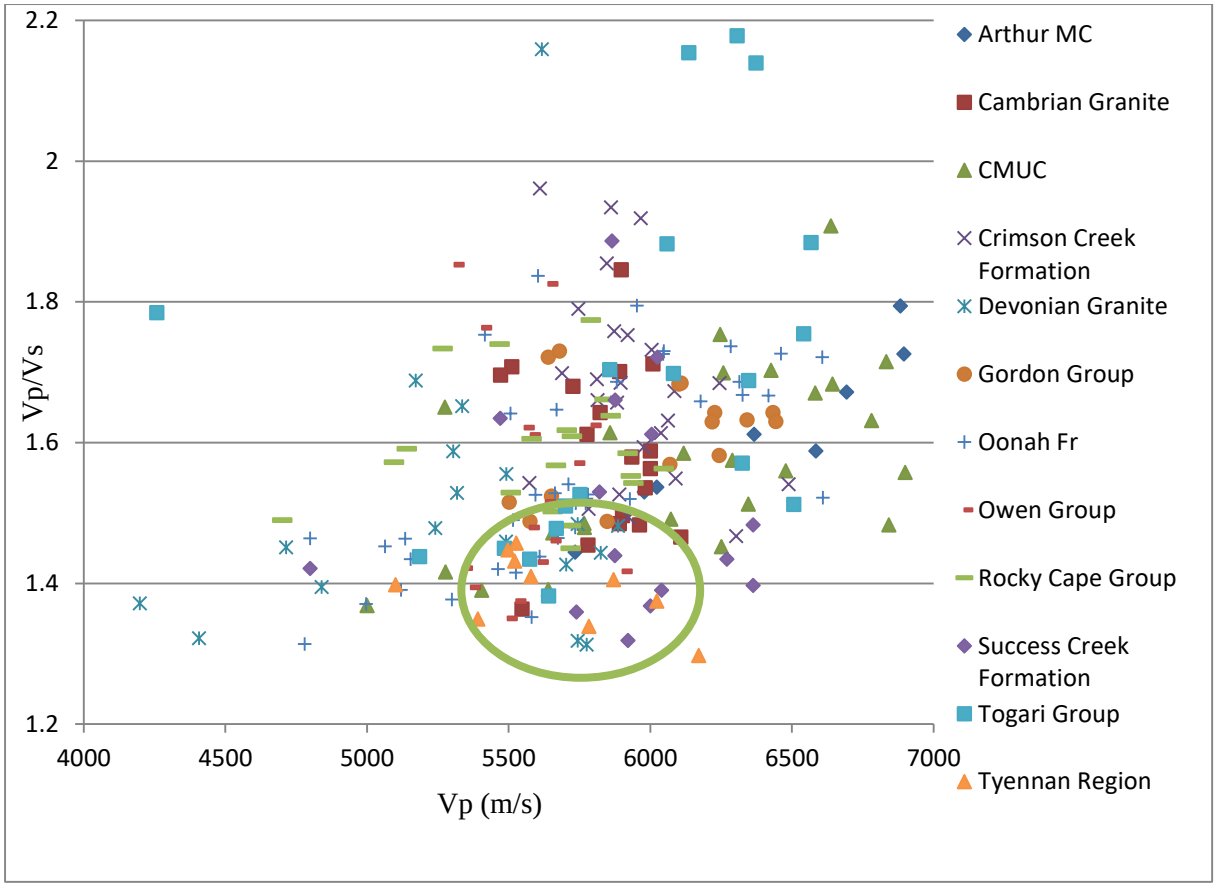

Figure 3. 12 - Scatter plot of V_p/V_s ratio against P-wave velocities measurements (m/s) from drill cores. Green circle represents Tyennan region.

3.8. Summary

Petrophysical properties of rock units from West Tasmania were estimated from measurements carried out in this study integrated with pre-existing measurements. The improved database now contains sufficient number of density and magnetic susceptibility measurements based on limited time and access to samples to properly characterise all the rock units with the exception of the Eldon Group and Tyennan region. For the latter two rock units, the values may be considered as useful reconnaissance estimates that improve on previous knowledge.

The Precambrian Basement units measured in this study display higher density values compared to previous studies as outlined in Table 3.6. In general, magnetic susceptibility measurements match the range of values recorded by previous studies (Table 3.7), although with a wider range of variation. CMUC were divided into two sub-populations: 1) population characterised by generally low density and high magnetic susceptibility and 2) population displaying high density and low magnetic susceptibilities.

For the first time, seismic velocity measurements have been systematically collected to characterise both P-wave and S-wave velocities across West Tasmania. Acoustic velocity estimations in this chapter have been characterised to improve modelling relating to P-wave values while S-wave velocities have been added to the database for future interpretations and are not used in this thesis. P-wave velocities for most rock units broadly lie in a range between ~5400 m/s and 6450 m/s. In contrast, S-wave values lie between ~3450 m/s and 4100 m/s. Anomalous P-wave velocities are apparent for the Arthur MC, CMUC and Devonian Granites. Devonian Granites also display low S-wave velocities. The Success Creek Formation and Tyennan region have relatively greater S-wave velocities across the study area in comparison with other units.

3.9. Estimated properties

The estimated petrophysical values supported from the improved database have been utilised in the potential field modelling of Chapters 5 and 6. These values provide better constraints for the properties of rock units during forward modelling and inversion. There can be a large amount of spatial variability within geological units in properties such as chemical composition, mineralogy and porosity, all of which can affect physical properties. Variations at this scale are not necessarily observed at drill core/ laboratory scale samples and, therefore, I used a range of acceptable properties, including but not limited to those observed in drill holes, for each unit during modelling. Table 3.8 provides a summary of the petrophysical values for each rock unit as determined or assigned in this chapter.

In this chapter, I measured properties of different stratigraphic units consisting of variable rock types and minerals. Therefore, is it not warranted to find stratigraphic units containing identical components in other regions in Australia or globally compared to lithological units measured in this study. However, where it is possible to lithology for global density range, I found that the density range of 2.57—2.67 g cm^{-3} for Devonian Granites and 2.62—2.74 g cm^{-3} for Cambrian Granites are compatible with the global average density range of 2.60—2.72 g cm^{-3} for granites characterised by Olhoeft and Johnson (1989).

Unit	Density (g cm^{-3})		Magnetic Susceptibility ($\times 10^{-3}$ SI)		P-wave velocity (m/s)		S-wave velocity (m/s)	
	Value	SD	Value	SD	Value	SD	Value	SD
Rocky Cape Group	2.74	0.05	0.415	0.29	5356	462	3539	279
Tyennan region	2.77	0.04	0.265	0.13	5498	576	4068	339
Togari Group	2.80	0.03	0.100	1.92	5900	555	3546	485
Arthur Metamorphic Complex	2.79	0.08	0.161	0.19	6378	513	3948	100
Burnie-Oonah Formations	2.74	0.09	0.588	1.59	5585	553	3678	253
Success Creek Formation	2.80	0.10	0.650	3.79	5895	383	3943	480
Crimson Creek Formation	2.88	0.10	7.250	19.92	6057	420	3617	371
Cambrian Mafic-Ultramafic Complex	2.73	0.23	10.290	14.82	6087	551	3916	306
CMUC- unit 1	2.65	0.19	14.451	16.08	-	-	-	-
CMUC- unit 2	2.86	0.14	0.745	0.66	-	-	-	-
Cambrian Granites	2.68	0.06	25.720	17.20	5873	167	3780	269
Owen Group	2.63	0.07	0.080	3.52	5578	165	3648	366
Gordon Group	2.71	0.04	0.280	0.44	5929	438	3733	218
Eldon Group	2.64	0.07	0.070	0.08	-	-	-	-
Devonian Granite	2.62	0.05	0.390	1.19	5223	497	3543	552

Table 3. 8 - Estimated properties utilised in this study for rock units across West Tasmania. The Cambrian Mafic-Ultramafic Complexes are divided into two subunits of the CMUC- unit 1characterised by low density and high magnetic susceptibility properties and the CMUC- unit 2 characterised by high density and low magnetic susceptibility properties.

Chapter 4 - The onshore and offshore tectonic structure of Tasmania from 3D gravity modelling

4.1. Abstract

The tectonic structure of Tasmania is an area of current geological controversy. In general, Tasmania can be divided into the Western Tasmanian Terrane, of Precambrian origin, and the Eastern Tasmanian Terrane with Phanerozoic outcrop. Current estimates of crustal depth and composition beneath Tasmania have primarily been determined using seismic techniques (AuSREM model), however, a significant amount of updated gravity data are now available, providing a complementary means of studying deep structures. The study of deep tectonic structures in Tasmania is not straightforward geophysical undertaking due to the need to work across onshore and offshore regions, at a scale intermediate between continental and local investigations. In this study we compile more than 700,000 gravity observations and calculate the complete Bouguer Anomaly in order to investigate the density of the crust and uppermost mantle across onshore and offshore Tasmania and Bass Strait. The complete Bouguer Anomaly was used to generate 3D geometry and property inversions to refine Moho depth and density distributions. We performed several geometry inversions of Moho depth based on seismic Moho estimations to find the most representative and credible surface and density distribution. Moho depths generated by geometry inversions were systematically evaluated by a series of densities assigned to the lower crust to invert the properties of the upper crust. Inversion results show that existing seismic derived Moho depths are not compatible with the gravity Moho. We find that the seismic Moho is at a shallower depth across onshore Tasmania. The crustal thinning beyond the unstretched continental crust limit is not honoured in AuSREM model, while the gravity Moho surface clearly delineates this trend. Crustal thinning across Bass Strait is supported in our model with the gravity Moho surface displaying a shallower Moho depth than the AuSREM model. The final model indicates that the lower crust in Tasmania has an anomalously low average density which might suggest dominantly felsic composition of the lower crust.

4.2. Introduction

Tasmania exhibits rocks that range in age from 1450—1330 Ma (Halpin et al., 2014) to the current era. Onshore Tasmania is divided into two major geological domains, the Western Tasmanian Terrane (WTT), and the Eastern Tasmanian Terrane (ETT) (Chappell et al., 1988; Williams, 1989). The Tamar Fracture System is proposed as the boundary between the WTT and the ETT (Leaman et al., 1994; Rawlinson et al., 2010; Reed, 2001; Williams, 1989; Young et al., 2011).

The Mohorovičić discontinuity (Moho), the boundary surface between the Earth's crust and the mantle, defines transitions in the physical properties of the crust such as seismic wave velocity and density variations. The nature and geometry of the Moho across Tasmania has been the focus of seismic studies in both continental scale (e.g. Kennett and Salmon, 2012; Kennett et al., 2011; Salmon et al., 2013), and regional scale (e.g. Michibayashi et al., 2012; Rawlinson et al., 2001b; Rawlinson et al., 2001a; Rawlinson et al., 2010; Rawlinson and Urvoy, 2006; Young et al., 2011). Tectonic elements beneath Bass Strait and offshore east and west Tasmania have also been studied using passive seismic data (e.g. Drummond et al., 2000; Petkovic, 2004; Pilia et al., 2015a and 2015b). Seismic stations are relatively densely distributed across north and east Tasmania, while a low number of stations are available in south and southwest onshore and offshore Tasmania, leading to high uncertainty in these areas (Kennett and Salmon, 2012). Furthermore, the seismic Moho surface does not indicate crustal ocean-ward thinning in offshore regions.

Gravity data across onshore Tasmania have been compiled at both regional and local scales. The Tasmanian residual responses are calculated using various regional models (i.e. MANTLE88, MANTLE91, MANTLE07 and MANTLE09) (Leaman, 1988, 2009; Roach et al., 1993). State-scale models of crustal thickness using gravity data were first produced by Leaman and Richardson (1989b) and followed by Roach (1994) who compared techniques for calculation and removal of regional gravity fields. At these local scales, upper crustal architectures have been studied through integration of gravity and magnetic models (e.g. Leaman, 2003; Leaman and Richardson, 1989a, 2003; Webster, 2003).

In this study, Moho depth and the unstretched continental crust limit (UCCL) of Tasmania are investigated using models generated from gravity data. These gravity datasets, in contrast to data derived from the seismic networks mentioned above, are collected at a high spatial resolution and offer regular coverage across onshore and offshore Tasmania. A range of

different Moho surfaces, sourced from offshore gravity inversion (Kusznir, 2008), AuSREM seismic Moho depth (Kennett and Salmon, 2012), seismic sections (Drummond et al., 2000; Kennett et al., 2013) and the Airy Isostatic Moho, are assessed in order to generate a precise Moho surface. Tectonic structures derived from previous continental scale gravity studies (i.e. Aitken, 2010; Aitken et al., 2015; Aitken et al., 2013) are incorporated into our regional scale models as a means of assessing the tectonic context of Tasmania and surrounding offshore regions. In this research the inverted Moho depth, based on the Bouguer gravity data, is called the gravity Moho surface.

4.3. Tectonic background

The study area encompasses onshore Tasmania and offshore regions including Bass Strait and parts of the Tasman Sea, Otway and Sorell Basins and the South Tasman Rise (Figure 4.1). Across onshore Tasmania, the WTT comprises large areas of exposed Meso- to Neoproterozoic basement with a Late Paleoproterozoic mantle extraction age within the lower crust (Berry et al., 2008). In contrast, Palaeozoic rocks dominate the ETT with no outcrops of Proterozoic basement (Reed, 2001). The WTT rifted from the Proterozoic Australia-Antarctica margin in the Late Proterozoic and reattached to the ETT by the Early Ordovician (Berry et al., 2008) or Early to Middle Devonian (Reed, 2001). Cayley (2011) linked western Tasmania to perhaps south China, whereas Gibson et al. (2011) suggest it was part of the southern margin of Victoria Land, Antarctica. More recently, Halpin et al. (2014) and Mulder et al. (2015) identified similarities between the WTT and western North America. In contrast, eastern Tasmania shares an affinity with the Lachlan Fold Belt of southeast Australia (Reed, 2001). Granitoid intrusions are emplaced across large areas of northeast Tasmania and parts of western Tasmania during the Devonian, prior to and following the Tabberabberan Orogeny (Black et al., 2005).

Within offshore regions of the study area, the Bass, Sorell, Otway, Durroon and Gippsland Basins are extensional sedimentary basins with thick sequences of Late Mesozoic-Cainozoic aged rocks. The Bass, Durroon and Sorell Basins were initiated due to extension related to rifting between Australia and Antarctica; forming failed arms of the Southern Margin Rift System (SMRS) in the latest Jurassic to Early Cretaceous (Seymour and Calver, 1995). The Otway and Sorell Basins evolved through repeated episodes of extension, thermal subsidence and inversion during the breakup of eastern Gondwana from the Middle Jurassic to the Cainozoic (Stagg et al., 1990). The Otway, Gippsland and Bass Basins developed as an extensive series of half-grabens, associated with failed rifting in the Cretaceous that resulted in

crustal thinning in Bass Strait (Palmowski et al., 2004; Stagg et al., 1999; Veevers, 1986). Features associated with rift failure and consequent crustal thinning beneath Bass Strait are detected as a high velocity seismic anomaly (Pilia et al., 2015b). Across the Tasman Sea, seafloor spreading started from ~84 Ma and continued to ~53.3 Ma resulting in the separation of the Lord Howe Rise from eastern Australia (Betts et al., 2002; Gaina et al., 1998).

The tectonic evolution of Tasmania and Bass Strait remains an active area of investigation. Cayley (2011) proposed a Proterozoic microcontinent of VanDieland comprising Tasmania, Bass Strait, central Victoria and adjacent oceanic plateaus (e.g. South Tasman Rise continental fragment), which combined to form Tasmania and parts of southeast Australia during the Cambrian and Silurian. The link between northwest Tasmania and south central Victoria is supported by 3D shear wave-speed models (Pilia et al., 2015b).

The UCCL and continental-oceanic boundary (COB) of the southern part of the Australia, including Tasmania have been investigated in many studies. Eagles et al. (2015) generated more than 20 estimates of COBs from various sources for Australia. In addition, Scher et al. (2015) delineated the innermost and outermost possible COBs in southern Australia. Williams et al. (2011) investigated the boundary between stretched and unstretched continental crust in southern Australia. The continental margin in Tasmania is thought to be relatively narrow, with a uniform continental shelf width of less than 100 km. This includes a sharp transitional zone (~10–20 km wide) from the average crustal thickness to highly thinned continental and oceanic crust (Brown et al., 2003).

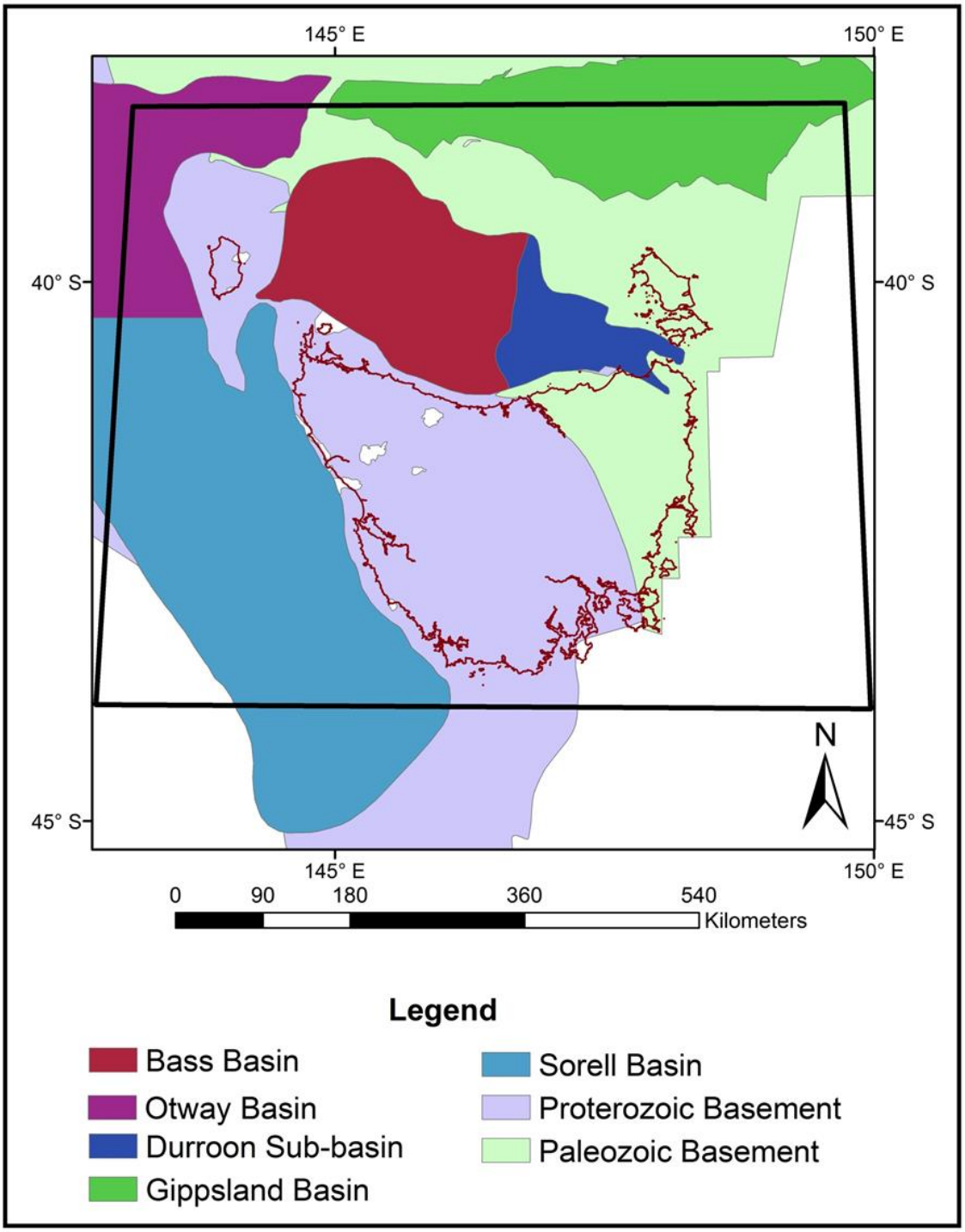

Figure 4. 1 - Map of the study area showing the major basement and basin features mentioned in the text (1:1 million geology map of Australia: Geoscience Australia- Raymond, 2012). The study area is shown with black polygon referring to the green rectangle in Figure 1.1. The exact geographic extent of the area used in the modelling in this chapter is listed in the caption to Figure 4.2 and following figures in Chapter 4 have the same spatial extent as that indicated by the box.

4.4. Gravity data processing

Over 700,000 gravity observations were compiled from various sources (Table 4.1). Collected data were processed for latitude, free-air and Bouguer correction. While most other studies have used free-air data, the topography effects result in uncertain geological and tectonic interpretations. To minimise this uncertainty, we calculated the complete Bouguer Anomaly by applying terrain corrections to onshore and offshore gravity data. For the Bouguer correction, we chose average densities of 2.67 g cm^{-3} for crustal rocks and 1.03 g cm^{-3} for water. A topography grid with 25 m resolution for onshore data, and 250 m spaced topography-bathymetry grid for offshore data have been used for the terrain correction. The terrain correction was calculated for a radius of 167 km to minimise the effects of the difference between the spherical cap and infinite horizontal slab (Nowell, 1999). The terrain correction varies between 0.05 and 142.86 mGal in this study. The Bullard B correction was calculated for onshore gravity data to account for the curvature of the Earth (Nowell, 1999).

Gravity data	Reference	Description
Onshore Tasmania	MRT	Gravity observation from MRT online database (2016)
Bass Strait marine	GSV	Data compiled by GSV and provided by Mark Duffett from MRT
West offshore Tasmania	GA	Data is provided by Michael Morse from GA
East offshore Tasmania	NOAA	Data for each ship track is downloaded separately and compiled into one database from NOAA (2016)

Table 4. 1 - Details of the gravity data compiled for this study and their sources (MRT: Mineral Resource Tasmania; GSV: Geology Survey of Victoria, GA: Geoscience Australia, NOAA: National Oceanic and Atmospheric Administration).

4.5. Initial model construction

The modelled area encompasses a region of 621 km × 577 km × 60 km, extending from 142° 46’ 50” to 149° 58’ 11” longitude and from -38° 20’ 29” to -43° 57’ 39” latitude (GDA94 datum) discretised into 1 km × 1 km × 0.5 km voxets. The onshore topography and offshore bathymetry grids (250 m cell resolution) were used to constrain the upper surface of the model. The model comprises seven layers: sediments, igneous intrusions in the Bass Basin, upper and lower crust within the UCCL, upper and lower crust beyond the UCCL, and a mantle

component.

4.5.1. Sedimentary basins

The SEEBASE^{TM} model (Oz SEEBASE^{TM}, 2005) was used as the lower boundary of the sedimentary basins. This boundary was fixed during modelling and did not vary. While Aitken (2010) used a constant density for sedimentary basin, Aitken et al. (2013) determined three different densities for sediments as a function of their burial depth. We applied both constant (2.40 g cm^{-3}) and variable densities (2.40—2.60 g cm^{-3}) during modelling.

4.5.2. Igneous intrusive rocks

Potential field anomalies in the Bass Basin within the Bass Strait have been ascribed to widespread mafic intrusions that were emplaced during the Mesozoic-Cainozoic (Cummings et al., 2004). Tasmania and parts of Bass Strait are affected by the intrusion of large volumes of dolerite and in some cases basalt extrusions overlying Late Triassic sediments at ~174 Ma (Burrett and Martin, 1989). Across the Bass Basin, high amplitude gravity observations are due to a combination of high density intrusions and crustal thinning. These intrusions are either part of the major Jurassic tholeiitic dolerite intrusions (Moore et al., 2013), common throughout eastern and northern Tasmania, or related to mantle depressurisation that occurred during basin extension and crustal thinning (Gunn et al., 1997). Across the Bass Basin, we placed a mafic body above the lower boundary of sedimentary basin consistent with sections presented by Cummings et al. (2004) and adjust its geometry using inversion of magnetic data.

4.5.3. UCCL and COB

Williams et al. (2011) used the shelf break as the most ocean-ward possible extent of the UCCL. Hence, we defined the shelf break as the UCCL boundary from the high resolution (250 m) bathymetry data. In the model generated by Eagles et al. (2015) the COB was placed beyond the extent of the study area. In our model, however, we considered the possibility of oceanic crust within the study area, which is discussed in the modelling and results sections.

4.5.4. Upper and lower crust

Aitken (2010) defined the upper-lower crust boundary as half of the Moho depth, while Aitken et al. (2015) predicted isosurfaces estimating the depth of upper-middle and lower crusts across Australia. Isosurfaces by Aitken et al. (2015) are not compatible with other boundaries across

the study area and are shallower than the SEEBASE^{TM} throughout Bass Basin and some other regions. Furthermore, the depth to a certain threshold in isosurfaces is not numerically reliable due to the vertical bias in the inversion and uncertainty in the AuSREM input model. Therefore, we defined the upper-lower crust boundary as half of the Moho depth.

According to Aitken et al. (2015), the depths of the densities of 2.75 g cm^{-3} and 2.8 g cm^{-3} isosurfaces are proxies for the base of the felsic upper crust and the top of the mid-crust in continental scale respectively. Seismic investigations by Drummond et al. (2000) and gravity modelling by Aitken et al. (2015) postulate the presence of a felsic middle to lower crust in Tasmania. Aitken (2010) also calculated a Tasmanian crustal density that is 1–2% lower than the Delamerian and Lachlan Orogens. Aitken et al. (2013) suggested an average crustal density anomaly of ~1–1.5% for western Tasmania and -0.5–-1% for east Tasmania. In a previous study, Leaman (1988) concluded that negative features on Bouguer anomaly data may be related to post Cretaceous sedimentation or granite intrusions.

4.5.5. Moho depth

A variety of Moho surfaces have been assessed in this study. Continental scale AuSREM (Kennett and Salmon, 2012) and state scale seismic (Rawlinson et al., 2010) Moho surfaces were used as initial constraints. Geometry inversion of the gravity data produced a Moho surface that was relatively poorly correlated with the seismic Moho. We used local seismic profiles from offshore Tasmania (Drummond et al., 2000; Kennett et al., 2013), seismic stations (e.g. Kennett and Saygin, 2015; Kennett et al., 2015; Rawlinson and Urvoy, 2006) and offshore gravity Moho estimation (Kusznir, 2008) to validate the final gravity Moho surface.

The Airy Isostatic Moho depth was calculated across the study area based on the Airy-Heiskanen model (Heiskanen and Moritz, 1967; Simpson et al., 1986). For the Airy Isostatic calculation, the initial crustal thickness of 32 km, a density contrast of 0.60 g cm^{-3} between crust and mantle and average crustal density of 2.67 g cm^{-3} have been used following Fitzgerald et al., (2009). The Airy Isostatic Moho surface displays the effect of crustal thickness and is several kilometres deeper than AuSREM surfaces in onshore regions.

We defined the mantle component that extends from the Moho, to beneath the cut-off depth of the study (60 km, Figure 4.2). The density of the mantle across the study area is thought to be between 3.22 g cm^{-3} to 3.25 g cm^{-3} (Aitken et al., 2015). In this study, the density of model components representing sedimentary units ranges between 2.40 and 2.60 g cm^{-3}following

Aitken et al., (2015). The density of the upper crust varies between 2.57 and 2.85 g cm^{-3} and a range of 2.65–2.95 g cm^{-3} is assigned to the lower crust based on geological and tectonic knowledge and the mantle is assigned a homogeneous density of 3.230 g cm^{-3} following model by Aitken et al., (2015).

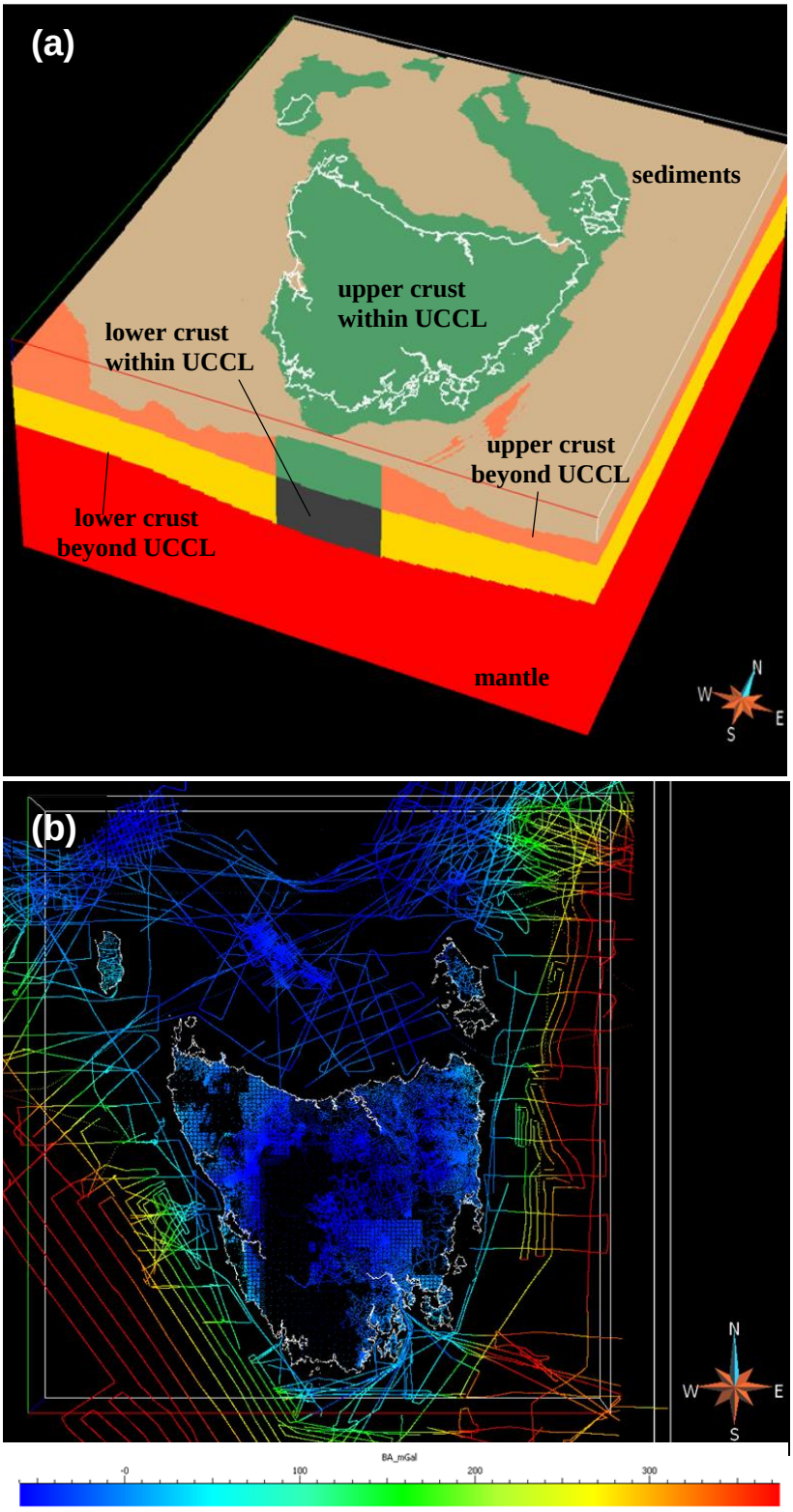

Figure 4. 2 – Initial model and gravity observations; (a) study area displaying modelled tectonic units (× 5 vertical exaggerations; down to 60 km depth) and the Tasmania coastline for reference. The mafic intrusive body in the Bass Strait occurs beneath the sedimentary basin and above the top of the upper crust. (b) Bouguer gravity observations across the study area (-60—375 mGal). The shelf break is defined as the unstretched continental crust limit (UCCL). Coordinates of the study area are 142° 46’ 50” longitude and-43° 57’ 39” latitude for the southwest corner and 149° 58’ 11” longitude and -38° 20’ 29” latitude for the northeast corner. This figure and subsequent 3D models are interactive GOCAD environment and are documented in the appendix.

4.6. Gravity inverse modelling

We used the Paradigm GOCAD (Mallet, 1992; http://www.pdgm.com) Version 2009.4 to generate and modify the 3D model and VPmg Version 7.1 (Fullagar, 2013; Fullagar et al., 2008) to carry out inversions. In VPmg, 3D inversion methods, used upon geologically-constrained models, are geometry and property inversions of potential field data. In a geometry inversion, the boundaries of geological units are allowed to move, following some constraints, to achieve the acceptable fit between responses calculated from the model and observed data. In contrast, a property inversion consists of a homogeneous inversion and a heterogeneous inversion. In a homogeneous inversion, the property of one or more geological units change, subject to upper and lower bound constrains, to improve the data fit. In a heterogeneous inversion each cell within the geological units is allowed to vary to improve the fit (Fullagar 2013, Fullagar and Pears 2007, Fullagar, et al. 2004).

To mitigate edge effects in modelling in this study, data within 7 degrees of the study area bounds are removed from the model before inversion. Multiple geometry and/or property (density) inversions were performed that tested different hypotheses for crustal thinning or thickening and variations in crustal components. The initial models, summarised in Table 4.2, are seismic AuSREM Moho model (Model-S) and Airy Isostatic Moho model (Model-A). Output models have been assessed to refine a new Moho depth reconcilable with gravity data. In this study the resulting models using geometry inversion have “Gx” suffix and models with “Px” suffix refer to property inversion. During geometry inversion, data were filtered using an upward continuation of 15 km to obscure the effects of shallow-burial depth features and enhance major, deep density contrasts (i.e. the Moho surface). A geometry inversion of the Moho, allowing a maximum 100% change of Moho depth compared to the initial model, was performed (initial Model-S; output Model-Sa-Gx). This geometry inverted model fits with offshore Moho surfaces proposed by Kusznir (2008) and is not compatible with the AuSREM Moho. Seismic Moho surfaces do not display crustal thinning beyond the UCCL which results in high uncertainty across these regions. Compared to the AuSREM Moho surface, this initial inverted gravity Moho surface is generally deeper within the UCCL and shallower beyond this boundary. The Airy Isostatic model displays a more compatible Moho depth compared to the geometry inverted from gravity data, representing thinning beyond the UCCL (initial Model-A: output Model-A-Gx). Geometry inverted outputs are relatively consistent with offshore seismic sections (Drummond et al., 2000; Kennett et al., 2013), and deployed seismic data across wet of the Tasman Sea. The inconsistency between the AuSREM and gravity Moho

surfaces could be due to the inherent uncertainties within seismic and gravity methods and models. These surfaces might also differ because of the assignment of inaccurate density values to tectonic units, uncertainty in geometry of other tectonic boundaries, or inaccurate interpolation of sparse seismic data. The possibility of onset of oceanic crust within the study area was investigated by assigning properties matching those of typical oceanic crust beyond the UCCL (initial Model-S; output Model-S-Gx-OceanicCrust).

To investigate the accuracy of P-wave derived values the AuSREM crustal model of Salmon et al. (2012) was used to convert P-wave velocities to densities using the empirical relationships established by Brocher (2005) and Ludwig et al. (1970). Forward modelling of calculated densities from P-wave velocities indicates a discrepancy between calculated and observed gravity values (Figure 4.3). These high misfits (root mean squared (RMS) errors >200 mGal) across the study area imply either the proposed relationships between velocity and density are not accurate or the AuSREM seismic model is not robust in Tasmania.

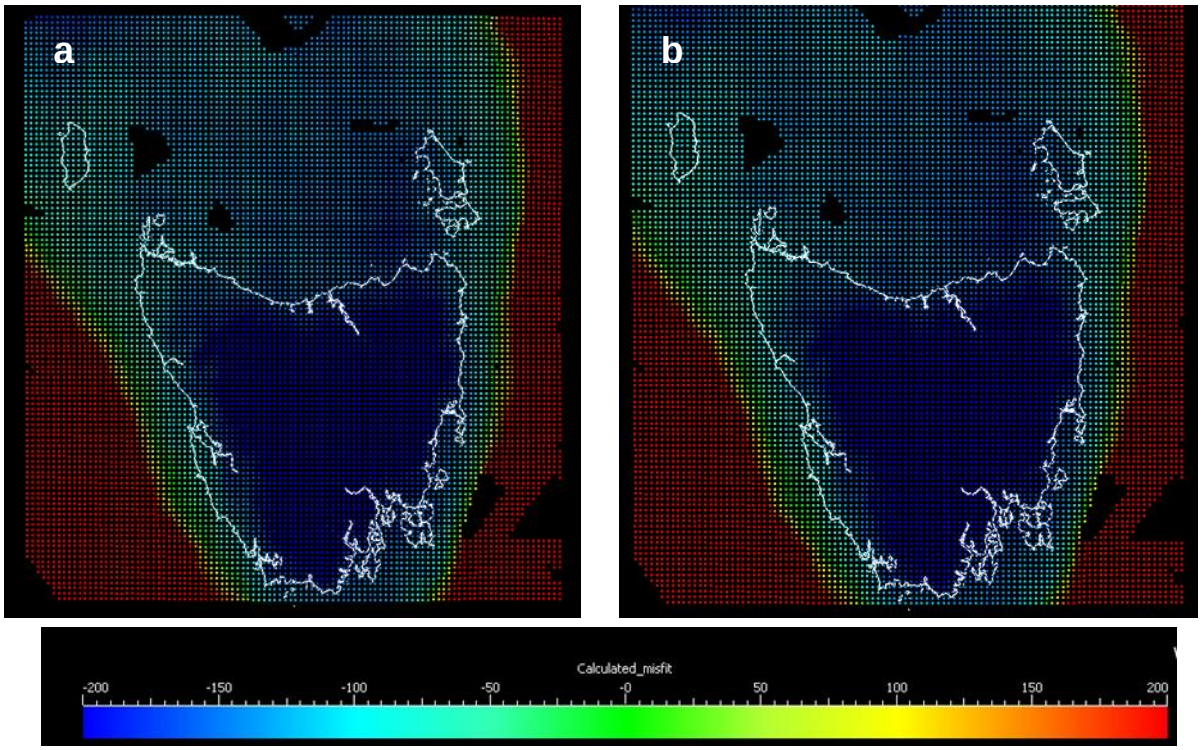

Figure 4. 3 - The misfit (mGal) between observed gravity and calculated gravity from density model extracted from seismic data using empirical relationship presented by a) Brocher (2005) formula; and b) Ludwig et al (1970) formula. Tasmanian coastline is shown as a guide for the scale and coordinates.

Property inversions for different Moho surfaces in this study were performed on AuSREM (initial Model-S.1; output Model-S-Px) and Airy Isostatic Moho surfaces (initial Model-A; output Model-A-Px). After heterogeneous inversions, low values of permitted densities (< 2.60 g cm^{-3}) were typically assigned to the crust within the UCCL and high density values (> 2.80 g cm^{-3}) to the component beyond the UCCL. These density values imply an adjustment of the geometry of the Moho surface is required to allocate representative density values to the crust.

Geometry and property inversions emphasize that a simple inversion using one of these methods does not adequately represent the Moho surface and crustal density variations across the study area. Hence, a new series of geometry and property inversions were performed to determine the gravity Moho surface and density variation. The goal was to find the geometry of Moho which resulted in a likely, or informative, density distribution within the upper crust. Multiple geometry inversions with various adjustments regarding the original AuSREM seismic Moho were performed and modelled surfaces were systematically evaluated by assigning three densities, 2.65, 2.70 and 2.75 g cm^{-3}, to lower crust and performing heterogeneous property inversions of upper crustal bodies (Table 4.2). Low density ranges assigned to the lower crust (2.65-2.75 g cm^{-3}) are interpreted based on initial property inversions. The first geometry inverted model with minimum change compared to the AuSREM model which displays representative density values to the upper crust was chosen as the gravity Moho surface. This model should display the minimum deviation from the reference model and be compatible with geological and tectonic understandings.

Initial model	**Aim**	**Initial comments**	**Inversion results**	**Output model**
Model-S	Geometry inversion of AuSREM Moho	Geometry inversion (max 100% deviation from constrained-model). Homogeneous crust with a density of 2.67 g cm^{-3} (RMS misfit of forward model ~ 102.8 mGal).	Model shows deeper Moho surface within the UCCL and shallower beyond the UCCL. Moho looks very different compared to the constrained seismic model (RMS misfit ~ 13.58 mGal)	Model-Sa-Gx
Model-S	Assess possibility of oceanic crust	Geometry Inversion, assigning properties of the oceanic crust (ρ=2.95 g cm^{-3}) to the crust beyond the UCCL (RMS misfit of forward model ~ 46.59 mGal)	The depth of the crust (depth >18 km) shows the presence of oceanic crust within the study area is unlikely (RMS misfit ~ 20.3 mGal)	Model-S-Gx-OceanicCrust

Model-S.1 (Lower resolution of 'Model 1", 1.5 km cell-size)	Property inversion of AuSREM Moho	Heterogeneous inversion of the crust (density ranges -0.10 to 0.28) (RMS misfit of forward model ~ 102.8 mGal)	Density histograms show most densities are around minimum or maximum bounded values (RMS misfit ~ 17.2 mGal).	Model-S-Px
Model-A (Isostatic Moho Surface)	Geometry inversion of the Isostatic Moho	Geometry inversion of Moho (100% max deviation from the initial model) (RMS misfit of forward model ~69.7 mGal)	Model is compatible with initial model beyond the UCCL and is deeper across onshore Tasmania. Initial model does not show crustal thinning in the Bass Strait (RMS misfit ~19.4 mGal)	Model-A-Gx
Model-A	Property inversion of the Isostatic Moho	Heterogeneous inversion of the crust (ranges -0.1 to 0.28)	Density histograms shows density are predominantly around 2.57 g cm^{-3} or 2.83 g cm^{-3} (RMS misfit ~ 13.2 mGal)	Model-A-Px
Model-S	Geometry inversion	Geometry inversion of Moho with maximum 10% variations	Inversion shows 69.35 mGal RMS misfit.	Model-Sb-Gx-10%
Model-Sb-Gx-10%	Property inversion of Model-Sb-Gx-10%	Heterogeneous inversion of the crust	Very low densities to the crust within the UCCL and anomalously high densities beyond the UCCL (RMS misfit 11.5 mGal).	Model-Sb-Px
Model-S	Geometry inversion	Geometry inversion of the Moho with maximum 15% variations	Inversion shows 49.97 mGal RMS misfit.	Model-Sc-Gx-15%
Model-Sc-Gx-15%	Property inversion of Model-Sc-Gx-15%	Heterogeneous inversion of the upper crust (density of lower crust is homogeneous and 2.75 g cm^{-3})	Density distribution shows that the geometry of the model needs more adjustment upon gravity observations or lower densities are required for the lower crust (RMS misfit ~ 16.2 mGal)	Model-Sc- Px-1

Model-Sc-Gx-15%	Property inversion of Model-Sc-Gx-15%	Heterogeneous inversion of the upper crust (density of lower crust is homogeneous, 2.65 g cm^{-3})	Low density of the lower crust does not compensate the low densities within the upper crust. Geometry needs further adjustment (RMS misfit ~ 15 mGal)	Model-Sc-Px-2
Model-S	Geometry inversion	Geometry inversion with maximum 25% variations	Inversion shows 36.77 mGal RMS misfit.	Model-Sd-Gx-25%
Model-Sd-Gx-25%	Property inversion of Model-Sd-Gx-25%	Heterogeneous inversion of the upper crust (density of lower crust is homogeneous, 2.70 g cm^{-3})	The upper crust shows very low densities in onshore Tasmania (RMS misfit ~ 15.8 mGal)	Model-Sd-Px-1
Model-Sd-Gx-25%	Property inversion of Model-Sd-Gx-25%	Heterogeneous inversion of the upper crust (density of lower crust is homogeneous, 2.65 g cm^{-3})	Very low densities are distributed within onshore Tasmania (RMS misfit ~16.6 mGal)	Model-Sd-Px-2
Model-S	Geometry inversion	Geometry inversion with maximum 30% variations	Inversion shows 23.18 mGal RMS misfit.	Model-Se-Gx-30%
Model-Se-Gx-30%	Property inversion of Model-Se-Gx-30%	Heterogeneous inversion of the upper crust (density of lower crust is homogeneous, 2.70 g cm^{-3})	Distributed low densities shows either low densities of the lower crust are needed or the geometry is not credible (RMS misfit ~14.8 mGal).	Model-Se-Px-1
Model-Se-Gx-30%	Property inversion of Model-Se-Gx-30%	Heterogeneous inversion of the upper crust (density of lower crust is homogeneous, 2.65 g cm^{-3})	Low density of the lower crust shows that the geometry is not precise (RMS misfit ~15.4 mGal)	Model-Se-Px-2
Model-S	Geometry inversion	Geometry inversion with maximum 35% variations	Inversion shows 17.80 mGal RMS misfit.	Model-Sf-Gx-35%
Model-Sf-Gx-35%	Property inversion of Model-Sf-Gx-35%	Heterogeneous inversion of the upper crust (density of lower crust is homogeneous, 2.75 g cm^{-3})	Inversion shows 19.54 mGal RMS misfit. Very low densities are required to adjust with observed gravity.	Model-Sf-Px-1
Model-Sf-Gx-35%	Property inversion of	Heterogeneous inversion of the upper crust (density of lower	Inversion shows 15.39 mGal RMS misfit. Density distribution looks slightly	Model-Sf-Px-2

	Model-Sf-Gx-35%	crust is homogeneous, 2.70 g cm^{-3})	lower than what expected regarding the geological understandings.	
Model-Sf-Gx-35%	Property inversion of Model-Sf-Gx-35%	Heterogeneous inversion of the upper crust (density of lower crust is homogeneous, 2.65 g cm^{-3})	Inversion shows 13.01 mGal RMS misfit. Density distributions slightly correspond to the geological information.	Model-Sf-Px-3
Model-S	Geometry inversion	Geometry inversion with maximum 40% variations	Inversion shows 13.11 mGal RMS misfit.	Model-Sg-Gx-40%
Model-Sg-Gx-40%	Property inversion of Model-Sg-Gx-40%	Heterogeneous inversion of the upper crust (density of lower crust is homogeneous, 2.75 g cm^{-3})	Relatively low density values are distributed across the upper crust (RMS misfit ~14 mGal).	Model-Sg-Px-1
Model-Sg-Gx-40%	Property inversion of Model-Sg-Gx-40%	Heterogeneous inversion of the upper crust (density of lower crust is homogeneous, 2.70 g cm^{-3})	Density distribution within the upper crust is consistent with geological understandings (RMS misfit ~15.6 mGal).	Model-Sg-Px-2
Model-Sg-Gx-40%	Property inversion of Model-Sg-Gx-40%	Heterogeneous inversion of the upper crust (Density of lower crust is homogeneous and 2.65 g cm^{-3})	Density distribution within the upper crust is consistent with our geological understandings (RMS misfit ~14.4 mGal).	Model-Sg-Px-3

Table 4. 2 - Details of the modelling procedure including important input models, inversions and output models. Model-S is the initial model using AuSREM seismic Moho and Model-A is the initial model using Isostatic Moho surface. For pure geometry inversion of Moho, data were upward continued by 15 km. The resulting models using geometry inversion have "Gx" suffix and models resulted from property inversion have "Px" suffix.

4.7. Results

Referring to inversions documented in Table 4.2, the model addressed as the "Model-S-Gx-OceanicCrust" indicates that there is no oceanic crust within the study area. As stated in "Inversion results" column in Table 4.2, the accepted geometry inversion comprised 40 iterations with 1% maximum change per iteration (initial Model-S; output Model-Sg-Gx-40%; Figure 4.4). Other geometry inverted models, stated in the table, do not provide a density distribution within the upper crust compatible with geological understandings. This model displays major tectonic boundaries (e.g. the UCCL) and features related to significant tectonic

events (e.g. crustal thinning within Bass Strait) with a low misfit. Our geological understanding (e.g. Seymour and Calver, 1995; Seymour et al., 2007) and petrophysical measurements (e.g. Keele, 1992; Leaman, 2003; McAdam, 2015; Poker, 2013; Webster, 2003) emphasise on a consistent density range of 2.62—2.75 g cm^{-3} for western Tasmania. In contrast, northeast Tasmania is dominated by intrusions of Devonian granites (Black et al., 2005) with an expected density range of ~2.60–2.68 g cm^{-3}. Investigation of the accepted model using a range of crustal densities for property inversion of the upper crust indicates a density distribution that is compatible with existing geological models across Tasmania with a lower crustal density of 2.70 g cm^{-3} (initial Model-Sg-Gx-40%; output Model-Sg-Px-2; Figure 4.5.).

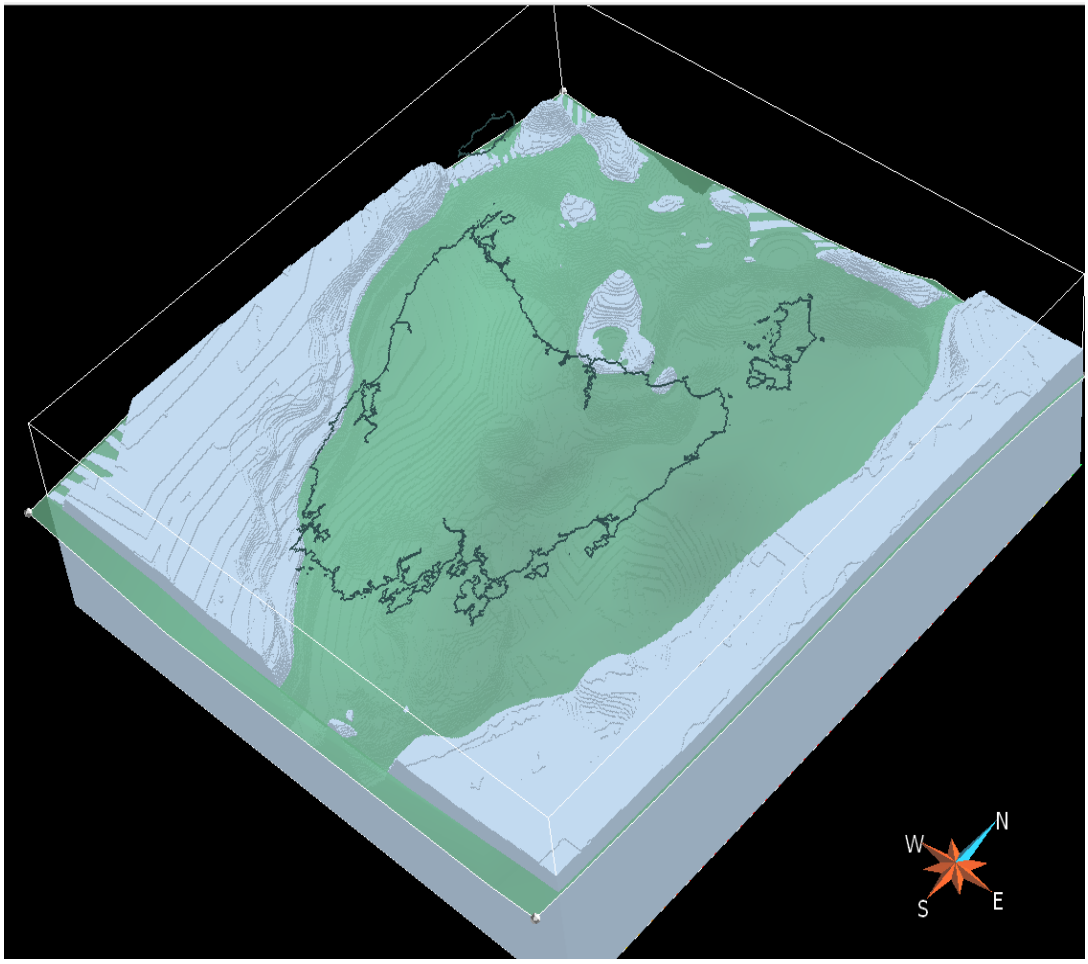

Figure 4. 4 – Final geometry inverted Moho surface using gravity data (× 3 vertical exaggerations). The upper surface of the volume represents the Moho surface. The original AuSREM Moho is shown as a translucent surface intersecting the model. The Moho surface resulting from the geometry inversion is generally deeper than the AuSREM Moho model within the UCCL and shallower beyond this boundary. Crustal thinning is interpreted using gravity data across Bass Strait. The depth extent is down to 60 km in this model. Tasmanian coastal boundary is shown as a geographic reference. Coordinates of the study area are 142° 46’ 50” longitude and-43° 57’ 39” latitude for the southwest corner and 149° 58’ 11” longitude and -38° 20’ 29” latitude for the northeast corner.

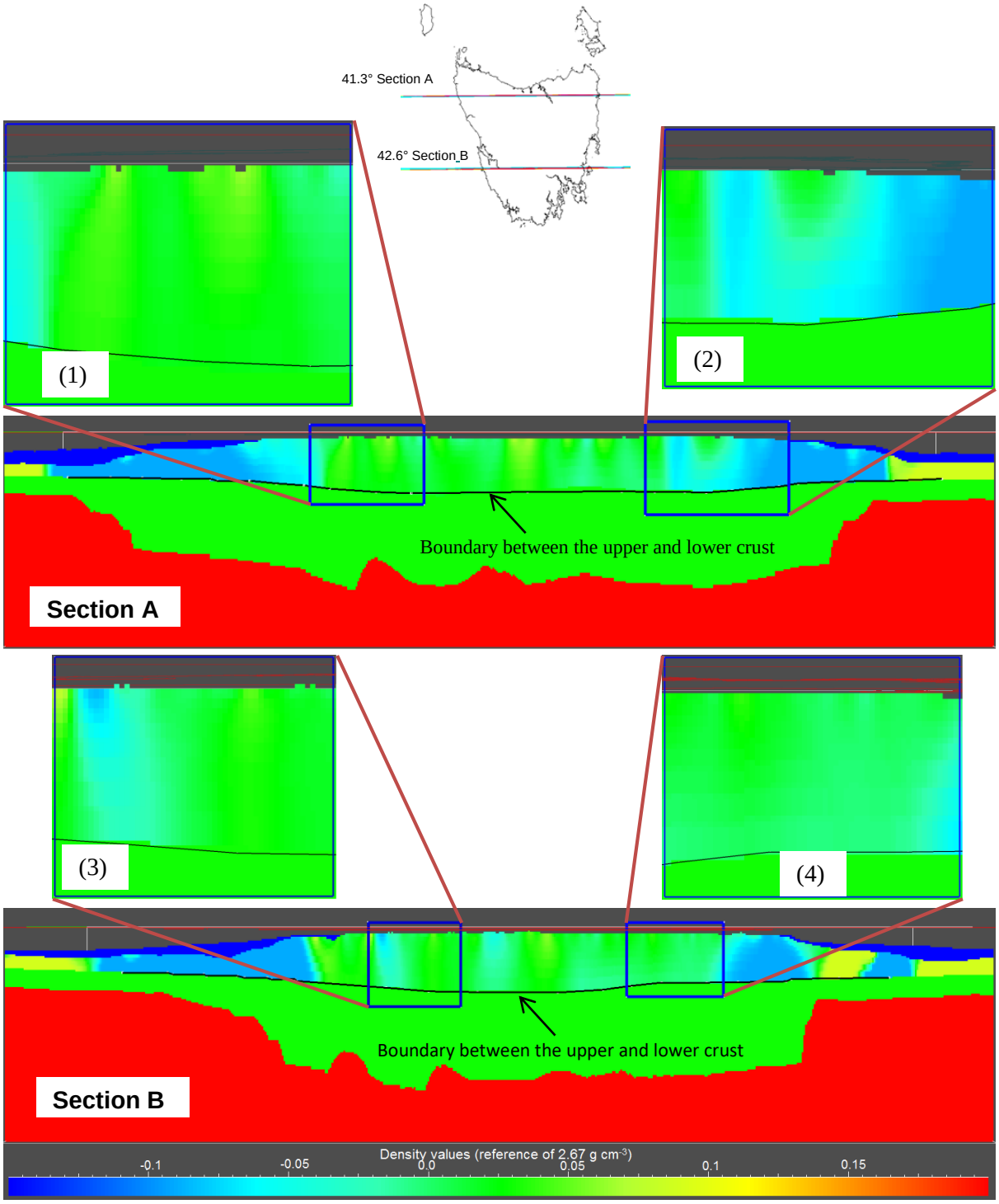

Figure 4. 2 - Results of heterogeneous inversion of the upper crust (× 2 vertical exaggeration, down to 60 km) upon geometry inverted model obtained from 40 iterations of Moho and a lower crustal density of 2.70 g cm^{-3}. Sections show the density distribution ranging 2.52–2.87 g cm^{-3} within the upper crust. The map of Tasmania is shown with locations of E-W sections: A (latitude -41.3°) and B (latitude -42.6°). Windows display the density distribution within the lower crust in NW Tasmania (Window 1), NE Tasmania (Window 2), SW Tasmania (Window 3) and SE Tasmania (Window 4). Through assigning the lower crustal density of 2.70 g cm^{-3}, density range across the upper crust is compatible with geological understandings associated with abundance of granites characterised with low density values.

4.8. Discussion

4.8.1. Modelling uncertainty

There is a limitation to the accuracy with which we can refine the Moho surface due to the uncertainty associated with modelling of granite bodies in the upper crust. This uncertainty inevitably has an effect on the properties and depths required in the lower regions to solve the inverse problem to within a reasonable misfit. In contrast, uncertainties for seismic Moho depth and gravity Moho depth are ±2–5 km (Aitken, 2010), which is up to 25% of the depth range for the estimated Moho surface across Tasmania. In addition, areas with a lack of gravity observations (i.e. the southwest corner of the study area; see Figure 2b) and low sensitivity of data due to the low resolution of topographic surfaces may affect the accuracy of our model.

4.8.2. Comparing the seismic-defined and gravity-defined Moho

While the seismically defined Moho may represent changes in the Earth's physical properties that produce a significant effect in the observed seismic data, this does not spatially coincide with density variations required to produce the observed gravitational field. Hence, the estimations of seismic and gravity Moho surfaces may not be comparable. This is because seismic and gravity derived models are investigating different physical properties. Therefore, it is possible that these surfaces represent transitions in the crust that are defined differently between the respective modelling outputs (Rivero et al., 2002). Alternatively, the seismic Moho estimates might be inaccurate or the seismic Moho does not reflect a compositional transition zone.

The final selected geometry for Moho has the minimum difference from the initial AuSREM Moho surface which represents reasonable density distribution within the upper crust consistent with geological understandings. The final gravity Moho surface, reconciled using both geometry and property inversions, indicates that the AuSREM Moho surface within the study area has a difference in depth of up to ~40% (Figure 4.4). Investigations into the geometry and density properties of deeper model components were not pursued as there are inherent trade-offs in accuracy between mass placed in the upper and lower volumes of the model.

The gravity inverted Moho surface is generally deeper than the seismic interpreted Moho surface within onshore Tasmania. The Moho surface across onshore northeast Tasmania is very deep (~40 km). The deep Moho depth in this region could be due to either the assignment of

excessively high densities to the crust or possible crustal thickening. The upper crust across northeast Tasmania in the new model is characterised by very low densities (~ 2.60 g cm^{-3}) associated with abundance of Devonian granites. Therefore, the likely pragmatic solution is a deep Moho depth across northeast Tasmania which has been suggested in the model. This interpretation is compatible with Black et al. (2005) who concluded that crustal thickening in Tasmania happened during the Tabberabberan Orogeny and resulted in the intrusion of felsic S- and I-type granites in northeast Tasmania. In addition, the Mathinna Terrane in northeast Tasmania is very similar, based on stratigraphic and structural history, to the Melbourne Zone in the Lachlan Orogen (Cayley, 2011). Similar to the Lachlan Orogen characterised by a very deep Moho surface (~50 km) (Kennett and Salmon, 2012), it can be concluded that a deep Moho depth is present beneath northeast Tasmania.

The gravity model shows shallower Moho surface across Bass Strait compared to the seismic Moho surface, which is consistent with crustal thinning (e.g. Gunn et al., 1997; Pilia et al., 2015b; Veevers, 1986) and asthenospheric upwelling (Sutherland et al., 2014) hypotheses. This crustal thinning was not clearly captured in the AuSREM model which is possibly because of a low number of deployed seismic stations across Bass Strait.

The gravity Moho surface beyond the UCCL decreases to minimum of ~15 km depth without the presence of oceanic crust. This finding is consistent with other studies that suggest oceanic crust appears beyond the extent of the study area (e.g. Brown et al., 2003; Scher et al., 2015; Williams et al., 2011). In addition, the transitional zone beyond the UCCL shows a relatively shallower Moho surface off the west coast of Tasmania compared to Tasman Sea.

4.8.3. Lower crustal densities

The new model shows a relatively low density of 2.70 g cm^{-3} for the lower crust which this low density value can be debated. Higher density values assigned to the lower crust result in either a much deeper Moho surface or pronounced lower density distributions within the upper crust which is not compatible with geological observations. Rudnick and Gabriel (2014) and Rudnick and Gao (2003) interpreted that composition of the lower crust is 80% mafic. This interpretation was updated by Huang, et al. (2013) who inferred the composition of the middle/lower crust from amphibolite-facies terranes. In this study, however, very low density of 2.70 g cm^{-3} would be consistent with a very small proportion of mafic components and

dominantly felsic compositions (low density silicate contents) in the lower crust such as feldspar and granitic entities.

4.9. Conclusion

Newly compiled Bouguer gravity data are used to investigate Moho depth and crustal heterogeneity across Tasmania, Bass Strait and surrounding offshore areas. We carried out geometry and property inversions of this newly compiled gravity data for the Moho and upper and lower crustal domains. Our findings indicate that the gravity-constrained Moho surface is not consistent with the previously available Moho surface constrained using broad scale seismic data. We carried out exhausting geometry and property inversions and modelled several versions of Figure 4.2 to better display the geometry of the gravity derived Moho depth and property distribution of the upper crust.

The gravity Moho surface is up to ~10 kilometres deeper than the seismic Moho below onshore Tasmania, varying from ~30–40 km depth. A gravity Moho surface with a depth of ~40 km is present in northeast Tasmania, which suggests crustal thickening during the Tabberabberan Orogeny. This deep Moho surface correlates with a similarly deep Moho surface beneath the Lachlan Orogen and supports the similarities in tectonic evolutionary models between these terranes. The Bass Basin displays a Moho surface of ~25 km depth which is consistent with later crustal thinning during the Cretaceous. This is the only major region on the landward side of the UCCL that shows a shallower gravity Moho surface compared to AuSREM Moho. On the ocean side of the UCCL, crustal thinning continues to ~16 km depth.

The results of the property inversion suggest that the lower crust across Tasmania is associated with a very low average density of 2.70 g cm^{-3}. This pronounced low density implies that Tasmania comprises more felsic lithologies in the middle and lower crust.

4.10. Acknowledgement

The authors would like to thank Michael Morse from Geoscience Australia for providing offshore gravity data in east Tasmania. EE is supported by a Tasmanian Graduate Research Scholarship from the University of Tasmania (UTas). We thank our colleagues at UTas and MRT for many productive discussions that greatly assisted the development of the models used in this study.

Chapter 5 - Major granite bodies beneath prospective regions of West Tasmania: geometry redefined by potential field modelling

5.1. Abstract

Tasmania is well endowed with mineral deposits, but notable for its exploration challenges due to cover sequences, topography and vegetation. It is also noted for the diversity of the mineralisation, which is a result of complex tectonic history and host structures. Three major separate granite intrusions occurred within Tasmania in the Neoproterozoic, Cambrian and Devonian. Granite plutons have been associated with mineralization in west and northwest Tasmania and have the potential to be used as an indicator for mineral exploration.

In this study, a regional model which refines the three-dimensional geometry of the subsurface geology beneath west and northwest Tasmania has been developed. This has been achieved using potential field inversions constrained by surface geology and by a newly extended petrophysical dataset. New 3D modelling can lead to a significant improvement in geometry of geological features, reconciling tectonic boundaries and identifying likely new mineral deposits. Forward modelling and property-based inversions of the pre-existing geological model show that the previously interpreted sub-surface geometry of geological units is not compatible with potential field data. Four major regions displayed a large discrepancy between calculated and observed data. These regions are the Housetop region, the eastern region of Rocky Cape Group outcrop, the region encompassing the Heemskirk-Meredith Granites, and a zone within the southern part of the Mount Read Volcanics. Modelling in this study redefines the subsurface geometries of these regions through individual, detailed geometry inversions. The density and magnetic susceptibility ranges of units are further refined through property inversions.

The modified geometry of the Devonian Granites may be summarised as follows: the Housetop Granite is relatively thin with maximum 5 km thickness while the Heemskirk and Meredith Granites are very thick and granite units extend at a shallower depth than interpreted between these bodies in previous models. The region between Heemskirk and Meredith plutons have associated with mineralisation and is thus a more prospective region than previously identified. This study has also interpreted, for the first time, an intrusive body underlying the eastern basement region of the Rocky Cape Group The petrophysical properties of this body are similar

to a granite body, and the top of this body is interpreted at a depth of > 3 km. This interpreted low density unit (granitic) may be either Neoproterozoic or Devonian. A new non-magnetic, low density Cambrian Granite, with a minimum burial depth of 1000 m, is also modelled in 3D in the south of the study area.

5.2. Introduction

West Tasmania is an area prospective for multiple mineral deposits styles. New 3D models of western Tasmania that are consistent with geophysical information can improve our understanding of regional geology, structures and tectonic history and aid mineral exploration through provision of pre-competitive information available to industry (through MRT).

5.2.1. Mineral exploration in West Tasmania

Multiple significant mineral deposits (Figure 5.1) are known to occur within western Tasmania associated with either the Mount Read Volcanics (MRV), Cambrian Mafic-Ultramafic Complexes (CMUC), or granite intrusions. The MRV contains large volcanic-hosted massive sulphide (VHMS)-type deposits with the main mineralised belt being the Central Volcanic Zone. Mt Lyell (Cu-Ag-Au), Henty (Au), Rosebery (Cu-Pb-Zn), Hercules (Zn-Pb-Cu-Ag-Au), Que River (Cu-Pb-Zn), Hellyer (Cu-Pb-Zn) and Fossey (Cu-Au) Mines are located within and close to the Central Volcanic Complexes (Corbett et al, 2014a; Taheri and Bottrill, 2005).

The CMUC includes three distinctive types of layered ultramafic successions that are the primary source of alluvial platinum-group element (PGE, ‘osmiridium’) deposits, chromite concentrations, and nickel mineralisation (Brown, 1998; Corbett et al, 2014a). Most of PGE minerals are associated spatially the Heazlewood River Complex and the Adamsfield Complex. Multiple mineral deposits are associated with the CMUC including the Magnet Mine (Ag-Pb-Zn), Stonehenge Mine (Pb-Ag), Wilson River area (mixed Au-osmiridium placers), Sunday Creek (Au-bearing alluvial deposits) associated with the Heazlewood River Complexes; and the Cuni area (Cu-Ni) linked to the Serpentine Hill Complexes (Corbett et al, 2014a).

The granite intrusions across northern and western Tasmania are the source of both skarn and vein-hosted deposits. For example, the Cambrian Granites are potentailly linked to the Cu-Au system of the Prince Lyell deposit (Murphy et al., 2003; Seymour et al., 2007). Devonian Granites are associated with a wide variety of deposit types including distal skarn Sn and W deposits (e.g. Renison, Mount Bischoff, Cleveland, Queen Hill and Rezorback), proximal Sn skarns (Mount Lindsay), greisens (e.g. Heemskirk), and quartz-cassiterite-wolframite systems

(e.g. Shepherd and Murphy, Balfour, Oakleigh Creek and Interview River; Champion et al, 2009). Examples of the Devonian Granite-related deposits are: the Kara deposit (Fe, W) associated with the Housetop Granite; the Mt Bischoff (Sn), Magnet (Pb, Ag, Zn) and Cleveland (Sn, Cu) deposits related to the Meredith Granites; the Queen Hill (Sn), Avebury, Burbank and Nickel Reward (epigenetic Ni) deposits associated with the Heemskirk Granites; the Murray Reward deposit (Cu) linked to the Interview Granites; and the North Mount Farrell (Pb, Zn, Ag) and Renison Bell (Sn) deposits associated with the Granite Tor Granites (Seymour et al., 2007).

5.2.2. Three-dimensional modelling of upper crustal structure

The main geological components of complex geological regions can be simplified and modelled in three-dimensions. The rapid development of three-dimensional (3D) inversion modelling packages and increases in computing power have made it easier to integrate geophysics and geology into a spatially consistent framework (e.g. Fullagar and Pears, 2007; McGaughey, 2006; Monoury et al., 2015; Calcagno, et al. 2008; Guillen, et al. 2008). Model construction and refinement can be achieved through the reconciliation of field observations, geophysical interpretation, incorporation of geological data uncertainty and inclusion of prevailing tectonic models (Lindsay et al., 2013).

The nature and distribution of density contrasts and variable concentrations of magnetic minerals in subsurface bodies make it possible to obtain crucial information from poorly exposed terranes through the integration of petrophysical and potential field datasets. Integration of detailed structural information with potential field modelling assists in understanding of buried 3D distributions of lithologies (Armit et al., 2014). Petrophysical data provide numerical constraints on the minimum and maximum values of model components used in VPmg during inversions in this study. The improved dataset (Chapter 3, Figure 3.3) also provides sufficient information on the distribution of petrophysical values which may be of value to alternative inversion approaches. This could be applied to subsets of this model in more detailed follow-up works.

This study focuses on regional-scale modelling of subsurface structures across western and northwestern Tasmania. Using a pre-existing 3D geological model, both forward modelling and potential field inversions were implemented to improve the subsurface geometry of regional-scale of structures and geological units. The aim of this study is not to precisely replicate the detailed geology but to generate a model that facilitates a better understanding of

the regional structures. The resulting model is also used to investigate the geometries and properties of major units and to determine anomalous regions for subsequent local-scale investigations.

5.3. Tectonic and geological framework

Tasmania is characterised by a diverse geology. It contains rocks ranging in age from Mesoproterozoic to Cainozoic (e.g. Seymour and Calver, 1995; Seymour et al., 2007; Berry and Bull, 2012; Halpin et al., 2014). These rocks are divided into different stratigraphic units/groups associated with different origins within larger domains of the WTT and ETT (Seymour and Calver, 1995; Seymour et al., 2007). This chapter investigates the geological-stratigraphic units with a focus on western Tasmania. The geology and tectonic structures of western Tasmania are complex due to a series of major tectonic events and orogenies. Three major orogenic events have been identified; the Wickham Orogeny (~760 Ma; Black et al., 1997), the Tyennan Orogeny (520—490 Ma; Berry and Crawford, 1988; Crawford and Berry, 1992), and the Tabberabberan Orogeny (390 Ma; Black et al., 2004).

The main Tasmanian Proterozoic basement rocks within the study area are the Rocky Cape Group (RCG, Mesoproterozoic; 1450 Ma), the Tyennan Element (Neoproterozoic; 1000—750 Ma), the Oonah and Burnie Formations (Neoproterozoic; 1000—750 Ma) and the Togari Group and correlates (Neoproterozoic-Lower Cambrian; 750—520 Ma; Seymour and Calver, 1995; Seymour et al., 2007). In the Meso- to Neoproterozoic (1450—1330 Ma) Tasmania (e.g. the RCG, King Island and correlates) was a small continental fragment on the margin of Gondwana (Berry and Bull, 2012; Halpin et al., 2014). The RCG contains several kilometres of marine shelf deposits partly overlain by sequences of the Smithton Synclinorium and Togari Group (Seymour et al., 2007). The RCG contacts Neoproterozoic-Late Cambrian quartzwacke turbidite successions of the Burnie and Oonah Formations at the Arthur Lineament. This Cambrian aged lineament is a narrow, northeasterly-trending metamorphic belt of pelitic, dolomitic and quartzose schists with interbanded amphibolite-facies rocks. The southern margins of Burnie and Oonah Formation outcrops are overlain by Neoproterozoic Success Creek and Crimson Creek Formations, which are correlates of the Togari Group (Seymour and Calver, 1995; Seymour et al., 2007).

The Tyennan Element represents a central, autochthonous basement core with the largest area of exposed Precambrian rocks in Tasmania. The Tyennan Element protolith was similar to

rocks of the RCG but this element experienced high grade metamorphism during the Cambrian (Seymour and Calver, 1995; Seymour et al., 2007).

The palaeogeographic feature lying between the Tyennan Element and the Rocky Cape block is known as the Dundas Trough. The Dundas Trough consists of formations and sequences of Late Proterozoic and Early to Middle Palaeozoic sedimentary and volcanic rocks deposited during the Tyennan Orogeny (Brown, 1986; Seymour and Calver, 1995; Seymour et al., 2007). The development of the Dundas Trough coincided with the emplacement of basic to intermediate volcanic complexes and sedimentary sequences of the MRV related to post-collisional volcanism of the Tyennan Orogeny (Berry and Bull, 2012; Berry and Crawford, 1988; Crawford and Berry, 1992). The last phase of the Tyennan Orogeny coincided with volcanic eruptions and the emplacement of sub-volcanic Cambrian Granites such as the Murchison and Darwin Granites between 503—498 Ma (Berry and Bull, 2012; Seymour and Calver, 1995; Seymour et al., 2007).

The Tyennan Orogeny was followed by a period of sedimentation and deposition of the Wurawina and Parmeener Supergroups. The Wurawina Supergroup covers areas of central, northern, southern and western Tasmania and comprises three sedimentary sequences; the Late Cambrian-Ordovician conglomerate and sandstone sequence of Owen Group; the Ordovician Gordon Group limestone with minor siltstone and sandstone, and the Silurian- Devonian Eldon Group consisting of a succession of quartz sandstone and siltstone with minor conglomerate horizons and limestone lenses (Seymour and Calver, 1995; Seymour et al., 2007).

During the Mid to Late Devonian, Tasmania was affected by the Tabberabberan Orogeny resulting in polyphase deformation and reactivation of older structures, followed by intrusion of late- to post-kinematic granite batholiths (Black et al., 2004). Devonian granite intrusions across Tasmania began around 400 Ma in the east and continued until the early Carboniferous in the west and northwest (Black et al., 2005; Seymour et al., 2007). Across the study area, these intrusions include the Housetop Granite (~380—343 Ma), Heemskirk Granite (~362—330.5 Ma), Pieman Granite (~356—338.5 Ma), Meredith Batholith (~338.5—336 Ma), and the Granite Tor Granite (~375— 344 Ma; Black et al., 1997; Seymour and Calver, 1995; Seymour et al., 2007).

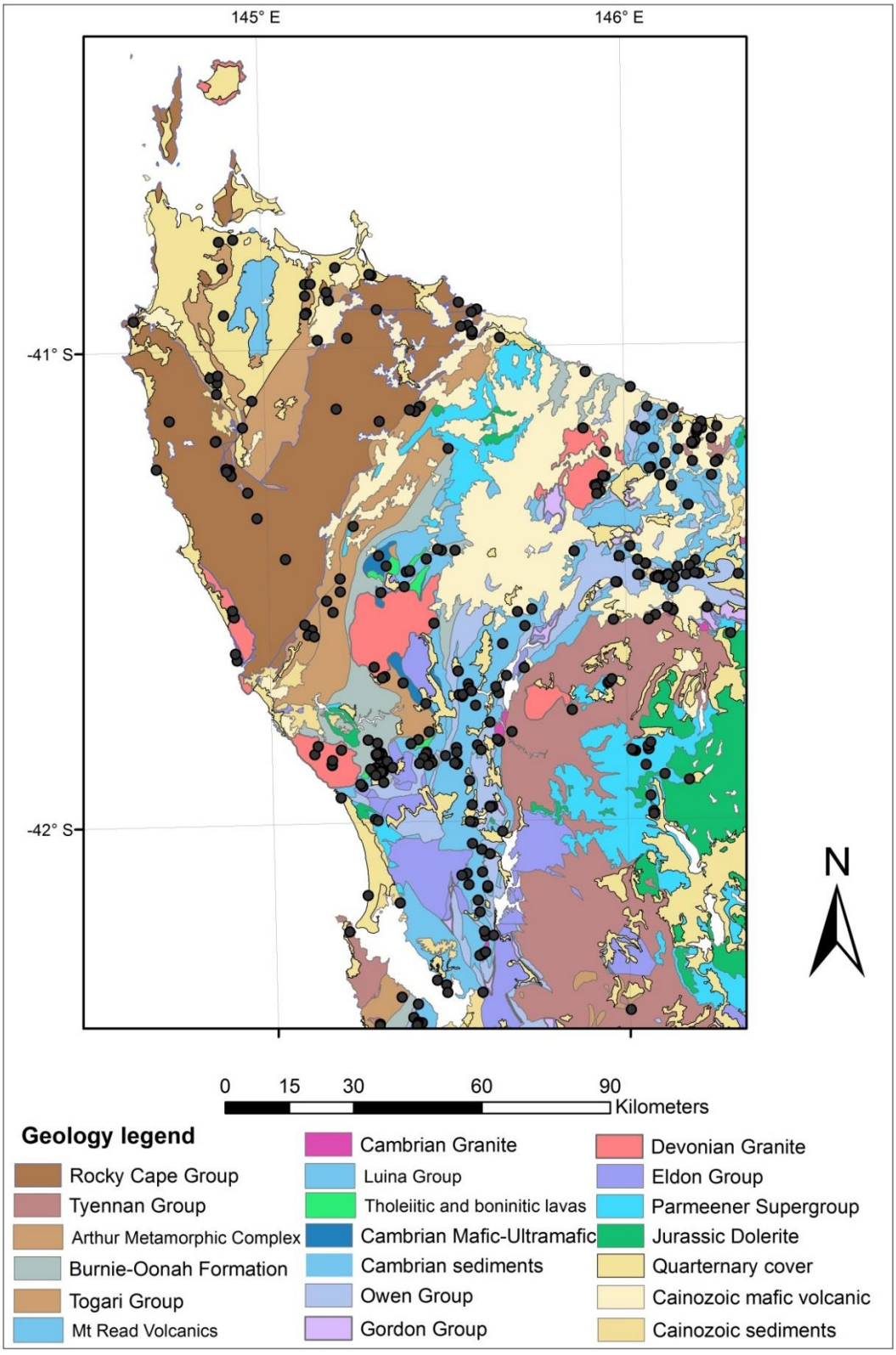

Figure 5. 1 - Geology map of the study area referring to the red rectangle in Figure 1.1. Small regions have been reclassified to correspond to the major units within the 3D model. Mineral occurrences are shown as dark dots (MRT online database, 2016; Geological Survey of Tasmania and Tasmania Development and Resources, 1995).

5.4. Previous petrophysical and geophysical studies

Across western and northwestern Tasmania, multiple regional 2D and 3D models have been interpreted by integrating geophysical data and geological observations (e.g. Leaman, 1990, 2003; Leaman and Richardson, 1992; Leaman and Richardson, 1989a; Murphy et al., 2003; Webster, 2003). The 3D regional geological model developed by Murphy et al. (2003) has been distributed by MRT and widely utilised. Constructing the Devonian Granites in the model, the models of Leaman (2003) and Murphy et al. (2003) include an isosurface indicating the depth to top of the Devonian Granites which mostly extend to depths of 9–12 km (Black et al., 2010).

The densities and magnetic susceptibilities of major units across Tasmania have been investigated in a number of studies (e.g. Payne, 1991; Keele, 1992; Roach, 1994; Tyson, 2002; Webster, 2003; Leaman, 2003; Poker, 2013;McAdam, 2015). Nevertheless, some of the estimated properties are not entirely reliable due to samples obtained from weathered surfaces, a paucity of samples collected for some rock units, or scale variability due to the local nature of some petrophysical studies. New petrophysical measurements were required to improve the database for detailed geophysical modelling (Chapter 3).

5.5. Data

The Paradigm GOCAD (Mallet, 1992;, http://www.pdgm.com) Version 2009.4 was used in this study to generate and modify a forward 3D model with dimensions of 157.5 km (west to east) by 216 km (north to south) and 10 km in depth (total volume of 3.4×10^{14} m^3). This model was discretised into a voxet model with resolutions of 500 m in x and y directions and 250 m in the z direction resulting in > 6.7 million voxels. The initial model was based on the published 3D onshore fault structure and geological model of Murphy et al. (2003; Figure 5.2). Details of this model are available on supplement 1.

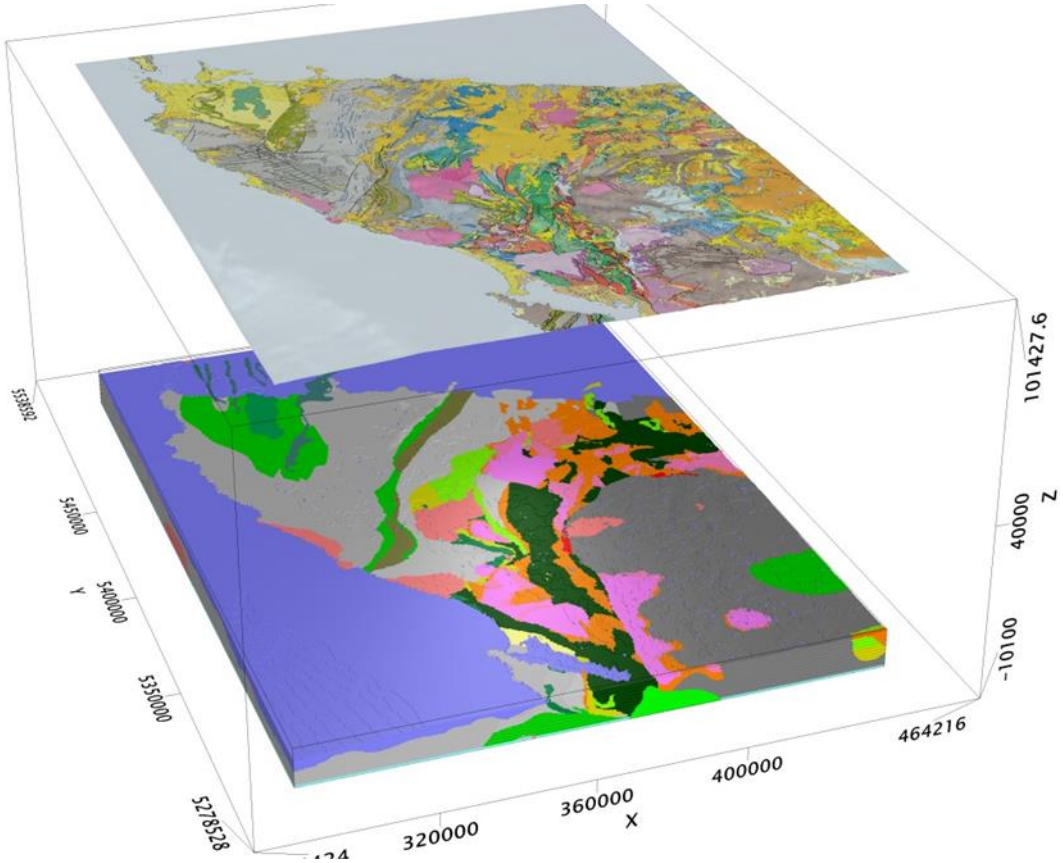

Figure 5. 2 – The initial model based on surface geology, serial sections and geophysical data (coordinates on GDA 94 datum, MGA zone 55). The model has a maximum depth of 10 km. The 1:250,000 scale geology map is shown on top for reference. For detailed information on geological features refer to Figure 1. A 3D view of major faults and geological units of this model is shown in the supplement 1. The geographic extent of the study area used in modelling is shown in this figure (e.g. Figure 5.4 and subsequent figures).

5.5.1. Petrophysical data

Core samples from non-weathered key rock units, deeper than 100 m, within the study area were collected and their densities and magnetic susceptibilities were measured to build a comprehensive petrophysical database. Overall, we collected 443 core samples from > 100 drill holes distributed across the 14 major rock units. Other recent measurements (MRT database, McAdam, 2015; Poker, 2013) were also included and finally 802 density and 2051 magnetic susceptibility measurements were combined to estimate density and magnetic susceptibility (Table 5.1).

Petrophysical data indicate that the CMUC is divided into two distinct units of low density and high magnetic susceptibility (CMUC- unit 1) and high density and low magnetic susceptibility (CMUC- unit 2). A difference in the degree of serpentinisation is likely to cause the density

and magnetic variations within this unit (Griggs, 2009). Dunites and harzburgites are typically characterised by higher density and less magnetic susceptibility than equally serpentinised peridotites (Saad, 1969). Units such as Devonian Granites and Owen Group display relatively low densities, while the Crimson Creek Formation, Togari Group and rocks within the Arthur Lineament present higher densities. In contrast, high magnetic susceptibilities are measured within Cambrian Granites and CMUC- unit 1 (Table 5.1).

Unit	Layer ID	Density (g cm^{-3})		Susceptibility ($\times 10^{-3}$ SI)	
		Mean	Ranges	Mean	Ranges
Devonian Granite	DGR	2.62	2.57-2.65	0.390	0-1.58
Eldon Group	Eldon	2.64	2.57-2.71	0.080	0-0.15
Gordon Group	Gordon	2.71	2.67-2.75	0.440	0-0.72
Owen Group	Owen	2.63	2.56-5.7	0.080	0-3.60
Cambrian Granite	CGR	2.68	2.62-2.74	25.720	8.52-42.92
Cambrian mafic-ultramafic complexes- unit 1	CMUC- unit 1	2.65	2.5-2.83	14.451	0-46.63
Cambrian mafic-ultramafic complexes- unit 2	CMUC- unit 2	2.86	2.67-3.05	0.745	0-2.06
Crimson Creek Formation	PCCC	2.88	2.78-2.98	7.250	0-27.17
Success Creek Formation	PCSC	2.80	2.7-2.9	0.650	0-4.44
Burnie-Oonah Formation	BOF	2.74	2.65-2.83	0.588	0-2.18
Arthur Metamorphic Complex	Arthur MC	2.79	2.71-2.87	0.161	0-15.31
Togari Group	TG	2.8	2.77-2.83	0.130	0-2.02
Tyennan region	TR	2.77	2.66-2.74	0.265	0-0.39
Rocky Cape Group	RGG	2.74	2.68-2.81	0.415	0-0.70

Table 5. 1 - Estimated petrophysical properties utilised for major rock units across West Tasmania. The Cambrian Mafic-Ultramafic Complexes is are divided into two subunits of the CMUC- unit 1characterised by low density and high magnetic susceptibility properties and the CMUC- unit 2 characterised by high density and low magnetic susceptibility properties.

5.5.2. Geophysical data

The residual Bouguer gravity anomaly and total magnetic intensity (TMI) data (MRT online database, 2016) were used in this study. The residual Bouguer anomaly, with the resolution of 250 m and a dynamic range of 64 mGal, was calculated using the MANTLE09 model (Leaman, 2009) to study upper 10 kilometres of the crust. The prominent feature in the gravity grid is the distribution of long-width negative anomalies (width of >40 km and amplitude of up to ~-35 mGal) corresponding to the Devonian Granites. TMI data, with a resolution of 100 m and

dynamic range of 9092 nT, is characterized by northeast-southwest trending features correlating with the MRV, Arthur Lineament, and local anomalies corresponding to the Tertiary Basalts, CMUC and Cambrian Cleveland-Waratah (CCW; Luina Group) associations. For example, the Housetop region displays a local magnetic anomaly associated with up to ~9 km width and an amplitude exceeding 1900 nT.

5.6. Method

Forward modelling and constrained geophysical inversions were carried out using VPmg^{TM} Version 7.1 (Fullagar, 2013; Fullagar et al., 2004; Fullagar et al., 2008). This software performs potential field, geometry and/or property inversions in a discretised volume using vertical rectangular prisms subdividing geological boundaries in each prism.

The inversion workflow used in this study is shown as a flowchart in Figure 5.3. Firstly, the initial model compared to potential field observations. This is achieved by considering the root mean square (RMS) misfit between the observed gravity and magnetic fields and those calculated from the model. The forward modelling provides the basis for our decisions regarding the choice of different property and/or geometry inverse modelling. Secondly, property inversion is conducted to reduce the overall misfit between observed and calculated values. The model will be validated if it yields a negligible misfit. Regions with high misfit are identified and geometry inversion is carried out on these model subsets to make further refinements.

We assessed the initial model using modelling techniques (i.e. geometry and property inversions) as described in supplement 2 and found four areas with high misfit (step 5-flowchart, Figure 5.3) on which we focus for detailed investigation (Figures 5.4 and 5.5). Region No.1 corresponds to the Housetop region with a positive residual gravity anomaly and pronounced positive magnetic anomaly. Region No.2 is located in the eastern portion of the RCG which shows that less dense bodies are required. Region No.3 shows a pronounced negative residual anomaly between Heemskirk and Meredith Granites which likely corresponds to the geometry of Devonian Granites. Region No.4 indicates a high amplitude negative residual anomaly in south of the MRV with a slightly negative residual magnetic anomaly. More detailed geometry inversion was applied to these four regions.

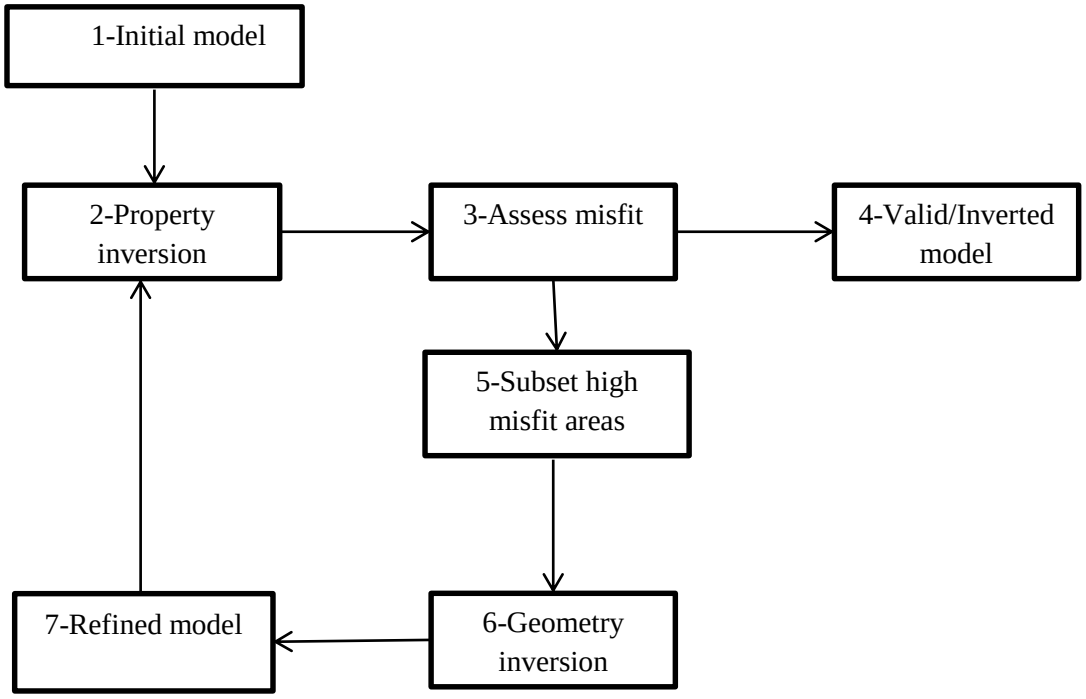

Figure 5. 3 - Flowchart outlining the inversion procedure

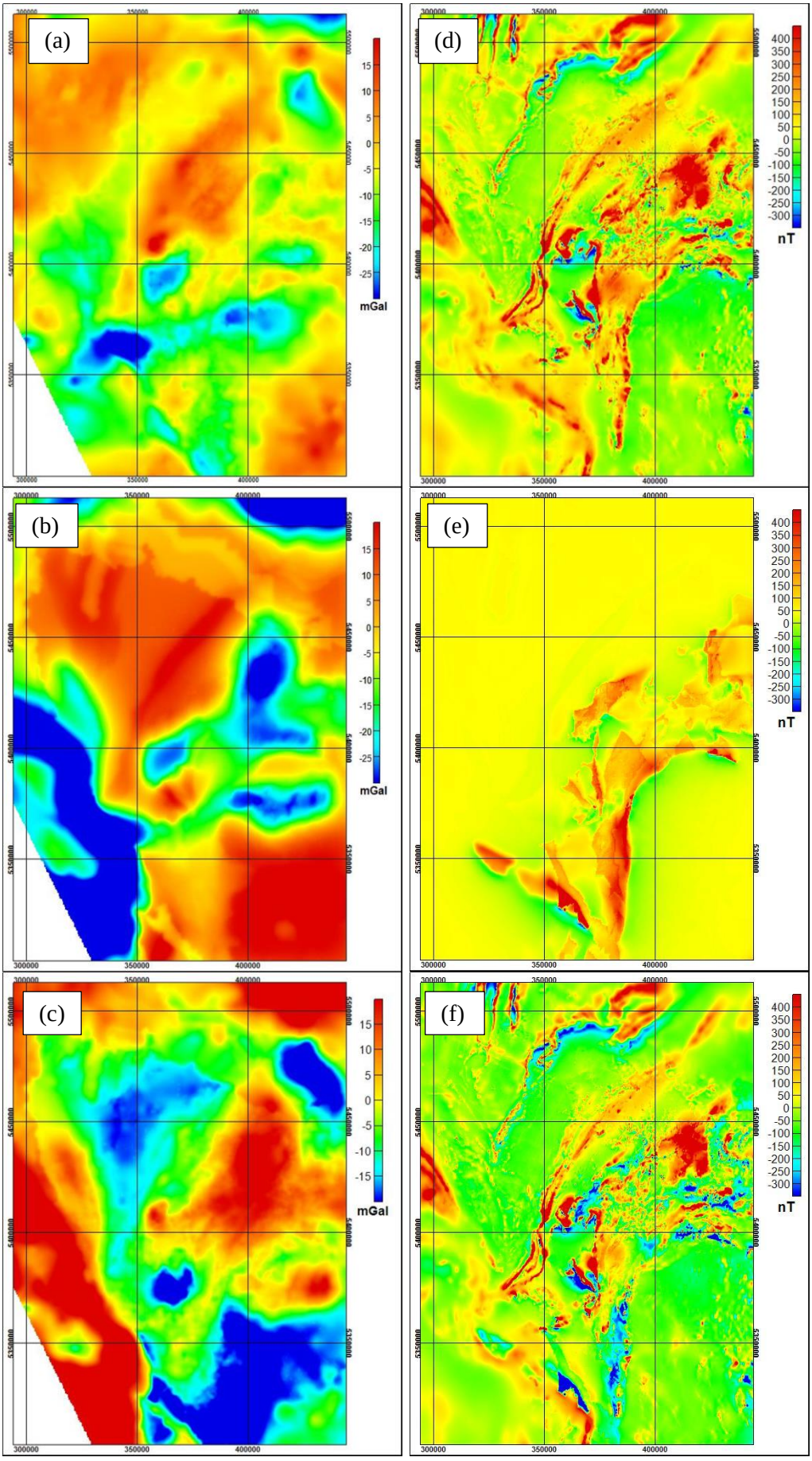

Figure 5. 4 - Potential field observations, calculations and residual of the initial model of the study area; a) observed gravity data; b) calculated gravity values from the initial model; c) residual gravity data between observed and calculated data; d) observed Total Magnetic Intensity (TMI); e) calculated TMI from initial model; f) residual TMI data between observed and calculated data.

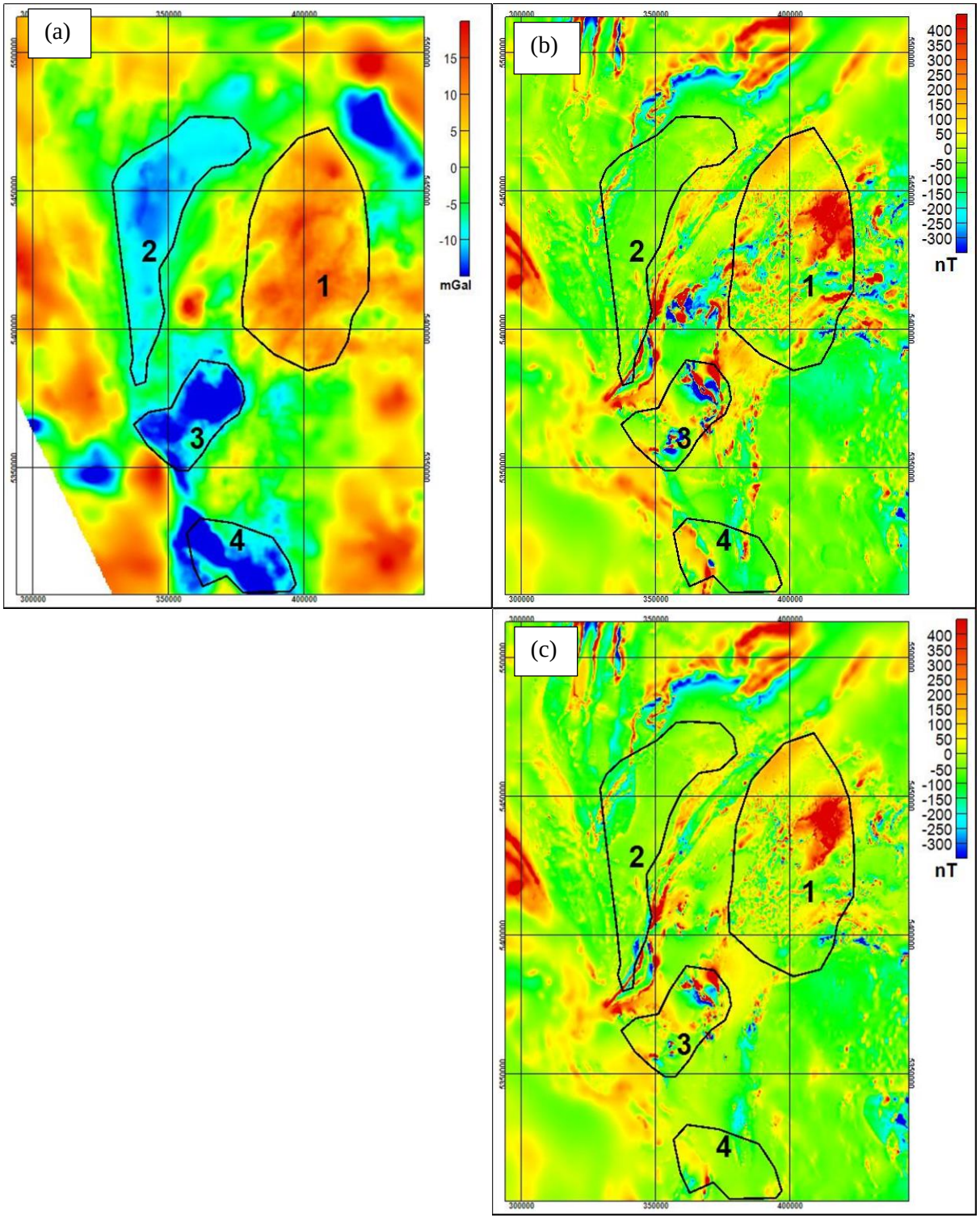

Figure 5. 5 - Residual potential fields resulted from property inversion of the initial model. a) residual gravity of homogeneous inversion; b) residual TMI of homogeneous inversion; c) residual TMI of heterogeneous inversion of Cambrian mafic-ultramafic complexes, Cleveland-Waratah associations and Mount Read Volcanics. Regions 1-4 are the Housetop region, eastern Rocky Cape Group, Heemskirk-Meredith Granites region and south of the Mount Read Volcanics in the text respectively.

5.6.1. Housetop region

Across the Housetop region, Devonian Granites are characterized by long-wavelength (10–15 km) positive residual gravity anomalies with moderate amplitude (-12 mGal). Compared to the Housetop Granite, other granite outcrops show much larger anomalies (e.g. the residual gravity of Heemskirk Granites is < -25 mGal). In the magnetic data, a large (~26 km wavelength), high amplitude (~1650 nT) anomaly occurs in this region. The source of this magnetic anomaly is interpreted to be at a depth of ~3–6 km, likely correlated with the Heazlewood River Ultramafic Complexes anomalies 50 km apart to the west of this region (Le Clerc, 1996).

Le Clerc (1996) proposed that Housetop Granite is thin with a maximum depth of 3–4 km. Le Clerc (1996) modelled an ultramafic sheet at depth of 3–4 km with maximum thickness of 1200 m to account for this magnetic anomaly. Our 2D gravity and magnetic modellings show that the Housetop Granite has average and maximum depths of 4 and 6 km and a thick magnetic sheet (maximum 2 km thick) at a depth of 3–5 km can account for this large magnetic anomaly. These 2D models are implemented to constrain new 3D geometry across this region.

5.6.2. East of RCG

The eastern portion of the RCG shows much lower residual values, in excess of ~8 mGal, than the western portion. Since modelling of potential field data is limited by the non-uniqueness of potential field source distribution (Blakely, 1995), different possibilities are evaluated based on geology and tectonic information across this region.

The first scenario reconsiders the residual gravity data. The MANTLE09 model was used to calculate the residual gravity data (Leaman, 2009). This model is likely to have large uncertainties with respect to constraining the Moho, however, the wavelength of this negative anomaly (widths raging ~1—25 km) suggests a source within the upper parts of the crust. Previous seismic Moho models (e.g. Kennett and Salmon, 2012; Rawlinson et al., 2001a; Rawlinson et al., 2001b; Rawlinson et al., 2010; Young et al., 2011) and gravity Moho model show no evidence of sharp changes in Moho depth within the RCG, which can account for this anomaly.

Dividing the RCG into two subpopulations with different density properties was considered, however, geology maps and sections do not suggest any major differences in sedimentary successions or a distinct boundary within the unit. Detrital zircon data show similar deposition ages for middle to lower parts of this unit in the east and west at 1800—1600 Ma (Halpin et

al., 2014). In addition, radiometric maps and remote sensing data do not highlight any evidence of major metamorphism or lithological changes across the RCG.

Another scenario is to assign lower density to the entire of the RCG. Some studies investigated the RCG by assigning low median density of 2.65 g cm^{-3} (e.g. Leaman, 1990; Tyson, 2002). Tyson (2002) studied west of the RCG and proposed a comparatively dense unit (Crimson Creek Formation) underlying west of the unit to account for positive gravity observations. Leaman (1990) assigned a similar density of 2.65 g cm^{-3} to study east of the RCG. Our petrophysical measurements were mostly sampled from west of the RCG and consistently returned higher densities (Table 5.1). A small number (5 samples) were measured by Mineral Resources Tasmania (MRT) across the eastern portion of the RCG and show densities consistently higher than 2.70 g cm^{-3} and no density as low as 2.65 g cm^{-3}. The geological context of the RCG and previous 3D modelling (MRT west Tasmania 3D model, 2016) suggest a density range of 2.68—2.72 g cm^{-3} for this group. Hence assigning a low mean density to the entire RCG is unlikely to be appropriate. In contrast, the influence of a bulk low density of 2.65 g cm^{-3} rarely exceeds -2 mGal observed in the residual gravity and cannot account for residual values of -6 to -8 mGal in this region.

High contrast in density between the eastern portion of the low density RCG and west of the high density Arthur Lineament (Table 5.1) is considered. This contrast cannot, however, account for the pronounced negative anomaly observed. The boundary between the RCG and eastern units also extends offshore, while this negative anomaly is present in onshore regions.

A pragmatic solution to this conundrum is to introduce a unit with low density (2.61 g cm^{-3}) below the eastern portion of the RCG. This solution provides a mathematical solution to the discrepancy in likely density properties of the RCG and the presence of anomalously low gravity observations. A density of 2.62 g cm^{-3} corresponds to acceptable densities of granites distributed within Tasmania and is consistent with 2D interpretations by Leaman (1990). Seismic shear wave model provided by Young et al. (2013) interpreted the presence of a unit with higher shear-wave velocity values (~3500 m/s) with respect to surrounding units in this area. These relatively high velocities are consistent with the properties of intrusive igneous rocks. The 3D geometry inversion shows that this inferred granitic unit has a minimum depth of > 3 km. The absence of major metamorphism and/or mineralisation on the surface across this region is indicates of substantial depth to this intrusive body.

The occurrence of high frequency northeast-southwest trending linear magnetic anomalies in some parts of the RCG and Smithton Basin are likely because of a Proterozoic magnetic tholeiitic basalt dyke swarm which outcrops in the area. Our 2D modelling and geological interpretations indicate these basaltic dykes have a maximum depth of a few hundred metres.

5.6.3. Heemskirk-Meredith Granites

Outcrops of the Heemskirk and Meredith Granites coincide with negative residual gravity anomalies, suggest that the geometry of the Devonian Granites requires adjustment. We used a recently constructed detailed granite surface resulting from the high precision Rosebery-Lyell 3D model (MRT West Tasmania 3D model, 2016) to reconstruct upper surfaces of granite in this region. Subsequent geometry inversions with petrophysical property constraints show that the granites have a shallow burial depth in this region. Our inverted geometry model from the recent granite model does not completely compensate the residual misfit. This result emphasises that this granite body is likely to extend to depths greater than 10 km and there is likely higher contrast between granites and other units.

5.6.4. South of MRV

A negative anomaly in excess of -10 mGal in the south of the MRV cannot be explained by the forward 3D modelled. Lithologies underlying this region are mostly relatively dense units of the MRV, Success Creek and Crimson Creek Formations. Leaman (2003) proposed that the source of this negative anomaly is not in the basement, nor due to basement rocks. Leaman (2003) modelled a new mass of non-magnetic, low density (2.62 g cm^{-3}) Cambrian Granite intruding along the major structural boundary on the western side of the Tyennan core and eastern side of the early Palaeozoic basin complex at a minimum depth of 1000 m below the surface. We modelled this Cambrian Granite body using 2D sections modelled by Leaman (2003).

5.7. Results of the geometry refined model

The geometry refined model is constructed following the flowchart in Figure 5.3. Figure 5.6 shows the new granitic unit below the eastern part of the RCG, non-magnetic Cambrian Granite in south of the study and newly refined geometry of Devonian Granites and CMUC. Forward gravity modelling of the refined 3D model shows a RMS misfit of 6.41 mGal (10% of the total dynamic range). Homogeneous inversion of the density values reduces the RMS misfit to 5.02 mGal (7.8% of the total dynamic range; Figure 5.7a) with an acceptable range of petrophysical

values. The final petrophysical values assigned to units are within the bounding constraints and only less discussed non-magnetic, low dense Cambrian Granite entity in the south of the MRV identified by Leaman (2003) displays very low densities of 2.60 g cm^{-3}. Onshore study area highlights the RMS misfit of 3.64 mGal (~5.7% of the total dynamic range).

Forward modelling of magnetic data of the refined 3D model displays RMS misfit of 189.59 nT (2.1% of the total dynamic range). Homogeneous inversion slightly decreases this misfit to 189.05 nT (2.1% of the total dynamic range). Inverted properties for some of non-magnetic features are close to the bounding constraints which could be expected as allowed ranges of properties are very narrow, around 0 SI, whereas features associated with high magnetic properties (e.g. Cambrian Granites, Crimson Creek Formation and CMUC- Unit 1) indicate properties within the maximums and minimum ranges. Heterogeneous inversion of CMUC, CCW, MRV and basalt reduces the RMS misfit to 138.81 nT (1.5% of the total dynamic range; Figure 5.7b) with a RMS misfit of 156.07 nT (1.7% of the total dynamic range) across onshore study area.

Small sources of model errors contributing to the misfit are beyond the resolution of this model. A positive gravity anomaly, located in the southeast corner of the study area, coincides with the Tyennan region. Interpreted geological sections (Murphy et al., 2003) have the Tyennan region extending to the base of the model but further investigation of subsurface lithologies in this location is beyond the scope of the current study.

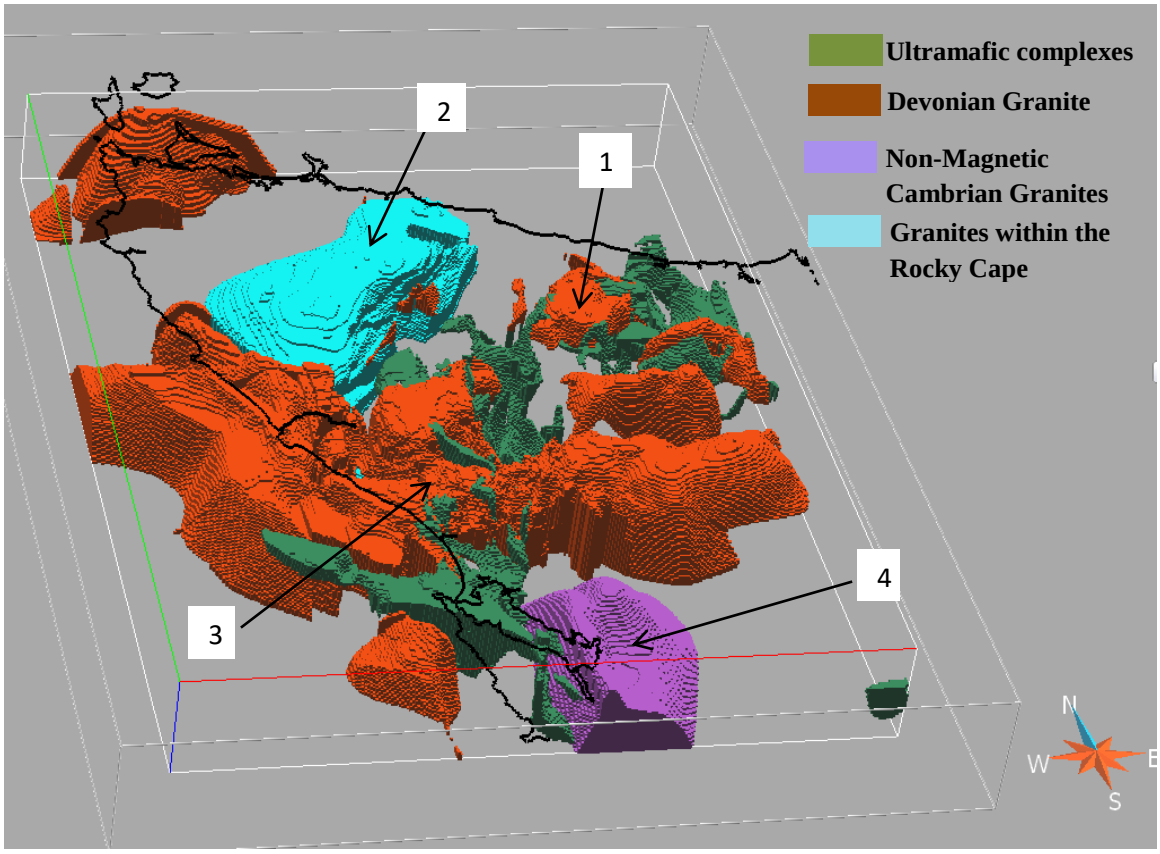

Figure 5. 6 - 3D model in the final form (× 2 vertical exaggeration). This figure shows the geometry refinement of major granite bodies and includes the likely presence of CMUC. Regions 1-4 display geometry of subsurface features corresponding to regions with high misfit in Figure 5. 5. The Tasmania coastline is shown by the dark-line colour.

5.8. Discussion

Modelling of potential field data is limited by a component of ambiguity due to the non-uniqueness of potential field source distribution (e.g. Blakely 1995, Jessell, et al. 1993, McLean and Betts 2003). Inclusion of geological data and field observations to constrain the model can help to a limit the range of possible solutions (Aitken and Betts, 2009). Constraints on subsurface geology have been improved using multi-disciplinary techniques and modelling of gravity and magnetic data as outlined below.

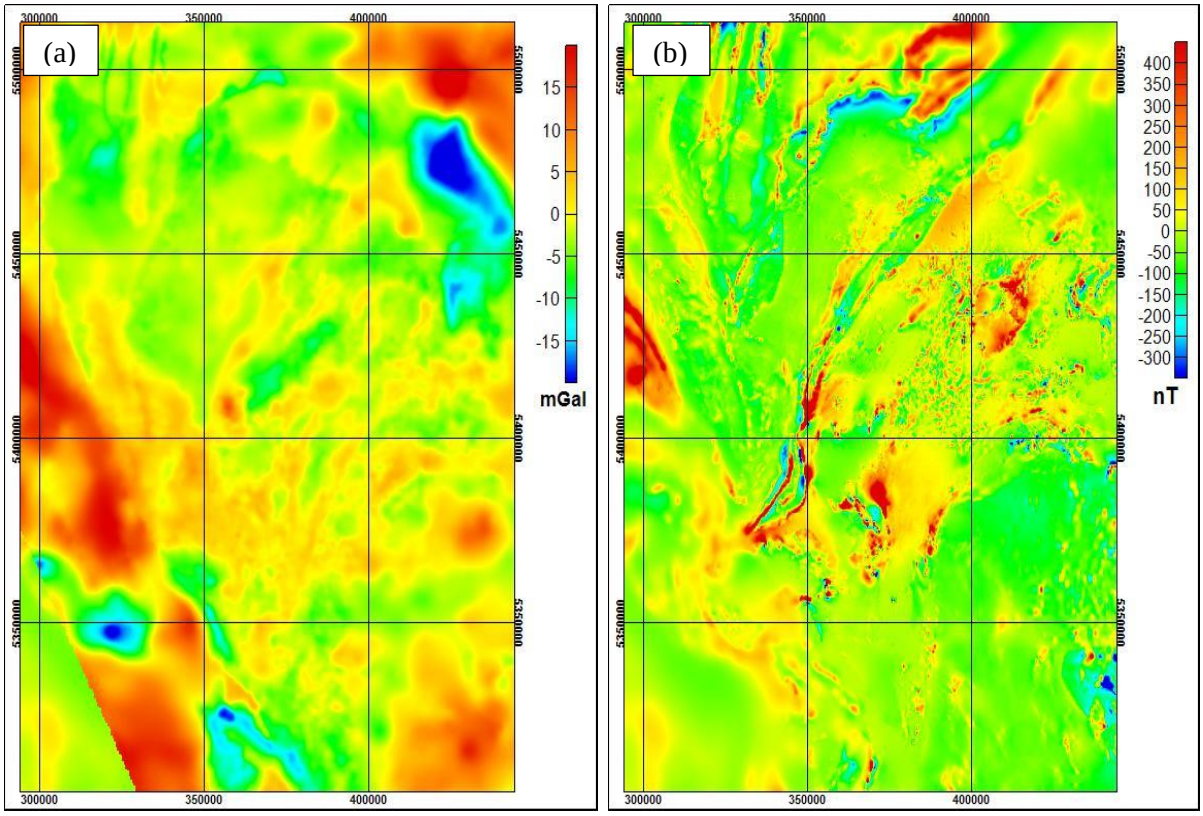

Figure 5. 7 – Residual gravity and magnetic of the refined model; a) residual gravity of homogeneous inversion of the refined 3D model, b) residual magnetic intensity of the refined model after homogeneous inversion of all units and heterogeneous inversion of Cambrian Mafic-Ultramafic Complexes, Cleveland-Waratah associations, Mount Read Volcanics and basalts of the new 3D model.

In any 3D geological modelling project, some fundamental geological problems are addressed in terms of geometry of subsurface units. These problems raise significant questions for the research and exploration communities to tackle (Murphy et al., 2003). It is fundamental that surface geology, containing abundant structural and lithological field observations, and geology at depth, usually represented by a paucity of structural observations, are simultaneously represented in a model (Lindsay et al., 2012).

Calculated potential field data from previously 3D geological models of onshore west and northwest Tasmania by Murphy et al. (2003) are inconsistent with potential field observations. Refinements to the geometry of major geological units have improved the understanding of tectonic processes across West Tasmania. The initial model presented the Housetop Granite as a relatively thick intrusive unit (Murphy et al., 2003). This intrusive unit, interpreted from both 2D and 3D inversion models, is significantly thinner, $\leq$ 5 km, in the new model. Top of the intrusive unit was constrained with geology map across the study area and characterised

petrophysical properties. Our new model also suggests a thick sheet, between 1–2 km, of very high magnetic susceptibility material equivalent to the Heazlewood River Ultramafic Complexes consistent with Le Clerc (1996) which proposed that the Housetop Granite is a partly overthrust body underlain by ultramafic units.

The presence of a deep felsic igneous body is a likely scenario in the east of the RCG. There are three possible tectonic origins for this inferred granitic body. Firstly, this body could have originated at 1800–1600 Ma as part of the basement of the RCG. Berry et al. (2008) suggested that the western Tasmanian lower crust has a Late Palaeoproterozoic (1740–1650 Ma) mantle extraction age. Black et al. (2010) interpreted an excess of 1630–1600 Ma inherited zircon in Palaeozoic western Tasmanian granites relative to the overlying RCG. Berry, et al. (2001) and Black et al. (2004) concluded that the best match for Tasmania is the Southwestern USA. More recently, Mulder et al. (2015) indicated that the majority of sediments in the RCG, deposited at 1450–1300 Ma, was sourced from Laurentia as part of Nuna supercontinent between the southern portion of the Mawson continent, and the Yavapai, Mazatzal, and Mojave Provinces. Granitoids intruded the southern Laurentia in the USA between and within Mazatzal and Yavapai provinces at 1650–1600 Ma (Whitmeyer and Karlstrom, 2007). Hence, the presence of basement ~1800–1600 Ma Proterozoic granites equivalent of Proterozoic granites in southwest USA is an acceptable scenario. The main hurdle to the validity of this hypothesis is that the lower-middle RCG consists of > 10 km thick package of sedimentary rocks and the presence of basement at shallower depth is unlikely, while the minimum depth of this granitic basement body modelled at depths of < 4 km. An alternative possibility is the Neoproterozoic granites emplaced during the Wickham Orogeny between 780–700 Ma and are present on King Island and Ahrberg Group in the southern region of the Arthur Lineament (Black et al., 1997; Holm et al., 2003). Neoproterozoic granites in the Arthur Lineament have similar emplacement ages with rift-related granites exposed in King Island during the Wickham Orogeny (Black et al., 1997; Holm et al., 2003). There is also evidence of fluid flows in the east of the RCG dated to 750–700 Ma (J.A. Mulder, unpublished data). The issue with this hypothesis is that this body has a very large size, with maximum extent of 31 km (west to east) × 85 km (north to south), compared to other two 780—700 Ma aged granite bodies. The other possibility for this felsic igneous body is Devonian age distributed within onshore and offshore Tasmania (e.g. Black et al., 2010). This idea is supported by Leaman (1990) which modelled the extent of Devonian Granites in the east of the RCG, correlating with southern margin of this new granitoid body. Hence, this body may be a continuation of Devonian felsic igneous rocks at depth despite little evidence at the surface.

New detailed geometry of the granites within Heemskirk-Meredith regions (MRT West Tasmania 3D model, 2016) and the RCG (modelled in this study) represent a refined surface of top of Devonian Granites across the study area. In the southern region of the MRV, a bulk of essentially non-magnetic, low density body the Cambrian Granites is modelled that controls the extent of previously modelled highly magnetic Cambrian Granite unit.

5.9. Conclusion

A revised regional 3D model of the west and northwest Tasmania has been constructed based on regional geological mapping, geologically constrained cross-sections, and geophysical modelling and interpretation. The new modelling reveals regional scale information about the geometry and property of underlying units and proposes new geological intrusive units that could not otherwise be detected. The new interpretation provides a framework for future and more detailed mineral exploration.

Our revised 3D model honours both the known geology and potential field observations and local petrophysical measurements. It shows that the Housetop Granite is thinner than previously interpreted and that an ultramafic unit, likely equivalent to the Heazlewood River Ultramafic Complexes, underlies this intrusive body. We also interpret a new bulk intrusive body with petrophysical properties similar to granite intrusions within the eastern portion of the RCG. The age of the modelled granite body could be either Neoproterozoic aged, intruded during the Wickham Orogeny, or Devonian aged, emplaced in the Tabberabberan Orogeny. This concealed low density body has a minimum burial depth of > 3 km. The lack of obvious surficial geological evidence (metamorphic, thermal or mineralisation footprint) for this body is explained by its significant burial depth.

The Devonian Granite intrusive bodies are modelled at a shallower depth (between that of the Heemskirk and Meredith Granites) than in previous interpretations and appear to be thicker than previously thought within western RCG. A new body of non-magnetic, low density felsic igneous rocks, likely to be correlated with Cambrian Granite intrusions, has been interpreted in the south of the MRV. This accounts for the observed negative residual anomaly and are likely to control the depth of the MRV and adjacent lithologies.

5.10. Acknowledgement

The authors would like to thank Stephen Kuhn, Thomas Ostersen, Jacob Mulder, Ron Berry, and Sasha Stepanov and many other colleagues from School of Physical Sciences (Earth

Sciences), University of Tasmania and MRT for very helpful discussion. EE is supported by a Tasmanian Graduate Research Scholarship from the University of Tasmania.

5.11. Supplementary materials

5.11.1. Supplement 1- Construction of the initial model

The initial model was based on a reference 3D onshore geological model by Murphy et al. (2003). Topography and bathymetry data at 250 m resolution, obtained from MRT online database (2016) was used to define top of geological surfaces. Across the modelled area elevation (relative to sea level) ranges from -5027 m in the southwest offshore corner to a height of 1539 m in the Central Highlands of Tasmania.

Fault network data by Murphy et al. (2003) that honour the geology map and subsurface information, provided primary constraints for our initial model. The Tyennan Margin Fault (TMF) is one of the major arcuate faults, it determines the western boundary of the Tyennan Element and eastern boundary of the Cambrian Granites, Dundas Element and CMUC. While Murphy et al. (2003) interpreted the TMF as an easterly and southerly dipping fault, new seismic interpretations show this fault as a steeply west dipping fault (Young et al., 2013). We therefore constrained the TMF in the initial model with this more recent interpretation (Figure 5.8). We used the surfaces which delineates the depth to top of the Devonian Granites modelled by Leaman (2003) to construct this unit extending to a depth of 9.5 km.

While a detailed study of the offshore structures is beyond the scope of this research, offshore regions were modelled with a coarse resolution to consider offshore extent of lithological structures. The structural patterns within onshore Tasmania can be traced into Bass Strait. We used offshore seismic profiles (Drummond et al., 2000; Kennett et al., 2013) and WORMS maps (Newnham, 2004) to trace major offshore faults and geological context. The SEEBASE^{TM} model (Oz SEEBASE^{TM}, 2005; Richardson, 2014) were used to model the basement of the sedimentary basins in offshore areas. Different sub-units within the MRV were merged in this study. A total of 20 units were defined based on elements and lithologies to produce the initial model (Figures 5.2 and 5.8).

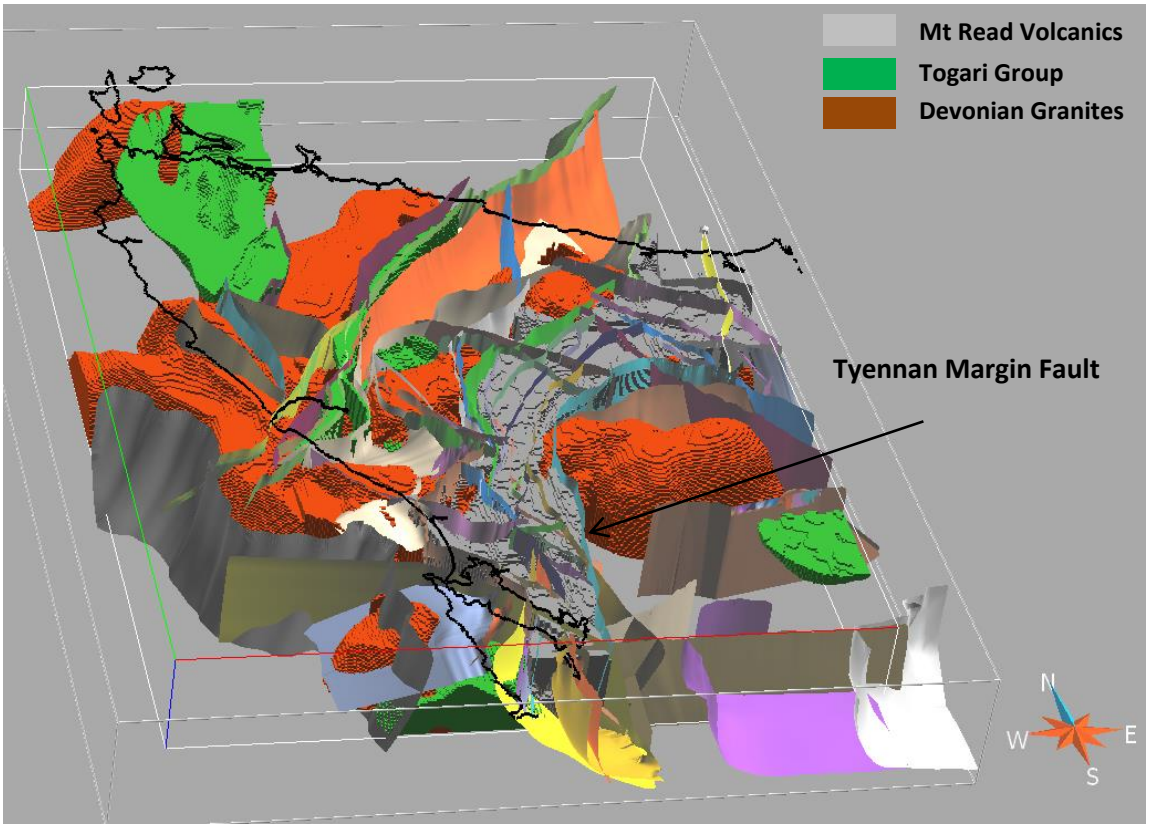

Figure 5. 8 - The initial model based on surface geology and geological sections. The figure displays the study area, fault network (different surfaces) and three geological components (× 2 vertical exaggeration). The Tasmania coastline is shown in grey line. The Tyennan Margin Fault refined using seismic models of Young et al., (2013) is shown.

5.11.2. Supplement 2- Assessment of the initial model

The initial model characterises and describes the distribution of petrophysical properties within lithological units. Observed gravity (Figure 5.4a) and calculated gravity (Figure 5.4b) values show the initial model has a RMS misfit of 15.17 mGal (~24% of the total dynamic range). Residual gravity data (observed-calculated, Figure 5.4c) of high positive misfit (> 15 mGal) correspond to the Housetop region. In contrast, east of the RCG, region between Heemskirk and Meredith Granites and south of the study area show a negative residual (< -10 mGal). This initial model indicates that the densities or geometries of structures within these regions of the model need to be reconciled.

Comparison of observed magnetic (Figure 5.4d) and calculated magnetic (Figure 5.4e) responses of the initial model shows an RMS misfit of 202.03 nT (2.2% of the total dynamic range; Figure 5.4f). Despite the misfit obtained being relatively low, the residual magnetic anomaly indicates pronounced positive anomalies (> 500 nT) in some parts of the study area such as the Housetop region, Arthur Lineament and areas correlating with CMUC and CCW.

In contrast, the south of the study area shows a negative residual anomaly which coincides with Cambrian Granites. This initial model also highlights that the magnetic susceptibility of Arthur Lineament is likely to be higher than the assigned magnetic susceptibility. It indicates that either the geometry or magnetic properties of CMUC, CCW and Cambrian Granites need adjustment.

Homogeneous inversion of gravity data produces a RMS misfit of 7.65 mGal (12% of the total dynamic range, Figure 5.5a). The large reduction in the misfit is principally a function of the increase in the density of the Devonian Granites to a mean density of 2.65 g cm^{-3} to compensate the residual anomaly in the Housetop region. The petrophysical database shows that a density of 2.65 g cm^{-3} is equal to the maximum permitted density of the granites. This suggests that the geometry of this unit needs further refinement.

Homogeneous inversion of magnetic data reduces the RMS misfit to 191.10 nT (2.1% of the total dynamic range, Figure 5.5b) by assigning higher magnetic susceptibility to Arthur Lineament. We treat this lineament as one unit and accept an average magnetic susceptibility of 10.161×10^{-3} SI as the representative value. The optimised magnetic susceptibilities obtained from magnetic homogeneous inversion are then applied to a new reference model for heterogeneous and geometry inversion. In the final model the CMUC, CCW and MRV units were considered as heterogeneous whereas the other units were considered as homogeneous. Once the magnetic susceptibility values of the homogeneous units were set, the magnetic susceptibility was adjusted for the heterogeneous units. The heterogeneous inversion decreases the misfit to 165.67 nT (1.8% of the total dynamic range; Figure 5.5c).

Chapter 6 - 3D inverse modelling of the prospective Heazlewood-Luina-Waratah region combining improved geological mapping and constraints from petrophysics

The Heazlewood-Luina-Waratah area is a prospective region in northwest Tasmania with several historically important mineral mines including the Cleveland and Magnet deposits. Major generations of mineralisation (Sn-Cu, Ag-Pb, Sn) across this region are mostly related to the emplacement of ultramafic complexes and/ or granite intrusions. Despite this, the complex geology of the area is poorly understood due to the difficult terrane and dense vegetation. Airborne geophysical data show several zones of high magnetic intensity, mainly due to ultramafic complexes and contact aureoles surrounding granite intrusions. Due to difficult access, there are large areas covered by very few gravity observations.

The recently published 1:25,000 Waratah geological map (Cumming and Everard, 2017), as well as the recently revised 1: 25,000 Luina map (Everard and Cumming, 2016a) and a detailed geological map of the Heazlewood River Ultramafic Complex (Peck, 1990) provide an opportunity to further study the geological structure by combining datasets through modelling. In this study, I construct a high resolution 3D geological model of the area using constraints from geological maps, and geological and geophysical sections. This new 3D model aims to refine the geometry and properties of major geological units as an aid to future mineral exploration. In addition, the model aims to provide new information on the tectonic history of the Heazlewood-Luina-Waratah region with win the context of western Tasmanian geological evolution.

6.1. Geological/tectonic overview

The Heazlewood-Luina-Waratah study area is located in northwest Tasmania between 355 000 to 375 000 mE and 5 400 000 to 5 420 000 mN (all coordinates on GDA 94 datum, MGA zone 55). The dimensions of the constructed 3D model are 20 km by 20 km with a depth extent of 10 km. This area encompasses a range of lithological units including Proterozoic metasedimentary units, Cambrian allochthonous sequences, complex ultramafic packages, Cambrian volcano-sedimentary rocks, Devonian granites and extensive Cainozoic basalt flows (Figure 6.1).

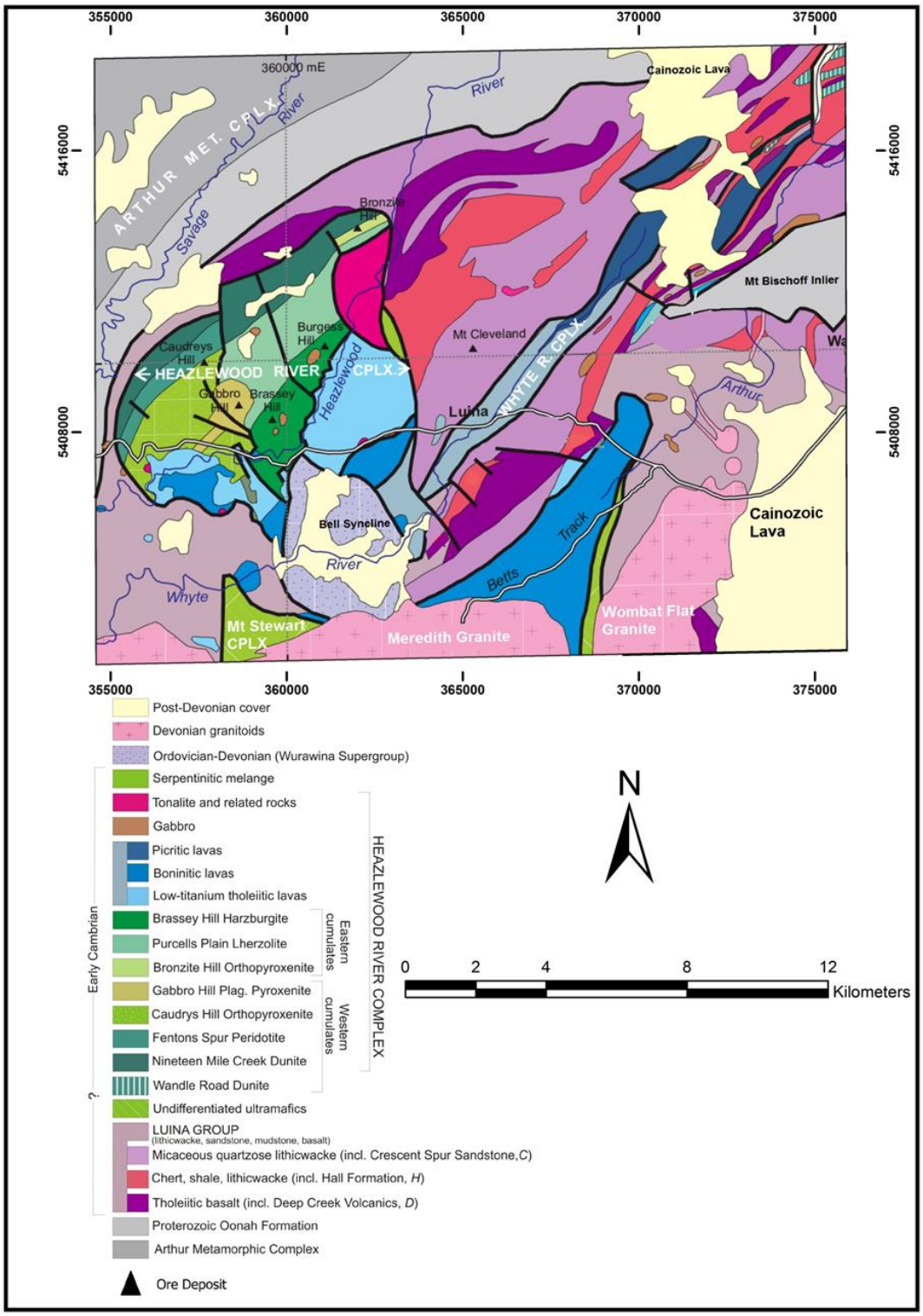

Figure 6. 1 - Geology map and major mineral deposits of the Heazlewood-Luina-Waratah region (Plum box in Figure 1.1; Reference: (Cumming et al., 2016) modified from Corbett et

Late Mesoproterozoic-Early Neoproterozoic sedimentary successions of the Oonah Formation are thought to form basement and outcrop in the west of the Luina-Waratah area. To the northwest, rock units of the Late Neoproterozoic Arthur Metamorphic Complexes were

metamorphosed in the Cambrian Tyennan Orogeny (Chmielowski and Berry, 2012) and are bound to the Heazlewood River Complexes and Luina Group. To the east, the fault bounded Mt Bischoff Inlier comprises pelites, quartz- sandstone and less abundant dolomite. The Mt Bischoff Inlier is correlated with the Oonah Formation also recent age-dating suggests the inlier is younger (Cumming et al., 2016; Seymour and Calver, 1995; Seymour et al., 2007). The Luina Group (previously known as the Cleveland-Waratah association- CCW) is a series of Early Cambrian allochthonous volcaniclastics, rift related basaltic lava flows, maroon siltstone and chert. These units were obducted over the Oonah Formation and Mt Bischoff Inlier (Corbett et al., 2014a). Three major formations of the Luina Group across the study area include: (1) the Deep Creek Volcanics; made up of tholeiitic basalts with locally developed pillows and minor intercalated tuff (basaltic Luina Group in this study), (2) the Crescent Spur Sandstone comprised the quartzose lithickwacke with interbedded siltstone, mudstone and minor mafic tuff and (3) the Hall Formation of maroon siltstone and mudstone, carbonaceous mudstone (Collins, 1983). Large areas of Early Cambrian boninitic and low titanium tholeiite lavas, of island arc-origin, were also emplaced during the obduction event (Corbett et al., 2014a).

Three mafic-ultramafic complexes have been mapped in this region: The Heazlewood River Ultramafic Complex (UC), the Mt Stewart UC and the Whyte River Complex. These UCs are predominately enclosed by the Luina Group (Griggs, 2002). The Heazlewood River UC, the largest and most lithologically diverse ultramafic complex in Tasmania, is thought to have a thickness of ~ 5 km. It comprises commonly layered and partly serpentinised peridotites and pyroxenites, probably representing cumulates derived from boninitic and low-titanium tholeiite lavas, together with gabbros, troctolites, tonalites and mafic and ultramafic dykes. The UC has two major cumulates: (1) the Eastern cumulates contains formations of the Brassey Hill Harzburgite, Parcells Plain Lherzolite and Bronzite Hill Orthopyroxenite, and (2) the Western cumulates are characterised by presence of the Gabbro Hill Plagioclase Pyroxenite, Caudrys Hill Orthopyroxenite, Fentos Spur Peridotite, Nineteen Mile Creek Dunite and Wandle Road Dunite. Tonalite and gabbro are also distributed within this UC. (Corbett et al., 2014a; Peck, 1990; Peck and Keays, 1990a, b). A westward transport direction for this complex has been suggested associated with the Cambrian tectonic evolution of Tasmania during the emplacement of complexes (Mulder et al., 2016; Peck, 1990; Peck and Keays, 1990a). The Heazlewood River UC is composed of several highly magnetic sheet-like bodies and a larger less-magnetised central unit (Poker, 2013). The last phase of igneous activity in the complex

was the Heazlewood Tonalite which has been dated at 513.5 ± 5 Ma (Turner et al., 1998). The Mt Stewart UC dominantly comprises layered cumulates of dunite, harzburgite and orthopyroxenite dykes and veins which are metamorphosed and intruded by the Meredith Batholith, probably at shallow depth (Corbett et al., 2014a). The Whyte River UC contains both boninites and low-titanium tholeiites which is bounded within the Luina Group toward east of the Heazlewood River UC (Brown, 1986; Collins, 1983).

The Bell Syncline, referred as the Huskisson Syncline by Newnham (2001), is located northwest of the Mt Stewart UC. This syncline contains Ordovician Moina Sandstone and Gordon Limestone overlain by Silurian-Devonian Eldon Group sandstones and siltstones and Crotty quartzite. Cambrian and Devonian deformations have changed the geometry of allochthonous sheets to steeply dipping and fault bounded units (Richardson, 2014). The Late Devonian Meredith batholith, which crops out in the south and west of the study area, consists of an unfractionated hornblende-bearing monzogranite, the Wombat Flat Granite (373.2 ± 1.9 Ma; Black et al., 2005) and the more fractionated and felsic Meredith Granite (372.2 ± 1.9 Ma; Kositcin and Everard, 2013). Although their dates are within error, the form of their contacts suggests that the Wombat Flat Granite may be the younger. Both are considered I-types and have been assigned to the same suite (Seymour et al., 2014). The contact aureole of the Meredith batholith displays an enhanced magnetic response that extends up to 2 km into the host rocks, which include the Luina Group, boninites, ultramafics and Eldon Group sandstones (Griggs, 2002). Cainozoic basalts and glacial deposits locally form a thin cover (Seymour et al., 2007) and pendants of Permian siltstone and diamictite (Cumming and Everard, 2017).

6.1.1. Mineralisation

The study area encompasses a wide variety of ore deposits, notably the Cleveland Sn-Cu deposit and the historically important Magnet silver-lead deposit. In contrast, the Mount Bischoff tin deposit, the world's largest at the time of its discovery in 1871, lies just to the east. In addition, there are numerous smaller historic mines and prospects in the area; other commodities recorded and investigated include gold, zinc, tungsten, nickel, osmiridium and chromite (Corbett et al., 2014b; Figure 6.1). At least two major generations of mineralisation have been documented across the area: (1) mineralisation directly related to the emplacement of UCs (e.g. Ni, chromite, osmiridium); and (2) mineralisation associated with Devonian hydrothermal events (e.g. Cu, Pb, Zn) related to granite intrusions (Newnham, 2001). The Heazlewood River and Mt Stewart UCs are considered prospective for Avebury-style Ni

deposits especially proximal to granite intrusions (Newnham, 2004). Mt Bischoff and similar, smaller Sn-W deposits (e.g. the Mt Youngbuck and Contact Creek anomalies) formed throughout the action of fluids emanating from Devonian granites and granite porphyry dyke swarms, which reacted with alkaline carbonate rocks (Morrison, 2002; Richardson, 2014). Devonian vein-related Pb-Zn deposits and polymetallic skarns are situated within the contact aureole of the Meredith Batholith (Griggs, 2002). The alteration halo associated with Meredith Batholith is also linked to three substantial deposits: the Mt Bischoff (Sn), Magnet (Ag-Pb-Zn) and Cleveland (Sn, Cu) deposits (Newnham, 2001).

Deposits associated with UCs can be grouped as follows: platinum group elements (PGE; largest producer of osmium and iridium in the early 1900's), Cu-Au (Old and New Jasper, Duff's Hill), Ag-Pb-Zn (Mt Stewart, Mt Wright-Heazlewood and Godkin Mines), Ni sulphide (Purcells, Fentons Knob and Lord Brassey Mines), W skarns (Mt Youngbuck) (Newnham, 2001). Furthermore, at Mt Bischoff deposit, to the east of the study area, three styles of mineralisation are observed: stratiform replacement of dolomite horizons by massive sulphide containing cassiterite; altered porphyry dykes enriched in topaz, cassiterite and disseminated sulphide; and fractures and fault fissures mineralised with vein quartz, sulphide and cassiterite (Halley, 1987).

6.2. 3D model construction

In this study the Paradigm GOCAD Version 2009.4 geological modelling package (Mallet, 1992; http://www.pdgm.com) was used to generate and modify an initial 3D model. The software VPmg^{TM} Version 7.1 (Fullagar, 2013; Fullagar et al., 2004; Fullagar et al., 2008) has been used to perform forward modelling and property and/or geometry geophysical inversions.

While the study area has been part of some regional scale geophysical/geological studies (e.g. Eshaghi et al., 2016; Eshaghi et al., 2016; Murphy et al., 2003; Webster, 2003), Poker (2013) focussed on this region via 2D modelling and unconstrained 3D inversion of potential field data. Nevertheless, this area is predominantly unstudied at high resolution. In this study, three newly drawn geological sections provided by MRT and 2D geophysical models by this study, Webster (2003) and Poker (2013) have been used to construct the initial 3D model. The fault network was constructed using the following: 1:25,000 Luina map (Everard and Cumming, 2016a); the 1: 25,000 Waratah geological map (Cumming and Everard, 2017), the detailed geological map of the Heazlewood River Ultramafic Complex (Peck, 1990), the 1: 50,000 Corina Map (Turner et al., 1991), MRT 1: 250,000 digital geological coverage (Geological

Survey of Tasmania, 1995) and MRT geological sections (Everard and Cumming, 2016b). Surfaces by Murphy et al. (2003) have been used to construct the Meredith Batholith component of the model. This granite body is widely distributed across the Luina-Waratah area to a subsurface depth of 7.5 km (Webster and Leaman 2002). The initial model (Figure 6.2) contains 28 geological units including: basement; Oonah Formation; Arthur Metamorphic Complex; UCs (13 groups); boninites (3 groups); Luina Group (5 groups); Gordon Group; Eldon Group; Devonian Granites and Cainozoic Basalts.

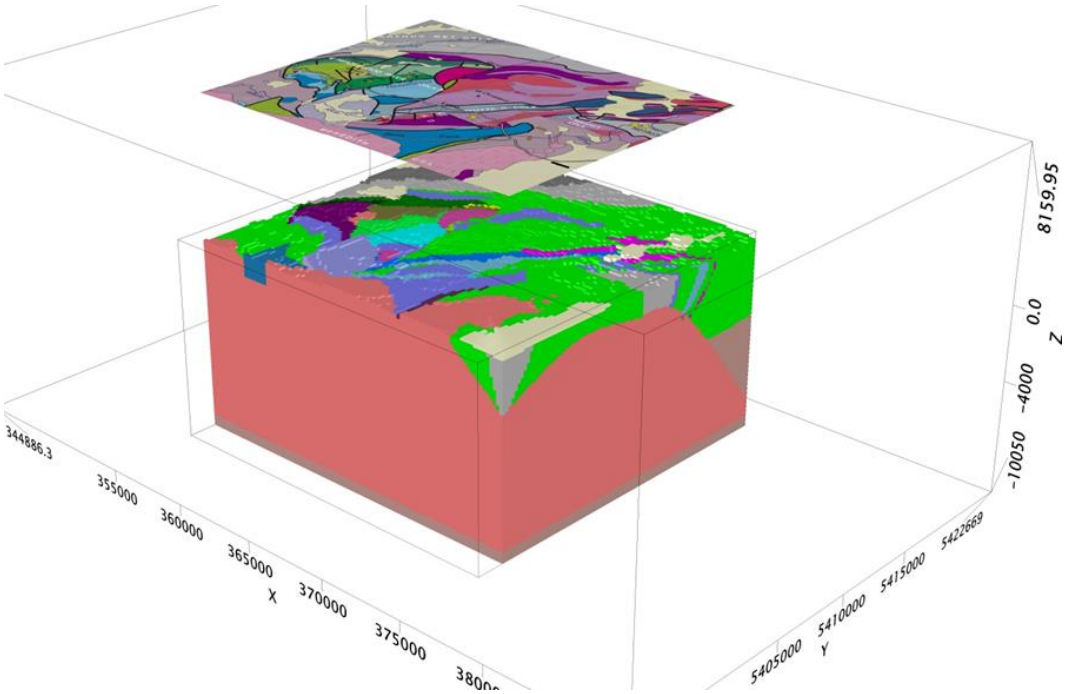

Figure 6. 2 - Constructed initial 3D model (total 28 geological units) displayed to a depth of 10 km (GDA94 datum, MGA55S). Geology map is shown above the model. For geological units refer to geological map in Figure 6.1. The geographic extent of the study area used in modelling is shown in this figure (e.g. Figure 6.3 and subsequent figures).

6.3. Geophysical data and petrophysical constraints

Geophysical data have been compiled by MRT and sourced from MRT online database (2016). Available gravity data consist of 276 observations irregularly distributed throughout the study area. These observations were compiled as part of the state scale gravity grid and the residual Bouguer gravity, with 250 m resolution, is compiled using MANTLE09 model (Leaman, 2009) as described in Chapter 1. MANTLE09 model is consistent with gravity Bouguer data system used by MRT data and hence, Bouguer gravity data calculated based on this model have been used. Across the study area the residual grid has a total dynamic range of ~55 mGal, encompassing significant regions with no gravity observations resulting in high uncertainty

(Figure 6.3a). Hence, the distribution of gravity observations must be taken into account when modelling. The magnetic grid has a resolution of 40 m with a total dynamic range of ~5447 nT (Figure 6.3d).

The Heazlewood River UC is characterised by a high-density zone because of the abundance of gabbro and pyroxenite rich units (Poker, 2013). However, the Heazlewood River UC is clearly a composite body with variable magnetisation due to serpentinisation and unaltered ultramafic materials. Furthermore, the contact aureole to the northeast of the Meredith Batholith displays a high magnetic response. Initial petrophysical properties and allowed ranges were assigned based on estimations by Poker (2013), MRT online database (2016) and this research.

6.4. Modelling

I divide the modelling workflow into two parts: (1) forward modelling and homogeneous inversion are used to investigate the initial 3D model and bulk density and magnetic susceptibility of geological components, and (2) heterogeneous and geometry inversions are employed to study variations of properties within units and refine their geometries. The first part of modelling was performed to assess the initial model and compare calculated responses with observed potential field data and, consequently, identify regions with high misfits. The second part was carried out to better reconcile the model with observed gravity and magnetic data and improved geometry of subsurface features. Unconstrained inversions, for both gravity and magnetic data, have been performed to remove large regional effects while modelling. For this purpose, larger size models (40 km mE × 40 km mE × 15 km mZ) were constructed encompassing the study area and unconstrained inversion modelling carried out upon this area. These unconstrained inversion models numerically assign density and magnetic susceptibility distributions of subsurface based on observed gravity and magnetic data which have been used as the regional model during inversion.

6.4.1. Forward modelling and homogeneous inversion

Forward modelling of gravity data returns a root mean squared (RMS) misfit of 3.12 mGal (5.7% of the total dynamic range) with high misfits within some regions (Figure 6.3b). Homogeneous inversion of the gravity model reduces the misfit to 1.99 mGal (3.6% of the total dynamic range) and partially accounts for regions with pronounced misfit (Figure 6.3c). Pronounced misfits after homogeneous inversion, constrained by petrophysical properties, are

predominantly distributed across the western edge of the Heazlewood River UC (Figure 6.3c; No. 1), north of the study area (No. 2) and within the Bell Syncline (No. 3), as there are no gravity observations available for interpolation. Nevertheless, some areas containing gravity observations (i.e. the Heazlewood River UC; No. 4, north of the Mt Stewart UC; No. 5, north of the Meredith Batholith; No. 6 and in the northeast of the study area; No. 7) also display high misfit.

Forward modelling of magnetic data shows a RMS misfit of 359 nT (6.6% of the total dynamic range) with pronounced misfit throughout the Heazlewood River UC, Bell Syncline and contact aureole (Figure 6.3e). Homogeneous magnetic property inversion, constrained by petrophysical properties, resulted in 336 nT RMS misfit (6.2% of the total dynamic range; Figure 6.3f). The homogeneous inverted model displays locally high positive misfits across the Heazlewood River UC (Figure 6.3f; No. 1), the western half of the Bell Syncline (No. 2) and the Meredith Batholith contact aureole (No. 3). A linear feature of high misfit is observed on the western edge of the Heazlewood River UC and continues toward the Mt Stewart UC (No. 4). Local misfits of the homogeneous inverted models, after taking into the account of the distribution of gravity observations, provide significant insights into further property and/or geometry inversions as discussed in the following section.

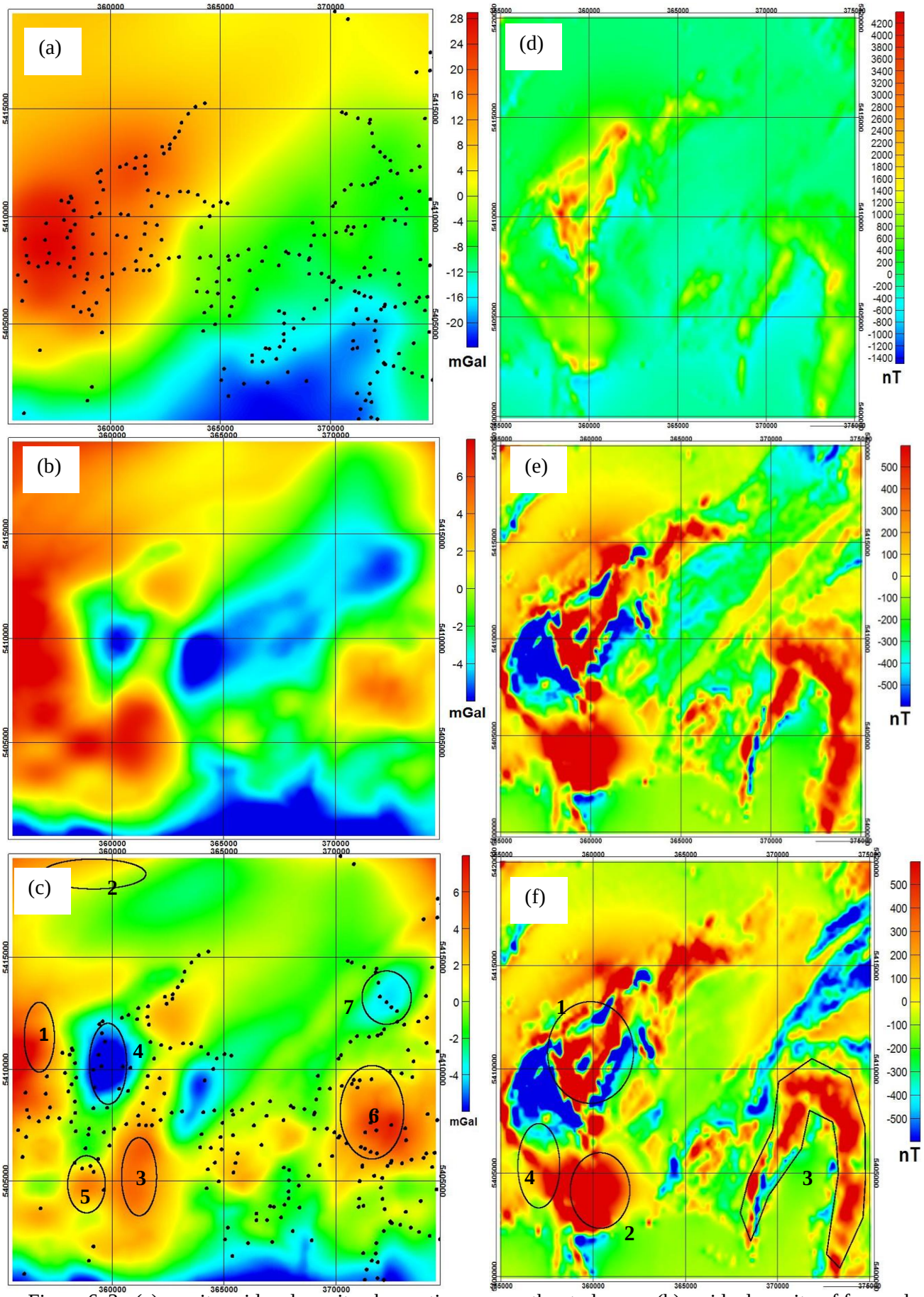

Figure 6. 3 - (a) gravity grid and gravity observations across the study area, (b) residual gravity of forward modelling of the initial model, (c) residual gravity of homogeneous inversion of the initial model, (d) TMI grid across the study area, (e) residual magnetic of forward modelling of the initial model, (f) residual magnetic of homogeneous inversion of the initial model. Polygons and numbers in figures (c) and (f) indicates regions with high misfit in homogenous inverted gravity and magnetic results discussed in the text.

6.4.2. Geometry and heterogeneous inversions

The heterogeneous gravity inversion was performed for components within the Heazlewood River UC and Meredith Batholith contact aureole. The heterogeneous inversion reduces the RMS misfit to 1.80 mGal (3.3% of the total dynamic range; Figure 6.4a). The heterogeneous magnetic property inversion was conducted on components within the UCs, Meredith Batholith contact aureole and basaltic Luina Group. Heterogeneous inversions were performed on features characterised by highly variable petrophysical properties, based on measurements and lithological contexts, and other units were assumed homogeneous. Magnetic heterogeneous property inversion results in a RMS misfit of 106.73 nT (1.96% of the total dynamic range; Figure 6.4b).

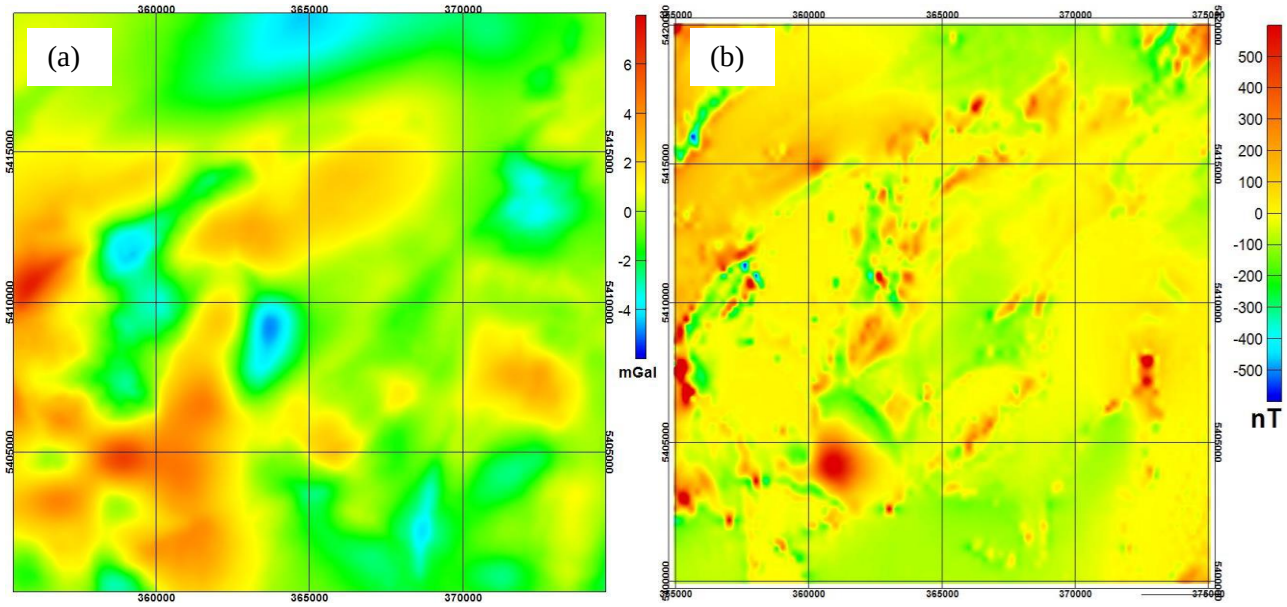

Figure 6. 4 - Heterogeneous inversion of the initial model, (a) residual gravity; (b) residual magnetic

Gravity data and property inversion indicates that the geometry of the northern margin of the Meredith Batholith needs further investigation. Hence geometry inversion for this Devonian granite body was performed. Furthermore, homogeneous and heterogeneous inversions of gravity and magnetic data show that the southern boundary of the Heazlewood River UC has an anomalously high misfit. This area was modelled based on 1:250,000 geological map and is likely to have a high level of uncertainty. Newnham (2001) suggested that the Heazlewood River UC and the Mt Stewart UC are linked beneath relatively shallow cover throughout this region. In a recent study, Radford (2016) used machine learning combined with field observations to study this region and found UCs in an area previously mapped as Luina Group.

I, therefore, modified the geology of this area by placing an UC in this region following the changes indicated by Radford (2016). This geometry refined model (Figure 6.5) was used for heterogeneous gravity and magnetic property inversions.

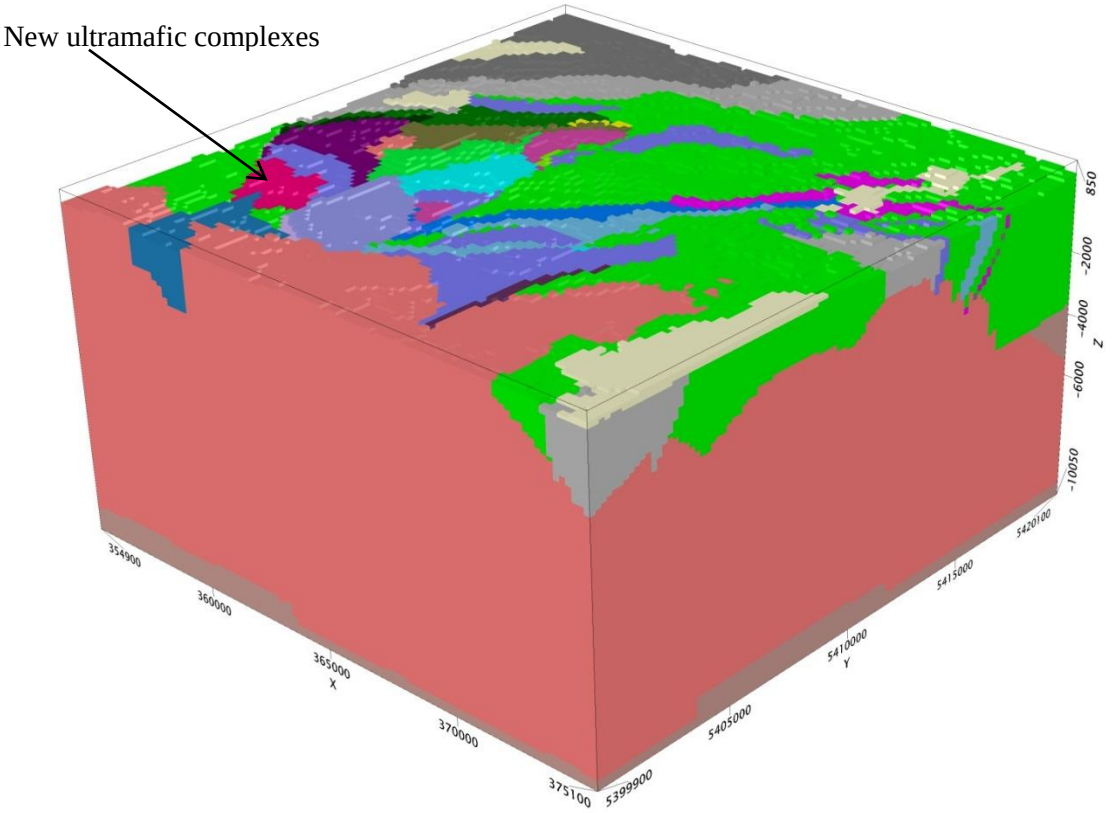

Figure 6. 5 – Geometry inverted refined 3D model. This model shows newly observed ultramafic complexes in south of the Heazlewood River Ultramafic Complexes. The geometry of Devonian Granites has been improved displaying steeply dipping boundaries in the northeast of the batholith. Geology units refer to Figure 6.1

6.5. Sensitivity

The refined model, based on a heterogeneous property inversion, was assessed to investigate the sensitivity of magnetic data with respect to variations in depth. The model was reconstructed for different depths levels (i.e. 1, 2, 3, 4, 5 and 10 km below sea level) and heterogeneous inversions of magnetic data were performed upon these models. Through this sensitivity test, the maximum depth that affects the magnetic property distributions was investigated.

6.6. Results

Property inversions were performed upon the newly refined model to compare results with the initial model. The refined model based on the homogeneous inversion of gravity data returned a RMS misfit of 1.66 mGal (3.02% of the total dynamic range; Figure 6.6a). Heterogeneous inversion of the UCs and Meredith Batholith contact aureole reduces the RMS misfit to 1.25 mGal (2.27% of the total dynamic range; Figure 6.6b). These results may be compared to the values obtained from the initial model stated previously (3.12 mGal). Heterogeneous inversion has not significantly improved the total RMS misfit, whereas it has a significant impact on misfit on the misfit within the Heazlewood River UC and contact aureole and displayed density distribution of subsurface units across these regions. The heterogeneous inversion displays a better consistency with geological knowledge and observed data and also represents petrophysical properties compatible with previously characterised values. This property inversion indicates that the Heazlewood River UC associated with generally pronounced high density values as previously stated in other studies (e.g. Poker, 2013).

The magnetic homogeneous inversion of the refined model displays 244 nT RMS misfit (4.49% of the total dynamic range; Figure 6.6c). Heterogeneous inversion of components within the UCs, Meredith Batholith contact aureole and basaltic Luina Group resulted in 65 nT RMS misfit (1.2% of the total dynamic range; Figure 6.6d). Compared to the residual values obtained from the initial model stated previously (3.59 nT), heterogeneous inversion significantly improved the misfit due to the high variation of magnetic properties within UCs and contact aureole. This inversion improved the understanding of magnetic susceptibility distribution within the UCs, contact aureole and basaltic Luina Group. The heterogeneous inversion displays a better consistency with geological knowledge and observed data and represents petrophysical properties compatible with previously characterised values across the UCs, contact aureole and basaltic Luina Group. This newly heterogeneous model provides valuable insights into serpentinisation of UCs associated with anomalously high magnetic susceptibility values within the features.

The sensitivity test upon the inverted model provided general insights into the depth of features affecting the magnetic observations. This test shows that the maximum depths of the contact aureole and Bell Syncline affecting magnetic observations are between 2 and 3 km and display pronounced changes in residual magnetic data. The test upon the Heazlewood River UC is sensitive to depths between 3 and4 km. The sensitivity test does not show any major impact on

magnetic observation throughout the Mt Stewart UC. Hence the Mt Stewart UC is not sensitive to depths > 1 km, indicating relatively very shallow magnetic sources across this UC.

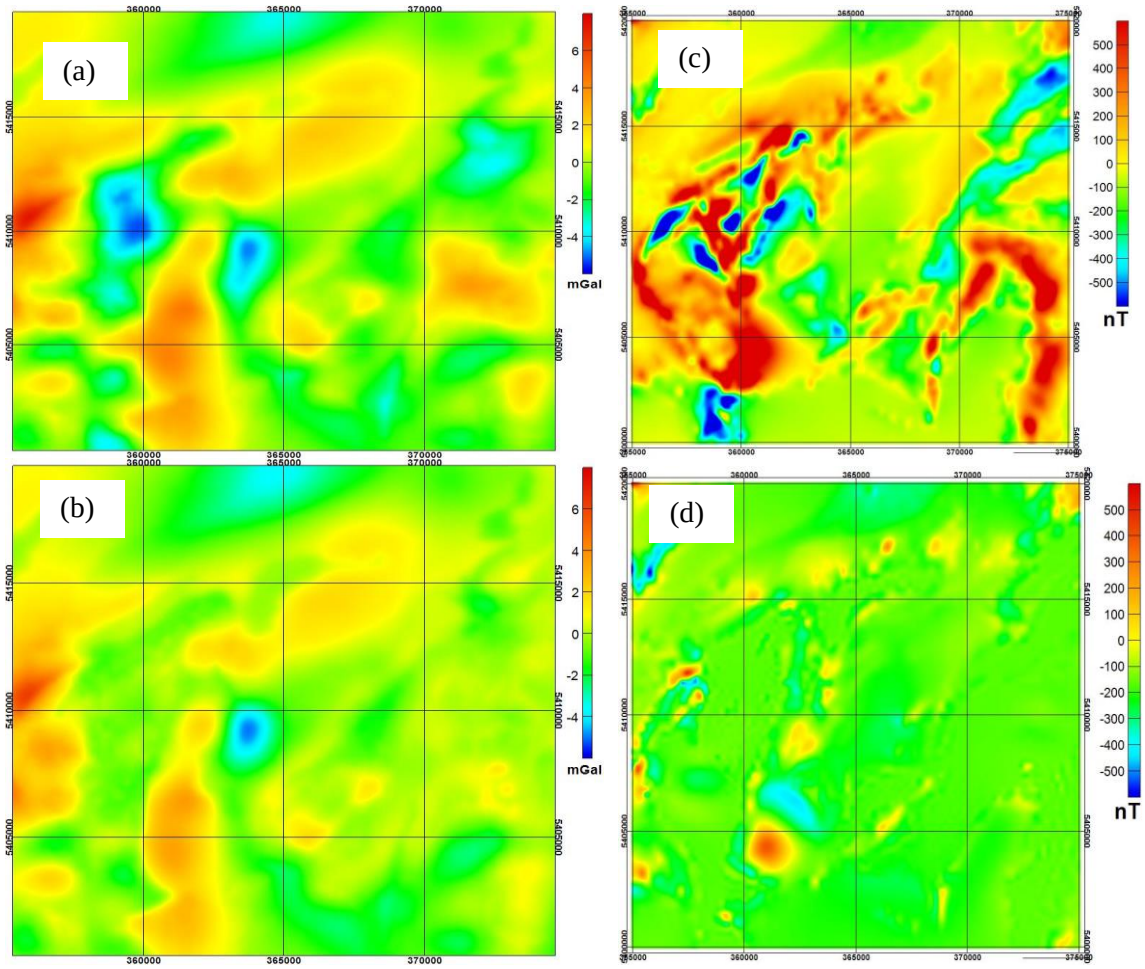

Figure 6. 6 - Property inversion results of the refined model consisting of the recently observed ultramafic complex; (a) residual gravity homogeneous inversion, (b) residual gravity heterogeneous inversion, (c) residual magnetic homogenous inversion, (d) residual magnetic heterogeneous inversion.

6.7. Discussion

The primary challenge with inversion of potential field data is the principle of "non-uniqueness" whereby a known field distribution on a bounding surface can produce an infinite number of source distributions. Resolution at depth must also be considered in the inversion of data to define geological boundaries because geophysical signals may be dominated by the response of shallow features (e.g. Fedi et al., 2005; Li and Oldenburg, 1998; Li and Oldenburg, 1996). In this study, multiple geological, geophysical, and petrophysical data have been used

to constrain some aspects of the model and limit the possibilities for non-unique solutions, and the sensitivity test previously described is carried out to provide insights into the depth resolution of the inversion.

The refined model has improved geometry of major geological units associated with mineralisation (i.e. Devonian Granites) that can help to direct the activities of mineral explorers. Geometry inversion of the Meredith Batholith (Figure 6.7) shows that this unit is more than 10 km thick in south of the study area and the northern boundary of this unit is dipping at a steeper angle than previous models. One of the most notable differences between the initial and refined 3D models is the newly identified geometry of the ultramafic outcrops. The new model is compatible with the recently discovered ultramafic outcrops linking the Heazlewood River UC and Mt Stewart UC. The low residual gravity observed in northeast of the study area may indicate the presence of a near surface granite cupola, possibly analogous to the abundant Devonian porphyry dykes at the Mt Bischoff. As the Devonian porphyry dykes at the Mt Bischoff have associated with mineralisation (Groves and Solomon 1964) , this newly postulated granite cupola is a potential target for future detailed exploration.

The Bell Syncline, displayed in Figure 6.7, indicates high residual magnetic anomalies for both the homogenous and heterogeneous inversions with a relatively shallow source. Newnham (2001) suggested that the Bell anomaly could be an accumulation of magnetite and sulphide within a roofed section of a zone of serpentinised ultramafics. The Ifield Creek magnetite skarn to the east of the Mt Stewart UC is suggested to lie close to the contact with the Bell Syncline remnant and in an embayment of the Meredith Batholith and may be associated with another magnetic skarn on the southeast corner of the syncline (Newnham, 2001). The 1:25,000 Luina geology map supports the presence of a skarn mineralisation in west of the syncline and matches the model across this region. The moderately deep Bell Syncline magnetic anomaly is attractive for mineral exploration because it suggests the presence of altered UCs and a potential geometry as a trap site (Newnham, 2001). In addition, the relative shallow granite depth in this area (~1200 m depth; Figure 6.7) is adjacent to major NNE trending structures (Newnham, 2001) and may be a result of possible reactions between granitic intrusions and Gordon Group carbonate rocks. Absence of gravity observations in this area prevents detailed investigation of anomaly geometry.

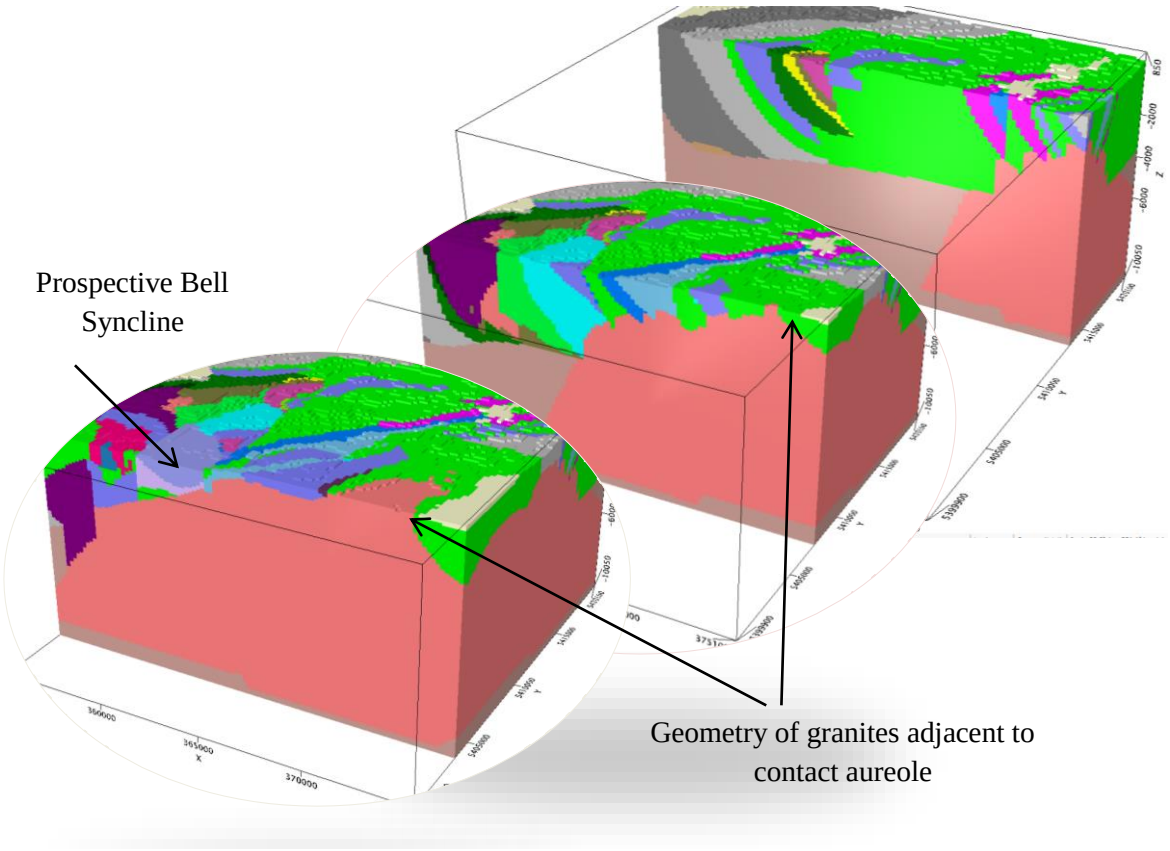

Figure 6. 7 – Slices through the refined model of Figure 6.6 displaying geometry of subsurface units.

Using initial petrophysical properties, property inversion estimates the optimum density and magnetic susceptibility upon the model and observed gravity and magnetic responses. Table 6.1 displays initial and homogeneous inverted petrophysical properties in this study. Density and magnetic susceptibility values can provide insights about the degree of serpentinisation and alteration within subsurface lithologies (Griggs, 2002) and therefore, can be used as an evidence for prospective mineral exploration (e.g. Gonzalez-Alvarez, Ignacio et al, 2010). For example, serpentinisation usually increases the magnetic susceptibility and reduces the density. In addition, mineral content, chemical variation and coherency typically lead to large amount of variability in density of igneous and metamorphic rocks. Increase in metamorphic grade generally increases density (Telford et al., 1990a), similar to the high densities observed across the contact aureole in this study. Property inversion of data shows that the Heazlewood River UC is characterised by high variations in density and magnetic susceptibility. These high density values are relatively unusual compared with petrophysical measurements for other UCs in West Tasmania (e.g. MRT online database 2016, Keele, 1992; Leaman, 2003; McAdam, 2015; Poker, 2013; Webster, 2003). Within the Heazlewood River UC, the Nineteen Mile

Creek Dunite and the Gabbro Hill plagioclase pyroxenite are characterised by high densities (up to 3.07 g cm^{-3}), while the Brassey Hill Harzburgite represents an average density of 2.86 g cm^{-3}. With regards to gravity data, boninites are characterised by low to medium densities based on the MRT petrophysical database (2016). In this study, boninites and low-titanium lavas of the Whyte River Complex, Cb, display a mean density of 2.66—2.71 g cm^{-3}, whereas the porphyritic boninitic lavas) represents a density of ~2.81 g cm^{-3}. Petrophysical measurements by Poker (2013) estimated an average density of 2.79 g cm^{-3} for the flow banded boninitic lavas. The unusually high proportion of dense material in Heazlewood River UC is likely to indicate the presence of gabbro, or other dense lithologies and it implies that the complex may be less serpentinised relative to others in West Tasmania.

Based on the magnetic data, components within the Heazlewood River UC have a wide range of magnetic susceptibilities between ~0 and > 200 × 10^{-3} SI. The heterogeneous inversion displays a highly magnetised thick unit (~1 km thickness) at depths greater than 3 km. Across the Heazlewood River UC, pillowed and flow-banded boninitic lavas and the Nineteen Mile Creek Dunite have a wide range of magnetic susceptibility values emphasising on variable alteration and serpentinisation, while the Heazlewood Tonalite is not magnetised. Likewise, the Mt Stewart UC and the newly modelled UC linking this with the Heazlewood River UC display variable magnetic susceptibilities with a maximum of > 250 × 10^{-3} SI. Additionally, the Luina Group displays heterogeneous magnetic susceptibility values between 0 and 80 × 10^{-3} SI, indicating variable lithological contexts within this unit. Across the contact aureole of the Meredith Batholith geophysical anomalies can be utilised to monitor metamorphism and potential related skarn-type mineralisation (Webster, 1984). According to the 3D model, the contact aureole has a radius of ~ 2 km and depth impact of up to ~ 1.4 km with a maximum magnetic susceptibility of ~ 90 × 10^{-3} SI near the granite intrusion. Figures 6.8 and 6.9 show density and magnetic susceptibility values within regions with anomalously high petrophysical properties. These figures indicate that there is high petrophysical variations across the Heazlewood River UC and contact aureole varying between non-magnetic entities to regions characterised with magnetic susceptibilities of > 320 × 10^{-3} SI. These highly variable petrophysical property distributions are consistent with complex tectonic evolution of West Tasmania and Tabberabberan Orogeny event during the Jurassic (e.g. Berry and Bull, 2012; Berry and Crawford, 1988; Crawford and Berry, 1992; Seymour and Calver, 1995; Seymour et al., 2007). Throughout the syncline, property inversion of magnetic data assigns very high magnetic susceptibility values to Gordon and Eldon Groups in response to the pronounced magnetic anomaly.

Unit	Group (ID)	Density (reference of 2.67 g cm^{-3})		Magnetic susceptibility (×10^{-3} SI)	
		Initial	Inverted	Initial	Inverted
Cainozoic basalt	TB	0.23	0.230	42.70	12.976
Devonian Granite	DGR	-0.06	-0.052	0.39	0.000
Eldon Group	SD	-0.03	0.016	0.39	3.940 (?)
Grodon Group	Ol	0.04	0.049	0.28	4.000 (?)
Boninitic and low-Ti lava	Low-titanium tholeiite (Cbm)	0.07	0.043	0.30	0.000
Boninitic and low-Ti lava	Boninite and low-Ti lava (Cb)	0.03	-0.012	0.11	0.000
Boninitic and low-Ti lava	Porphyritic boninitic lava (Cba)	0.11	0.137	0.60	17.999
Luina Group	Contact aureole (Ecwc-Aureole)	0.12	0.068	12.00	25.237
Luina Group	Ccwc	0.11	0.032	12.00	0.000
Luina Group	Crescent Spur Sandstone (Ccwq)	0.08	0.071	8.60	3.501
Luina Group	Beneath Bell Syncline (Ccw-Depth)	0.15	0.177	18.05	25.368
Luina Group	Basaltic Luina Group (Ccwb)	0.13	0.119	30.11	29.969
Ultramafic Complex	Nineteen Mile Creek Dunite (Csdn)	0.35	0.327	80.00	48.715
Ultramafic Complex	Purcells Plain Lherzolie (Cspsl)	0.35	0.250	140.00	60.218
Ultramafic Complex	Whyte River Complex (Cbbp)	0.11	0.012	8.00	0.646
Ultramafic Complex	Serpentinised orthopyroxene dunites (Csps)	0.35	0.339	89.90	79.657
Ultramafic Complex	Gabbro Hill Plagioclase Pyroxenite (Cgh)	0.35	0.345	50.00	78.689
Ultramafic Complex	New ultramafic Complex (New UC)	0.35	0.301	20.00	55.983
Ultramafic Complex	Fentons Spur Peridotite (Cfs)	0.35	0.370	10.00	5.612
Ultramafic Complex	Caudreys Hill Orthopyroxenite (Cch)	0.35	0.370	12.18	8.000
Ultramafic Complex	Brassey Hill Harzburgite (Cspsh)	0.23	0.186	40.00	27.494
Ultramafic Complex	Beneath Bell Syncline (Cs-Depth)	0.09	0.112	100.00	105.865
Ultramafic Complex	Heazlewood Tonalite (Ctt)	0.09	0.114	2.80	2.410
Ultramafic Complex	Bronzite Hill Orthopyroxenite (Cspsb)	0.35	0.350	90.40	83.860
Ultramafic Complex	Mt Stewart	0.12	0.160	9.00	39.996
Ultramafic Complex	Massive serpentinite (Csm)	0.35	0.350	80.00	57.131
Arthur Metamorphic	Arthur MC	0.12	0.161	15.00	16.863
Oonah Formation	Po	0.07	0.057	0.59	3.000
Basement	Base	0.00	0.002	0.08	0.000

Table 6. 1 - Summary table displaying initial and homogenous property inverted density and magnetic susceptibility values of units. Initial assigned properties were estimated based on Poker (2013), MRT online database (2016) and Eshaghi (2017). High average magnetic susceptibilities marked with "?" symbol are anomalously high, representing misleading geometry or highly altered units across the Bell Syncline. Group (ID) is presented to distinguish different sub-units. Density values are with respect to the average density of 2.67 g cm^{-3} used in Bouguer gravity data processing.

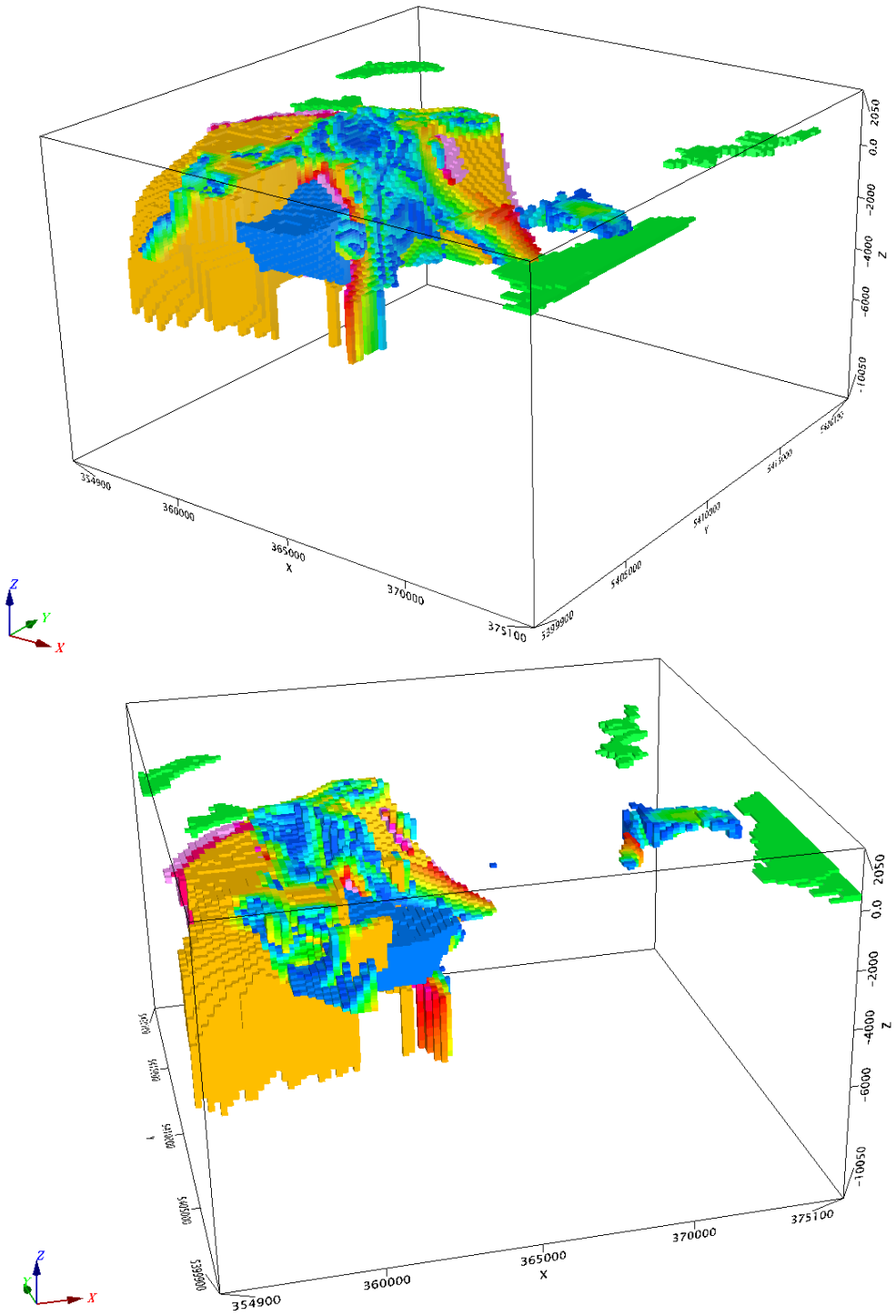

Figure 6. 8 - Density properties ranged 2.83—3.07 g cm^{-3} displaying the Cainozoic basalt, contact aureole and Ultramafic Complexes across the study area. Colours represent density values (green: low; red: high). This figure displays density properties. For unit names, refer to Figures 6.5 and 6.7.

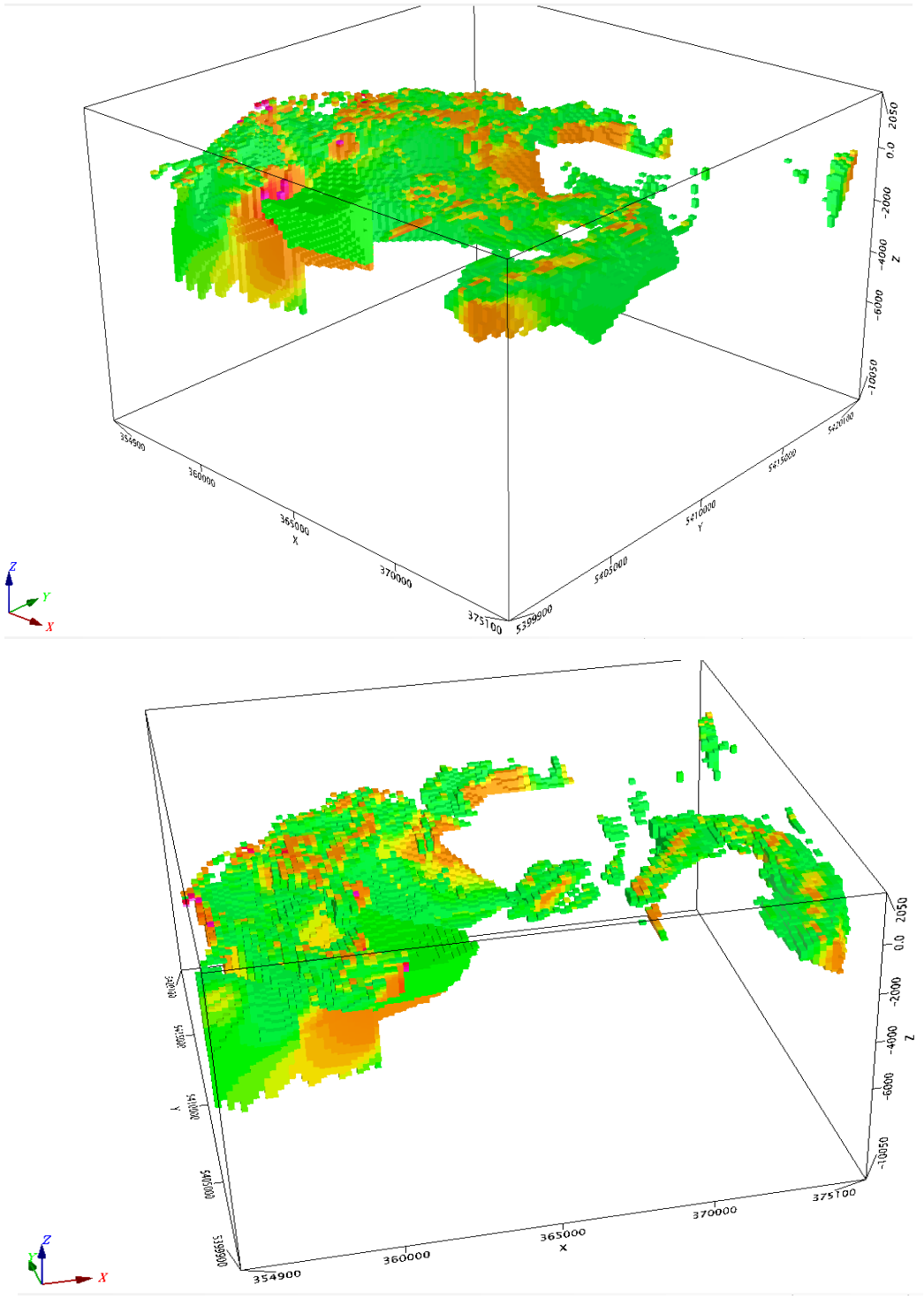

Figure 6. 9 - Magnetic susceptibility values between 0.035 and 0.33 SI distributed across the study area. These values predominantly display the Ultramafic Complexes and contact aureole. Colours represent the magnetic susceptibility values (green: low; red: high). This figure displays magnetic susceptibility properties. For unit names, refer to Figures 6.5 and 6.7.

The geometry of western edge of the Heazlewood River UC is debated in several studies. For example, geophysical studies (i.e. Poker, 2013; Webster, 2003) suggested a west-dipping

boundary for western edge of this UC. Poker (2013) modelled the boundary of this UC as shallowly dipping toward the west. Geological maps (i.e. Peck, 1990) and cross-sections suggest the western edge of this UC is dipping towards the east. The 3D model, incorporating the geological maps and cross-sections, has resulted in an east dipping fault network throughout the western boundary of the UC. The magnetic data inversion is confirmed as compatible with an east dipping contact with the heterogeneities identified likely giving rise to the westward dipping models previously suggested by 2D geophysical inversions.

6.8. Conclusions

I have constructed an initial 3D geology model based on all available geological, geophysical and petrophysical information for the Heazlewood-Luina-Waratah region of western Tasmania. This initial model has been first investigated using a geometry inversion of Devonian granites and information from recent geological field work (Everard and/or Cumming, in prep and pers comm). An UC linking the Heazlewood UC and the Mt Stewart UC has been modelled in this study for the first time. This newly identified complex is a likely target for future mineral exploration. The refined geometry shows a very thick Meredith Batholith (> 10 km) in south and a possible near surface granite cupola toward northeast of the study area.

Further modelling using property inversion has revealed a high degree of variation in petrophysical properties within the ultramafic complexes in this area. The range of density and magnetic susceptibility values throughout the UCs indicates a variable degree of serpentinisation and alteration within these units. The Bell Syncline is characterised by shallow magnetic sources which could indicate skarn mineralisation. The sensitivity test, and the final refined model, show that the Heazlewood UC is characterised by a thick complex (~4 km), while the contact aureole and Mt Stewart UC are thinner (< 2 km).

Chapter 7- Summary

The research documented in this thesis has investigated the deep geological structure of Tasmania, in the context of eastern Australia, and with a focus on west Tasmania. This investigation was carried out through the integration of multiple geophysical datasets, petrophysical characterisation of significant lithological units, and application of geologically and petrophysically constrained 3D modelling of potential field data. This research comprises the estimation of the CPD across east Australia at a sub continental scale, moving toward refining Moho depth at a regional scale study across onshore and offshore Tasmania, investigating major geological features across West Tasmania at a local scale and finally concentrating on the prospect scale modelling of the Heazlewood-Luina-Waratah region.

In this chapter, the research advances are summarised together with the main limitations. The major questions that were outlined in Section 1.4 are discussed in this chapter. This chapter also provides a summary of how the results from separate chapters might be interpreted together (where appropriate) in the context of improved pre-competitive information for mineral explorers, and finally in the context of the refinement of 3D geological structures in Tasmania.

7.1. Research Advances

7.1.1. New petrophysical constraints

One of the main challenges in the 3D modelling of potential field data is to assign representative petrophysical (i.e. density and magnetic susceptibility) values and ranges (maximum and minimum) to the lithological units. Previously available petrophysical measurements were dominantly characterised based on surface/shallow subsurface sampling with weathering effect or samples were collected from local investigations resulting in characterisation with a high level of uncertainty.

Because of paucity of petrophysical measurements from deep major units, I collected samples from depths > 100 m with negligible weathering effect and improved petrophysical database in Chapter 3 to better constrain density and magnetic susceptibility properties assigning to each unit. The newly measured and characterised density and magnetic susceptibility values have significantly added knowledge into the database of representative petrophysical properties across West Tasmania. For example, Precambrian basements across West Tasmania were previously characterised by a density range of 2.64—2.69 g cm^{-3}, while the new measurements

show these units are characterised by densities higher than 2.73 g cm^{-3}. I used this newly improved database during the local and prospect scale modelling.

7.1.2. New geophysical modelling

During 3D modelling at different scales of this study, one difficulty was using different types of data, which could be contradictory, to construct an improved, refined, model. Geological observations, seismic models, potential field interpretations and tectonic scenarios, used to construct a representative model, might individually imply different results in some cases.

I prioritised particular input databases while addressing these contradictions/inconsistencies. For example, during the construction of the Tyennan Margin Fault within the local scale model of West Tasmania, the seismic data showed a steeply west dipping geometry for this boundary, while the magnetic data indicated a dip in the opposite (eastward) direction. I prioritised and used the seismic interpretations with a higher level of certainty to construct this boundary. Another instance of data inconsistency concerns the geometry of western edge of the Heazlewood River UC during construction of the prospect scale model. While, previous geophysical models suggest that this boundary is west dipping, geological observations and sections suggest an east dipping boundary. I used geological sections to construct the initial model, with the boundary dipping east, and inversion showed this east dipping geometry can successfully account for geophysical observations. Therefore, the newly constructed models are, to some extent, different from previous models because of using recently published and more reliable data.

7.2. Response to major research questions

The questions posed in "Section 1.4: major research questions to be addressed" were pursued in chapters 2, 4, 5 and 6 and the responses are summarised in this section. Correlations between tectonic boundaries (i.e. Moho and CPD) using different geophysical data and methods have been investigated in Chapters 2 and 4. In addition, subsurface geology was better constrained using a multi-disciplinary approach and 3D potential field modelling across West Tasmania (local scale, Chapter 5) and the Heazlewood-Luina-Waratah region (prospect scale, Chapter 6) to address the questions.

7.2.1. On a sub continental scale, does the Curie Point Depth (CPD) determined from spectral analysis of magnetic data correlate with Moho depth

determined from seismic data throughout east Australia? What do any disparities between these depth surfaces tell us about the overall context of tectonic structure and evolution?

Chapter 2 showed a sub continental scale CPD model, with a resolution of 100 km × 100 km across east Australia and 50 × 50 km across Tasmania, that improved knowledge in comparison to previous studies. Relationships between the CPD and seismic Moho depth across east Australia indicate that these boundaries correlate to some extent. The range of differences between these two boundaries is usually within the expected uncertainties of models. Nevertheless, Proterozoic basements and northern parts of the Thomson and Lachlan Orogens indicate deeper CPDs than the seismic Moho depth. This could be because of presence of features associated with low thermal gradient (i.e. Precambrian terranes). The other scenario is that upper parts of the lithosphere are magnetised and the Moho boundary is not necessarily a magnetic boundary. The estimated CPDs are predominantly deeper than expected from geothermal gradients estimated from the OZTemp model. This paradox between estimated and expected CPDs could be due to the uncertainty in large scale spectral analysis of aeromagnetic data and/or the incomplete understanding of the thermal regime and undergoing terranes associated with low geothermal gradient at depths deeper than 5 km.

Tasmania generally exhibits shallower CPD ranges compared to the average CPD values across east Australia indicating the possibility of more recent active tectonics associated with a higher average geothermal gradient. In detail, northeast Tasmania shows a shallower CPD range compared to western parts of Tasmania which would be consistent with the presence of younger terranes and tectonic evolution of this region.

7.2.2. Does the Moho depth defined by gravity data correlate with the Moho depth defined by seismic data for the Tasmania region? What do any disparities between these depth surfaces tell us about the evolution of Tasmania?

Chapter 4 examined a 3D regional scale model, with a resolution of 1000 mE × 1000 mN × 500 mZ, to improve knowledge about the gravity constrained Moho depth compared to the previous seismic Moho depth across onshore and offshore Tasmania. The refined gravity derived Moho depth can assist to better reconcile tectonic structures throughout Tasmania. Findings in this chapters show that the gravity Moho depth does not correlate with the seismic constrained Moho model. The gravity model shows that the study area is characterised by the continental crust without the presence of the (purely) oceanic crust. Compared to the seismic

Moho depth, the gravity Moho depth is generally deeper across onshore Tasmania. Northeast Tasmania is characterised by very deep Moho depths (up to 40 km), unlike the seismic model. This is likely due to the crustal thickening across this region during Tabberabberan. The gravity constrained Moho depth delineates the crustal thinning across the Bass Basin and beyond the unstretched continental crust limit.

7.2.3. Is it possible to better constrain subsurface geology in the region of West Tasmania using a multi-disciplinary approach and 3D potential field modelling? How might any improvements aid the understanding of tectonic processes and help to direct the activities of mineral explorers?

The local scale model in Chapter 5, with a resolution of 500 mE × 500 mN × 200 mZ, has improved knowledge into distribution of major geological features (e.g. Devonian Granites) using a multi-disciplinary approach and 3D potential field modelling across West Tasmania. In this chapter, I found that the Devonian Granites have shallower depths between the Heemskirk and Meredith Granites and are deeper toward west of the Rocky Cape Group compared to the initial model. In addition, the refined model shows the maximum thickness of Housetop Granites is < 6 km with likely thick (1—2 km thickness) and highly magnetised ultramafic complexes at depth throughout the Housetop region. This model also identifies two granitic intrusions: 1) a new granitic body across east of the Rocky Cape Group, with minimum depth of > 3 km, with a possible emplacement age of either Neoproterozoic or Devonian, and 2) a non-magnetic, low density Cambrian Granite component in south of the MRV following 2D models presented by Leaman (2003). The newly identified granitic intrusion across east of the Rocky Cape Group suggests a wider distribution of either Neoproterozoic or Devonian Granites across West Tasmania. Therefore, the implication of the newly identified granitic body in the east of the Rocky Cape Group is to suggest a greater extent of the Neoproterozoic or Devonian tectonic events across Tasmania. If this granitic unit has a Neoproterozoic origin, it would improve our insights into the possible extent of Wickham Orogeny and its impact across northwest Tasmania. The newly identified granitic body to the west of the Rocky Cape Group has a minimum depth of deeper than 3 km and would be challenging to drill directly, whereas the likely Cambrian Granite component in south of the MRV has an estimated burial depth of ~1 km and can be accessed by a deep drill hole for a direct sampling for petrophysical characterisation and determining the exact age of the component via geochronology.

To direct the activities of mineral explorers, the refined geometry across West Tasmania suggests the presence of possible deep mineralisation (e.g. Ag, Pb-Zn, Fe, W skarn) across the Housetop region, similar to the Heazlewood UC. In addition, the Heemskirk and Meredith Granites are linked at shallower depths, compared to previous models, and that this is compatible with known and potential mineralisation between these two components. Hence, the local scale model emphasises that the area between the Heemskirk and Meredith Granites units could be a target for further future exploration activities.

7.2.4. Is it possible to make similar improvements on a local and prospect scale and how might these improvements help to direct the activities of mineral explorers?

Chapter 6 showed a prospect scale model, with a resolution of 200 mE × 200 mN × 100 mZ, providing insights into distribution and geometry of major units across the Heazlewood-Luina-Waratah region. The model improved constraints on the geometry of the Meredith Batholith and exhibited recently observed ultramafic complexes linking the Heazlewood River and Mt Stewart UCs. The refined geometry of batholiths indicates that the northern part of this component has a steeply dipping boundary at depth with likely granite cupolas at shallow depths (less than 2 km depth) toward northeast of the study area. Property inversions of the model show that the Heazlewood River UC are characterised by a high internal variation of density and magnetic susceptibility values. These complexes are also characterised by high average density values. In addition, geometry and property inversions of the contact aureole of the Meredith Batholith and Mt Stewart UC show these units have a maximum depth extent of < 2 km with variable density and magnetic properties. This model identifies three regions with potential for mineralisation for future explorations at a deposition scale which are discussed in Section 7.3.

7.3. Improved pre-competitive information to direct mineral explorers

The Mineral System framework, noted in Chapter 1, links locations that may be prospective for ore deposits to their wider context. According to the mineral system framework, deep tectonic events are a source of energy to drive fluids (and intrusions) through the crust at a very large scale. Investigation of the CPD across east Australia provides a significant insight into the geometry and source of deep crustal fluids associated with shallow CPDs and prevailing geothermal regime. In this study, the sub continental scale CPD investigation can help to identify high heat flow throughout the lower parts of the crust and highlight regions

inconsistent with previous large scale scenarios for further detailed investigations. Across Tasmania, the CPD is generally shallower than the average CPD values across east Australia. It indicates a generally higher geothermal gradient compared to east Australia and consequently a shallower source of crustal fluids across Tasmania.

The regional and local scale studies link the coarse resolution continental scale models to detailed prospect/ deposit scale studies and bridge between the large scale understanding and any prospect scale study. The regional scale study has concentrated on crustal scale tectonic boundaries, refining the gravity constrained Moho depth, and also provides insights into the upper lithospheric architecture. The regional model indicates that the upper crust throughout Tasmania is associated with distribution of low density components, typically Devonian granites. The granites are the mid-to deep sources of the fluid that migrate to the shallower depths through fault system. Intrusion of granites provides an appropriate environment for a favourable transient geodynamic event that might give rise to a mineral system based on McCuaig et al. (2010) and McCuaig and Hronsky (2014) across West Tasmania. Sources of fluids and minerals (i.e. granite) need to interact with trap sites to initiate mineralisation. In this research, the local and prospect scale models have focused on the metal deposition window, i.e. the top 10 km. The intrusion of magmatic components (i.e. granite) as the major source of mineral fluids is the main objective of local scale modelling in this research.

The metallogenic evolution of Tasmania shows that significant mineralisation occurred during the Delamerian Orogeny (550—490 Ma; Rosebery, Hercules, Que River, Hellyer deposits), the Benambran Orogeny (490—435 Ma; Mt Lyell, Henty deposits) and the Tabberabberan Orogeny (~435—380; Mt Bischoff, Queen Hill, Renison Bell, Zeehan, Beaconsfield deposits; Huston et al., 2012b). The refined geometry of Devonian Granites and newly identified granitic bodies at depth can assist to better study sources of fluids and help to identify new fertile regions at the local scale across West Tasmania.

The prospect scale model aims to highlight traps and halos for future exploration. This area showed possible new fertile areas, with conditions to preserve minerals. The pronounced residual gravity anomaly of the local scale model across the Heazlewood area is characterised by high magnetic observations. Across the Heazlewood-Luina-Waratah region, the lithology of units and geometry of faults likely incorporates fluids and generate appropriate conditions and trap sites to preserve minerals. For example, the dolomite content of the Gordon Group could interact with the Meredith Batholith and result in skarn mineralisation. The prospect scale

model resulting from inversion indicates three regions with potential for mineralisation for future explorations at a deposition scale: 1) northeast of the Waratah region associated with possible granite cupolas and ultramafic outcrops, 2) above the Bells Syncline associated with high magnetic observations, intrusion of Devonian Granites and abundance of carbonate units of Gordon Group, and 3) in the vicinity of a recently explored ultramafic complex linking the Heazlewood River and Mt Stewart UCs.

7.4. Refined 3D geological structure and towards improved understanding of tectonic evolution

The geophysical inversions carried out in this thesis have refined the understanding of major geological features and tectonic context. By studying the CPD throughout east Australia in Chapter 2, I found that the northern part of the Queensland and regions associated with broad volcanism across the east coastline are characterised by relatively shallow CPDs. In contrast, northern parts of the Delamerian, Thomson and Lachlan Orogens show deep CPDs which suggest these regions are potentially associated with low geothermal gradients at depth. Across Tasmania, the northeast of Tasmania and Bass Strait are characterised by a shallower CPDs in comparison with western Tasmania.

In addition to refining the Moho depth using gravity data in Chapter 4, this chapter also shows the density distribution of major components throughout the upper and lower crust across the area. In the model, the density distribution of the upper crust is characterised by an abundance of low density components which is compatible with abundance of Devonian Granites across east and west Tasmania. In contrast, the model indicates that the lower crust across Tasmania has an anomalously low density range which might suggest that the lower crust in this area consists of unusually felsic compositions (e.g. a relatively high percentage of feldspar).

Synthesising the findings from Chapters 2 and 4, the CPD is consistently deeper than the seismic Moho depth across onshore Tasmania (up to ~15 km). Since the mantle rocks are not magnetic, these CPDs are likely the basement of the magnetic crust corresponding to the Moho boundary (Saad, 1969). Therefore, the Moho depth might be slightly deeper than the previous seismic Moho model. The refined gravity Moho depth successfully indicates deeper Moho boundary, compatible with the CPD estimations. In contrast, across offshore east and west Tasmania, the CPD is predominantly deeper than the Moho depth. The newly refined gravity Moho model implies shallower Moho depths which result in a more pronounced misfit between the CPD and gravity Moho boundary. This could be due to the presence of the oceanic crust

associated with magnetic properties. However, the gravity constrained Moho model suggests that continental crust dominates the study area. In addition, the more recent tectonic evolution of offshore Tasmania, compared to onshore Tasmania, suggests a high geothermal gradient leading to a shallow CPD. This paradox could be an objective for further investigations.

Synthesising the findings from Chapters 4 and 5, I found that the regional scale model is characterised by the distribution of low and high density features within the upper crust across West Tasmania. This is compatible with presence of low density Devonian Granites adjacent to other units characterised by higher densities across the local scale model.

Synthesising the findings from Chapters 5 and 6, the local scale model of West Tasmania displays pronounced residual gravity values across the Heazlewood region. The prospect scale model showed that the high residual gravity anomaly is due to the unusual high density of the Heazlewood River UC (> 3.00 g cm^{-3}) compared to other UCs across West Tasmania. In addition, the local scale study suggests the Meredith Batholith is a thick (> 10 km thickness) component. Across the prospect scale model, the newly refined geometry of the Meredith Batholith similarly shows a thick granitic component.

The orientations of 3D structures across Tasmania are affected by a variety of tectonic influences. Major tectonic influences are continental collision and rifting, orogenic events (e.g. Tyennan and Tabberabberan Orogenies), and the subsequent regional stress field throughout tectonic history. Other influences include the effects of sedimentation, erosion and subsidence, emplacement of large intrusive hot bodies (e.g. Devonian granites), regional and local metamorphism. The final models produced in this study, have refined the geometry of major geological units and structures while defining new intrusive bodies. The new models will be available for public consultation and usage through Mineral Resources Tasmania.

Bibliography

Abd El Nabi, S., H, 2012, Curie point depth beneath the Barramiya–Red Sea coast area estimated from spectral analysis of aeromagnetic data: Journal of Asian Earth Sciences, v. 43, p. 254-266.

Aitken, A., and P. Betts, 2009, Constraints on the Proterozoic supercontinent cycle from the structural evolution of the south-central Musgrave Province, central Australia: Precambrian Research, v. 168, p. 284-300.

Aitken, A. R. A., 2010, Moho geometry gravity inversion experiment (MoGGIE): A refined model of the Australian Moho, and its tectonic and isostatic implications: Earth and Planetary Science Letters, v. 297, p. 71-83.

Aitken, A. R. A., C. Altinay, and L. Gross, 2015, Australia's lithospheric density field, and its isostatic equilibration: Geophysical Journal International, v. 203, p. 1961-1976.

Aitken, A. R. A., M. L. Salmon, and B. L. N. Kennett, 2013, Australia's Moho: A test of the usefulness of gravity modelling for the determination of Moho depth: Tectonophysics, v. 609, p. 468-479.

Arkanihamed, J., 1991, Thermoremanent magnetization of the oceanic lithosphere inferred from a thermal evolution model - implications for the source of marine magnetic-anomalies: Tectonophysics, v. 192, p. 81-96.

Arkanihamed, J., 2007, Differential reduction to the pole: Revisited: Geophysics, v. 72, p. 13-20.

Armit, R. J., L. Ailleres, P. G. Betts, B. F. Schaefer, and T. N. Blaikie, 2014, High-heat geodynamic setting during the Palaeozoic evolution of the Mount Painter Province, SA, Australia: evidence from combined field structural geology and potential-field inversions: Geophysical Journal International, v. 199, p. 253-275.

Arnaiz-Rodríguez, M., S., and N. Orihuela, 2013, Curie point depth in Venezuela and the Eastern Caribbean: Tectonophysics, v. 590, p. 38-51.

Artemieva, I. M., 2006, Global 1°×1° thermal model TC1 for the continental lithosphere: Implications for lithosphere secular evolution: Tectonophysics, v. 416, p. 245-277.

Bansal, A. R., S. P. Anand, M. Rajaram, V. K. Rao, and V. P. Dimri, 2013, Depth to the bottom of magnetic sources (DBMS) from aeromagnetic data of Central India using modified centroid method for fractal distribution of sources: Tectonophysics, v. 603, p. 155-161.

Bansal, A. R., G. Gabriel, V. P. Dimri, and C. M. Krawczyk, 2011, Estimation of depth to the bottom of magnetic sources by a modified centroid method for fractal distribution of sources: An application to aeromagnetic data in Germany: Geophysics, v. 76, p. L11-L22.

Bektaş, Ö., 2013, Thermal structure of the crust in Inner East Anatolia from aeromagnetic and gravity data: Physics of the Earth and Planetary Interiors, v. 221, p. 27-37.

Berry, R. E., and S. W. Bull, 2012, The pre-Carboniferous geology of Tasmania: Episodes: International Geoscience Newsmagazine, v. 35, p. 195-204.

Berry, R. F., and A. J. Crawford, 1988, The tectonic significance of Cambrian allochthonous mafic-ultramafic complexes in Tasmania: Australian Journal of Earth Sciences, v. 35, p. 523-533.

Berry, R.F., Jenner, G.A., Meffre, S., and Tubrett, M.N., 2001, A North American Provenance for Neoproterozoic to Cambrian Sandstones in Tasmania? Earth and Planetary Science Letters 192, 207-22.

Berry, R. F., D. A. Steele, and S. Meffre, 2008, Proterozoic metamorphism in Tasmania: Implications for tectonic reconstructions: Precambrian Research, v. 166, p. 387-396.

Betts, P. G., D. Giles, G. S. Lister, and L. R. Frick, 2002, Evolution of the Australian lithosphere: Australian Journal of Earth Sciences, v. 49, p. 661-695.

Bhattacharyya, B. K., 1966, Continuous spectrum of the total-magnetic-field anomaly due to a rectangular prismatic body: Geophysics, v. 16, p. 97-122.

Bhattacharyya, B. K., and L. K. Leu, 1975, Analysis of magnetic anomalies over Yellowstone National Park: Mapping of Curie point isothermal surface for geothermal reconnaissance: Journal of Geophysical Research, v. 80, p. 4461-4465.

Black, L. P., C. R. Calver, D. B. Seymour, and A. Reed, 2004, SHRIMP U-Pb detrital zircon ages from Proterozoic and Early Palaeozoic sandstone and their bearing on the early geological evolution of Tasmania: Australian Journal of Earth Sciences, v. 51, p. 885-900.

Black, L. P., J. L. Everard, M. P. McClenaghan, R. J. Korsch, C. R. Calver, A. M. Fioretti, A. V. Brown, and C. Foudoulis, 2010, Controls on Devonian–Carboniferous magmatism in Tasmania, based on inherited zircon age patterns, Sr, Nd and Pb isotopes, and major and trace element geochemistry: Australian Journal of Earth Sciences, v. 57, p. 933-968.

Black, L. P., M. P. McClenaghan, R. Korsch, J. L. Everard, and C. Foudoulis, 2005, Significance of Devonian-Carboniferous igneous activity in Tasmania as derived from U-Pb SHRIMP dating of zircon: Australian Journal of Earth Sciences, v. 52, p. 807-829.

Black, L. P., D. B. Seymour, K. D. Corbett, S. F. Cox, J. E. Streit, R. S. Bottrill, C. R. Calver, J. L. Everard, G. R. Green, M. P. McClenaghan, J. Pemberton, J. Taheri, and N. J. Turner, 1997, Dating Tasmania's Oldest Geological Events. Tasmania National Geoscience Mapping Accord, Mineral Resources Tasmania: Australian Geological Survey Organisation, Record 1997/15, p. 1-57.

Blackney, P. C. J., 1982, The petrology and conditions of metamorphism of the Fitzmaurice Bay to Stokes Point area, King Island: B.Sc. (Hons) thesis, University of Tasmania.

Blakely, R. J., 1988, Curie temperature isotherm analysis and tectonic implications of aeromagnetic data from Nevada: Journal of Geophysical Research, v. 93, p. 11817-11832.

Blakely, R. J., 1995, Potential theory in gravity and magnetic applications, Cambridge University Press.

Bouligand, C., J. M. G. Glen, and R. J. Blakely, 2009, Mapping Curie temperature depth in the western United States with a fractal model for crustal magnetization: Journal of Geophysical Research, v. 114, p. B11104

Brocher, T. M., 2005, Empirical Relations between Elastic Wavespeeds and Density in the Earth's Crust: Bulletin of the Seismological Society of America, v. 95, p. 2081-2092.

Brown, A. V., 1986, Geology of the Dundas-Mt Lindsay-Mt Youngbuck Region: Bulletin Geological Survey Tasmania, v. 62.

Brown, A. V, 1998, Platinum Group Elements and Their Host Rocks in Tasmania: A Summary Review. in Record 1998/04 Tasmanian Geological Survey (ed.).

Brown, A. V., C. R. Calver, M. J. Clarke, K. D. Corbett, J. L. Everard, S. M. Forsyth, B. A. Goscombe, D. C. Green, G. Green, M. P. McClenaghan, J. Pemberton, D. Seymour, M. J.

Vicary, and G. P. Woollard, 2012, Geology of Tasmania. Edition 2012.1. Geological Atlas 1:500 000 digital series.

Brown, A. V., and R. H. Findlay, 1992, The 10th Legion Thrust, Zeehan District: distribution, interpretation, regional and economic significance: Tasmania Geological Survey Report 1992/2.

Brown, B. J., R. D. Müller, C. Gaina, H. I. M. Struckmeyer, H. M. J. Stagg, and P. A. Symonds, 2003, Formation and evolution of Australian passive margins: implications for locating the boundary between continental and oceanic crust: in Evolution and Dynamics of the Australia Plate, edited by R. R. Hillis et al., Special Papers - Geological Society of America, v. 372, p. 223-243.

Calver, C. R., L. P. Black, J. L. Everard, and D. B. Seymour, 2004, U-Pb zircon age constraints on late Neoproterozoic glaciation in Tasmania: Geology, v. 32, p. 893-896.

Calver, C. R., J. L. Everard, R. Berry, F.,, R. S. Bottrill, and D. B. Seymour, 2014, Proterozoic Tasmania, in K. D. Corbett, P. G. Quilty, and C. R. Calver, eds., Geological Evolution of Tasmania, v. Special Publication 24, Geological Society of Australia, p. 61-94.

Calver, C. R., and M. R. Walter, 2000, The late Neoproterozoic Grassy Group of King Island, Tasmania: correlation and paleogeographic significance: Precambrian Research, v. 100, p. 299-312.

Cawood, P. A., and R. J. Korsch, 2008, Assembling Australia: Proterozoic building of a continent: Precambrian Research, v. 166, p. 1-38.

Cayley, R., A., 2011, Exotic crustal block accretion to the eastern Gondwanaland margin in the Late Cambrian–Tasmania, the Selwyn Block, and implications for the Cambrian–Silurian evolution of the Ross, Delamerian, and Lachlan orogens: Gondwana Research, v. 19, p. 628-649.

Cayley, R. A., and R. J. Musgrave, 2013, A paradigm change -the giant Lachlan Orocline: consequence of microcontinent ingestion, stalled subduction and southeast-directed Siluro-Devonian subduction rollback superimposed on a single accreted Ordovician arc assemblage: the Lachlan Fold Belt of eastern Australia. (Invited): American Geophysical Union, Fall Meeting, v. abstract #T23H-07.

Cayley, R. A., D. H. Taylor, A. H. M. VandenBerg, and D. H. Moore, 2002, Proterozoic-Early Palaeozoic rocks and the Tyennan Orogeny in central Victoria: the Selwyn Block and its tectonic implications: Australian Journal of Earth Sciences, v. 49, p. 225-254.

Cermak, V., and E. Hurtig, 1978, The preliminary heat flow map of Europe and some of its tectonic and geophysical implications: Pageoph, v. 117, p. 92-103.

Champion, D. C., and D. L. Huston, 2016, Radiogenic isotopes, ore deposits and metallogenic terranes: Novel approaches based on regional isotopic maps and the mineral systems concept: Ore Geology Reviews, v. 76, p. 229-256.

Champion, D.C., N. Kositcin, D.L, Huston, E. Mathews, and C. Brown, 2009, Geodynamic Synthesis of the Phanerozoic of Eastern Australia and Implications for Metallogeny. in 2009/18 Geoscience Australia Record (ed.), p. 254.

Chappell, B. W., A. J. R. White, and R. Hine, 1988, Granite provinces and basement terranes in the Lachlan Fold Belt, southeastern Australia: Australian Journal of Earth Sciences, v. 35, p. 505-521.

Chmielowski, R. M., and R. F. Berry, 2012, The Cambrian metamorphic history of Tasmania: The Metapelites: Australian Journal of Earth Sciences, v. 59, p. 1007-1019.

Chopping, R., and B. Kennett, L, N., 2013, The Curie depth of Australia, and its uncertainty: 23rd International Geophysics Conference and Exhibition, Melbourne, Australia, p. 1-3.

Chopping, R., and B. Kennett, L, N., 2015, Maximum depth of magnetisation of Australia, its uncertainty, and implications for Curie depth: GeoResJ, v. 7, p. 70-77.

Christensen, N. T., 1996, Poisson's ratio and crustal seismology: Journal of Geophysical Research, v. 71, p. 5921-5931.

Chulliat, A., Macmillan, S., Alken, P., Beggan, C., Nair, M., Hamilton, B., Woods, A., Ridley, V., Maus, S., and Thomson, A., 2015, The Us/Uk World Magnetic Model for 2015-2020:. Technical Report, National Geophysical Data Center, NOAA.

Clark, D., 1997, Magnetic petrophysics and magnetic petrology; aids to geological interpretation of magnetic surveys: AGSO Journal of Australian Geology and Geophysics, v. 17, p. 83-103.

Collins, P. L. F., 1983, Geology and mineralisation at the Cleveland mine, western Tasmania, PhD thesis, University of Tasmania.

Corbett, K. D., R. Berry, F., J. L. Everard, C. R. Calver, M. Cracknell, J., M. J. Vicary, and R. S. Bottrill, 2014a, Cambrian Tasmania, in K. D. Corbett, P. G. Quilty, and C. R. Calver, eds., Geological Evolution of Tasmania, v. Special Publication 24, Geological Society of Australia, p. 95-240.

Corbett, K. D., P. G. Quilty, C. R. Calver, and editors, 2014b, Geological evolution of Tasmania: Geological Society of Australia, Special Publication 24, Geological Society of Austalia (Tasmania Division), p. 639

Corbett, K. D., and M. Solomon, 1989, Cambrian Mt Read Volcanics and associated mineral deposits, in: Burrett C. F.; Martin, E. L. (ed.). Geology and Mineral Resources of Tasmania: Special Publication Geological Society of Australia, v. 15, p. 84-153.

Corbett, K. D., and M. J. Vicary, 2014, Middle Cambrian Post-Collisional Volcanism and Sedimentation, in K. D. Corbett, P. G. Quilty, and C. R. Calver, eds., Geological Evolution of Tasmania, v. Special Publication 24, Geological Society of Australia, p. 145-183

Cox, S. F., 1973, The structure and petrology of the Cape Wickham area, King Island: B.Sc. (Hons) thesis, University of Tasmania.

Crawford, A. J., and R. F. Berry, 1992, Tectonic implication of Late Proterozoic-Early Paleozoic igneous rock associations in western Tasmania: Tectonophysics, v. 214, p. 37-56.

Cumming, G., and J. L. Everard, 2017, Digital Geological Atlas 1:25 000 series, Sheet 3641. Waratah: Mineral Resources Tasmania.

Cumming, G., J. L. Everard, and S. Meffre, 2016, Age constraints and provenance of the Mount Bischoff inlier and the Luina Group - evidence from La-ICPMS U-Pb dating of detrital zircon, in UR2016-04, ed., Mineral Resources Tasmania, p. 27.

Cummings, A. M., R. R. Hillis, and P. R. Tingate, 2004, New perspectives on the structural evolution of the Bass Basin: implication for petroleum prospectivity: PESA Eastern Australia Basins Symposium II, v. (2004: Adelaide, South Australia), p. 133-149.

Direen, N. G., and A. J. Crawford, 2003, The Tasman Line: where is it, what is it, and is it Australia's Rodinian breakup boundary?: Australian Journal of Earth Sciences, v. 50, p. 491-502.

Doser, D. I., and H. Kanamori, 1986, Depth of seismicity in the Imperial Valley Region (1977–1983) and its relationship to heat flow, crustal structure and the October 15, 1979, earthquake: Journal of Geophysical Research-Solid Earth and Planets, v. 91, p. 675-688.

Doutch, H. F., and E. Nicholas, 1978, The Phanerozoic sedimentary basins of Australia and their tectonic implications: Tectonophysics, v. 48, p. 365-388.

Duffett, M., L. M. Richardson, 2014, Total Magnetic Intensity Map of Tasmania, scale: 1:500 000. Mineral Resources Tasmania.

Drummond, B. J., T. J. Barton, R. J. Korsch, N. Rajaram, A. N. Yeates, C. D. N. Collins, and A. V. Brown, 2000, Evidence for crustal extension and inversion in eastern Tasmania, Australia, during the Neoproterozoic and Early Paleozoic: Tectonophysics, v. 329, p. 1-21.

Eagles, G., L. Pérez-Díaz, and N. Scarselli, 2015, Getting over continent ocean boundaries: Earth-Science Reviews, v. 151, p. 244-265.

Edwards, R. P., and K. Atkinson, 1986, Ore Deposit Geology and its Influence on Mineral Exploration, London-New York [Chapman and Hall], p. 466.

Eshaghi, E., A. M. Reading, M. J. Roach, M. Cracknell, J., M. Duffett, and D. Bombardieri, 2016, 3D modelling of granite intrusions in northwest Tasmania using petrophysical and residual gravity data, SEG Technical Program Expanded Abstracts 2016, Dallas, USA, p. 1637-1642.

Eshaghi, E., A. M. Reading, M. J. Roach, M. Duffett, D. Bombardieri, and M. Cracknell, J., 2016, 3D modelling of granite intrusions in northwest Tasmania using petrophysical and residual gravity data, SEG Technical Program Expanded Abstracts 2016, p. 1637-1640.

Everard, J. L., and G. Cumming, 2016a, Digital Geological Atlas 1:25 000 Series, Sheet 3640. Luina.

Everard, J. L., and G. Cumming, 2016b, Geological sections across the Heazlewood-Luina-Waratah region: Mineral Resources Tasmania.

GEO F/X., 1997, User's guide for KT-9 Kappameter magnetometer, in Exploranium radiation detection systems, ed.

Farquharson, C., G., M. Ash, R., and H. Miller, G, 2008, Geologically constrained gravity inversion for the Voisey's Bay ovoid deposit: The Leading Edge, v. 27, p. 64-69.

Fedi, M., P. Hansen, C., and V. Paoletti, 2005, Analysis of depth resolution in potential-field inversion: Geophysics, v. 70, p. A1-A11.

Fergusson, C. L., R. A. Henderson, and R. Offler, 2017, Late Neoproterozoic to Early Mesozoic sedimentary rocks of the Tasmanides, Eastern Australia: Provenance switching associated with development of the East Gondwana Active Margin. In R. Mazumder (Ed.): Sediment Provenance: Influence on Compositional Change from Source to Sink, p. 325-369.

Fielding, L. R., R. Sliwa, R. J. Holcombe, and J. T. Jones, 2001, A new palaeogeographic synthesis for the Bowen, Gunnadeh and Sydney basins of eastern Australia. In: Berecher, T. & Hill, K. (eds) PESA Eastern Australian Basins symposium. Australian Institute of Mining and Metallurgy, Melbourne, 269-279.

Fishwick, S., M. Heintz, B. L. N. Kennett, A. M. Reading, and K. Yoshizawa, 2008, Steps in lithospheric thickness within eastern Australia, evidence from surface wave tomography: Tectonics, v. 27, p. TC4009.

Fitzgerald, D., R. Paterson, and p. B. Skladzien, 2009, Isostatic and decompensative correction of Victoria gravity data, in Geoscience Victoria 3D Victoria Report 3, ed. Department of Primary Industries.

Foster, D.A., and Gray, D.R., 2000, Evolution and Structure of the Lachlan Fold Belt (Orogen) of Eastern Australia. Annuan review of Earth and Planetary Science 28, 47-80.

Fox Maule, C., M. E. Purucker, and N. Olsen, 2009, Inferring magnetic crustal thickness and geothermal heat flux from crustal magnetic field models: Danish Climate Centre, Report 09-09, p. 13-15.

Fullagar, P. K., 2013, VPmg User Documentation, Version 7.1, Fullagar Geophysics Pty Ltd, Report FGR01F-4.

Fullagar, P. K., G. N. Fallon, P. J. Hatherly, and D. W. Emerson, 1996, Implementation of geophysics at metalliferous mines, in final report AMIRA Project P436: CRC for Mining Tech. and Equipment Report No MM1-96/11, ed.

Fullagar, P. K., and G. A. Pears, 2007, Toward geologically realistic inversion, In "Proceeding of Exploration 07: Fifth Decennial International Conference on Mineral Exploration" edited by B. Milkereit, p. 444-460.

Fullagar, P. K., G. A. Pears, D. Hutton, and A. Thomson, 2004, 3D Gravity and Aeromagnetic Inversion for MVT Lead-Zinc Exploration at Pilbara, Western Australia: Exploration Geophysics, v. 35, p. 142-146.

Fullagar, P. K., G. A. Pears, and B. McMonnies, 2008, Constrained inversion of geologic surfaces - pushing the boundaries: The Leading Edge, v. 27, p. 98-105.GADDS, 2016, Geophysical Archive Data Delivery System from Geoscience Australia to download potential field data across Australia, http://www.geoscience.gov.au/cgi-bin/mapserv?map=/nas/web/ops/prod/apps/mapserver/gadds/wms_map/gadds.map&mode=browse. Accessed 8-11-2016

Gaina, C., D. R. Muller, J. Y. Royer, J. Stock, J. Hardebeck, and P. Symonds, 1998, The tectonic history of the Tasman Sea: A puzzle with 13 pieces: Journal of Geophysical Research-Solid Earth, v. 103, p. 12413-12433.Gerner, E., and F. Holgate, 2010, OZTemp - Interpreted temperature at 5 km depth, Canberra: Digital data, Geoscience Australia.

Gibson, G. M., M. P. Morse, T. R. Ireland, and G. K. Nayak, 2011, Arc–continent collision and orogenesis in western Tasmanides: Insights from reactivated basement structures and formation of an ocean–continent transform boundary off western Tasmania: Gondwana Research, v. 19, p. 608-627.

Glen, D., 2006, The Lachlan Orogeny: new boundaries, new data, new ideas, new deposits, in P. C. Lewis, ed., ed., Mineral Exploration Geoscience in New South Wales, SMEDG Mines and Wines Conference, Cessnock NSW, Expended abstract, p. 1-6.

Glen, R. A., 2005, The Tasmanides of eastern Australia. In: Vaughan A. P. M., Leat P.T & Pankhurst R. J. eds. Terrane processes at the margins of Gondwana: Geological Society of London, Special Publications 246, v. 246, p. 23-96

Glen, R.A., 2013, Refining Accretionary Orogen Models for the Tasmanides of Eastern Australia. Australian Journal of Earth Sciences 60, 315-70.

Glen, R. A., I. G. Percival, and C. D. Quinn, 2009, Ordovician continental margin terranes in the Lachlan Orogen, Australia: implications for tectonics in an accretionary orogen along the east Gondwana margin: Tectonics, v. 28, p. TC6012.

Glen, R., and Roberts, J., 2012, Formation of Oroclines in the New England Orogen, Eastern Australia. Journal of the Virtual Explorer 43.

Groves, D.I., and Solomon, M., 1964, The Geology of the Mt Bischoff District. Papers and Proceedings Royal Society of Tasmania 98, p. 1-22.

Guillen, A., Calcagno, P., Courrioux, G., Joly, A., and Ledru, P., 2008, Geological Modelling from Field Data and Geological Knowledge: Part Ii. Modelling Validation Using Gravity and Magnetic Data Inversion. Physics of the Earth and Planetary Interiors 171, 158-69.

Goes, S., F. J. Simons, and K. Yoshizawa, 2005, Seismic constraints on temperature of the Australian uppermost mantle: Earth and Planetary Science Letters, v. 236, p. 227-237.

González-Álvarez, I., F. Pirajno, and R. Kerrich, 2013, Hydrothermal nickel deposits: Secular variation and diversity: Ore Geology Reviews, v. 52, p. 1-3.

Goscombe, B. D., 1990, Equilibrium thermodynamics of the Lyell Highway eclogites: Report Department of Mines Tasmania 1990/19, p.1-10.

Gray, D. R., and D. A. Foster, 2004, Tectonic evolution of the Lachlan Orogen, southeast Australia: historical review, data synthesis and modern perspectives: Australian Journal of Earth Sciences, v. 51, p. 773-817.

Griggs, D., 2002, Interpretation of the HEM Survey Northwest Tasmania, B.Sc (Hons) thesis, University of Tasmania.

Groves, D. I., R. J. Goldfarb, M. Gebre-Mariam, S. G. Hagemann, and F. Robert, 1998, Orogenic gold deposits: A proposed classification in the context of their crustal distribution and relationship to other gold deposit types: Ore Geology Reviews, v. 13, p. 7-27.

Gunn, P., J. Mitchell, and A. Meixner, 1997, The structure and evolution of the bass basin as delineated by aeromagnetic data: Exploration Geophysics, v. 28, p. 214-219.

Hallett, M., J. Vassallo, R. Glen, and S. Webster, 2005, Murray-Riverina region: an interpretation of bedrock Palaeozoic geology based on geophysical data: Quarterly Notes of the Geological Survey of New South Wales v. 118, p. 1-16.

Halley, S. W., 1987, Genesis of the Mount Bischoff Tin Deposit, PhD thesis, Australian National University.

Halpin, J. A., T. Jensen, P. McGoldrick, S. Meffre, R. F. Berry, J. L. Everard, C. R. Calver, J. Thomson, K. Goemann, and J. M. Whittaker, 2014, Authigenic monazite and detrital zircon dating from the Proterozoic Rocky Cape Group, Tasmania: Links to the Belt-Purcell Supergroup, North America: Precambrian Research, v. 250, p. 50-67.

Harrison, C. G. A., 1976, Magnetization of the oceanic crust: Geophysical Journal of the Royal Astronomical Society, v. 47, p. 257-283.

Heincke, B., M., J. Moorkamp, M., J. Chen, and R. Hobbs, W. , 2010, Adaptive coupling strategy for simultaneous joint inversion that use petrophysical information as constraints, 80th Annual International Meeting, SEG, Expanded Abstracts p. 2805–2809.

Heiskanen, W. A., and H. Moritz, 1967, Physical Geodesy: In W. H. Freeman, San Francisco, California, p. 364

Holm, O. H., and R. F. Berry, 2002, Structural history of the Arthur Lineament, northwest Tasmania: An analysis of critical outcrops: Australian Journal of Earth Sciences, v. 49, p. 167-185.

Holm, O. H., C. A. J, and R. F. Berry, 2003, Geochemistry and tectonic setting of meta-igneous rocks in the Arthur Lineament and surrounding area, northwest Tasmania: Australian Journal of Earth Sciences, v. 50, p. 16-918.

Howard, L.E., and Sass, J.H., 1964, Terrestrial Heat Flow in Australia. Journal of Geophysical Research 69, 1617-26. Hronsky, J., 2015, The future of mineral exploration – and what it means for geophysics, ASEG-PESA 2015; 24th International Geophysical Conference and Exhibition, Perth.

Huang, Y., Chubakov, V., Mantovani, F., Rudnick, R.L., and McDonough, W.F., 2013, A Reference Earth Model for the Heat-Producing Elements and Associated Geoneutrino Flux. Geochemistry, Geophysics, Geosystems 14, 2003-29.

Hussein, M., K. Mickus, and L. F. Serpa, 2013, Curie Point Depth estimates from aeromagnetic data from Death Valley and surrounding regions, California: Pure and Applied Geophysics, v. 170, p. 617-632.

Huston, D. L., R. Blewett, R. Skirrow, A. McQueen, J. Wang, L. Jaques, and D. Waters, 2012a, Foundations of wealth—Australia's major mineral provinces, in R. Blewett, ed., Shaping a Nation: A Geology of Australia, Geoscience Australia, p. 380-431.

Huston, D. L., R. S. Blewett, and D. C. Champion, 2012b, Australia through time: A summary of its tectonic and metallogenic evolution: Episodes, v. 35, p. 23-43.

Huston, D. L., T. P. Mernagh, S. G. Hagemann, M. P. Doublier, M. Fiorentini, D. C. Champion, A. Lynton Jaques, K. Czarnota, R. Cayley, R. Skirrow, and E. Bastrakov, 2016, Tectono-metallogenic systems — The place of mineral systems within tectonic evolution, with an emphasis on Australian examples: Ore Geology Reviews, v. 76, p. 168-210.

Jago, J. B., and A. V. Brown, 1989, Middle to Upper Cambrian fossiliferous sedimentary rocks, in: Burrett, C. F.; Martin, E. L. (ed.). Geology and Mineral Resources of Tasmania: Special Publication Geological Society of Australia, v. 15, p. 74-83.

Jaireth, S., I. C. Roach, E. Bastrakov, and S. Liu, 2016, Basin-related uranium mineral systems in Australia: A review of critical features: Ore Geology Reviews, v. 76, p. 360-394.

Jaques, A. L., S. Jaireth, and J. L. Walshe, 2002, Mineral systems of Australia: an overview of resources, settings and processes: Australian Journal of Earth Sciences, v. 49, p. 623-660.

Jenning, C. W., 1997, Geological map of California, scale 1/7500000 (California Division of Geology and Mines, Sacramento, California, 1977).

Jessell, M.W., R.K. Valenta, G. Jung, and A. Geiro, 1993, Structural Geophysics. Exploration Geophysics, v. 24, p. 599-602.

Johnson, R. W., J. Knutson, and S. R. Taylor, 1989, Intraplate Volcanism in Eastern Australia and New Zealand: Cambridge University Press, Melbourne.

Joly, A., A. Porwal, and T. C. McCuaig, 2012, Exploration targeting for orogenic gold deposits in the Granites-Tanami Orogen: Mineral system analysis, targeting model and prospectivity analysis: Ore Geology Reviews, v. 48, p. 349-383.

Joly, A., A. Porwal, T. C. McCuaig, B. Chudasama, M. C. Dentith, and A. R. A. Aitken, 2015, Mineral systems approach applied to GIS-based 2D-prospectivity modelling of geological regions: Insights from Western Australia: Ore Geology Reviews, v. 71, p. 673-702.

Kamm, J., I. Lundin, A., M. Bastani, M. Sadeghi, and L. Pedersen, B., 2015, Joint inversion of gravity, magnetic, and petrophysical data—A case study from a gabbro intrusion in Boden, Sweden: Geophysics, v. 80, p. 131-152.

Kamperman, M., 1984, The Precambrian metamorphic geology of the Lyell Highway-Collingwood River area: B.Sc. (Hons) thesis, University of Tasmania.

Keele, R., 1992, The King River regional cross-section: a transitional through the Dundas Trough: CODES: AMIRA Project P291 - Report 4, p. 11-30.

Kennett, B., E. Saygin, T. Fomin, and R. Blewett, 2013, Deep Crustal Seismic Reflection Profiling: Australia 1978-2011: ANU Press and Geoscience Australia, Canberra, p. 180.

Kennett, B. L. N., S. Fishwick, A. M. Reading, and N. Rawlinson, 2004, Contrasts in mantle structure beneath Australia: relation to Tasman Lines?: Australian Journal of Earth Sciences, v. 51, p. 563-569.

Kennett, B. L. N., and M. Salmon, 2012, AuSREM: Australian Seismological Reference Model: Australian Journal of Earth Sciences, v. 59, p. 1091-1103.

Kennett, B. L. N., M. Salmon, E. Saygin, and G. AusMoho Working, 2011, AusMoho: the variation of Moho depth in Australia: Geophysical Journal International, v. 187, p. 946-958.

Kennett, B. L. N., and E. Saygin, 2015, The nature of the Moho in Australia from reflection profiling: A review: GeoResJ, v. 5, p. 74-91.

Kennett, B. L. N., E. Saygin, and M. Salmon, 2015, Stacking autocorrelograms to map Moho depth with high spatial resolution in southeastern Australia: Geophysical Research Letters, v. 42, p. 7490-7497.

Kerrich, R., and D. A. Wyman, 1997, Review of developments in trace-element fingerprinting of geodynamic settings and their implications for mineral exploration: Australian Journal of Earth Sciences, v. 44, p. 465-487.

Korsch, R.J., and Doublier, M.P., 2015, Major Crustal Boundaries of Australia [Digital Dataset]. Geoscience Australia, Commonwealth of Australia, Canberra. http://www.ga.gov.au.

Kositcin, N., and J. L. Everard, 2013, New SHRIMP U-Pb zircon ages from Tasmania: July 2012-June 2013, in Geoscience Australia Record 2013/22, Tasmania Geological Survey Record 2013/02, ed., Canberra, Geoscience Australia.

Kreuzer, O. P., A. V. M. Miller, K. J. Peters, C. Payne, C. Wildman, G. A. Partington, E. Puccioni, M. E. McMahon, and M. A. Etheridge, 2015, Comparing prospectivity modelling results and past exploration data: A case study of porphyry Cu–Au mineral systems in the Macquarie Arc, Lachlan Fold Belt, New South Wales: Ore Geology Reviews, v. 71, p. 516-544.

Kusznir, N., 2008, South Australia-Antarctica conjugate rifted margins: Mapping crustal thickness & lithospheric thinning using satellite gravity inversion, p. 65.

Leaman, D. E., 1988, MANTLE88 - Regional gravity field, Tasmania: Geophysical Report Mt Read Volcanics Project Tasmania 7.

Leaman, D. E., 1990, Geophysical-structural review, Rocky Cape Block, NW Tasmania for Geopeko: Leaman Geophysics [TCR91-3213].

Leaman, D. E., 2003, Quantitative interpretation of magnetic and gravity data for the Western Tasmania Regional Mineral Program - Part 1: Mineral Resources Tasmania- Tasmanian Geological Survey, v. Record 2002/15, p. 9-51.

Leaman, D. E., 2009, MANTLE-09 - a new crustal gravity model for Tasmania: Report GPCR2009-01, p. 6.

Leaman, D. E., P. W. Baillie, and C. M. Powel, 1994, Precambrian Tasmania: a Thin-skinned Devil: Exploration Geophysics, v. 25, p. 19-23.

Leaman, D. E., and L. M. Richardson, 1992, A geophysical model of the major Tasmanian Granitoid: Tasmania Department of Mines - Report 1992/11.

Leaman, D. E., and R. G. Richardson, 1989a, The granites of west and north-west Tasmania - a geophysical interpretation: Bulletin Geological Survey Tasmania, v. 66.

Leaman, D. E., and R. G. Richardson, 1989b, Production of a residual gravity field map for Tasmania and some implications: Exploration Geophysics, v. 20, p. 181-184.

Leaman, D. E., and R. G. Richardson, 2003, A geophysical model of the major Tasmanian granitoids, Mineral Resources Tasmania. Tasmanian Geological Survey. Record 2003/11.

Le Clerc, M., 1996, The geophysics of the Housetop Granite: B.Sc. (Hons) thesis, University of Tasmania.

Li, C. F., X. Shi, Z. Zhou, J. Li, J. Geng, and B. Chen, 2010, Depths to the magnetic layer bottom in the South China Sea area and their tectonic implications: Geophysical Journal International, v. 182, p. 1229-1247.

Li, C., F, J. Wang, Z. Zhou, J. Geng, B. Chen, F. Yang, J. Wu, P. Yu, X. Zhang, and S. Zhang, 2012a, 3D geophysical characterization of the Sulu–Dabie orogen and its environs: Physics of the Earth and Planetary Interiors, v. 192-193, p. 35-53.

Li, P., and G. Rosenbaum, 2014, Does the Manning Orocline exist? New structural evidence from the inner hinge of the Manning Orocline (eastern Australia): Gondwana Research, v. 25, p. 1599-1613.

Li, P., G. Rosenbaum, and P. J. T. Donchak, 2012b, Structural evolution of the Texas Orocline, eastern Australia: Gondwana Research, v. 22, p. 279-289.

Li, Y., and D. W. Oldenburg, 1998, 3D inversion of gravity data: Geophysics, v. 63, p. 109-119.

Li, Y., and D. W. Oldenburg, 1996, 3D inversion of magnetic data: Geophysics, v. 61, p. 394-408.

Lindsay, M. D., L. Aillères, M. W. Jessell, E. A. de Kemp, and P. G. Betts, 2012, Locating and quantifying geological uncertainty in three-dimensional models: Analysis of the Gippsland Basin, southeastern Australia: Tectonophysics, v. 546-547, p. 10-27.

Lindsay, M. D., M. W. Jessell, L. Ailleres, S. Perrouty, E. de Kemp, and P. G. Betts, 2013, Geodiversity: Exploration of 3D geological model space: Tectonophysics, v. 594, p. 27-37.

Lisitsin, V. A., I. González-Álvarez, and A. Porwal, 2013, Regional prospectivity analysis for hydrothermal-remobilised nickel mineral systems in western Victoria, Australia: Ore Geology Reviews, v. 52, p. 100-112.

Lisitsin, V. A., and I. K. Pitcairn, 2016, Orogenic gold mineral systems of the Western Lachlan Orogen (Victoria) and the Hodgkinson Province (Queensland): Crustal metal sources and cryptic zones of regional fluid flow: Ore Geology Reviews, v. 76, p. 280-295.

Hot Dry Rocks Pty Ltd., 2013, Petrophysical properties of core samples MRT001-MRT083, Prepared for Mineral Resources Tasmania, p. 1-23.

Ludwig, W. J., J. E. Nafe, and C. L. Drake, 1970, Seismic refraction: the Sea. Vol. 4 (Part 1), Wiley Intersection, New York, p. 53-84.

Mallet, J. L., 1992, Gocad: A computer-aided design program for geological applications . in A. K. (ED) In: Turner (ed.) Three-Dimensional Modelling with Geoscientific Information System. Series C, Mathematical and Physical Sciences, 354., Kluwar Academic Publisher, Springer eBook, NATO-ASI, 123-41.

Mamillan, M., 1972, Connaissances Actuelles pour Mesurer le Degré d'Altération des Pierres et l'Efficacité des Méthodes de Traitement, 1st International Sympo-Soium on the Deterioration of Building Stones, La Rochelle, p. 47-56.

Martin, E. L., and C. F. Burrett, 1989, Geology and mineral resources of Tasmania: Geological Society of Australia, Special Publication, v. 15, p. 574.Maus, S., D. Gordin, and D. Fairhead, 1997, Curie-temperature depth estimation using a self-similar magnetization model: Geophysics, v. 129, p. 163-168.

Mavko, G., T. Mukerji, and J. V. Dvorkin, 1998, The Rock Physics Handbook: Tools for Seismic Analysis in Porous Media: Cambridge University Press, Cambridge, U.K, p. 329 pp.

McAdam, W. J., 2015, A geophysical interpretation of the Mole Creek area, central Tasmania: B.Sc. (Hons) thesis, University of Tasmania.

McCuaig, T. C., S. Beresford, and J. Hronsky, 2010, Translating the mineral systems approach into an effective exploration targeting system: Ore Geology Reviews, v. 38, p. 128-138.

McCuaig, T. C., and J. Hronsky, 2014, The Mineral System concept: The key to exploration targeting, 2014 Society of Economic Geologists, Inc. Special Publication, p. 153-175.

McEnroe, S., K. Fabian, P. Robinson, C. Gaina, and L. Brown, 2009, Crustal magnetism, lamellar magnetism, and rocks that remember: Elements, v. 4, p. 241-246.

McGaughey, J., 2006, The common earth model: A revolution in mineral exploration data integration, in GIS Application in the Earth Sciences, Geological Association of Canada Special Publication#44, edited by J.R. Harris, ed., p. 567-576.

McLaren, S., Sandiford, M., and Hand, M., 1999, High Radiogenic Heat–Producing Granites and Metamorphism—an Example from the Western Mount Isa Inlier, Australia. Geology 27, 679-82.

McLean, M.A., and P. Betts, 2003, Geophysical Constraints of Shear Zones and Geometry of the Hiltaba Suite Granites in the Western Gawler Craton, Australia. Australian Journal of Earth Sciences, v. 50, p. 525-41.

Meffre, S., R. F. Berry, and M. Hall, 2000, Cambrian metamorphic complexes in Tasmania: Tectonic implications: Australian Journal of Earth Sciences, v. 47, p. 971-985.

Meffre, S., N. G. Direen, A. J. Crawford, and V. Kamenetsky, 2004, Mafic volcanic rocks on King Island, Tasmania: evidence for 579 Ma break-up in east Gondwana: Precambrian Research, v. 128, p. 475-496.

Michibayashi, K., Y. Kusafuka, T. Satsukawa, and S. J. Nasir, 2012, Seismic properties of peridotite xenoliths as a clue to imaging the lithospheric mantle beneath NE Tasmania, Australia: Tectonophysics, v. 522-523, p. 218-223.

Milligan, P. R., R. Franklin, B. R. S. Minty, L. M. Richardson, and P. J. Percival, 2010, Magnetic anomaly map pf Australia (Fifth edition), 1:15 000 000 scale, Geoscience Australia, Canberra.

Mishra, D. C., and L. B. Pedersen, 1982, Statistical analysis of potential fields from subsurface reliefs: Geoexploration, v. 19, p. 247-265.

Monoury, S., B. Jupp, and A. Foley, 2015, Mine scale constrained geophysical inversion; a case study at the Darlot-Centerary Gold Mine, ASEG-PESA 2015 - Perth, Australia, p. 4.

Moore, D. H., P. G. Betts, and M. Hall, 2013, Towards understanding the early Gondwanan margin in southeastern Australia: Gondwana Research, v. 23, p. 1581-1598.

Moresi, L., P. G. Betts, M. S. Miller, and R. A. Cayley, 2014, Dynamics of continental accretion: Nature, v. 508, p. 245-8.

Morrison, K., 2002, Mt Bischoff Mine remediation project, geology report, in Mineral Resources Tasmania ed., p. 1-14.

MRT West Tasmania 3D model, 2016, The West Tasmania 3D geophysical modelling, http://www.mrt.tas.gov.au/portal/west-tasmania-3d-geological-geophysical-modelling, Accessed: 14-11-2016

MRT online database, 2016, Download online geophysical and geological database from Mineral Resources Tasmania. http://www.mrt.tas.gov.au/portal/database-searches. Accessed 8-11-2016.

Mulder, J. A., R. F. Berry, S. Meffre, and J. A. Halpin, 2016, The metamorphic sole of the western Tasmanian ophiolite: New insights into the Cambrian tectonic setting of the Gondwana Pacific margin: Gondwana Research, v. 38, p. 351-369.

Mulder, J. A., J. A. Halpin, and N. R. Daczko, 2015, Mesoproterozoic Tasmania: Witness to the East Antarctica–Laurentia connection within Nuna: Geology, v. 43, p. 759-762.

Murphy, B., K. Denwer, R. Keele, P. Stapleton, R. Korsch, D. Seymour, and G. Green, 2003, Tasmania Mineral Province Geoscientific database, 3D Geological Modelling, Mines and Mineral Prospectivity, Project T3: Release Notes.

Murray., C. G., and A. G. Kirkegaard., 1978, The Thomson Orogen of the Tasman Orogenic Zone: Tectonophysics, v. 48, p. 299–325.

Musgrave, R. J., 2013, Oroclines in the Tasmanides of eastern Gondwana: Geophysical Research Abstracts, v. 15.

Musgrave, R. J., 2015, Oroclines in the Tasmanides. Journal of Structural Geology 80, 72-98.

Newnham, L., 2001, EL 14-2001 Heazlewood Area, Tasmania. Review of Exploration Potential for Avebury Style Nickel Sulfide Deposits. In EL 14/2001- Heazlewood Area Annual Report Year Ending 14 September 2002 Prepared for Allegiance Mining NL, 51 p. MRT CR 02-4765.

Newnham, L., 2004, EL 14/2001 - Heazlewood Area, in A. Report, ed., Sydney, Allegiance Mining NL, p. 35.

NOAA, 2016, National Oceanic and Atmospheric Administration, National centre for environmental information, internet website to download marine geology and geophysics data, https://www.ngdc.noaa.gov/mgg/mggd.html

Nowell, D. A. G., 1999, Gravity terrain corrections — an overview: Journal of Applied Geophysics, v. 42, p. 117-134.

Okubo, Y., R.J. Graf, R. O. Hansen, and K. Ogawa, 1985, Curie point depths of the island of Kyushu and surrounding areas, Japan: Geophysics, v. 53, p. 14.

Okubo, Y., H. Tsu, and K. Ogawa, 1989, Estimation of Curie point temperature and geothermal structure of island arcs of Japan: Tectonophysics, v. 159, p. 279-290.

Olhoeft, G.R., and Johnson, G.R., 1989, Densities of Rocks and Minerals, Section II. Handbook of Physical Properties of Rocks and Minerals, R.S. Carmichael (Ed.). Oldenburg, D. W, and Y. Li, 2005, Inversion of applied geophysics: a tutorial: Near-Surface Geophysics, 9. 89-150.

Olorunfemi, M. O., A. A. Adepelumi, D. E. Falebita, and O. A. Alao, 2011, Crustal thermal regime of Ikogosi warm spring, Nigeria inferred from aeromagnetic data: Arabian Journal of Geosciences, v. 6, p. 1657-1667.

Oz SEEBASE™, 2005, Public domain report to Shell Development Australia by Frog Tech Pty Ltd., Brisbane.

Palmowski, D., K. C. Hill, and N. Hoffman, 2004, Structure and hydrocarbons in the Shipwreck Trough, Otway Basin: half-graben gas fields abutting a continental transform: APPEA Journal, v. 44, p. 417-440.

Patison, N. L., R. F. Berry, G. J. Davidson, B. P. Taylor, R. S. Bottrill, B. Manzi, J. Ryba, and R. E. Shepherd, 2001, Regional metamorphism of the Mathinna Group, northeast Tasmania: Australian Journal of Earth Sciences, v. 48, p. 281-292.

Payne, B., 1991, Geophysics of Mt. Sedgwick Red Hills Area: B.Sc. (Hons) thesis, University of Tasmania.

Peck, D., 1990, PGE geochemistry and petrogenesis of the Heazlewood River Mafic-Ultramafic Complex, Tasmania, PhD thesis, University of Melbourne.

Peck, D., and R. Keays, R., 1990a, Geology, geochemistry and origin of platinium-group elements-chromitite occurrences in the Heazlewood River Complex, Tasmania: Economic Geology, v. 85, p. 765-793.

Peck, D., and R. Keays, R., 1990b, Insights into the behaviour of precious metals in primitive, S-undersaturated magmas: Evidence from the Heazlewood River Complex, Tasmania: Canadian Mineralogist, v. 28, p. 553-577.

Petkovic, P., 2004, Time-depth functions for the Otway Basin: Geoscience Australia Record 2004/02.

Pilia, S., N. Rawlinson, R. A. Cayley, T. Bodin, R. Musgrave, A. M. Reading, N. G. Direen, and M. K. Young, 2015a, Evidence of micro-continent entrainment during crustal accretion: Scientific Reports, v. 5, p. 8218.

Pilia, S., N. Rawlinson, N. G. Direen, A. M. Reading, R. Cayley, L. Pryer, P. Arroucau, and M. Duffett, 2015b, Linking mainland Australia and Tasmania using ambient seismic noise tomography: Implications for the tectonic evolution of the east Gondwana margin: Gondwana Research, v. 28, p. 1212-1227.

Pilkington, M., 1997, 3D magnetic imaging using conjugate gradients: Geophysics, v. 62, p. 1132-1142.

Pirajno, F., 2016, A classification of mineral systems, overviews of plate tectonic margins and examples of ore deposits associated with convergent margins: Gondwana Research, v. 33, p. 44-62.

Poker, S., 2013, A geophysical investigation of the northern extent of the Meredith Granite, northwest Tasmania: B.Sc. (Hons) thesis, University of Tasmania.

Porwal, A., R. D. Das, B. Chaudhary, I. Gonzalez-Alvarez, and O. Kreuzer, 2015, Fuzzy inference systems for prospectivity modelling of mineral systems and a case-study for prospectivity mapping of surficial Uranium in Yeelirrie Area, Western Australia: Ore Geology Reviews, v. 71, p. 839-852.

Proceq, 2016, Proceq test equipment manufacturer, Pundit Lab Information Page. http://www.proceq.com/nondestructivetestequipment/concrete-testing/ultrasonic-pulse-velocity/pundit-lab.html. Accessed 7-11-2016.

Radford, D. G., 2016, Geological mapping from radar imagery with Machine Learning: B.Sc. (Hons) thesis, University of Tasmania.

Rawlinson, N., G. A. Houseman, C. D. N. Collins, and B. J. Drummond, 2001a, New evidence of Tasmania's tectonic history from a novel seismic experiment: Geophysical Research Letters, v. 28, p. 3337-3340.

Rawlinson, N., G. A. Houseman, and C. D. N. Collins, 2001b, Inversion of seismic refraction and wide-angle reflection travel times for three-dimensional layered crustal structure: Geophysics, v. 145, p. 381-400.

Rawlinson, N., H. Tkalčić, and A. M. Reading, 2010, Structure of the Tasmanian lithosphere from 3D seismic tomography: Australian Journal of Earth Sciences, v. 57, p. 381-394.

Rawlinson, N., and M. Urvoy, 2006, Simultaneous inversion of active and passive source datasets for 3D seismic structure with application to Tasmania: Geophysical Research Letters, v. 33, p. L24313.

Raymond, O. L., 2012, Surface Geology of Australia (1:1M scale dataset) A3 map: Geoscinec Australia, Canberra.

Raymond, O. L., S. Liu, R. Gallagher, W. Zhang, and L. M. Highet, 2012, Surface Geology of Australia 1:1 million scale dataset 2012 edition.

Reed, A. R., 2001, Pre-Tabberabberan deformation in eastern Tasmania: A southern extension of the Benambran Orogeny: Australian Journal of Earth Sciences, v. 48, p. 785-796.

Reynold, J., M., 1997, An introduction to applied and environmental geophysics: In New York, John Wiley & Sons Ltd (ed).

Richardson, S., 2014, EL31/2003 Heazlewood Tasmania Contact Creek project, in F. report., ed., Base Metals Ltd, Mineral Resources Tasmania, p. 12.

Ritis, R., D. Ravat, G. Ventura, and M. Chiappini, 2013, Curie isotherm depth from aeromagnetic data constraining shallow heat source depths in the central Aeolian Ridge (Southern Tyrrhenian Sea, Italy): Bulletin of Volcanology, v. 75, p.1-11.

Rivero, L., V. Pinto, and A. Casas, 2002, Moho depth structure of the eastern part of the Pyrenean belt derived from gravity data: Journal of Geodynamics, v. 33, p. 315-332.

Roach, M. J., 1994, The regional geophysical setting of gold mineralisation in northeast Tasmania, PhD Thesis, University of Tasmania.

Roach, M. J., D. E. Leaman, and L. M. Richardson, 1993, A comparison of regional - residual separation techniques for gravity surveys: Exploration Geophysics, v. 24, p. 779-784.

Rosenbaum, G., 2012, Oroclines of the southern New England Orogen, eastern Australia: Episodes, v. 35, p. 187-194.

Royer, J. Y., and N. Rollet, 1997, Plate-tectonic setting of the Tasmanian region: Australian Journal of Earth Sciences, v. 44, p. 543-560.

Rudnick, R.L., and Gabriel, G., 2014, The Composition of the Continental Crust- Holland, Heinrich D. in Karl K. Turekian (ed.) Treatise on Geochemistry, Pregamon, 1-51.

Rudnick, R.L., and Gao, S., 2003, 3.01 - Composition of the Continental Crust A2 - Holland, Heinrich D. in Karl K. Turekian (ed.) Treatise on Geochemistry, Pergamon, 1-64.

Saad, A., F., 1969, Magnetic properties of ultramafic rocks from Red Mountain, California: Geophysics v. 34, p. 974-987.

Salmon, M., B. L. N. Kennett, and E. Saygin, 2012, Australian Seismological Reference Model (AuSREM): crustal component: Geophysical Journal International, v. 192, p. 190-206.

Salmon, M., B. L. N. Kennett, T. Stern, and A. R. A. Aitken, 2013, The Moho in Australia and New Zealand: Tectonophysics, v. 609, p. 288-298.

Sandiford, M., Hand, M., and McLaren, S., 1998, High geothermal gradient metamorphism during thermal subsidence. Earth and Planetary Science Letters 163, 149-65.

Sandwell, D.T., Müller, R.D., Smith, W.H.F., Garcia, E., and Francis, R., 2014, New global marine gravity model from Cryosat-2 and Jason-1. Reveals Buried Tectonic Structure. Science 346, 65-67.

Sandwell, D.T., and Smith, W.H.F., 2009, Global marine gravity from retracked geosat and Ers-1 altimetry: Ridge segmentation versus spreading rate. Journal of Gephysical Research 114, 1-18.

Sandwell, D.T., and Smith, W.H.F., 1997, Marine gravity anomaly from Geosat and Ers 1 satellite altimetry. Journal of Geophysical Research 102, 10039-54.

Sandwell, D.T., 2005, Retracking Ers-1 altimeter waveforms for optimal gravity field recovery. Geophysical Journal International 163, 79-89.

Scher, H., D., J. Whittaker, M., S. Williams, E., J. Latimer, C., W. Kordesch, E. C., and M. Delaney, L., 2015, Onset of Antarctic Circumpolar Current 30 million years ago as Tasmanian Gateway aligned with westerlies: Nature, v. 523, p. 580-583.

Seymour, D., M. P. McClenaghan, G. Green, J. L. Everard, R. Berry, F., G. J. Callaghan, G. J. Davidson, and P. B. Hills, 2014, Mid-Palaeozoic orogenesis, magmatism and mineralisation, in K. D. Corbett, P. G. Quilty, and C. R. Calver, eds., Geological Evolution of Tasmania, v. Special Publication 24, Geological Society of Australia, p. 273-362.

Seymour, D. B., and C. R. Calver, 1995, Explanatory notes for the Time-Space Diagram and Stratotectonic Elements map of Tasmania: Tasgo NGMA Project: Sub-Project 1: Geological Synthesis, v. Tasmanian Geological Survey record 1995/01.

Seymour, D. B., and C. R. Calver, 1995, Stratotectonic Elements Map Of Tasmania (1:500 000 Scale), NGMA Tasgo project, Mineral Resources Tasmania.

Seymour, D. B., G. R. Green, and C. R. Calver, 2007, The geology and mineral deposits of Tasmania: a summary: Geological survey, v. Bulletin 72, p. 32.

Shaw, R.D., P. Wellman, P.J. Gunn, A.J. Whitaker, and C.Z. Tarlowski, 1995, Australian Crustal Elements (National Geoscience Dataset Geoscience Australia.

Shuey, R. T., D. K. Schellinger, A. C. Tripp, and L. B. Alley, 1977, Curie depth determination from aeromagnetic spectra: Geophysical Journal International, v. 50, p. 75-101.

Simpson, R. W., R. C. Jachens, R. J. Blakely, and R. W. Saltus, 1986, A new isostatic residual gravity map of the conterminous United States with a discussion on the significance of isostatic residual anomalies: Journal of Geophysical Research, v. 91, p. 8348.

Spector, A., and F. S. Grant, 1970, Statistical models for interpreting aeromagnetic data: Geophysics, v. 35, p. 293-302.

Stacey, F. D., and S. K. Banerjee, 1974, The physical principles of rock magnetism: Elsevier, Amsterdam, v. 195 pp.

Stagg, H. M. J., C. D. Cockshell, J. B. Willcox, A. J. Hill, D. V. L. Needham, B. Thomas, G. W. O'brien, and L. P. Hough, 1990, Basins of the Great Australian Bight region, geology and

petroleum potential, Bureau of Mineral Resources, Geology and Geophysics, Continental Margins Program Folio, 5.

Stagg, H. M. J., J. B. Willcox, P. A. Symond, G. W. O'brien, J. B. Colwell, P. J. Hill, C. S. Lee, A. M. G. Moore, and H. I. M. Struckmeyer, 1999, Architecture and evolution of the Australian continent margin: AGSO Journal of Australian Geology and Geophysics, v. 17, p. 17-33.

Sutherland, F. L., I. T. Graham, J. D. Hollis, S. Meffre, H. Zwingmann, F. Jourdan, and R. E. Pogson, 2014, Multiple felsic events within post-10 Ma volcanism, Southeast Australia: inputs in appraising proposed magmatic models: Australian Journal of Earth Sciences, v. 61, p. 241-267.

Tanaka, A., Y. Okubo, and O. Matsubayashi, 1999, Curie point depth based on spectrum analysis of the magnetic anomaly data in East and Southeast Asia: Tectonophysics, v. 306, p. 461-470.

Geological Survey of Tasmania, and Tasmania Development and Resources, 1995, Geological atlas 1:250 000 digital series: [Tasmania]/ Tasmanian Geological Survey.

Taheri, J., and R.S. Bottrill, 2005, Devonian Granites and Associated Mineralisation in Northeast and Northwest Tasmania. Mineral Resource Tasmania, Tasmanian Geological Survey, Record 2005/03, 73.

Telford, W., L. Geldart, and R. Sheriff, 1990a, Gravity Methods, Applied Geophysics, Cambridge University Press, p. 6-61.

Telford, W., L. Geldart, and R. Sheriff, 1990b, Magnetic Methods, Applied geophysics, Cambridge University Press, p. 62-135.

Telford, W., L. Geldart, and R. Sheriff, 1990c, Seismic Methods, Applied Geophysics, Cambridge University Press, p. 136-282.

Tetley, M. G., R. D. Muller, P. W. Schmidt, and S. E. Williams, 2013, Macquarie Arc and the Lachlan Orocline hypothesis: Magnetic analysis and development of geologically constrained forward model of lithospheric magnetisation: 23rd International Geophysics Conference and Exhibition, Melbourne, Australia, p. 1-3.

Turner, N. J., 1989, Precambrian, in: Burrett, C. F.; Martin, E. L. (ed.). Geology and Mineral Resources of Tasmania: Special Publication Geological Society of Australia, v. 15, p. 5-46.

Turner, N. J., L. P. Black, and M. Kamperman, 1994, Pre-Middle Cambrian stratigraphy, orogenesis and geochronology in western Tasmania, in: Cooke, D.R.; Kitto, P. A. (ed.). Contentious issues in Tasmanian geology: Abstracts Geological Society of Australia, v. 39, p. 51-56.

Turner, N. J., L. P. Black, and M. Kamperman, 1998, Dating of Neoproterozoic and Cambrian orogenies in Tasmania: Australian Journal of Earth Sciences, v. 45, p. 789-806.

Turner, N. J., R. S. Bottrill, A. J. Crawford, and I. Villa, 1992, Geology and prospectivity of the Arthur Mobile Belt.: Bulletin Geological Survey Tasmania, v. 70, p. 227-233.

Turner, N. J., A. V. Brown, M. P. McClenaghan, and I. R. Soetrisno, 1991, Geological Atlas 1:50 000 Series. Sheet 43 [7914N].

Tyson, T., 2002, Gravity and magnetic of the Woolnorth area, Northwest Tasmania: B.Sc. (Hons) Thesis, University of Tasmania.

Vasconcelos, G., P. B. Lourenco, C. S. A. Alves, and J. Pamplona, 2007, Prediction of the Mechanical Properties of Granites by Ultrasonic Pulse Velocity and Schmidt Hammer Hardness, Masonry Conference, Missouri, p. 998-1009.

Veevers, J., 1986, Breakup of Australia and Antarctica estimated as mid-Cretaceous (95 ± 5 Ma) from magnetic and seismic data at the continental margin: Earth and Planetary Science Letters, v. 77, p. 91-99.

Wasilewski, P. J., and M. A. Mayhew, 1992, The Moho as a magnetic boundary revisited: Geophysical Research Letters, v. 19, p. 2259-2262.

Webster, S., 1984, A magnetic signature for tin deposits in south-east Australia: Exploration Geophysics, v. 15, p. 15-31.

Webster, S. S., 2003, Quantitative interpretation of magnetic and gravity data for the Western Tasmanian Regional Mineral Program, Part 2: Mineral Resources Tasmania- Tasmanian Geological Survey, Record 2002/15, p. 52-91.

Weissel, J. K., and G. D. Karner, 1989, Flexural uplift of rift flanks due to mechanical unloading of the lithosphere during extension: Journal of Geophysical Research, v. 94, p. 13919-13950.

White, R.M., 2007, Quantum Theory of Magnetism: Magnetic Properties of Materials. Springer Science & Business Media.Whitmeyer, S. J., and K. E. Karlstrom, 2007, Tectonic model for the Proterozoic growth of North America: Geosphere, v. 3, p. 220-259.

Williams, E., 1989, Summary and synthesis: in Geology and mineral resources of Tasmania (edu), in edited by Burrett, C. F. and Martin, E.L, ed., Special Publication Geological Society of Australia 15, p. 468-499.

Williams, N., C., 2008, Geologically constrained UBC-GIF gravity and magnetic inversion with examples from the Agnew-Wiluna Greenstone Belt, Western Australia, University of British Columbia, 509 p.

Williams, S., E., J. Whittaker, M., and R. D. Müller, 2011, Full-fit, palinspastic reconstruction of the conjugate Australian-Antarctic margins: Tectonics, v. 30, p. TC6012.

Wyborn, L. A., C. A. Heinrich, and A. L. Jaques, 1994, Australia Proterozoic Mineral System: Essential Ingredients and Mappable Criteria, The AusIMM Annual Conference, Darwin, p. 109-115.

Yoshii, T., 1979, A detailed cross-section of the deep seismic zone beneath northeastern Honshu, Japan: Tectonophysics, v. 55, p. 349-360.

Young, M. K., N. Rawlinson, P. Arroucau, A. M. Reading, and H. Tkalčić, 2011, High-frequency ambient noise tomography of southeast Australia: New constraints on Tasmania's tectonic past: Geophysical Research Letters, v. 38, p. L13313.

Young, M. K., N. Rawlinson, and T. Bodin, 2013, Transdimensional inversion of ambient seismic noise for 3D shear velocity structure of the Tasmanian crust: Geophysics, v. 78, p. WB49- WB62.